# Urban planning support based on the photovoltaic potential of buildings: a multi-scenario ranking system

**Thèse N° 9051**

**Présentée le 24 janvier 2019**

**à la Faculté de l'environnement naturel, architectural et construit**
**Laboratoire de Performance Intégrée au Design**
**Programme doctoral en architecture et sciences de la ville**

**pour l'obtention du grade de Docteur ès Sciences**

**par**

GIUSEPPE PERONATO

**Acceptée sur proposition du jury**

**Prof. F. Golay, président du jury**
**Prof. M. Andersen, Prof. E. Rey, directeurs de thèse**
**Prof. M. C. Brito, rapporteur**
**Prof. C. Reinhart, rapporteur**
**Prof. F. Maréchal, rapporteur**

**2019**

ÉCOLE POLYTECHNIQUE
FÉDÉRALE DE LAUSANNE

# Abstract

An increased use of renewable energy and of energy efficiency measures in buildings is needed to face the urgency of climate change. Buildings are in fact among the highest worldwide consumers of primary energy, mostly of fossil fuel origin, while still making insufficient use of in-situ renewable energy sources. To find a solution to this situation, many municipalities have promoted the use of solar cadastres mapping the solar energy potential of the existing building stock. However, their implementation has limits from different points of view including assessment accuracy, representation methods, and decision-support.

To overcome these limits, this thesis proposes a planning-support system based on the photovoltaic (PV) potential of buildings. The goal is to provide decision-makers and stakeholders with a robust method to assess the potential of photovoltaic electricity generation of existing buildings under uncertain environmental conditions.

The developed methodology is based on an urban-scale modeling workflow that includes the simulation of the photovoltaic electricity production and a simplified estimation of the building energy retrofit potential. Existing state-of-the-art models for solar radiation, building energy and PV performance are coupled in the workflow, which relies on a vector 3D city model featuring an accurate representation of buildings, terrain, and vegetation. The proposed modeling workflow also includes an innovative approach for simulating the arrangement of PV modules on the building envelope, which influences both the energy yield and the acceptability of the system. The modeling workflow is in turn integrated into a planning-support system that provides a robust assessment of the photovoltaic potential through risk-averse scenarios. We consider here two crucial yet underestimated uncertainty factors: weather and vegetation. The results are aggregated at different scales and, for each scale, the spatial locations are ranked through pairwise comparisons according to relevant energy indicators. The results are finally displayed in a 3D-mapping tool featuring false-color overlays at the considered aggregation scales to address different objectives and inform decision-makers.

We conducted sensitivity analyses towards different input data resolutions and modeling scenarios so as to achieve a good trade-off between accuracy and computational cost and define confidence intervals for the calculated values. The simulated PV yield was also compared against measured data from an existing PV installation.

The proposed modeling workflow and planning-support system were tested in an urban district within the city of Neuchâtel (Switzerland). The analysis highlighted areas with the highest potential and provided a priority list of interventions. It also showed the impact of vegetation on absolute results and especially on the ranking of the spatial locations evaluated by their energy potential.

**Keywords**: *3D city model, urban building energy modeling, PV forecasting, decision-making*

# Résumé

Pour faire face aux changements climatiques, il est nécessaire d'encourager l'utilisation d'énergies renouvelables et l'adoption de mesures d'efficacité énergétique dans les bâtiments. Les bâtiments sont de fait parmi les plus grands consommateurs d'énergie primaire à l'échelle mondiale, la plupart d'origine fossile, et intègrent encore insuffisamment les sources d'énergie renouvelables disponibles sur site. Afin de remédier à cette situation, beaucoup de communes ont promu l'utilisation de cadastres solaires cartographiant le potentiel solaire des bâtiments existants. Ces cadastres ont toutefois des limites en termes de précision du calcul, de méthodes de représentation ou d'aide à la décision.

Pour surmonter ces limites, cette thèse propose un système d'aide à la planification urbaine basé sur le potentiel photovoltaïque (PV) des bâtiments. Le but est de donner à tous les acteurs du processus décisionnel une méthode solide pour évaluer et comparer le potentiel de génération d'énergie électrique photovoltaïque des bâtiments existants dans un contexte de conditions environnementales incertaines.

La méthodologie développée est basée sur une procédure de modélisation à l'échelle urbaine comprenant des simulations de la production photovoltaïque et une estimation simplifiée du potentiel de rénovation des bâtiments. Cette procédure met ensemble des modèles d'avant-garde pour la simulation du rayonnement solaire, des besoins énergétiques des bâtiments et de la production photovoltaïque avec une analyse à la grande échelle basée sur une maquette numérique vectorielle 3D. La maquette permet une représentation détaillée des bâtiments, du terrain e de la végétation. La procédure de modélisation inclut en outre une approche novatrice pour simuler le positionnement des modules PV sur l'enveloppe du bâtiment, ce qui influence non seulement la production d'électricité mais aussi l'acceptabilité du système. La procédure de modélisation est intégrée à son tour dans un système d'aide à la planification qui permet une évaluation robuste du potentiel photovoltaïque à travers des scénarios de minimisation du risque. Nous considérons ici deux facteurs d'incertitude cruciaux bien que sous-estimés : les conditions météorologiques et la végétation. Les résultats sont agrégés à différentes échelles et, pour chaque échelle, les emplacements spatiaux sont classés par une comparaison par paires selon les indicateurs énergétiques appropriés. Les résultats sont finalement visualisés dans un outil cartographique 3D avec des couches en fausses couleurs superposées aux échelles d'agrégation considérées pour atteindre différents objectifs et informer les décideurs.

Nous avons conduit des analyses de sensibilité au regard de différentes résolutions des données et scénarios de modélisation afin d'atteindre un bon compromis entre la précision et le temps du calcul et de définir les intervalles de confiance des résultats. La production photovoltaïque simulée a été aussi comparée avec les données mesurées d'une installation existante.

Finalement, la procédure de modélisation et le système d'aide à la planification ont été testés dans un secteur de la ville de Neuchâtel, en Suisse. L'analyse a mis en lumière les zones avec le potentiel le plus haut et a établi une liste de priorités d'intervention. Elle a aussi montré l'impact de la végétation sur les valeurs absolues et surtout sur le classement des emplacements spatiaux évalués sur base de leur potentiel énergétique.

**Mots-clés :** *modèle urbain 3D, modélisation énergétique des bâtiments à l'échelle urbaine, estimation de la production photovoltaïque, processus de décision*

# *Abstract*

Per far fronte ai cambiamenti climatici, è necessario incoraggiare l'uso di energia rinnovabile e l'adozione di misure di risparmio energetico negli edifici. Gli edifici sono infatti tra i maggiori consumatori di energia primaria alla scala mondiale, la maggior parte di origine fossile, ed integrano in modo ancora insufficiente le fonti energetiche rinnovabili disponibili in loco. Per porre rimedio a questa situazione, molti comuni hanno promosso l'uso di mappe solari che individuano il potenziale solare degli edifici esistenti. Queste mappe hanno però alcuni limiti in termini di precisione della valutazione, dei metodi di rappresentazione o del supporto alla decisione.
Per superare questi limiti, questa tesi propone un sistema di supporto alla pianificazione urbana basato sul potenziale fotovoltaico degli edifici. L'obiettivo è di fornire a tutti gli attori del processo decisionale un metodo solido per valutare e confrontare il potenziale di produzione di energia elettrica fotovoltaica degli edifici esistenti in un quadro di condizioni ambientali incerte.
La metodoologia sviluppata si basa su una procedura di modellazione alla scala urbana che comprende simulazioni della produzione fotovoltaica ed una stima semplificata del potenziale di riqualificazione energetica degli edifici. Questa procedura unisce modelli avanzati per la simulazione della radiazione solare, del consumo energetico degli edifici e della produzione fotovoltaica con un'analisi alla grande scala basata su modelli urbani vettoriali tridimensionali, che permettono una rappresentazione accurata degli edifici, del terreno e della vegetazione. La modellazione include anche un approccio innovativo per stimare la disposizione dei moduli fotovoltaici sulle superfici degli edifici, un fattore che influisce non solo sulla produzione di elettricità, ma anche sull'accettabilità di questi sistemi. La procedura di modellazione è integrata a sua volta nel sistema di supporto alla pianificazione che permette una valutazione robusta del potenziale fotovoltaico attraverso degli scenari di minimizzazione del rischio. Sono considerati due fattori di incertezza tanto importanti quanto sottostimati: le condizioni meteorologiche e la vegetazione. I risultati sono aggregati a diverse scale e, per ogni scala, le unità spaziali sono classificate con il metodo del confronto a coppie, sulla base dell'indicatore energetico appropriato. I risultati sono infine visualizzati in un programma di geovisualizzazione 3D con una rappresentazione sovrapposta in falsi colori alle diverse scale considerate, dando così informazioni pertinenti sui diversi obiettivi agli attori rilevanti.
Sono state condotte delle analisi di sensibilità rispetto a diversi scenari di modellazione e risoluzioni dei dati, al fine di trovare un buon compromesso tra precisione e tempo di calcolo e di definire gli intervalli di confidenza dei risultati. La produzione fotovoltaica simulata è stata inoltre confrontata con i dati reali di un impianto esistente.
La procedura di modellazione ed il sistema di supporto alla pianificazione proposti sono stati infine sperimentati in un settore della città di Neuchâtel, in Svizzera. L'analisi ha evidenziato le zone con maggiore potenziale, contribuendo così a stilare una lista di priorità d'intervento. L'analisi ha altresì mostrato l'impatto della vegetazione sui risultati assoluti e, soprattutto, sull'ordine relativo delle unità spaziali valutate per il loro potenziale di energia.

**Parole chiave:** *modello urbano tridimensionale, modellazione energetica degli edifici alla scala urbana, previsione di produzione fotovoltaica, processo decisionale*

# Table of Contents

# 1 Introduction

Currently, 55% of the world population live in cities and this share is expected to increase to 68% by 2050 [303]. Buildings represent about 40% of the total primary energy use in the U.S. and in Europe, the largest portion coming from fossil fuels [42].

In this context, it is essential to provide energy production where it is mostly consumed. As everywhere else on earth, also in urban environments solar energy is a key renewable energy source. In particular, solar photovoltaics produce electricity, which can be used for all energy uses in buildings, including lighting, appliances, heating and cooling. Self-consumption of on-site energy production reduces the stress of the grid [199] and helps the financial viability of the system [161].

In terms of carbon content, photovoltaic-generated electricity is cleaner than the current electricity primary energy mix in Switzerland and many other countries (see Table 2.3 and [299]). Moreover, with an expected progressive decarbonization of electricity generation, electrification of heating can help reduce the carbon content of building energy consumption compared to the use of fossil fuels (e.g., in the Netherlands [185] and in China [212]). Using electricity, heat pumps generate heating by an efficiency that is usually three times or more the one of conventional boilers. Moreover, with global warming increasing the global cooling demand [42], they provide flexible space conditioning, adapted both for heating and cooling purposes. However, because heat pumps are best at low-temperature heating, they are effective only in high-performing buildings, with reduced heat losses.

The new buildings conceived with current high-performance standards represent only a small share of the total building stock. In Switzerland, more than 85% of the building stock was built in the last century or before. In many developed countries with a decreasing or stable population, the existing building stock can accommodate the current housing needs. However, the performance of existing buildings is often poor, as their envelope was conceived with no or little attention to insulation and use of passive solar gains.

The refurbishment of the thermal envelope is a typical energy retrofit intervention that can greatly improve the energy performance of a building. Leaving substantially unaltered the in-going energy flux (e.g., unchanged windows size) and the inertia (e.g., addition only of low-density insulating materials), the energy losses are highly reduced by the increased insulation level of the opaque envelope and the glazings.

In an envelope retrofit intervention, Building-Integrated Photovoltaics (BIPV) can substitute conventional cladding, i.e., the outermost layer of the building skin, both on roofs and façades. Some examples

are photovoltaic roof tiles, that can be used instead of traditional roofing, and semi-transparent photovoltaics, that can be used as energy-producing glazings in windows. Interventions on the building skin are particularly sensitive because of the change of the building appearance, affecting human perception both from an aesthetical (e.g., integration in a historical building) and comfort point of view (e.g., glare). In this sense, Building-Integrated Photovoltaics (BIPV) systems, as well as carefully-designed Building-Applied Photovoltaics (BAPV) systems, increase the aesthetic acceptability of PV technologies. They also allow the application of PV systems on all available building surfaces. Moreover, the diversification of tilts and azimuth orientations can smooth the production curve throughout day and seasons, improving the match with the local demand curve.

Building-installed solar systems could give a substantial contribution to renewable energy production. The IEA [119] estimated that they could cover about one third of the current electricity demand of some developed countries. The Swiss government set a 20% share of photovoltaic electricity production as part of its 2050 energy strategy [63].

Many countries have implemented subsidies and facilitations both for building energy retrofitting and solar energy installations. However, traditional mechanisms such as the feed-in-tariff have often become victim of their own success. Such financial-support mechanisms have contributed to boost the share of renewable energy production in the European market in the last 10-15 years, at the expense though of the distortion of electricity market prices and imbalance in the electrical power systems [238]. Many countries, including Switzerland, have recently reduced the financial support to photovoltaics.

In this context, the increase of renewable production energy is slowing down in many European countries [238]. There is hence the need to drive the potential of photovoltaics towards the targets fixed by the renewable energy transition, both in the European Union and Switzerland, which are far from being reached. We believe that the combination of energy retrofit intervention of the existing building stock with solar energy systems can help the energy transition. Mapping the energy potential and supporting decision-making is a first step towards the implementation of ambitious planning decisions, both from public authorities and private investors.

## 1.1 Research scope

This thesis aims at providing novel advancements on the analysis of solar energy generation potential in urban environments. The research is articulated around some specific research gaps that will be highlighted in the state of the art (Chapter 4). However, we can anticipate here some broader objectives that target the main research gaps and constitute the core of the thesis investigation.

#### Coupling state-of-the-art assessment methods and 3D city models

The assessment of BIPV production in urban environments requires adequate tools and input data. In dense urban environments, a relevant share of the available energy hitting the surfaces is reflected from the urban canopy, as will be shown Section 6.2.2. Similarly, vegetation is highly affecting solar radiation on façades and, to some extent, on rooftops, as will be shown in Chapter 7.

Therefore, we need to account for inter-reflections and vegetation shading to have a comprehensive analysis of the available solar radiation, but the time-varying complex shape and semi-transparency of trees is challenging to model. It requires computationally-expensive calculations, such as raytracing or radiosity algorithms, as well as an accurate sensing and representation of both vegetation and the

surrounding built environment. The last generation of geodata including a full modeling of vertical discontinuities such as overhangs on building façades provide a high level of accuracy in the geometric Level of Detail (LOD). We will show that a gap exists between advanced simulation methods and their application to urban-scale analysis, which can be bridged by the use of these new-generation urban geodata and efficient computational workflows.

**Supporting robust decisions**

As in many other problems dealing with limited resources, also in solar potential assessments there is the need to set some priorities. Setting priorities, as all decision-making actions, requires a perfect knowledge of the resources or adequate methods to deal with the uncertainties.

Modeling urban scale PV potential involves epistemic uncertainties, such limited data availability and computational power, and intrinsically aleatory uncertainties, such as the weather variability. These factors are rarely included in the decision-making problem, while we argue that they would improve the robustness of energy planning decisions. In the thesis, we will show the application of a decision-support method including some crucial environmental uncertainties, such as weather and vegetation. We will also test the sensitivity of the results to some simulation parameters so as to find a good compromise between the accuracy of the results and the computational cost.

### 1.1.1 Research actions

We can consider the thesis scientific contribution as the direct outcome of the following three research actions:

- *review* the broad spectrum of disciplines composing the studied topic, to show the potential and limits of current methods;
- *develop* a new method combining existing and new knowledge;
- *test* the method and show its added value in a real case study.

Regarding the review action, in the previous section we have seen that analyzing the photovoltaic potential in urban environments offers perspectives on a wide range of topics, belonging to very distant disciplines. The review is indeed part of the thesis contribution, as we want to draw from the contributions of each discipline, in particular:

- Geographic Information Systems (GIS), for the sensing, representation and analysis of the built environment in a virtual 3D model;
- spatial decision-support systems, for improving traditional decision-making including multiple analysis granularities and uncertainties;
- solar radiation, building thermal and PV performance simulation, by coupling existing state-of-the-art models and adapting them for urban-scale applications;

We also want to show the links between the disciplines and hence highlight the need for a comprehensive method of solar potential analysis, which will be then the object of the development and testing phases.

### 1.1.2 Local context

This thesis is in inscribed in the Swiss context. In this sense, it deals with the legal and political framework of Switzerland, with respect for example to planning tradition and energy objectives. Even if the developed method can be considered country-agnostic, the subsequent application has to deal with the specificities of the local context.

In general, the characteristics of Switzerland are those of a developed country, with a favorable technical and regulatory framework for photovoltaic implementation. These characteristics can be summarized as follows:

- favorable climatic conditions for PV applications, with mid-high solar irradiation and mid-low temperature;
- ambitious policy and long-term objectives for the energy decarbonization;
- (recent) regulatory framework encouraging self-consumption of building-produced PV electricity;
- subsidies for building energy retrofit and photovoltaics at different institutional levels;
- availability of high-quality and -resolution geodata, in particular 3D city models;

We argue that the contribution to the Swiss context will be a good test for future applications to other countries, assuming that at least some of the conditions listed here above will be met elsewhere in the near future (Section 1.1.3).

### 1.1.3 Premises

The thesis is based on some premises drawn from facts and evidence in the multi-disciplinary review conducted in the Part I. Although they are not part of the thesis direct scientific investigation, which is grounded on a more specific review (Chapter 4), these premises form the *boundary conditions* for the wide applicability of the thesis proposed method.

- Photovoltaics are one the most promising micro-energy generation sources and will significantly increase their share in the future energy mix;
- Thanks to their flexibility, 3D city models will become the common practice to conduct solar and building energy assessments on existing buildings and on their possible transformation strategies; their availability, today limited to some countries and cities, will increase in the future, thanks to the increasing availability and popularity of acquisition methods;
- Due to the ongoing urbanization process, urban energy planning actions will be increasingly important in the energy transition;
- The encouraging regulatory framework for energy saving and renewable energy, in particular financial or other public-driven incentives, will continue play an important role in the energy transition;

We argue that the validity of this thesis's method will not be jeopardized in case some of these premises are not verified in the future, although we acknowledge that the concrete applicability of some parts of the thesis might be limited.

## 1.2 Content overview

We present here a short summary of the thesis content along with its structure.

**Part I - Research context and state of the art**

In the first part, we will conduct a literature review at different levels of detail and relation with the research scope. This part is meant to introduce the topic, but also to prove the assumptions that were listed in Section 1.1.3.

**Chapter 2** will give an overview of the multi-disciplinary research background of the thesis;

**Chapter 3** will report about the Swiss situation with regards to solar energy, building energy and urban planning, investigating the legal and policy framework;

**Chapter 4** will describe the current state of the art regarding the assessment of solar energy potential in urban areas and the use of such information in decision making. This section will highlight more specifically the research gaps targeted by the thesis.

**Part II - Preliminary development and test applications**

This part constitutes a collection of autonomous and self-contained preliminary studies and, as such, can be read independently from the other parts. However, to facilitate a direct comparison with the thesis method presented in Chapter 11, we follow the same structure for presenting the methodology. We also highlight the main differences and the contributions to the thesis development at the end of each section. For further information, the reader can refer to the original complete publications that are referenced at the beginning of each section.

**Chapter 5** summarizes the characteristics of the analysis method used in this part and the goals of its chapters;

**Chapter 6** presents sensitivity analyses with regards to the Level of Detail (LOD), the discretization of the 3D model and the raytracing ambient settings;

**Chapter 7** contains studies regarding the vegetation modeling, showing its relevance in solar potential assessment and proposing modeling strategies to deal with the seasonal variability;

**Chapter 8** deals with the arrangement of PV modules on tilted surfaces and on flat roofs;

**Chapter 9** investigates the stability of ranking with regards to different hypotheses and modeling scenarios, and discuss the findings in decision-making.

**Chapter 10** summarizes the findings of this part, also in relation with their application in Part III.

Along with the differences, we will also highlight the main findings that contributed to the method development.

**Part III - Core development and verification**

In the third part of the thesis, we will present the novel research contribution of the thesis based on the research background and with regards to the gaps highlighted in the state of the art, in particular:

**Chapter 11** describes the methodology and software workflow developed for the analysis;

**Chapter 12** presents a case-study application of the developed methodology in a Swiss city;

**Chapter 13** compares the simulated results with measurements and alternative methods;

In **Chapter 14**, we summarize the results of the thesis and discuss the limitations and future work.

# Part I
# Research context and state of the art

# 2 Multidisciplinary research background

This thesis deals with topics inherent to various disciplines, including energy engineering, semiconductor physics, geographic information systems, law, urban planning and decision theory. Far from pretending to be in-depth and exhaustive, this section aims at providing the reader with a general introduction to the specific topics in these fields relevant for the thesis. It also aims at informing some choices that will be taken in the following chapters, based on current practice and state of the art. To this end, at the end of each section, we will summarize and discuss the main facts that are revelant for the thesis development.

## 2.1 Urban micro energy generation

Urban energy micro generation allows the offsetting of building energy demand by producing on-site energy (either thermal or electrical) that can be directly used by the consumers-producers. We consider here only systems that can be installed at the building scale and whose primary energy source is possibly available on-site, i.e. wind, geothermal, hydro, solar energy and biomass, while a more comprehensive list can be found in Table 2.1. These systems are considered as "city-integrated" renewable energy sources and their exploitation is crucial to face the challenges of climate change and urban influx [139].

If we consider electricity production, we can identify three types of generation systems: photovoltaics, micro wind turbines and micro-hydro systems. For thermal energy, we can find geothermal (both shallow and deep) and solar thermal. Micro-CHP systems combine the production of electricity and thermal energy from both renewable and non-renewable fuels. Even if bio-mass CHP systems exist, at the size of single buildings these systems usually rely on the combustion of natural gas.

We will focus hereinafter on energy sources that are "visible" and "building-attached", as they provide a series of challenges in their assessment, which intersect with architecture and urban planning disciplines and are hence relevant to the interdisciplinary scope of this thesis.

The importance of user perception and acceptance of renewable energy systems is often underestimated. In this sense, solar and wind energy are visibly technologies, as their components, i.e., solar modules or wind turbines, are usually exposed to the view and in some cases part of building envelope or of the landscape. Nonetheless, many research works are aimed at masking the appearance of the solar cells [264, 228] and at finding locations in which they are not visible [84], as many PV modules are considered not aesthetically-suitable for certain locations. Similarly, some research has investigated

the negative effect due to the visibility of solar systems, as a source of discomfort and disability glare [130, 258].

There are also several constraints linked to the fact that they are attached or integrated to the building. In this sense, they can in some cases be part of the building envelope. Moreover, their installation involves a transformation of the building surfaces, which could have potential benefits (but also conflicts) in the design and planning process.

### 2.1.1 Solar energy vs Wind energy

Both solar and wind energy systems attached to buildings provide the challenges of being usually visible systems and of generating energy discontinuously. Unlike for micro wind turbines, which have a lower efficiency than those used in wind farms, for solar energy we can find comparable efficiencies in urban applications and in large plants [329].

Ishugah et al. [123] reports some examples of building-integrated wind turbines. Just like for building-applied and building-integrated solar photovoltaics (Section 2.2.5), wind energy can be used for the energy retrofitting of existing buildings or as part of the design concept for a new (usually high-rise) building. The most common type for urban applications is the horizontal-axis wind turbine (HAWT) [123], as it better suits the design constraints of such installations (e.g., low speed and turbulent wind, little space).

Building-integrated wind turbines were popular in the UK but had a subsequent poor performance which led to negative feedbacks, because of turbulence, noise and vibration [284, p. 341]. Noise, safety (e.g. damage from broken blades), resonance, flicker shadow, and aesthetics are some of the typical concerns about wind energy [329, 123, 39]. On the other hand, glare and aesthetics are the main concerns that can be found for solar installations.

Wind in urban areas is subjected to microclimate variations, which are difficult to predict at the large scale without long-time monitoring or complex CFD modeling. This makes wind energy more difficult to assess than solar energy in urban areas [329]. Solar irradiation can be, in fact, more easily modeled even in complex urban environments, even if an accurate prediction of boundary conditions affecting the efficiency of solar cells is also difficult to obtain.

### 2.1.2 Solar thermal vs Photovoltaics

Solar thermal is often seen as a direct competitor to photovoltaics, because they both exploit the same energy source and both occupy a part of the building envelope. Goetzberger and Hoffmann [96, p. 219] deny that PV and solar thermal compete for roof space, as there is usually enough space to fit both of them. The main arguments cited by Goetzberger and Hoffmann [96, p. 219] are that:

- thermal collectors need only limited space, because they have higher efficiency and they are likely sized for the consumption of Domestic Hot Water (DHW);
- the efficiency of thermal collectors is not sensitive to partial shading and can be hence placed on locations that are not suitable for PV.

However, the first condition is not met when solar thermal is used also for space heating. In this case, even if the target temperature for space heating can be much lower than for DHW (around 30° instead of 60°), the need of space for solar collectors is greater.

*Table 2.1 – Examples of microgeneration technologies*
*Source: Staffell et al. [284, p. 9]*

| Technology | Energy conversion process | Renewable | Higher efficiency |
|---|---|---|---|
| Condensing boilers | Gas → Heat | | |
| Biomass boilers | Sustainable fuel → Heat | ✓ | |
| Heat pumps | Electricity + Sun→ Heat | | ✓ |
| Solar photovoltaic | Sun → Electricity | ✓ | |
| Solar thermal | Sun → Heat | ✓ | |
| Micro wind | Sun* → Electricity | ✓ | |
| Internal combustion engines | Gas → Heat + Electricity | | ✓ |
| Stirling engines | Gas → Heat + Electricity | | ✓ |
| Fuel cells | Gas → Heat + Electricity | | ✓ |

*Atmospheric wind due to air density variations caused by the sun.

The hybrid solar thermal and photovoltaic (PV-T) modules can partially solve the space problem, while increasing the efficiency of the PV modules by dissipating the heat, provided that this can be used or stored (for example in a swimming pool). However, so far there are only few products available on the market and the popularity of this system is very country-specific, depending on locally-available products and subsidies [97].

Even when solar energy is used for space heating, there are some more arguments that favor PV solutions over solar thermal:

- for low-temperature space heating, the total efficiency of top-tier PV modules (around 20%) coupled with a heat pump (COP around 3) is comparable to the one of solar thermal collectors;
- solar thermal systems sized for space heating result in overproduction of hot water during summer that cannot be easily used or stored, while electricity can be more easily self-consumed, stored or injected into the grid.

### 2.1.3 Synthesis and discussion

There is a growing interest towards micro energy generation sources, most of which have the advantage of building- and city-integration as well as make use of renewable energy sources.

In the cases of wind and solar energy, the visibility of the systems and the application or integration to the building envelope opens challenges related to the acceptability and the assessment of their potential in urban areas. This brings about a crossing interest of disciplines such as urban planning and architecture, which can favor the conditions for the deployment of such energy sources.

Despite an interest for micro wind turbines in some wind-exposed countries, the potential for a larger number of locations and the easier integration into existing urban areas make solar energy particularly interesting to be evaluated in the context of Switzerland, but also of a larger number of countries.

With regards to solar energy, photovoltaic energy provides some benefits as for storage and flexibility of use. From an efficiency point of view, the coupling with modern heat pumps makes photovoltaics also competitive for space heating and domestic hot water.

In terms of occupied surface area in the building envelope, photovoltaics have clearly more require-

ments than both wind turbines and solar thermal collectors. In this sense, it can be seen as complementary to these sources, as all of them can be fitted in the same building. In addition, there are synergies between building design and retrofitting and the installation of photovoltaic systems, in the sense that many photovoltaic modules can substitute traditional building materials.

To conclude, photovoltaic systems are a promising micro energy source adapted for building integration, while the evaluation of their potential is challenging from many point of views, which make them worth to investigate in this thesis.

## 2.2 Photovoltaic systems

In this section, we will analyze the main photovoltaic technologies and how their yield can be evaluated through performance models. Finally, we will examine the typical regulatory framework.

The goal is to review the most promising models and trends for further application in the thesis.

### 2.2.1 Technologies

A photovoltaic module is composed of multiple solar cells, which are connected in series, or a as layer of thin-film solar cells which is also internally connected in series [96, p. 2]. Photovoltaics cells produce electricity from solar radiation through the properties of semiconductor materials. Goetzberger and Hoffmann [96, p. 2] cite some typical strong points of photovoltaics:

- “direct conversion of solar radiation into electricity”;
- “no mechanical moving parts, no noise”;
- “no high temperatures”;
- “no pollution”, if we exclude the fabrication process [322];
- “PV modules have a very long lifetime”, with many manufacturers guaranteeing their modules for 25 years, which is though a shorter period than the operation of most buildings;
- “the energy source, the sun, is free, ubiquitous, and inexhaustible”;
- “PV is a very flexible energy source, its power ranking from microwatts to megawatts”.

The most-used semiconductor material is silicon, both in crystalline and amorphous forms. There is also an infinite number of compound materials that could be considered for use as solar cells, but in practice the most promising ones are Copper Indium Diselenide (CIS) and Cadmiun Telluride (CdTe). Finally there are some cells that do not or only partially rely on semi-conductors, such as the dye-sensitized and organic solar cells.

The power of a solar cell is the product of current and voltage. The IV curve represents the product of current and voltage from short-circuit (where current is at the maximum, but voltage is zero) to open-circuit (where voltage is at its maximum, but current is 0. The maximum power $P_{max}$ is hence located at the Maximum Power Point (MPP). The ideal IV curve will be a rectangle defined as $I_{SC} \cdot V_{OC}$, with the MPP being its outer corner.

*Table 2.2 – Efficiencies of PV module technologies.*
*Table based on data retrieved by ISE [122, p. 27] in 2015. Values for CdTe and CIS modules were updated using the values given by the manufacturers in their websites (March, 2018).*

| Material | Typical module efficiency | Sources |
|---|---|---|
| *First generation* | | |
| Mono-crystalline silicon (c-Si) | 16-18% | ISE [122, p. 27] |
| Poly-crystalline silicon (p-Si) | 16-17% | ISE [122, p. 27] |
| Heterojunction (HJT) | 18-21% | ISE [122, p. 27] |
| *Second generation* | | |
| Cadmium telluride (CdTe) | 17-18% | First Solar Series 6™ |
| Copper indium (di)selenide (CIS) | 12-14% | Solar Frontier PowerModule |

### 2.2.2 Market products

All technologies listed in the previous section are present in the market, while the relative share is very different, in terms of sales, power installed and actual energy production.

In the CEC database we can find an updated list of PV modules characteristics, including nameplate ratings and temperature coefficients, as self-reported by the manufacturers and reviewed by the California Energy Commission. This database is used by software such as SAM and PVLIB. In March 2018, the list reported data from 21'151 PV modules. As can be seen in fig. 2.3, mono- and poly-crystalline represent the largest share of the products in the list, with only 3% of modules being of other types (mostly thin-film). Because of this repartition, the average power is hence fairly high (260 W), while it is only 158 W for thin-film modules.

This repartition is partially confirmed by the data of Figure 2.1 referring to the global installed power, which shows a more pronounced share of poly-Si modules though, despite their generally lower nominal power.

It is difficult to establish trends for future systems, but at the moment it looks that silicon-based modules cover the largest share of the market. Historically, thin-film materials had a larger share and, among these, Cd-Te cells have become preponderant in the last decade, as can be seen in the historical trends published by ISE [122, p. 21].

In terms of sizes, we can see that there is a large variety of shapes and surface areas of PV modules. There is not a clear difference between BIPV modules and standard modules, while in the former category there are more products with lower shape factors, i.e. the (see Figure 2.2). In general, we can argue that the spread of products with so different characteristics should be considered in building applications where the space to be fitted with modules is particularly important. In this sense, given a surface for which a maximization of the active area is aimed, there might be a significant difference on the effective module total area depending on the size and the shape factor of the selected module.

### 2.2.3 Life cycle analysis

PV use a renewable energy source (solar radiation) to produce electricity and in this sense are carbon-free. However, from a life-cycle analysis perspective, the manufacturing, transportation, installation and disposal of PV systems do contribute to carbon emissions. In particular, manufacturing and transportation are highly dependent on the origin of the production, in terms of distance from the

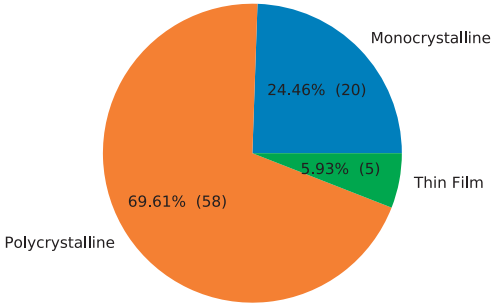


*Figure 2.1 – Global power installed of PV modules per technology in 2016 [GWp].*
*Data source: ISE [122]*

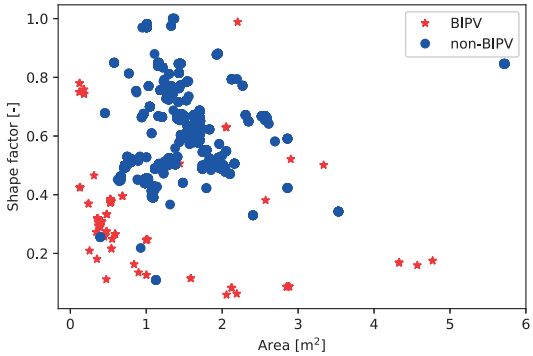


*Figure 2.2 – Shape factor (i.e., the ratio between the short and long sides) and area of standard commercial modules.*
*Data source: California Enegy Commission (CEC) PV module list, March 1, 2018*

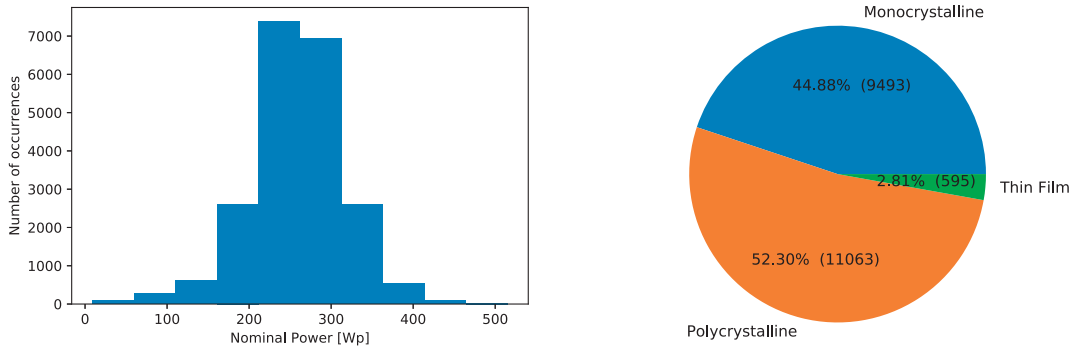


(a) Nominal Power

(b) Technology

*Figure 2.3 – Characteristics of commercial modules in the CEC database.*
*Data source: California Enegy Commission (CEC) PV module list, March 1, 2018*

installation site and of carbon content of the energy used for the manufacturing.

If we compare the carbon content of electricity produced with PV and the one of the grid (Table 2.3), PV systems provide clean energy in relation to coal-predominant mixes like the German one and comparable to nuclear-predominant mixes like the French-one. The carbon content is also expected to reduce in future years, mainly due to the increasing efficiency and duration of PV modules [92]. However, as shown by Vuarnoz and Jusselme [308], the carbon content of grid electricity is dynamic and the value at different times of the year can be significantly different from the annual mean. Moreover, competitive renewable energy sources such as run-of-the-river hydroelectricity provide lower carbon emissions than photovoltaics, even in optimistic future scenarios. In this sense, the placement of solar modules could be done so as to minimize the carbon content with respect to alternative energy sources.

*Table 2.3 – Carbon content of electricity from different sources as calculated in Life Cycle Analysis studies. For grid electricity means, the table shows the annual mean and the hourly Standard Deviation.*

| | Mean [$gCO_{2\ eq.}$/kWh] | STD [$g/CO_{2\ eq.}$/kWh] | Source |
|---|---|---|---|
| German electricity mix | 851 | 66 | [308] |
| French electricity mix | 78 | 24 | [308] |
| Swiss electricity mix | 206 | 84 | [308] |
| Swiss domestic electricity production mix | 40 | 16 | [308] |
| Swiss run-of-the-river hydroelectricity | 4 | - | [180] |
| Single-si 15.1% today | 80 | - | [92] |
| Single-si 22.9% 2050 Business-as-Usual scenario | 52 | - | [92] |
| Single-si 25.2% 2050 Realistic scenario | 26 | - | [92] |
| Single-si 27.6% 2050 Optimistic scenario | 14 | - | [92] |

### 2.2.4 Boundary conditions

The energy generation potential of a photovoltaic system is given by several boundary conditions that limit the theoretical efficiency of the solar cell. We will review here some of these boundary conditions, with the purpose of later introducing appropriate models for the prediction of their effect on the PV performance.

#### 2.2.4.1 Temperature

It is known that high temperatures negatively affect the performance of solar cells, in particular crystalline silicon ones. This is particularly important in building applications, as surface temperatures are usually higher than air temperatures due the absorptivity of the building materials and ventilation might be limited, both because of urban obstructions or the type of installation (integrated or applied) of the PV module.

The performance of PV cells linearly decreases with the increment of surface temperature. Several models expressing the electrical efficiency of the solar cells based on the temperature [74] and predicting the temperature in function of climatic parameters [126] exist in the literature.

#### 2.2.4.2 Spectral differences and low irradiance

In low and mostly diffuse light conditions, such as in the case of facade-installed systems with non-optimal exposition, crystalline modules might present a significant drop in their performance. Conversely, this drop is expected to be not that relevant for thin-film technologies, which have generally lower efficiencies, though.

Heterojunction technologies (HJT) show interesting properties compared to standard crystalline cells. Even under low irradiation conditions, their efficiency remains high and maintains 80% of its STC performance at only 10 W/m$^2$, as shown by [37].

#### 2.2.4.3 Partial shading

Partial shading significantly affects PV performance of solar cells connected in series. In fact, as soon as a solar cell is shaded, the cell becomes a hotspot. In this sense, not only the performance of the entire system is affected, but there is also the risk of damage because of the overheating. This can happen at different scales: from the one of the module, in which all cells are connected in series to maximize the power, or the one of multiple modules also connected in series.

Possible solutions can be adopted to overcome this problem. In general, multiple by-pass diodes are inserted in a single module so that if the cells around a bypass diode are shaded, the rest of the module will not be affected. At the scale of an installation composed by multiple modules connected in series, the use of a single inverter for each module (or a limited number of modules) can solve the problem.

### 2.2.5 Building integration

This thesis deals with photovoltaic systems installed on buildings. We can identify two main types of building integration: building-applied and building-integrated photovoltaic systems. According to Peng et al. [211], Building-Integrated Photovoltaics (BIPV) are a "functional part of the building envelope, or they are integrated into the building's design", while Building-Applied Photovoltaics (BAPV) are "an add-on to the building, not directly related to the structure's functional aspects". In addition, BIPV products can be divided into BIPV-modules or PV constructive elements [134]), whereas in the BAPV category we can find standard open rack-mounted panels and roof-attached PV panels.

However, there is no consensual definition of BIPV and a gradient of integration exists between fully BAPV (Figure 2.4, at left) and fully BIPV solutions (Figure 2.4, at right) [133]. James et al. [133] showed that partially integrated PV systems (Figure 2.4, in the middle) are sometimes described as BIPV and even given specific incentives.

#### 2.2.5.1 Normative definitions

In terms of norms, the European Norm EN 50583-1:2016 "Photovoltaics in buildings - Part 1: BIPV modules" provides a clear definition of building-integrated photovoltaics. BIPV systems must "form a construction product providing a function as defined in the European Construction Product Regulation CPR 305/2011". These requirements are: "mechanical resistance and stability", "safety in case of fire", "hygiene, health and the environment", "safety and accessibility in use", "protection against nose", "energy economy and heat retention", and "sustainable use of natural resources".

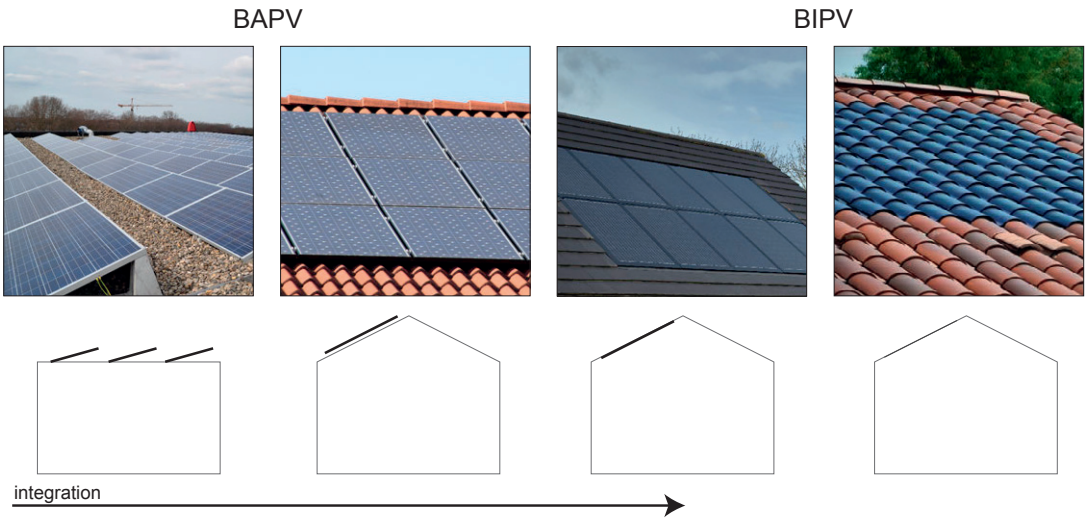


*Figure 2.4 – Gradient of building integration.*
*Image sources, from left ro right: Public Domain, Public Domain, CC BY-SA 2.0* Solar Trade Association *via* Flickr, *CC BY-SA 4.0* Bête spatio-temporelle *via* Wikimedia Commons

The EN 50583-1:2016 norm specifies also the building's function that are relevant for BIPV, which are: "mechanical rigidity orstructural integrity", "primary weather impact protection: rain, snow, wind, hail", "energy economy, such as shading, daylighting, thermal insulation", "fire protection", "noise protection", "separation between indoor and outdoor environments", and "security, shelter or safety".

#### 2.2.5.2 Application to existing buildings

BAPV products seem the most convenient ones for application to existing buildings, which are the target of this thesis. However, BIPV and BAPV products do not necessarily compete against each other but are rather complementary in different situations.

As we will discuss in Section 3.4.1, BIPV are a financially- and architecturally-viable solutions in the case of a complete retrofit of the roof and/or the building envelope. In this sense, depending on the thermal performance of the building and the investment attitude and availability of the owner, BIPV can be effectively used in existing buildings, contributing to the overall energy strategy. Differently, for buildings for which a complete refurbishment is not a viable solution (either because of lack of need or of funding), BAPV products are still an effective solution.

Moreover, depending on the sensitivity and visibility of the building and of the urban location (as proposed by [188] and discussed in Section 4.2.4), either BIPV or BAPV products can be the appropriate solution for each context.

### 2.2.6 Prediction models

There are several models aimed at the prediction of the photovoltaic potential. Klise and Stein [153] provide an extensive review of the most common PV assessment methods. As a subsequent work, the Sandia National Laboratories worked on a set of collaborative open-source libraries providing access to three of these models, namely the PVwatts model [73], the Sandia Array Performance Model [150] and

the Single Diode Model [66].

These PV assessment methods are composed of multiple physical models. We list here below the main models, describing their fundamental parameters and highlighting the aspects of complexity.

#### 2.2.6.1 Plane of Array Irradiance

In spite of PV technologies having different spectral responses, standard PV prediction models do not include such information. Similarly, they do not make difference between the components of solar radiation, which have typically very different spectra. For solar energy applications, the target solar radiation quantity is therefore the global irradiance incident on the Plane of Array (POA), also called Global Tilted Irradiance (GTI). The POA irradiance is usually modeled based on the main components of solar radiation at the horizontal surface (GHI, DHI) and normal to the sun (DNI) [271].

The calculation of the *direct incident solar radiation* is straightforward, once the angle of incidence of the DNI on the tilted plane is known [271]. For most applications, the calculation of *reflected solar radiation* can be neglected (as its contribution for installation tilts is low below 45°tilts) or calculated with a number of assumptions, such as infinite, horizontal and isotropically-reflective foreground [271].

The *sky diffuse solar irradiance* is the most complex component to calculate. This component is crucial in overcast sky conditions, in which it constitutes the 100% of the GHI, while giving a relatively small contribution during clear or partly-cloudy conditions (<30% of GHI) [271]. Different models are available and a complete review was conducted by Yang [321], while the most popular are the ones developed by Perez et al. [215], which generally perform well with hourly data [271].

#### 2.2.6.2 Cell and module temperature

As seen in Section 2.2.4.1, the cell temperature is affecting the performance of many technologies of solar cells, in particular the crystalline silicon ones. Typically, the cell temperature is higher than the air temperature, because of the absorptivity of building materials. The type of installation also affects the ventilation. In this sense, BIPV modules are generally more subject to overheating because they are less ventilated than an open-rack system, through which the wind can freely flow.

The Sandia Array Performance Model [149] is a popular module for predicting the cell and module temperature. It differentiates between the module (back surface) $T_m$ and cell temperature $T_c$. These are calculated with two different empirical equations:

$$T_m = E \cdot \left\{ e^{a+b \cdot WS} \right\} + T_a \tag{2.1}$$

where $T_m$ is the back surface air temperature (°C), $T_a$ is the ambient air temperature (°C), E is the solar irradiance incident on module surface (W/m$^2$), WS is the wind speed measured at standard 10-m height (m/s)

$$T_c = T_m + \frac{E}{E_o} \cdot \Delta T \tag{2.2}$$

*Table 2.4 – PVWatts's temperature coefficients for different module types.*
*Source Dobos [73, p. 4]*

| Module type | Cover type | Temperature coefficient ($\gamma$) |
|---|---|---|
| Standard | Glass | -0.47%/°C |
| Premium | Anti-reflective | -0.35%/°C |
| Thin film | Glass | -0.20 %/°C |

#### 2.2.6.3 Module performance

The simplest module performance often used as a rule of thumb for energy production is the following:

$$E = I_{\text{POA}} \cdot \eta \cdot A \tag{2.3}$$

where $I_{\text{POA}}$ is the irradiance on the Plane of Array and $A$ and $\eta$ are respectively the Area and the efficiency of the module. This model does not consider the effect of boundary conditions presented in Section 2.2.4. Moreover, the accuracy of this model is largely dependent on the conditions at which the efficiency $\eta$ has been measured. Many manufacturers provide only efficiency at STC[1], which is usually larger than the efficiency at the actual test conditions (especially in hot climates), giving thus an overestimation of the energy production $E$. Some manufactures provide the PTC efficiency[2], which is closer to real world conditions.

It is also possible to have a more accurate estimate of the efficiency $\eta$ at the actual cell temperature by using a temperature coefficient $\gamma$. For example, PVWatts use the coefficients listed in Table 2.4. Some manufactures include the Temperature at NOCT[3] and the relative temperature coefficient $\gamma$ from which it is possible to estimate the efficiency:

$$\eta = \eta_{\text{STC}} \cdot [1 + \gamma(T_{\text{cell}} - T_{\text{STC}})] \tag{2.4}$$

Some computer software integrate more complex models for module performance. [153] provides a review of 23 PV performance models, among which we find PVWatts, the 5-parameter Array Performance Model [66]. These models are included in the popular software System Advisor Model (SAM), which aims at providing an assessment of PV as a system, including then also the financial part. They are also included in PVLib, a Python library for photovoltaic prediction [112], based on an original MATLAB version [286]. Because of their implementation in open-source libraries which make these models particularly suitable for this thesis application, we will briefly list their main characteristics:

- *PVWatts* is an on-line calculation tool developed by the National Renewable Energy Laboratory principally intended for rapid assessment of PV energy generation. *PVWatts* is a popular model for early-design estimations, as it requires few input, while providing validated results [73]. It was conceived for use in the homonym web tool by NREL[4], but it is also available as calculation model in SAM and PVLIB. The web application has been online since 1999 and is currently at

[1] Standard Test Conditions, i.e. cell temperature of 25°C, irradiance of 1000 W/m$^2$ and an air mass 1.5 (1.5 AM) spectrum
[2] PVUSA Test Conditions, i.e. air temperature of 20°C at 10 m above ground level, irradiance of 1000 W/m$^2$, 1.5 m/s wind speed and an air mass 1.5 (1.5 AM) spectrum
[3] Nominal Operating Cell Temperature conditions, i.e. air temperature of 20°C, irradiance of 800 W/m$^2$, 1 m/s wind speed and mounting with open back side [114, 12]
[4] http://pvwatts.nrel.gov/, last accessed on March 28, 2018

version 4 [73]. Unlike other models, it does not require a particular PV product as input, but it is rather intended for a family of products (e.g. “standard”, “premium” or “thin film” module types). For this reason, in additional to the prediction models, it contains also many default values.

- The *Sandia Array Performance Model* (SAPM) is an advanced performance model for estimating the DC current of an array. It can be coupled with the the Sandia Inverter Performance Model to provide the conversion from DC to AC current. It is based on a series of empirical measurements of commercial PV modules, which are listed in a database. This database is maintained and regularly updated by Sandia. At the time of writing, this list included 523 modules.

- The *5-parameter model*, or *De Soto model*, is a semi-empiric model which express the five parameters of the single-diode models as a function of cell temperature and POA irradiance. The IV-curve of a PV cell (but also of a module or an array) can be in fact described with ideal circuit models including a single diode under constant temperature and POA irradiance. All single-diode models are governed by five main parameters: light current, diode reverse saturation current, series resistance, shunt resistance, and ideality factor. The parameters for the De Soto model, i.e., short circuit current, open circuit voltage, voltage at maximum power point, current at maximum power point and the temperatures coefficients at both open circuit voltage and short circuit current, are usually provided by manufacturers in the technical data-sheet of the product or can be obtained many products through the California Energy Commission (CEC) database, already described in Section 2.2.2. This list is 40 times larger than the Sandia Modules database needed to run the SAPM model. The main advantage of using this model is therefore the applicability for a large number of market products.The 5-parameter model in its current version is based on the work by De Soto et al. [66], but its origin dates back to 1989 and is constantly evolving in its version maintained by the University of Wisconsin[5] This model is better suited for crystalline silicon modules, while it works also for thin-film technologies [153].

An experimental study conducted by Cameron et al. [41], compared these models as well as three other ones (a simple fixed efficiency model, an efficiency model with temperature coefficient correction, and PVmode, an early model developed by Sandia) on the performance of PV arrays of different size (1.1, 1.11 and 2.3 kW). The study shows that all models have generally error lower than 10%. The SAPM model has the best accuracy, while PVWatts and the 5-parameter model have similar results, with the latter improving for larger arrays.

#### 2.2.6.4 System and inverter performance

The system performance includes modeling losses due to different factors. Dobos [73] cites the following real-world system losses reducing the DC current: soiling, shading, snow, mismatch, wiring, connections, light-induced degradation, nameplate rating, system age, and operational availability. In the PVWatts model, the total system losses accounts for 14% of the DC energy [73].

In addition to these losses, the transformation from DC to AC energy needs an inverter performance to be modeled. Similarly than for module efficiency, typical data sheets provide only the maximum efficiency, while the inverter efficiency is a function of input power level and input voltage [41].

However, it should be considered that modeling the system and inverter performance, requires many hypothesis concerning the arrangement of the modules and the strings, so as to minimize the number

[5] http://sel.me.wisc.edu/software.shtml, last accessed on March 28, 2018.

of inverters while not undermining the performance due to partial shading. This problem has been treated by previous studies using optimization algorithms [89]. For the scope of our work, which focuses on comparisons rather than on absolute values, we argue that the DC yield is a good proxy of the solar potential. The AC performance will be confronted to a real system in Chapter 13 using a fixed Performance Ratio.

### 2.2.7 Regulatory aspects

Acciona et al. [2] identified the main challenge related to the diffusion of (BI)PV in the European market as the achievement of grid parity and the adoption of a facilitating regulatory framework. Grid parity is achieved when the Levelized Cost of Electricity (LCOE) produced by photovoltaic systems is equal or lower to the market price for electricity.

#### 2.2.7.1 Incentive and business models

Several business models and incentive schemes have been used to boost the use of solar energy. In general, these schemes do not differentiate between BIPV and BAPV applications. However, there are some notable exceptions, including Switzerland (sections 3.1.2 and 3.2.1.1).

We will describe here the main incentive and business models as classified by Acciona et al. [2].

**Public-supported or funded mechanisms**

**Feed-in tariff (FiT)** This is one of the most common incentive models, based on the principle that the actual costs of the injected electricity should be paid. This is done because the usual price of renewable energy, included photovoltaics, is or used to be higher than the market price. This term is used sometimes for the compensation given by the energy utility company for the sold electricity, which is usually lower than the retail price. However, in this work we consider the FiT as a public-funded mechanism and hence always higher than the retail price and fixed for a given number of years.

**Income tax credits** As for many interventions related to energy saving and renewable energy production, many countries and local governments provide income tax credits for investments in photovoltaic systems.

**Sustainable building requirements** This is a non-monetary mechanism to boost renewable energy, by requiring a minimum share of on-site renewable energy production. The same goal can be also achieved by requiring zero-energy or positive-energy buildings, for which the compensation of the residual energy demand through on-site renewable energy sources is needed. This mechanism is mostly applied for new buildings.

**Renewable portfolio standards** This is a requirement that can be imposed to energy utility companies to produce a share of electricity from renewable energy sources. Depending on the country-specific energy situation, in most of the cases the share includes also some electricity produced by photovoltaics.

#### Private-supported mechanisms

Some of these mechanisms are usually supported by companies through their environmental sustainability programs. Even if a profit cannot be directly achieved through some of these actions or is anyway lower than the usual, companies might show an interest towards the environment as part of marketing strategy.

**Investment funds for PV** A possible action is the creation and the acquisition of shares in private PV investment funds [2].

**Energy Service Company (ESCo) and Energy Performance Contracting (EPC)** An Energy Service Company (ESCo) manages energy-saving and renewable energy interventions for a client, assuming the investment and hence the risk of the financial operation. The operation is usually defined by Energy Performance Contacting (EPC) or Energy Savings Performance Contracting (ESPC). Public-private partnerships regulated by Energy Performance Contracting are often used to promote energy-saving projects in the public administration [44].

Energy Performance Contracting was first developed in the United States in the 1970s and in the US is still widely used to finance projects. Recently, EPC has been implemented by local governments to finance the installation of photovoltaic systems on their own building roofs with no upfront costs [52].

**Commercial bank activities** Green investments can be promoted by banks through preferred terms on mortages for buildings including PV and preferential loans on PV systems [2].

**Green electricity schemes** Energy utility companies promote green electricity schemes for customers interested in buying energy that is certified as renewable or even solar-produced-only. This electricity is usually sold at a higher price than the standard market one, and is hence intended for private customers or companies with an environmental-friendly attitude.

#### 2.2.7.2 Self-consumption business models

Self-consumption business models are allowed only in some countries and regions. In some cases, self-consumption is allowed but is not regulated so as to allow mixed schemes where part of the electricity not consumed on site can be injected into the grid. Acciona et al. [2] categorize and describes some of the most widespread models, which are listed here below.

**Pure self-consumption with constraints** This model is typical of countries where self-consumption is allowed but there is no regulatory framework or it is discouraging such application. In a pure-self consumption model, the injection of the over-production to the grid is not allowed. The grid is used only to buy electricity at the normal market price and a tax might be charged because of the use of self-consumption. Because of such circumstances, the installation of PV systems is usually not economically sustainable and, when it is, forces the system to be over-sized to use as much as possible the self-produced energy.

**Pure self-consumption with a Feed-in tariff (FiT)** This model is typical of a regulatory framework encouraging solar energy. The customers can use self-consumption and sell the surplus energy to the grid at a predefined price, which is usually guaranteed for a certain amount of years. This makes the projects economically viable, but public subsidies are needed to finance this model.

**Net-metering** In the net-metering scheme the price of both sold and bought energy is the same. In case the PV Levelized Cost of Electricity (LCOE)is still higher than the electricity market price, which is often the case, at least in this scheme, this model can be also publicly-funded.

**Net-billing** In the net-billing scheme, the price of the sold electricity is usually lower than the retail one. The costs and gains are netted at the end of the contract period and a single invoice is issued. If self-consumption is allowed, then users are encouraged to use this possibility, as it determines higher financial return.

### 2.2.8 Synthesis and discussion

Based on the review conducted in this section, we have identified the following challenges that need to be addressed to cover the research area of this thesis:

- even if crystalline silicon still have the highest market share, both BAPV and BIPV products are valid solutions for building applications, while their appropriateness is building-specific and depends on multiple factors (e.g. type and location of building, building owner attitude);
- advanced prediction models applicable to real market products are available, yet they have not been used in large-scale assessments;
- even in a grid-connected system and when grid-parity will be reached, self-consumption of PV electricity is an interesting business model.

This thesis will address the potential for building-applied solar systems, including therefore both BIPV and BAPV products. Because of the wide range of products and the constant evolution of the market, we could not identify a typical product. We targeted instead an evaluation method, which is applicable to a wide range of market products. With respect to the analysis of prediction models, the single-diode model coupled with the five-parameter model appears as one of the most promising module performance model, as it can be easily applied relying on information from manufacturers and/or contained in the CEC database. However, there are some limitations in the use of such model:

- we cannot consider partial shading effects on a single module, as it assumes a single-diode for module;
- spectral conditions (for example due to diffuse or direct light) are not taken into account;

We did not investigate the grid impact of photovoltaics, as this would have gone beyond the scope of this thesis. However, it should be noted that the large-scale deployment of photovoltaics can put in danger the grid resilience [90]. Increasing the self-consumption can help solve the problem of grid-overload during peak hours, while Freitas et al. [90]showed that it is only the case when using large storage capacities, while small battery systems may lead to even stronger power ramps. Self-consumption also provides an interesting business model for the diffusion of building-installed photovoltaics.

## 2.3 3D city models

3D geo-information is a nascent field in area in the field of geomatics and geographic information science. For decades, the analysis of geodata has been mostly 2D. More recently, the use of 3D geoinformation has emerged as a way to solve a wide range of spatial problems in many different disciplines [29].

We can also distinguish between different types of 3D representations of the built environment, some of which are not fully 3D but rather a 2D representation of the space including height information (the $z$ coordinate) and are thus classified as 2.5D models (Figure 2.5). 2.5D models are also sometimes referred to as *raster* models, from the type of data format that they use, i.e., *raster* images, as opposed to *vector* polygons commonly used to represent fully-3D geoinformation. As pointed out by Biljecki [26, chapter 2], 3D city models are a subset of 3D geoinformation, which include a broad quantity of data, such as 3D trajectories (e.g., from a GPS tracker), raster models (such as DSM and DTM, see Section 2.3.3.2), and voxels (i.e., the 3D equivalent of 2D pixels).

In this work, we associate 3D city models with a variety of data structures and origins, which allow the different objects of a city such as building, terrain and vegetation, while the main definition will apply to the representation of buildings. Biljecki [26, chapter 2] defines city models as "structured objects described by their boundary surfaces that may be semantically enriched". In this thesis, we will also consider this definition, while specifying that the semantic enrichment is seen as a support to the creation of parametric 3D city models. Implicit in this definition, is the use of vector data, rather than raster (e.g., DSM or DTM) or point-cloud (e.g., LiDAR) data. Only vector 3D city models support in fact semantics and boundary representation (BRep) of surfaces, while the 3D geometry can be reconstructed using raster or point-clouds.

When considering 3D geoinformation representing buildings, we can also distinguish between 3D city models and 3D cadastres. 3D city models are used for making decisions and improving local governance in cities, and as tools for urban planning and environmental simulations [26]. 3D cadastres are described as the the tool to digitally represent and/or manage and register land rights, restrictions and responsibilities in a 3D space [9, 10]. Even if both 3D cadastres and 3D city models contain a 3D representation of city objects, the former usually have smaller amount of detailed information, while having legal-binding status in their definition and for this reason can be used as the ground-truth for the validation of the latter [9]. Since their application in this work is environmental simulations, we will use here only 3D city models, while referring to some datasets also as 3D cadastres, when they are considered as such by the data provider. For example, the 3D city model of Neuchâtel (Appendix A.1.5) is considered as a 3D cadastre, as it is based on the building footprints from the official (2D) cadastre.

*Figure 2.5 – Example of a 2.5D (left) and 3D (right) representation.*
*Inspired by Peters [230]*

### 2.3.1 Level of Detail (LOD) [6]

The Level of Detail (LOD) is a concept originated in computer graphics [171] that has been adapted to 3D city modeling by the Open Geospatial Consortium in the framework of the definition of the CityGML standard OGC [201]. The LOD concept has an equivalent in similar datasets such as density for point clouds and resolution for voxels [26, chapter 2].

The CityGML standard defines five levels of detail, which are normally used in 3D city modeling fig. 2.6. Biljecki et al. [30] proposed a more extended definition of the LOD concept in 3D city modeling describing intermediate levels. In historical cities, such as the ones typical of Switzerland and other European countries, buildings usually present complex roof shapes, as well as overhangs and dormers, which limit the actual surface available for solar energy systems. To this regard, the LOD characteristics represented in Figure 2.6 should be intended as minimum features. Recent LOD2 models (e.g., the ones described in Appendices A.1.4 to A.1.6) do include more details, such as roofs overhangs and some rooftop superconstructions. We will refer to such models as LOD2+ or LOD2.3, using the LODX.X notation proposed by Biljecki et al. [30].

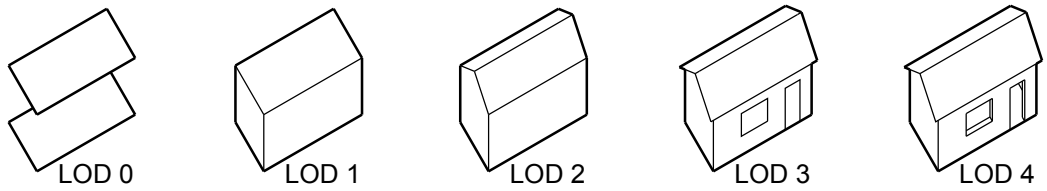


*Figure 2.6 – Representation of the LOD original scheme.*
*Adapted from Peronato et al. [220]*

For solar irradiation studies and building energy demand studies, LOD1 to LOD3 models are commonly used. We will discuss the implications for such uses in Section 4.2.1 and Section 4.1.5.

### 2.3.2 Parametric 3D city models

In this work, we advocate the use of parametric 3D city models as decision support tools in urban planning. The main application of such models is as a support for simulating densification strategies [269, 218], or as a visualization support for collecting residents' opinion about different urban landscape options [156].

So far the applications of such models are still based on simplifications of the existing 3D city models. For example, in our previous work [218], we used information of the building height and footprint from a static LOD2 model to build a parametric LOD1 model used to simulate different densification scenarios in Geneva. Also Seifert et al. [270] introduced different abstractions of building representation from a CityGML model to create a parametric 3D city model.

As pointed out by Seifert et al. [270], it is primordial that enough and good quality semantics are

[6] This section contain excerpts from a published conference paper [220]: Peronato, G., Bonjour, S., Stoeckli, J., Rey, E., & Andersen, M. (2016). Sensitivity of calculated solar irradiation to the level of detail: insights from the simulation of four sample buildings in urban areas. In *PLEA 2016 - Cities, Buildings, People: Towards Regenerative Environments, Proceedings of the 32nd International Conference on Passive and Low Energy Architecture; (Vol. 2)*. Los Angeles. The text is reproduced here as a courtesy of the conference organizers and with the agreement of the co-authors. G.P. contributed by conducting and writing the review presented here.

provided with the 3D city model in order to apply the simulation of building by-laws. We can argue that 3D city models derived either from BIM data or 3D cadastres can be easily adapted for the use as parametric 3D city models, as the presence of high-level semantics is part of their definition.

### 2.3.3 Acquisition and reconstruction

In this section, we will give a succinct description of the main acquisition and 3D reconstruction techniques. The goal is to show the potential and the limitations of such techniques in producing 3D vector city models.

The main acquisition methods include Aerial Laser Scanning (ASL) and aerial photography. Aerial photography is then processed with photogrammetrical method, while point clouds obtained thorugh ASL are processed using bottom-up or top-down approaches. In the first category, we find tessellation algorithms, for example using Delaunay, Voronoi, alpha-shape. Top-down approaches usually proceed by fitting the points to a given shape. For example, Kada and McKinley [138] using LiDAR data and a cell-decomposition of the footprints to reconstruct 3D roof shapes. This technique, together with photogrammetry, is more commonly used for building 3D reconstruction, while tessellation algorithms are commonly commonly applied to vegetation and terrain reconstruction.

We will detail here below the main tessellation algorithms, some of which will be later used in this work for terrain and vegetation reconstruction. Section 2.3.3.2 will introduce the geometrical components of the 3D city model used for solar irradiation assessments.

#### 2.3.3.1 Tessellation algorithms[7]

Delaunay triangulation, Voronoi diagrams, alpha-shape and convex-hull are related geometric constructions that can be used to construct 2D or 3D shapes from a set of points.

The notion of $\alpha$-shape was introduced by Edelsbrunner, first in 2D Edelsbrunner et al. [76] and finally in the 3D space Edelsbrunner and Mücke [77]. Fischer [83] reports an easy description by Edelsbrunner and Mücke:

> "Imagine a huge mass of ice-cream making up the space $\mathbb{R}^d$ and containing the points $S$ as hard chocolate pieces. Using one of these sphere-formed ice-cream spoons we carve out all parts of the ice- cream block we can reach without bumping into chocolate pieces, thereby even carving out holes in the inside (eg. parts not reachable by simply moving the spoon from the outside). We will eventually end up with a (not necessarily convex) object bounded by caps, arcs and points. If we now straighten all round faces to triangles and line segments, we have an intuitive description of what is called the $\alpha$-shape of $S$...."

Alpha-shapes are a generalization of the convex hull [76]. In a family of alpha-shapes, the $\alpha$ parameters controls the level of detail of the shape. In this sense, if $\alpha$ tends to 0 then the alphashape degenerates to the set of points S, while if $\alpha$ tends to $\infty$ the alpha-shape tends to the convex-hull of the set $S$ of points.

The alpha-shape can be constructed through a Delaunay triangulation, and removing the triangles whose circumcircle has radius greater or equal to $\alpha$. Figure 2.7 shows some 2D-examples of shape

[7] This paragraph is largely inspired on this Plotly tutorial https://plot.ly/python/alpha-shapes/ [Last accessed on April 10, 2018]

*Figure 2.7 – Examples of 2D-shape reconstruction algorithms.*
*Adapted from source code and explanations by Sean Gillies (https://sgillies.net/2012/10/13/the-fading-shape-of-alpha.html) and "pv." (https://stackoverflow.com/questions/6537657/python-scipy-delaunay-plotting-point-cloud) [Last accessed on April 10, 2018].*

(a) Delaunay triangulation (b) Convex hull (c) alpha-shape with $alpha = 0.3$

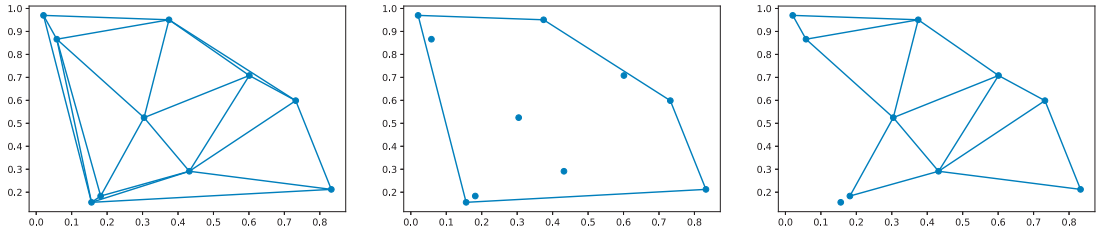

reconstruction.

#### 2.3.3.2 3D geometry

We will consider only buildings, vegetation and terrain, which are the main geometry types for solar potential studies.

**Buildings**

3D city modeling is based on the acquisition of information about building geometry using different techniques and tools. We will present here the main methods that are currently applied in the literature. Some of them are included in proprietary software or used by firms that are active in this field. In this work, we will not deal with acquisition and reconstruction, while using only available city models, which are listed in Appendix A.1. We describe here, however, the main techniques that are used to produce such models.

Existing 3D city models (Table 2.5) are created using remote-sensing techniques and (semi-)automated reconstruction methods. In fact, manual 3D-modeling of buildings is not feasible for large-scale applications, even if it should be considered that some local authorities are suggesting or even enforcing the use of BIM models for obtaining a building permit[8] and the subsequent use of these models to update existing 3D cadastres is studied [283, 291].

According to Agugiaro [7], the reconstruction of 3D city models can be obtained nowadays through an nearly-full automated workflow, as long as high quality input data are provided, such as a DSM obtained from a dense point cloud with at least 10-15 pts/m$^2$. Brenner [35] reviews the main building reconstruction methods, based on both ASL and aerial photography. In addition, these methods can be applied in a wide range of combinations (for example LiDAR surveys corrected with aerial photogrammetry) and there are different subcategories of each method (for example stereo- or ortho-photography) [26].

[8] For example the Singapore Building & Construction Authority has been accepting since 2016 voluntary e-submission of architectural designs in native BIM format (https://www.corenet.gov.sg/general/building-information-modeling-(bim)-e-submission.aspx)

### Vegetation

Vegetation is also included in 3D city models. The 3D modeling of vegetation requires two different steps: vegetation segmentation and 3D shape reconstruction.

The first step is sometimes not applied. For example, vegetation can be considered part of the context and as such modeled through a a Delaunay triangulation including all LiDAR points [132]. However, this method gives a rough representation of vegetation, as if it were directly connected to the soil. Moreover, this method does not allow the application of single-tree-specific models (e.g. growth model, transparency parameters), which will be more in-depth analyzed in Section 4.1.4.

LiDAR data have been extensively used in recent years for vegetation segmentation, and in particular for Individual Tree Crown Detection (ITCD), but only a small fraction of studies focused on 3D shape reconstruction [327]. Zhen et al. [327] lists the main techniques used for 3D shape reconstruction, including Convex hull, alpha-shape, superquadratics and Hough transform. The latter two methods are used to fit points to given shapes, while the former produce shapes directly originated from the position of the points. We argue that in urban environments where a large number of different trees are used,

An advantage of alpha-shape with regards to convex-hull algorithms is that they can be indirectly used for segmentation the point clouds into individual tree crowns, using the $\alpha$ parameter as the threshold for grouping the points (see Figure 2.7). $\alpha$-shape parameters can also be used as predictors to derive tree parameters [305]. For this reason, we will use

### Terrain

Terrain is a main part of a 3D city model. On the basis of the represented details, we can identify three main types of terrain data:

- Digital Elevation Model (DEM) i.e. a 2.5D representation of the earth surface in which all natural and man-made artifacts have been removed. Alternative definitions are given by [106, p. 48], mostly valid in the US.
- Digital Surface Model (DSM), i.e. a 2.5D representation of the earth surface including all natural and man-made artifacts
- Digital Terrain Model (DTM), i.e. a 2.5D representation of the earth surface in which all natural and man-made artifacts have been removed and, as such, can be considered as a synonymous of DEM, while an alternative, more specific definition used in the US is given by [106, p. 48]. Digital Height Model (DHM) is also a term that is sometimes used to describe terrain data, while with very different definitions depending on the country. Swisstopo's DHM corresponds to a DEM/DTM[9] interpolated from the 1:25'000 national map.

Because of country-specific definitions, there is no consensus on these definitions [10], while in this work we will use DEM, DSM and DTM with the above-given definitions.

Despite the convenient representation of terrain as raster grids in DTM, this is not computationally efficient, as the number of points is the same regardless of the complexity of the terrain. Conversely, TINs represent complex topography with more triangles than smoother areas [159]. Moreover, triangulation is needed for many computational operations, such as raytracing. A TIN can be directly constructed

[9] https://shop.swisstopo.admin.ch/en/products/height_models/dhm25200 [Last accessed: April 4, 2018]
[10] An interesting discussion on these terms can be found here [Last accessed: April 4, 2018].

*Table 2.5 – Comparison of features between different 3D city models for the assessment of solar energy potential.*

| | Raster 2.5D model | Vector 3D-city model |
|---|---|---|
| Standard input data (minimum requirements) | DSM | DSM and vector footprints |
| Availability of data | High | Still limited |
| Need for 3D reconstruction | No | Yes |
| Minimum size of roof superstructures | 0.25 $m^2$ [11] | 5 $m^2$ [12] |
| Façades | Possible | Yes |
| Overhangs | No | Yes, depending on the LOD |
| Interreflections | No | Yes, if supported by the solar radiation model |
| Parametric modifications | No | Yes, depending on the quality of the semantics |
| Interoperability with BIM | No | Possible |
| Use as building thermal model | No | Possible |

from raster grids (DTM) or LiDAR point clouds by tessellation algorithms. The most common algorithm to construct TINs is the Delaunay triangulation [159] (see also Section 2.3.3.1). The Rhinoceros3D *MeshPatch* command provides an implementation of the Delaunay algorihm in Rhinoceros, which will be implemented in this work (Section 11.2.1.3).

### 2.3.4 Application to environmental assessments

Biljecki et al. [29] reviewed typical applications of vector 3D city models. Despite most of their applications are linked to the visualization benefits, they identify some use cases in which visualization is not an essential component. Among these uses, we find two environmental applications such as the estimation of the solar irradiation and the energy demand. The assessment of solar energy potential is "arguably one of the most prominent use case in 3D city modeling" [29] . Some of the most advanced and recent works, make use of LOD1 and LOD2 models to evaluate the solar potential [78, 191]

Unlike other energy-related applications, the Level of Detail of the geometric model has a great impact on the predicted solar energy production [220]. That is why many applications are still based on raster models, which usually provide a better representation of the geometry of the roofs, whereas they have other limitations.

Table 2.5 presents a comparison of the features between the different models. Although raster 2.5D models are simpler to obtain and currently have higher resolution of rooftops, vector 3D city models provide a more complete representation of the buildings and have a more flexible use.

### 2.3.5 Availability of datasets

Stoter et al. [290] presented the situation of 3D mapping conducted by seven mapping authorities in European countries, included also in Table 2.6. The CityGML website lists some of the datasets that are freely available (https://www.citygml.org/3dcities/, last accessed on April 10, 2018), covering many European and North-American cities.

[11] Considering a Digital Surface model at 0.5-m resolution
[12] As provided in the 3D cadastre the City of Neuchâtel.

*Table 2.6 – Non-exhaustive list of available 3D vector city models in European countries. Only regional- and national-wide available products are considered here.*

| Country/State | Mapping agency | LOD | Acquisition[14] | Availability | | License | Ref. |
|---|---|---|---|---|---|---|---|
| | | | | Space | Time | | |
| E - Catalonia | IGCG | 1 | LiDAR | State | Available | CC-BY | [290] |
| E - Catalonia | IGCG | 2 | Photogramm. | | In-progress | | [290] |
| PL - Poland | GUGiK | 2 | LiDAR | State | end of 2018 | | [290] |
| FI - Finland | NLS | 1-2 | LiDAR | State | 2019 | | [290] |
| CH - Switzerland | Swisstopo | 1 | | State | | Payment | [290, 295] |
| CH - Switzerland | Swisstopo | 2+ | Photogramm. | State | End of 2018 | Payment | [290, 296] |
| CH - Geneva | SITG | 2+ | Photogramm. | State | Available | Open | [70] |
| CH - Neuchatel | SITN | 2+ | Photogramm. | State | Available | | |
| NL - Netherlands | Kadaster | 1 | LiDAR | State | Available | | [290] |
| DE - North Rhine-Westphalia | | 1-2 | LiDAR + Photogramm. | State | Available | Open | opengeodata.nrw.de |

It should be noted that mapping is often in charge to regions and state governments (for example in Italy, Spain and Germany), rather than national countries. For this reason, the situation is not uniform across countries. Nonetheless, Switzerland, despite its strongly federal configuration, provides the only country-wide dataset of LOD2+ model.

Unlike 3D vector city models, LiDAR data is much more widespread and many countries already have or have been constructing complete databases (including many EU countries, Switzerland, USA, Canada and New Zealand)[13]. As explained in Section 2.3.3.2, combined with vector footprints and depending on the resolution, LiDAR can be used to reconstruct 3D city models.

### 2.3.6 Synthesis and discussion

This section presented an overview of 3D city models, highlighting their current and potential use for environmental assessments. We defined their main characteristics and use applications, and analyzed the main algorithms and techniques for geometric reconstruction, with a particular emphasis on vegetation reconstruction from LiDAR point clouds.

The main goal was the choice of suitable datasets and reconstruction techniques for further analysis in the thesis.

Based on the conducted review, we can summarize the findings as such:

- despite some current disadvantages (e.g. limited availability of data and lower resolution in rooftop superconstructions), vector 3D city models present several advantages for the applications related to solar energy potential compared to 2.5D models; some of these features can be directly used in this thesis: the support for fully-3D representation, including façades and overhangs, and fully-3D simulation, including modeling building thermal performance and inter-reflections; other features are only considered for future applications, such as the integration with BIM and the exploration of densification strategies using parametric 3D city models;
- many mapping authorities have been creating vector 3D city models (Table 2.6), suggesting that

[13] Wikipedia maintains an updated list of these datasets: https://en.wikipedia.org/wiki/National_lidar_dataset [Last accessed on April 10, 2018].

[14] In most products vector footprints are used as well.

this form of data will become more popular; LiDAR is also very popular and can be used to produce such models;
- we have reviewed different tessellation algorithms used for reconstructing geometry from cloud points or raster models: we have seen that the Delaunay algorithm is appropriate for reconstructing terrain TINs and alpha-shapes can be used for segmenting and reconstructing vegetation point clouds in single trees. Vegetation will be futher discussed with regards to its use in solar potential studies in Section 4.1.4.

## 2.4 Planning for solar energy

Urban planning is intended to prepare the urban development of green-field areas as well as to guide the re-development of existing urban areas. In this thesis, we will tackle more specifically the second objective.

Since the origins of urban planning as a scientific discipline (normally attributed to Idelfonso Cerdà, the author "Eixample" extension plan for Barcelona (1855-1859), considering transport, ventilation and sunlight needs), solar access has been a crucial question in urban history, mostly in relations with health needs, questions brought up by the *hygienist* movement, and passive solar energy. Harzallah [103], Siret and Harzallah [280], Siret [279] provide an extensive review of these theories and their application in $19^{th}$ and $20^{th}$ urban planning.

Morley [186], referring to the situation in the US, cites five strategic points of interventions that can be used in planning process to support solar energy:

1. Visioning and goal setting, i.e., all participatory planning processes engaging residents and community stakeholders in prepare solar energy goals;

2. Plan making, i.e., the preparation of any planning document mentioning and supporting solar energy;

3. Regulations and incentives, including all supportive regulatory activities, such as for example solar access regulations;

4. Development work, i.e., all the activities supporting developers in solar development projects, including permitting assistance and development review, as well as public-private partnerships in this field;

5. Public investments, financing for example exemplary buildings, educational and informative activities (including solar cadastres, see Section 4.3.1).

We will focus here on the third point concerning regulatory tools that can be used in the planning practice, as these are the main actions that can be supported by assessment methods as the ones presented in this thesis. Other non planning-specific regulatory tools such as financial incentives have been already described in Section 3.2.1.1 and will be indirectly discussed as part of allocation problems in Section 2.5.

Finally, in Section 2.4.2, we will review some more general planning and urban theories and concepts that have applications to solar energy development.

### 2.4.1 Regulatory tools

We review here regulatory tools, intended both as legal instruments and as common planning strategies, that can be used by planning professionals and authorities to favor the deployment of solar energy in urban areas.

#### 2.4.1.1 Zoning

Zoning determines the land use of a parcel and is at the origin of urban planning as a discipline. Since the 1960s, zoning has often assumed a negative connotation as the results of the criticism from the book by Jane Jacobs [125], who pointed out as the development of mono-functional urban areas increases segregation and need for transportation. However, Temby et al. [298] suggested that solar zoning could be used "to determine and plan which urban neighborhoods are best suited to the many different applications of BIPV" and in this sense "allowing planners where BIPV makes sense and where it does not".

Kehoe [143] suggests some possible zone classifications for solar energy systems:

- principal use, such as the ones that can be used for solar farms;
- special use, where the principal use is subjected to specific restrictions to avoid nuisances and conflicts with other activities;
- accessory use, such as small-scale roof- or ground-mounted systems which produce electricity mostly for on-site use; for many communities, this use is allowed by default [186, p. 53] in all locations.
- secondary use, in which solar energy production is secondary to other main uses, such as an installation on a commercial or agricultural parcel, but a relevant share of the energy production is sold;

More detailed zoning rules can add more specific zones with specific requirements, related for example to solar access and aesthetics. In fact, zoning ordinances, which originally served only to segregate land uses, nowadays often prescribe design standards and even require building commissions to evaluate the pertinence of the design choices [163]. Some communities have also adopted use-specific standards, encouraging different types of solar developments (e.g. roof-top vs free-standing systems), and avoiding conflicting between uses as well as discretionary decisions, which increase the uncertainty and hence the cost and time of solar projects for developers [186, p. 53-54]. Rules could be also used to facilitate some specific design arrangements (e.g. maximizing afternoon production vs maximizing all-day production) depending on the type of electricity demand curve in that particular urban area (e.g. residential vs industrial).

#### 2.4.1.2 Solar access regulations

Regulations can help communities develop solar energy, by clarifying which types of solar energy systems are allowed, define their location and mitigate their potential associated nuisances [186]. They can also impose planning rules to maximize solar exposure in new dwellings and encourage our suggest the building of solar-ready homes [186]. As reported by Morley [186], as of February 2013, 39 states and the District of Columbia have adopted some sort of solar access laws.

Here below we review the main types of solar access regulations: solar easement, solar permit, and solar envelope.

#### Solar easement

An easement is the right of entering or using someone else property without owning it. "A solar access easements is a negotiated legal agreement between affected parties that is designed to protect a landowner's right to install PV and their access to sunlight" [75]. Solar easements are common in many North-American juridisctions [158], as the part of the right to solar access. It can be seen as a limitation to private property, as it limits an use of land that would obstruct someone else access to sun, but also as the right for everybody to take advantage of the solar resource.

Temby et al. [298] suggested integrating solar easements during large-scale and planned redevelopments of low-rise zones, "providing a legal right to receive future sunlight". DVRPC [75] suggests that municipalities encourage building owners to obtain easements from neighboring landowners, while they cannot enforce them through zoning or permitting process. Owners of multiple adjoining adjacent lots are encouraged to keep solar access easement to all their lots, so that, in case the parcels are sold to different owners, the easement is preserved [75].

Because of its nature of mutual agreement between neighbors, the solar easement is the solar access regulation that is the least prone to contentious situations, but is also considered the weakest form of protection [186, pp. 57-58].

#### Solar permit

Unlike solar easements, a solar permit is an official form of solar protection granted by a public authority and, in this sense, it is seen as a stronger protection than solar easements [186, pp. 57-58]. Morley [186, p. 58] presents the typical mechanisms for obtaining a solar permit: "a property owner provides documentation of a solar energy system to the local government and obtains a permit providing protection from shading caused by future construction or tree growth on neighboring properties".

#### Solar envelope

The solar envelope (or solar fence, in some sources Morley [186, p. 58]) is one of the typical instruments that are used in planning and building bylaws to guarantee solar access to every plot for a given number of hours. Its concept was created by Ralph Knowles [155] and its application as a planning zoning regulation was tested by the city of Los Angeles [200]. Morley [186, p. 58] reports the examples of Fort Collins and Boulder (Colorado, US), in which different solar fences were associated with a zoning system.

### 2.4.2 Planning trends

We review here historical and more recent planning trends that have been influenced the way we plan and design our cities for the deployment of solar energy.

#### 2.4.2.1 Density and compactness [15]

Early 20th century urban theories were dominated by low-density city planning, originated from the concept of Garden City [115], and rapidly diffused in Europe [304] and North-America [285], as a response to the overcrowded and noxious cities of that time. These positions were contrasted by most of the architects participating to the International Congress of Modern Architecture (CIAM) proposed instead an high-density schemes with multi-story buildings and wide open space at the ground level while focusing on solar access [190, p. 54]. Their presentation included the comparison with example of poor urban conditions in contemporary cities, whose criticisms ("chaotic", "over-dense, "sunless") paradoxically echoed those made by the Garden city advocates [190, pp. 54-60].

Even if high-density settlements have been popularized in the second post-world-war with often very negative results in terms of social *mixité* (such as the unfortunate *Grand Ensembles* in France), urban sprawl of low-density settlements has followed the urban development of most countries.

Following the Brundtland Commission report of 1987, the contemporary debate on the urban form was greatly influenced by the concept of sustainable development [135]. Since then, the model of the compact city has been seen as the most effective solution to face with global warming, and hence the reduction of pollution, as well as with the loss of greenfield sites caused by urbanization [33]. In this context, the necessity of reducing urban land use has become widely accepted because of the increasing awareness of the relationship between urban density and the impact of transportation in energy consumption.

#### 2.4.2.2 Urban resilience

In the last two decades, much interest is given to the resilience of urban areas, in particular towards climate change. If the Urban Heat Island (UHI) effect and the increase of flooding risk as well as of hazardous natural events are the main threats for urban areas, urban energy systems should be improved towards more resilience. Sharifi and Yamagata [274] identified some of these threats, some of which but not all are related to climate change, and reviewed in the literature the criteria that can be used to asses it. The deployment of solar panels and building-integrated modules is indeed part of the criteria for assessing the resilience of urban energy systems.

Addressing urban resilience requires some the trade-off to be made, as some strategies have might have discordant effects with other planning trends. For example, it was shown that UHI effect is directly correlated to built density [95]. The UHI effect in dense urban areas can be mitigated, but there might be eventually a risk of conflict between building-integrated photovoltaics and the use of vegetation or *cool* materials in the building envelope, the latter becoming popular tools for UHI mitigation.

#### 2.4.2.3 Urban renewal

The concept of urban renewal dates back to the first International Seminar on Urban Renewal in August 1958. Miller [181] listed the three constituents of urban renewal defined in this seminar: *redevelopment*, which deals with the clearance of existing buildings and the use of the cleared land as well as of any contiguous open land for building new projects; *rehabilitation*, which consists of "removing the physical results of deteriorated or obsolescent buildings" or "the conditions that tend to cause the

[15] This section contains excerpts from the author's master thesis [218, Ch. 1]: Peronato, G. (2014). *Built density, solar potential and daylighting: Application of parametric studies and performance simulation tools in urban design.* Università Iuav di Venezia, Venice. The excerpts are the author's own work.

deterioration of existing buildings by discouraging their maintenance"; *conservation*, which includes the practices aimed at keeping functional existing buildings.

In recent years, urban renewal has been often associated to sustainable development, as both concepts share the same spatial and temporal perspective while dealing with social, economic and environmental issues of urban areas [328]. Urban renewal is considered an effective strategy to increase the density of the city's inner core while maintaining or improving the urban qualities of the area [250]. Since both sustainable development and urban renewal are concerned with future spatial scenarios, Zheng et al. [328] suggested that scenarios should be integrated into a decision-support system, which helps visualize the future scenarios as well as analyze current plans and potential options.

Among the different urban renewal strategies, Power [234] suggested that the refurbishment of the existing building stock would have several economic, social and environmental benefits compared with demolition and reconstruction. Evidences from the literature showed that refurbishment makes sense in terms of "time, cost, community impact, prevention of sprawl, reuse of existing infrastructure and protection of existing communities" and "can lead to a reduced energy use in buildings in both the short and the long term" [234].

### 2.4.3 Synthesis and discussion

The review showed that there are many planning tools that can be used for the implementation of solar energy in urban areas. Many of them are in charge of municipalities and planning authorities.

Solar zoning, easements and other legal/planning tools are useful to prevent conflicting uses and uncertainty for solar developers. However, defining solar zones, requires an evaluation of the potential for solar energy, so as to evaluate the trade-off with other alternative uses. In this sense, mapping solar potential is crucial before any planning decision.

Regarding the urban tendencies, we have seen how the relation between solar energy has potential agreements with on-going urban transformations processes (resilience, self-sufficiency, renewal), but also potential conflicts with competitive strategies (reduction of area for solar systems due to UHI strategies, reduction of solar access due to high-density) that should be carefully evaluated by decision-makers.

## 2.5 Choice under scarcity of resources

Despite the abundance of the solar resource on Earth, its actual utilization is limited. Space, cost, installation time are some of the most typical constraints that make solar energy potential a scarce resource. Scarcity of resources is also typical of the allocation of public funds, such as financial incentives for solar energy. In economics, the allocation of limited resources is known as "the basic budgeting problem" [145] and is far to have a comprehensive solution embracing all situations [87].

Therefore, we review allocation theory that is used when decision-makers are faced to choices under scarcity. We analyze methods that have an application (or might have one in the future) in building energy retrofitting and photovoltaic installations, for example when public financial incentives or tax deductions are allocated. We are mostly interested in non-market methods, as in the case of financial incentives, the willingness to pay cannot be used as the allocation criterion ("money does not buy money").

Subsequently, we analyze ranking methods, which can be considered as a particular case of allocation methods, based on the *skill* or *need* of each evaluated object. As we will see in Section 2.5.2, ranking does not necessarily imply a choice, but can be used as the first approach to the decision problem.

### 2.5.1 Allocation methods

Decision-making is costly and for these reasons in every-day life we use methods that can reduce this cost. Demand-supply allocation is at the basis of economics and is considered to give the most efficient allocation of goods to individual, in absence of market restrictions. The willingness to pay (as in the case of an auction) allocates each good to the best buyer. However, there are some things that, in normal conditions, money cannot buy, like scarce medical resources, and, in general, the allocation of public resources is done through non-monetary systems [61].

In the literature, we find four types of non-market allocation systems: political allocations [40], lotteries, queues [40, 60], and priority lists [60]. Lotteries correspond to a random allocation (e.g. the one used for allocating a share of the green cards, the US working permits). According to Calabresi and Bobbitt [40, p. 43], provided that information about the goods is uniformly or randomly distributed and the need is not initiated by the user, queues are only a particular case of the lottery method in which the drawing is done *ex machina*. Political allocations correspond to a subjective and time-consuming evaluation, which we will not take into consideration in this review. Another typical case of non-market allocation is when the demand exceeds the supply, and some goods are rationed, instead of their price being increased [61].

Calabresi and Bobbitt [40] identify two separate sets of determinations dealing with allocation problems: first-order determinations define the global setting of imposed or natural scarcity of goods, while the second order ones allocate the available resources. We will deal with here only with second-order determinations, as we consider that the scarcity of the goods is a boundary condition of the system, in the case of allocation of public resources.

#### 2.5.1.1 Queues

Queues are one of the most common non-market allocation systems, also known as the "first come, first served" rule (FCFS) or, in queuing theory, as "first in, first out" principle (FIFO) [229], in which "resources are allocated to interested parties in their order of entry". Its effectiveness can be evaluated in terms of *efficiency*, i.e. "maximizing aggregate welfare", and *fairness*, i.e. "a morally defensible treatment of or distribution among those who take part in the process".

According to Perry and Zarsky [229], FIFO affects the benefit of the allocation participants in three possible ways:

- by the time of the allocation *per se*, notably because of the value of the time spent in the queue;
- by reducing the quality of the allocated good, because in some cases the last goods to be allocated are of worse quality (e.g. parking lots are usually filled in order of proximity to the amenity);
- by determining the actual entitlement of the good, because in some cases the goods are not enough to satisfy the demand (e.g. fixed quantity of goods to be allocated to a too large number of users) or because the demand is satisfied when it is too late (e.g. transplant queue);

The application of FIFO systems, and more generally of allocation methods, has been studied in the

context of nuisance law [318], traffic management [319], sport [319], housing, asylum and health-care rights [324].

According to Perry and Zarsky [229], "FIFO's most apparent strength is low administrative cost". This makes it particularly competitive with regards to alternative methods, which are subjected to complications due to the larger number of explanations needed, the verification of the rules and the possible disputes involved. Also for Elster [79, Ch. 3, p. 74], the waiting list has the advantage of being "a self-sorting device that does not require controversial and costly discretionary decisions". Moreover, some allocation principles are used as proxies for other principles because of easier decision-making [79, Ch. 3, p. 65]. In this sense, FIFO can be seen as a proxy for *need* [79, Ch. 3, p. 74] or willigness to pay, because of the time wasted in the queue [60].

Elster [79, Ch. 3] classified allocation principles along two dimensions: the need of discretionary assessment and the dependence on actions taken by the individuals. In this sense, we can consider FIFO as a method which is based on an objective assessment (the time spent in the queue) and on the willingness of the participants to stay in the queue. We can argue that these are some of the reasons why it is perceived as a fair method, as the sacrifice of waiting is seen as *desert*, and willingness to stay in the queue is seen as *need* for the good [79, Ch. 3, p. 74].

#### 2.5.1.2 Queue-alternative allocation methods

Perry and Zarsky [229] cite four main allocation methods alternative to queues, based on 1) willingness to pay, 2) service time, 3) need or expected enjoyment, 4) skills.

1. The *willingness to pay* is a market-based method and can be simply implemented with an auction mechanism, but, in addition to the possible welfare benefits, can only work if the good to be allocated is not money.
2. The *service time* is specific to shareable goods and services (e.g. a multi-user computational cluster), in which the allocation to participants with short service times (SST) might improve the quality of the service, which will be otherwise saturated by heavy users.
3. The *need* or *expected enjoyment* represents "two possible manifestations of the resource's value or utility for each participant"
4. *skill* (or *merit* according to [79, Introduction]) corresponds to the ability of the participant to make the most out of the allocated resource.

The allocation according to the skill of a participant might increase the resource's value and hence the aggregate welfare [319, 229]. However, these two methods are of difficult implementation, as they imply the evaluation of the needs or skills of the participants [229]. According to Young [325], algorithms can better perform the allocation, as they can efficiently target alternative allocation criteria such as need, proximity, urgency, or merit, and give hence a response to the conflict between the rights of individuals and the principle of the waiting list, although this can be perceived as a violation of the right of those in the queue [325].

Perry and Zarsky [229] described possible evasion of the queue system due to a special treatment that can be usually justified. In addition to the case of mutual consent, FIFO allocation can be excepted in case of special need, *special merit* or *special skill*. These correspond to some of the previously-described alternative methods to FIFO.

Therefore, it is crucial that the evaluation of the *need* or *skill* is perceived as fair as possible by the participants, in order to replace a classical FIFO mechanism. This is especially valid for evaluation algorithms which, while reducing administrative costs of the evaluation, might be perceived as a black-box.

### 2.5.2 Ranking methods

We will review here [16] ranking methods, which can be assimilated to skill- (or need-) based allocation systems. In many applications, the evaluation of the skill is too expensive and simpler allocation methods or rules-of-thumb such as FIFO methods are applied [319]. However, in this section, we will try to show how ranking can be effectively applied for (spatial) decisions, while application of a ranking-based evaluation will be part of the thesis' scientific contribution.

In spatial planning, multi-criteria methods are used to define priorities among different locations, i.e. by ranking them by priority of intervention. Recent sample applications include the definition of best locations for increasing urban tree canopy [168], treated wastewater instream use [148], or urban investments [179].

Ranking is in fact a typical problem in multi-criteria decision-making, along with choice and sorting [267, Ch. 4c]. The distinction between choice and ranking is not always clear, as ranking procedures can be adopted in decision problems that are more choice-like to give more options to the decision-maker [268, Ch. 10]. Sorting can also be applied to ranked solutions by subsequent attribution to different categories. In this sense, ranking provides the simplest way to approach a decision problem, while allowing the decision-makers to introduce further choice- and/or sorting-based decisions.

Pairwise comparisons are often used in decision problems, as they are an effective method to subdivide a complex decision problem in binary preference questions. This is especially necessary when the criteria by which the alternatives are ranked or chosen are subjective and hence prone to inconsistency. The Analytical Hierarchical Process (AHP) [262] and the outranking methods of the Electre [260] and Prométhée [32] families make use of pairwise comparisons for decision problems involving both tangible and intangible (e.g. qualitative) criteria.

Pairwise comparisons are also used when a preference model can be only applied to pairs of items at a time. This is the case, for example, in sport tournaments: only two teams can play each other at once, so a pool of $n$ teams will require $(n^2 - n)/2$ matches (or $n^2 - n$ matches if home- and away-games are considered) to obtain a final ranking of the teams.

Condorcet methods are some of the most popular pairwise ranking methods, with applications in both sport tournaments and elections. These methods calculate the score of each alternative as the number of victories by pairwise comparisons. Based on the score of each alternative a ranking, which might include some ties, can be established. An extension of the Condorcet method, the Copeland method [233, p. 122], also counts the defeats. It can be seen as a special case of the Borda count method [273], another popular method used in both elections and sports, which generally requires multiple matches between the same pair of opponents (or a ballot asking voters to rank the different candidates) to establish the final ranking.

[16] This section contains some excerpts from a published journal paper [226]: Peronato, G., Rastogi, P., Rey, E., & Andersen, M. (2018). A toolkit for multi-scale mapping of the solar energy-generation potential of buildings in urban environments under uncertainty. *Solar Energy*, 173, 861–874. https://doi.org/10.1016/j.solener.2018.08.017. The text is reproduced here as a courtesy of the publisher and with the agreement of the co-authors. G.P. contributed by conducting and writing the review.

The Copeland method provides simple, robust and optimal ranking from pairwise comparisons [273]. It is often criticized because it counts only the quantity of victories and defeats and ignore their magnitude. This limitation can be overcome by accepting fuzzy outcomes and introducing fractional scores, instead of the conventional boolean/crisp comparisons between alternatives, e.g., Naderi et al. [192].

### 2.5.3 Synthesis and discussion

We have reviewed methods used to deal with choice under scarcity of resources. The goal was the current state of the art and identify possible alternative methods to effectively assign incentives (not exclusively financial) to boost solar energy in buildings.

The most common allocation method based on the principle “first come, first served” is perceived as fair and efficient, but is undoubtedly advantageous for those who can wait longer, who are not necessarily the ones the can profit the most from the allocated good. Alternative methods have often too high administrative costs. However, can argue that algorithms can improve their performance and automation, reducing thus the cost of the allocation system.

In thin sense, rankings provide an efficient method to allocate resources on a *skill* or *need* basis. Pairwise comparison can help produce the score, and hence a ranking, when the *skill* of each participant is not directly apparent, but has to be evaluated in a tournament-like evaluation. This method will be more extensively explained in the implementation of Section 11.4.

# 3 The case of Switzerland

Switzerland has peculiar characteristics with regards to spatial planning and solar energy. As we will see, these two aspects, which normally belong to separate normative fields, are deeply interconnected. Moreover, we will describe also the various regulative framework, incentives, and corresponding allocation methods that were put in place to boost solar energy and building energy refurbishment.

Even if major revisions of the Federal Spatial Planning and Energy Acts were recently enforced (respectively in 2014 and 2018), it should be considered that these sector are rapidly evolving and this section depicts only the situation at the beginning of 2018.

## 3.1 Legal framework

Switzerland is a federal confederation, consisting of 26 Cantons. The federal legislative power is held by the Federal Assembly, i.e., a Parliament composed by two chambers with equal powers but a different composition.

The law-making process[1] is similar across the confederation, at both federal and cantonal level. The main legislative instrument is the law or act ("*Gesetz, Loi, Legge*"), which must be approved by the Parliament, and the ordinance ("*Ordnung, Ordonnance, Ordinanza*"), which is an implementing act established by the government (i.e., at the federal level, the Federal Council). Direct democracy instruments also intervene in the law-making process, as laws can also be implemented by popular vote ("*Volksinitiative, initiative populaire, iniziativa popolare*") or rejected by a referendum.

The Federal Constitution is the supreme law and defines matters that are in charge of the Confederation or the Cantons. Any change to the Federal Constitution must be approved through a referendum receiving a double majority of people and cantons. The constitutional principles regulating spatial planning and the energy policy are defined respectively in the Articles 75 and 89 of the Constitution, which also assign specific matters to the Cantons or the Confederation. For example, the definition of the principles for spatial planning and renewable energy policy are assigned to the Confederation (Articles 75(1) and 89(2)), while measures for building energy use are primarily assigned to the Cantons (Art. 89(4)).

[1] The titles of sources of law and other legal/country-specific terms will be cited by their original title or acronym in Switzerland's official languages, i.e., German, French and Italian, or in the canton's one(s). For sake of simplicity, we will also use their unofficial English denomination, whenever it is available, or our own translation.

### 3.1.1 Solar energy in urban planning [2]

Different laws and regulations exist at each political level regarding spatial planning. In this matter, the Confederation lays down the principles, which are binding on the cantons, and encourage and coordinates the efforts of the cantons (Federal Constitution, Art. 75) mainly through the Federal Spatial Planning Act (RPG-LAT-LPT) and its implementing ordinance (RPV-OAT-OPT). We review here the aspects related to solar energy, while the next sections will deal with the urban development policy and planning instruments defined in this act.

The RPG-LAT-LPT (Article 18a) encourages active solar installations, while granting a specific facilitation only to building-applied solar installations on non-protected sites respecting particular integration criteria. The RPV-OAT-OPT (Article 32a) defines these integration criteria for the solar systems that are considered as "roof-adapted" and hence given the building permit-waiver.

These criteria explicitly exclude from the permit-waiver open rack-mounted systems on roofs and any type of installation on façade (even as BIPV), while cantons are allowed to extend these criteria. In this sense, the Canton of Vaud allows for example the installation without authorization of solar modules up to 8 $m^2$ on façades and of any size on flat roofs in specific building zones (RLATC VD, Art. 68a(2 and 2ter)). The Canton of Neuchâtel gives an additional permit-waiver to any solar installation on flat roofs up to 120-cm high and 50-cm distant from the perimeter of the roof (RelConstr. NE, Art. 4d(d)). For solar systems not satisfying the permit-waiver criteria, the fact of requiring an authorization makes the implementation of these systems more difficult as the outcome of the authorization process is long and uncertain. In general, four main types of obstacles have been identified for the acquisition of a building permit, such as longer timeframes, higher costs, reduced design freedom, and an increasing insecurity of succeeding [331].

Solar access (see also Section 2.4.1.2) is generally regulated at a cantonal level. For example, in the Canton of Neuchâtel the executive regulation on spatial planning (RELCAT NE) defines the maximum building occupation profiles by setting minimum spacing angles that vary according the orientation and the building zone. These norms are meant to set the distance between buildings according to their height, so as to assure to each one the required space, sunlight and daylight (RELCAT NE, Art. 18).

### 3.1.2 Authorization process for solar installations

An article regarding solar energy was first introduced in 2007 in the Federal Planning Law by Parliament initiative.

> In building and agricultural zones, solar installations that are well integrated into roofs and façades are authorized as long as they do not cause major violations to any cultural heritage element or natural site of cantonal or national importance.[3]

The same article was modified only few years later, also by Parliament initiative. Proponents were not satisfied of the previous version of the article, as, according to them, it did not give the expected boost to solar installations [136] and was restricting the municipal licensing initiative [107]. The current

[2] This section contains some paragraphs jointly written with Emilie Nault in the framework of the task 51 "Solar Energy in Urban Planning" of the International Energy Agency (IEA) - Solar Heating and Cooling Programme (SHC)

[3] Own translation, original text in French: "*Dans les zones à bâtir et les zones agricoles, les installations solaires soigneusement intégrées aux toits et aux façades sont autorisées dès lors qu'elles ne portent pas atteinte à aucun bien ni à aucun site nature d'importance cantonale ou nationale.*"

version of the article enforced since the 1st of May 2014 includes hence major changes.

> In building and agricultural zones, solar installations that are enough adapted to roofs do not need any authorization as of Article 21(1)[4]. Such projects have just to be announced to the relevant authority.
>
> Cantonal legislation can:
>
> - designate other building zones in which aesthetic aspects are less relevant and therefore other solar installations can be also exempted from the building permit;
> - establish the obligation of building permit for precisely-defined building zones to protect.
>
> Solar installations on cultural heritage or natural sites of cantonal or national importance are always required a building permit. They must not cause any major violation to these sites.
>
> Otherwise, the interest in using solar energy on existing or new constructions prevails in principle over aesthetic principles. [5]

The introduction of this article brought about several comments in the juridical field [136, 231, 107, 1]. Jäger [136] highlighted the unprecedented innovation of this law, which introduced an authorization-free framework for some types solar installations applicable to the whole Switzerland. However, as for the previous article, many authors [136, 231] pointed out the possible conflict between federal and cantonal levels, the latter having exclusive or main competence in matters related to planning (Art. 75 Cst.), heritage and nature protection (Art. 78 Cst.), as well as in energy in buildings (Art. 89 Cst.). Piguet and Dyens [231] suggested that an amendment to the Constitution would have given to this law more solid basis. Similar concerns were expressed already in the parliamentary debate, both for the 2007 and 2014 versions of the article 18a [107]. In any case, according to the Article 190 of the Constitution, laws approved by the Federal Parliament cannot be judged for unconstitutionality by the Federal Court.

If on the one hand the 2014 version of the article introduced a permission-free framework for roof-adapted installations, on the other, the 2007 version included also a reference to façades, which are now excluded from the procedure defined in the 2014 version. However, as noticed by Jäger [136], the new version does not constitute any obstacle to other types as installations, but rather facilitates the use of specific ones, i.e., the "roof-adapted". In general, most of the cantons already provided special regulations facilitating the installation of some solar systems, and this simplification trend seemed to increase after the introduction of art. 18a at the federal level [107].

The Spatial Planning Ordinance RPV-OAT-OPT (Art. 32a) specifies the criteria defining "roof-adapted" installations which are granted the building-permit-free procedure.

[4] This article details the procedure for obtaining a building permit, which is needed for any transformation or new construction

[5] Own translation, original text in French: "*Dans les zones à bâtir et les zones agricoles, les installations solaires suffisamment adaptées aux toits ne nécessitent pas d'autorisation selon l'art. 22, al. 1. De tels projets doivent être simplement annoncés à l'autorité compétente.*
*Le droit cantonal peut: a) désigner des types déterminés de zones à bâtir où l'aspect esthétique est mineur, dans lesquels d'autres installations solaires peuvent aussi être dispensées d'autorisation; b) prévoir une obligation d'autorisation dans des types précisément définis de zones à protéger.*
*Les installations solaires sur des biens culturels ou dans des sites naturels d'importance cantonale ou nationale sont toujours soumises à une autorisation de construire. Elles ne doivent pas porter d'atteinte majeure à ces biens ou sites.*
*Pour le reste, l'intérêt à l'utilisation de l'énergie solaire sur des constructions existantes ou nouvelles l'emporte en principe sur les aspects esthétiques.*"

A solar installation is enough adapted to a roof (as of Art. 18a(1) RPG-LAT-LPT) if:

(a) it sticks out from the roof for maximum 20 cm orthogonally;

(b) it is contained in the roof shape from side and front orthogonal views;

(c) it is low-reflecting according to the scientific the state of the art;

(d) it has a compact shape;

Specific cantonal prescriptions based on the cantonal law are applicable if based on justified protection needs and if they do not limit solar energy use more than what prescribed in the former paragraph.

Projects that are not subjected to the building permits must be announced before the works start to the cantonal authority giving the building permit or other competent authority defined by cantonal legislation. Cantonal legislation establishes the delay for announcing the project and defines the drawings and documentation to enclose. [6]

Figure 3.1 exemplifies the prescriptions stated in the first paragraph. It should be noted that the last three examples of Figure 2.4 would comply with these requirements.

Nonetheless, according to Jäger [136], these guidelines are not much clear, in particular with regards to the paragraph 1d, which presents also slightly different translations in the three official languages. The intention of the legislator is to require that the installation is tending towards a rectangular shape. This follows the principles of many cantonal bylaws setting geometric rules for the visual appearance of solar installations. An interpretation mostly based on the German version of the law text [136] is that the installation should be as compact as possible, allowing hence installations composed by multiple surfaces when this is need. In any case, in pitched roofs, multiple standalone installations, one for each slope of a roof, are allowed [136, 231].

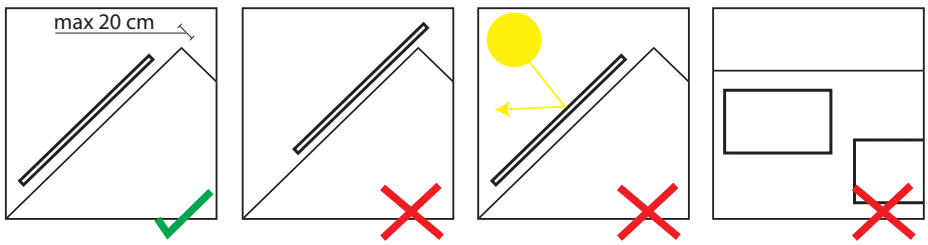


*Figure 3.1 – Criteria defining "roof-adapted installations" according to the Art. 32a RPV-OAT-OPT, adapted from [332]*

[6] Own translation, original text in French: "*Les installations solaires sont considérées suffisamment adaptées aux toits (art. 18a, al. 1, LAT) si les conditions suivantes sont réunies: a) elles ne dépassent pas les pans du toit perpendiculairement de plus de 20 cm; b) elles ne dépassent pas du toit, vu de face et du dessus; c) elles sont peu réfléchissantes selon l'état des connaissances techniques; d) elles constituent une surface d'un seul tenant.*
*Les dispositions concrètes fondées sur le droit cantonal traitant de l'intégration desdites installations s'appliquent lorsqu'elles visent de manière proportionnée la défense d'intérêts de protection justifiés et ne limitent pas l'exploitation de l'énergie solaire plus strictement que l'al. 1.*
*Les projets dispensés d'autorisation doivent être annoncés avant le début des travaux à l'autorité délivrant les autorisations de construire ou à une autre autorité déclarée compétente pour recevoir les annonces par la législation cantonale. La législation cantonale fixe le délai dans lequel l'annonce doit être faite et précise quels plans et autres documents doivent y être joints.*"

A second article in the Federal Spatial Planning Ordinance (Art. 32b) specifies what should be considered as "of cantonal or national relevance". In particular, it states that only some types of monuments in the federal inventories should fall into this category.

According to Jäger [136], traditional tilted installations on flat roofs are not included in the procedure of article 18a, as they do not respect the aptness criteria. On the contrary, roof-applied installations (BAPV) are included in the facilitated procedure, while the "well integrated" installations (which we can consider as a reference to BIPV systems) which were the only target of the previous version of the norm. Design regulations and guidelines at the cantonal level cannot be more restrictive that those of the Art. 32 OAT [107]. Jäger [136] summarized all cases that require a normal authorization procedure, which are:

- installations in cultural heritage elements or natural sites of cantonal or federal importance;
- installations in protected zones;
- isolated installations (e.g., not attached to buildings);
- installations applied or integrated to façades;
- tilted installations on flat roofs;
- installations that are not compact.

Despite the fact that the new norm highly simplifies the procedure for some types of installation, Piguet and Dyens [231] and Abegg and Dörig [1] raised the possibility that the procedure would not be completely straightforward both for constructors and local authorities. A simple notification procedure does not allow the competent authorities to carry out a comprehensive evaluation of the interests involved in each individual case [1].

Paradoxically, the longer, normal procedure requiring a building permit can be still considered a valuable option, as it allows the competent authorities to examine the compliance with the law before the works start. According to Abegg and Dörig [1], the absence of a preventive legality check in the framework of a building permit procedure postpones litigation to the time after the construction of the solar installation, which leads to considerable legal uncertainty. Similarly, it is impossible to apply recovery measures for unlawful installations, creating hence a problematic situation also for the public authorities [1]. Moreover, in its implementing normative at the cantonal level, the Canton of Zurich specified that the notification does not exempt the client from the duty to comply with the legislation when constructing the solar system [1].

### 3.1.3 Sample legal studies

The purpose of this section if to show the authorization process of some solar energy installations, that required multiple passages through authorities and law courts at different jurisdiction levels. This review was conducted in the framework of the IEA SHC Task 51.

***La Chaux de Fonds (NE)***

The building is located in a zone belonging to the Inventory of Swiss Heritage Sites (ISOS) and to the UNESCO world heritage list. The building permit waiver regulated by the federal planning law (RPG-LAT-LPT, Article 18a) for solar installations does not apply to heritage sites. The federal and cantonal law does not set a hierarchy between the public interest towards renewable energy sources and the conservation of heritage and landscape[7]. Building owners refused to use PV modules integrated in the roof as requested by the municipal authorities claiming that this would have augmented maintenance costs and caused a loss in

[7] At least till the addition of Article 18a(4)) to the RPG-LAT-LPT in 2012 (in force since May 2014) stating that the interest in using solar energy in existing and new buildings prevails - in principle - over aesthetical aspects.

the efficiency. The Municipality denied the building permit, motivating that the project would have jeopardized the heritage site. The building owners appealed to the Cantonal Government and to the Cantonal Court, claiming that an aesthetical judgement cannot prevail on the interest of promoting renewable energy sources. The Cantonal Court rejected the appeal of the building owners motivating that the municipal authorities did not exceeded their legitimate power of appreciation granted by the law.

- 10/28/2009 – Demand of building permit
- 01/20/2010 – Changes to the project asked by the municipality
- 05/12/2010 – Permit rejected by the Municipal Government
- 04/08/2013 – Appeal to the Cantonal government rejected
- 11/18/2013 – Appeal to the Cantonal Court rejected

Source: Jurisprudence Administrative de l'Etat de Neuchâtel, REC.2010.180

***Vaglio, Capriasca (TI)***

In the building permit referred to a refurbishment project the owners asked to install solar thermal panels. The Municipality granted the building permit but denied the installation of solar panels with the reference to cantonal laws and municipal bylaws. The building owners appealed to the Cantonal Government, which confirmed the judgment of the municipality, and then to the Cantonal Court. The Cantonal Court noted that the cantonal laws and municipal bylaws are in contrast with the Federal Planning Law (RPG-LAT-LPT article 18a) and that municipal authorities did not mention the federal legislation, which prevails on lower level one, in their motivations for the refusal. The Cantonal Court accepted the appeal and enforced the Municipality to reconsider the building permit for solar panels checking whether the integration criteria determined by the federal regulation are respected.

- 11/23/2008 – Demand of building permit
- 04/20/2009 – Building permit granted by the municipality but excluding solar panels
- 06/09/2009 – Appeal to the Cantonal government rejected
- 11/12/2009 – Appeal to the Cantonal Court approved

Source: Sentenze e decisioni del Tribunale Cantonale Amministrativo della Repubblica e Cantone del Ticino, 52.2009.255

***Vulcherens (VD)***

As a consequence of fire damages, the owners want to reconstruct the building raising the roof and rotating it by 90 degrees[8], so that one slope of the roof is oriented towards South and hence optimized for solar systems. According to the local bylaws[9], buildings roofs have to follow the main orientation of the surrounding buildings, which in this case is East-West. The municipality rejected the building permit with one of the motivations being that the installation of solar panels was not a sufficient reason to contravene the bylaws. The Cantonal Court accepted the appeal of the building owners, stating that the bylaws actually included an exception to the general orientation rule in case of the installation of solar panels also confirmed by a previous court case.

- 07/11/2008 – Building permit
- 08/08-09/07/2008 – Public inquiry: three oppositions from the neighbors
- 06/30/2008 – Building permit rejected
- 06/16/2009 – Appeal to the Cantonal Court approved

Source: Jurisprudence du Canton de Vaud, AC.2008.0267

[8] Other modifications were also part of the court case, but are not included in this summary as not related to the solar installation

[9] Règlement du plan général d'affectation et du plan partiel d'affectation du village, commune de Vucherens, 1995, Article 25(5)

### 3.1.4 Planning instruments [10]

The Federal Act on Spatial Planning (RPG-LAT-LPT) (see also Section 3.1.1) defines two planning instruments to be developed by each canton:

- the master plan ("*Richtplan*", "*Plan directeur*", "*Piano direttore*")
- the land use plan ("*Nutzungsplan*","*Plan d'affectation*", "*Piano di utilizzazione*")

Similarly, cantonal laws define the plans for the development of smaller areas such as cities and neighborhoods and regulate the role of municipalities in the planning process.

Master plans are intended for strategic planning, i.e., they define the needs and set the goals for the future development of a given territory. On the basis of the master plans, land use plans define for this territory the land use conditions, e.g. development purpose and size. Figure 3.2 shows the development process of master plans and land use plans in the Canton of Vaud. The main difference stands in the last part of the process, related in particular to the public participation and final ratification. For example, master plans are subjected to a public consultation (i.e., a referendum), while land use plans are subjected to public enquiries, consisting in period of 30 days during which stakeholders can present their arguments against the plan.

Master plans are usually composed by several documents addressing different themes. At the cantonal and city scales energy plans usually provide also an analysis of the potential for renewable energy.

### 3.1.5 Building integration

In Switzerland, energy and planning legal framework encourage the use of building-integrated solar energy systems. At the same time, heritage and landscape protection prevent the modification of certain buildings and areas or these are subjected to a specific planning/design restrictions and evaluation process. Both the Confederation, with the Inventaire fédéral des sites construits d'importance nationale â protéger en Suisse (ISOS), and cantons maintain a list of protected buildings and areas, for which a building permit is always needed for installing solar systems. Moreover, some cantons (for example, Neuchâtel with the Récensement Architectural du Canton de Neuchâtel (RACN)) maintain also a database of buildings architectural quality, in which a score is attributed to each building and according to the score different conservation regulations apply.

As seen in the general review Section 2.2.5, there is a gradient of definitions for BIPV products. In legal terms, two different definitions apply in Switzerland depending on the particular applications, i.e. either obtaining the building permit for installing a solar system or getting access to subsidies.

The Federal Spatial Planning Act (RPG-LAT-LPT) and the relative Ordinance include a definition of "roof-adapted" installations, which are granted a permit-free scheme (see section 3.1.2). This definition is quite generous in terms of prescription, allowing to be included in this scheme most of the BAPV installations on pitched roofs.

The Federal Ordinance on the Encouragement for Electricity produced by Renewable Energy Sources (ENFV-OEneR-OPEn) provides another definition of integrated photovoltaic systems (see section 3.2.1.1). This corresponds to a quite strict definition of BIPV, as the solar system must have a double function in the building (with regards to heat, weather or fall protection). Even if it the heat-protection definition

[10] This section contains some paragraphs jointly written with Emilie Nault in the framework of the task 51 "Solar Energy in Urban Planning" of the International Energy Agency (IEA) - Solar Heating and Cooling Programme (SHC)

is quite vague and could be interpreted in different ways, the ENFV-OEneR-OPEn identifies a subset of what is classified as BIPV by the European Norm EN 50583, which provides a broader and more detailed

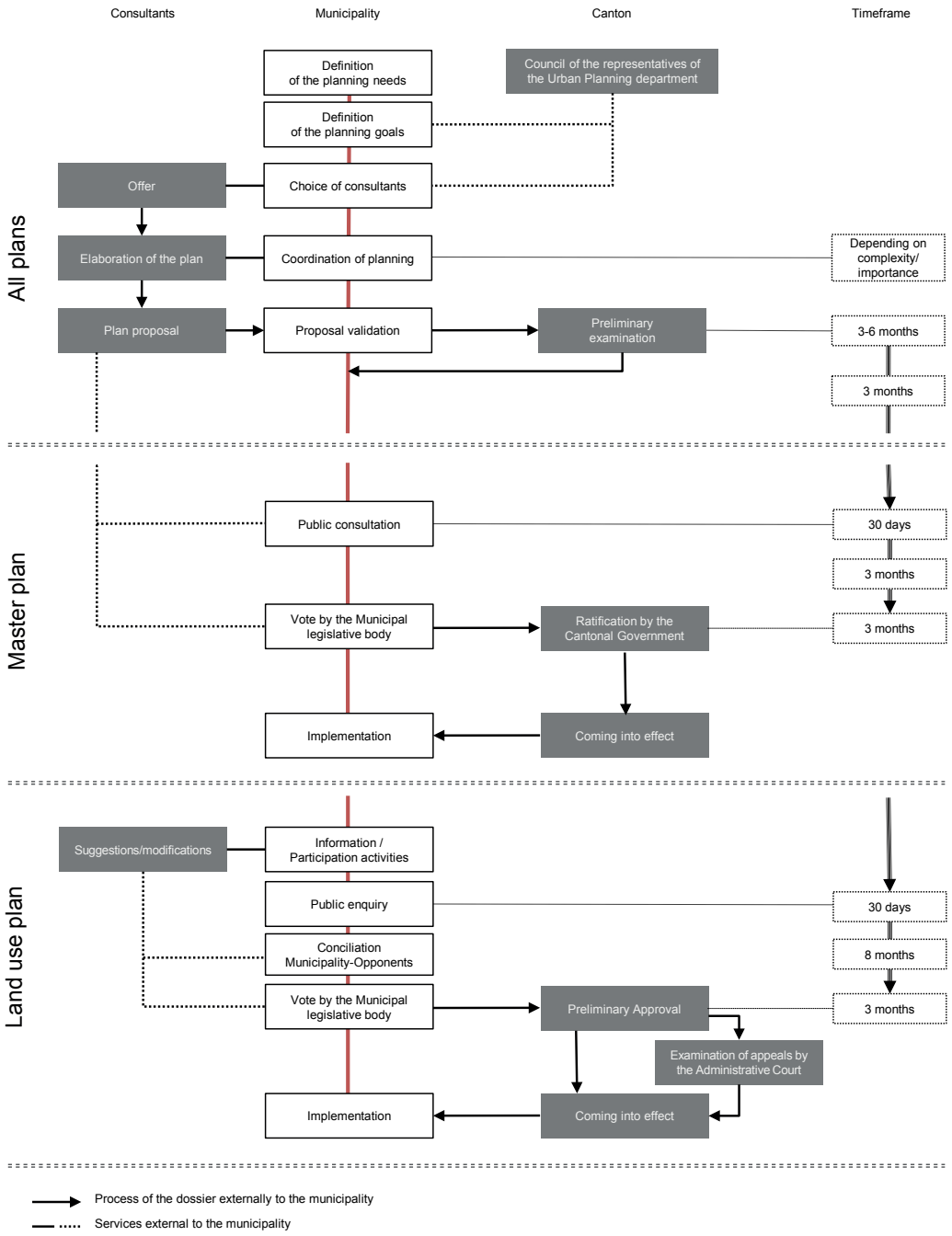


*Figure 3.2 – Planning process in the Canton of Vaud.*

definition of building functions (including for example noise and fire protection, see also Section 2.2.5). It should be noted that, at the moment this thesis is written, the EN 50583 has not been yet adopted by a Swiss norm.

## 3.2 Energy policy

The necessity of an energy transition has been in the public debate in Switzerland since 2011. As a consequence of the nuclear disaster in Fukushima, the Swiss government decided to update their energy policy. In particular, it was agreed to switch to a progressive withdrawal from nuclear power, with the support also of the Parliament.

The energy policy defined by the Federal Government in its message to the Parliament in September 2013 [63] set some ambitious goals, at short- (2020), mid- (2035), and long-term (2050). In order to meet the energy global warming targets, it has been foreseen a reduction of the $CO_2$ emission per capita to 1.5-1.0 t in 2050, which is supposed to be compatible with keeping the global temperature rise within the 2.0°-C limit fixed by the Paris agreement. The government also aims at keeping affordable energy prices and guarantee a high level of supply security. These overall objectives are possible due to planned energy saving measures, in particular a decrease of 54% of the average final energy consumption and of 18% of the electricity consumption in 2050 compared to 2010, as well as an increase of share of renewable energy sources. The main objectives for the different policy scenarios and target years are listed in Table 3.1.

With its message to the Parliament, the Government proposed a new Energy Act in substitution the previous one dating back to 1988. The parliamentary procedure started in fall 2013 and, after three debates in the upper and lower chambers, the bill was finally approved in September 2016. During this procedure, as a consequence of an initiative of the Green Party, a referendum on an immediate withdrawal from nuclear power was rejected by the the Swiss People in November 2016. An optional referendum on the Energy Act was held, due to popular request. The Swiss People finally adopted the Energy act in May 2017 by 58.2% of the vote and this came into force in January 2018.

With the exception of nuclear energy, the Energy Act substantially extends the previous energy policy, while fixing new goals, including energy and electricity saving, increase renewable energy share, guarantee the access to international energy markets, transform and develop the energy grid, promote energy research, strengthen the exemplary function of the public sector and intensify international cooperation (ENFV-OEneR-OPEn, Comments).

*Table 3.1 – Summary of electricity policy objectives.*
*Sources: Message of the Swiss Federal Council [63], Prognos AG [236]*

| | Scenarios | 2020 | 2035 | 2050 |
|---|---|---|---|---|
| Electricity demand | Busines as usual | 68 TWh/y | 70 TWh/y | 75 TWh/y |
| | Government measures | 64 TWh/y | 63 TWh/y | 66 TWh/y |
| | 2050 Energy Strategy | 63 TWh/y | 60 TWh/y | 58 TWh/y |
| Renewable electricity (without hydro) | 2050 Energy Strategy | 4 TWh/y | 15 TWh/y | 24 TWh/y |
| | Share of demand | 6% | 25% | 41% |
| PV electricity production | All scenarios | 1 TWh/y | 7 TWh/y | 11 TWh/y |
| | Share of demand | 2% | 12% | 19% |

### 3.2.1 Solar energy

With regards to renewable energy and photovoltaic energy in particular, the Energy Act (EnG-LEne-LEne), its implementing ordinance (EnV-OEne-OE) and the Ordinance encouraging electricity produced from renewal energy sources (ENFV-OEneR-OPEn) fix some important thresholds and principles.

Two types of subsidies are described by the law: one-time contribution up to 30% of the investments costs (EnG-LEne-LEne, Artt. 24 and 25 ) and feed-in incentives (EnG-LEne-LEne, Artt. 19, 20, 21, 22). These measures have fixed ending times for new projects, notably until 2022 for the feed-in incentives and 2030 for the one-time contributions (Art. 38).

These incentives are provided as long as enough funding is provided for these measures (EnG-LEne-LEne, Artt. 19(2) and 24(1)). The funding is based on compensations added to the cost of electricity, hence paid by all electricity consumers in Switzerland, fixed by the Government, but at maximum 0.023 CHF/kWh (EnG-LEne-LEne, Article 35(3)). This represents an augmentation with respect to the former supplement which was maximum 0.015 CHF/kWh (ENFV-OEneR-OPEn, Comments).

Grid managers are obliged to buy and remunerate the fed-in energy from installations smaller than 3 MWp of power or 5000 MWh of annual injection (EnG-LEne-LEne, Art. 15), unless the installations already benefit from the feed-in incentives.

Self-consumption is allowed also as part of communities formed by contiguous building lots (EnV-OEne-OEn, Art. 14(2)) as long as the power of the installation is at least 10% of the one of the grid connection (EnV-OEne-OEn, Art. 15).

#### 3.2.1.1 Federal Incentive scheme

The incentive scheme is based on the Energy Act (EnG-LEne-LEne) and its conditions are defined by the Ordinance encouraging electricity produced from renewal energy sources (ENFV-OEneR-OPEn). This framework was already present before the implementation of the Energy Act, but the amounts have been frequently changed in the last years (Tables 3.2 and 3.3). Provided that they comply with the Energy Act requirements, these values are expected to change frequently also in the future, as the ordinance can be modified by the Government, without the Parliament's approval.

The ENFV-OEneR-OPEn ordinance defines two categories of PV systems (art. 6):

- integrated systems, i.e. all systems integrated in a building and installations which, in addition to electricity, are used for weather, heat or fall protection;
- building-attached or isolated systems.

Installations are further divided into "large" and "small", with the defining threshold being fixed at 100 kWp (Art. 7).

As prescribed in the Energy act, two types of incentives are defined: a one-time subsidy ("*Einmalvergütung EV, rétribution unique RU, rimunerazione unica RU*") to reduce investment costs and a feed-in incentive ("*Einspeisevergütungssystem, système de rétribution de l'injection, sistema di rimunerazione per l'immissione di elettricità*") per kWh of injected energy. The one-time subsidy is further defined by the Ordinance as composed of two separate subsidies: a fixed one and a peak-power-based one.

Large installations can opt for one of these two schemes, while the small ones can choose only the

one-time subsidy scheme (Art. 8). If the owners decide to renounce the power-based subsidy for the power exceeding the 100 kWp, installations are considered as small ones (Art. 7(3)). Since the expected waiting time before subsidies are granted is shorter for small installations, this option might become more viable.

*Table 3.2 – One-time subsidies for isolated or building-attached installations.*

| In operation | Fixed (CHF) | Power-based (CHF/kWp) <30 kWp | Power-based (CHF/kWp) <100 kWp | Power-based (CHF/kWp) ≥100 kWp |
|---|---|---|---|---|
| As of 01.04.2018 | 1400 | 400 | 300 | 300 |
| 01.04.2017 – 31.03.2018 | 1400 | 450 | 350 | 350 |
| 01.10.2016 – 31.03.2017 | 1400 | 500 | 400 | 400 |
| 01.10.2015 – 30.09.2016 | 1400 | 500 | 450 | 450 |
| 01.04.2015 – 30.09.2015 | 1400 | 680 | 530 | 530 |
| 01.01.2014 – 31.03.2015 | 1400 | 850 | 650 | 600 |
| 01.01.2013 – 31.12.2013 | 1500 | 1000 | 750 | 700 |
| 01.01.2012 – 31.12.2012 | 1600 | 1200 | 950 | 850 |
| 01.01.2011 – 31.12.2011 | 1900 | 1450 | 1200 | 1000 |
| Before 2011 | 2450 | 1850 | 1500 | 1300 |

*Table 3.3 – One-time subsidies for building-integrated installations. Values with a star (*) are the same of Table 3.2 as the same conditions as for BAPV installations apply.*

| In operation | Fixed (CHF) | Power-based (CHF/kWp) <30 kWp | Power-based (CHF/kWp) <100 kWp | Power-based (CHF/kWp) ≥100 kWp |
|---|---|---|---|---|
| As of 01.04.2018 | 1600 | 460 | 340 | 300* |
| 01.04.2017 – 31.03.2018 | 1600 | 520 | 400 | 350* |
| 01.10.2016 – 31.03.2017 | 1800 | 610 | 460 | 400* |
| 01.10.2015 – 30.09.2016 | 1800 | 610 | 510 | 450* |
| 01.04.2015 – 30.09.2015 | 1800 | 830 | 630 | 530* |
| 01.01.2014 – 31.03.2015 | 1800 | 1050 | 750 | 600* |
| 01.01.2013 – 31.12.2013 | 2000 | 1200 | 850 | 700* |
| 01.01.2012 – 31.12.2012 | 2200 | 1400 | 1100 | 980 |
| 01.01.2011 – 31.12.2011 | 2650 | 1700 | 1400 | 1200 |
| Before 2011 | 3300 | 2100 | 1700 | 1500 |

A feed-in tariff (FiT) was first introduced in 2008 so as to match the cost of PV-generated electricity to the one of the market (the so-called "cost-covering renumeration for feed-in to the electricity grid", "*kostenorientiertes Einspeisevergütungssystem KEV, rétribution à prix coûtant RPC, rimunerazione a copertura dei costi RIC*"). Despite the attractive tariff (which has though been constantly lowered since 2008), a cap to the funding of this measure prevented a strong boosting effect for photovoltaics.

Since 2018, the feed-in tariff has lowered of about 20% in order to subsidize as many projects as possible in the waiting list, while it does not cover anymore the entirety of the levelized energy cost (ENFV-OEneR-OPEn, Comments).

For all type of subsidies, a first-come-first-served system is in place. Expected minimum waiting times in February 2018 are as follows[11]:

[11] https://pronovo.ch/fr/2017/12/06/sri-ou-ru/ [Last accessed on February 20, 2018]

- one-time subsidies for small installations (<30 kWp): 2.5 years
- one-time subsidies for large installations (≥100 kWp): 6 years
- feed-in incentive for large installations (≥100 kW): only applications in the waiting list submitted by June 30, 2012 are expected to be admitted in the program

## 3.3 Urban development

Starting from the 1970s, Switzerland, along with most of the western countries, experienced a loss of population in the cities [261]. This can be partially explained by an increase of housing consumption, due to the growth of smaller households living in larger dwellings, but also to a growth of suburban population. However, a demographic turnaround happened during the last decade, when Swiss cities have gained population thanks to international migrants, non-family households and other population belonging to well-off classes. This quantitative phenomenon is part of a process of reurbanization, i.e. "a new period of demographic growth after a period of decline" [261], which can be partly explained by a new attractiveness of core cities for segments of the middle and upper classes.

In addition to this spontaneous reurbanization process, the inner development of Swiss cities is also encouraged by the "Territorial Project Switzerland" ("*Raumkonzept Schweiz, Projet de territoire Suisse, Progetto territoriale Svizzera*") a non-normative document [12] jointly promoted by the Swiss Federal Government, Cantons and Municipalities, which aims at a sustainable development of the Swiss territory. One of the objectives promoted by this document is the preservation of natural resources, which, for what concerns urban areas, includes the stop to urban sprawl and the limitation of green-field urbanization. In order to achieve these goals, the document promotes actions of urban renewal, such as the densification of the urban areas by the construction of infill areas, the renovation of disused buildings and the redevelopment of brown-field areas [12, Strategy 2, p.43]. These actions are also intended to decrease the energy consumption of urban areas by reducing the need for transportation and promoting the energy refurbishment of existing buildings [12, Strategy 3, p. 54].

### 3.3.1 Planning policy

The latest revision (enforced in 2014) of the Federal Spatial Planning Act (RPG-LAT-LPT) has introduced the principle that future urban development (intended as new constructions) should be linked to the expected demographic increment in the following 15 years (Art. 15(1)) and that oversized building zones should be reduced (Art. 15(2)). This concept has been at the core of the partial revision process of the act, with the final goal of reducing oversized building zones or moving them to locations where new dwellings are justified by the demographic trends. Also, the size of building zones will be no more evaluated only at the municipal level, but it will take into account also the situation of neighboring municipalities (Art 15(3)).

If the general principle of urban inner development and densification is encouraged by the "Territorial Project Switzerland", the actual implementation of these principles in legal and planning documents is up to the Cantons. As already described in Peronato [218], the Canton of Geneva, in its Master Plan 2030, introduced a planning action called "strengthening urban renewal" aimed at promoting densification and extension of the dense urban center, for instance by setting minimum built density goals and applying roof-raising strategies. Roof-raising is also regulated in Geneva by a specific cantonal law, which after an initial bill proposed in 2005, was finally enacted by the Parliament in February and approved by a popular vote in February 2009 by 89.9% of the votes [218, Chapter 4, section 1.2.1 ]. This

law grants the possibility of roof-raising up to 2 additional stories of selected buildings in the city center, which comply with a townscape harmony principle, while fixing some rules to prevent gentrification. However, no specific measures are adopted to protect the solar access.

## 3.4 Energy in buildings

The Article 45 of the Energy Act gives specific measures for buildings. For example, it introduced a 20-cm exception to maximum size requirements for buildings, in case of energy retrofit interventions. However, due to the Constitutional limits assigning to the Cantons legislation on energy in buildings (Article 89(4)), the federal level provide mostly general principles, that cantons are invited to apply in their own legislation.

We will review here some studies that tried to assess the potential for building energy refurbishment in Switzerland. Subsequently, we will describe the main incentive scheme to support these interventions.

### 3.4.1 The potential for building energy refurbishment

In the Swiss context, the building energy refurbishment plays an important role. About one third of the residential building stock was built before 1946, and another third between 1946 and 1980 (data: BFS-OFS-UFS, 2016), with thus very different thermal standards than today. One of the goals of the 2050 Energy Strategy is hence to reduce the final energy consumption of buildings (all uses) from 100 TWh (2010-2015) to 55 TWh in 2050, while phasing out fossil fuels (75% of today's heating demand) and direct electricity heating [25].

In the framework of the Swiss National Research Project NRP 54, Schalcher et al. [263] described the characteristics of the two economic categories of renovation, aiming either at conserving the value or at creating an added value. They estimated that the actual investments for the renovations aiming at conserving the building economic value are much lower than what would be necessary to implement standard overhauling measures to the existing Swiss building stock. Since this type of renovations mostly follows the supply-demand model, one of the possible interpretations made by the authors is that the refurbishment cycle does not correspond anymore to the economic reality or that the market does not provide enough value for the standard refurbishment cycles. Conversely, refurbishments aimed at creating an added value have a secondary role in terms of investments in the Swiss context as they are mostly limited to single-family detached houses. The study also dealt more specifically with energy refurbishments showing their significant economic impact because of their higher specific costs. Unfortunately, the analysis was based on the latest available data, which were from the period 1990-2000. However, the authors assumed that the current and future potential for energy refurbishment could be actually higher because of the great augmentation of energy prices starting from 2004 and the effect of the Swiss Building Program (see Section 3.4.1.1).

In this context, it seems that energy refurbishment interventions have an immediate interest for building owners and a large potential for growing in Switzerland. Jakob [127] showed that energy refurbishment of previously non-insulated building envelopes is profitable in most cases. Also considering a typical multi-family house of the construction period from 1975 to 1990, which had been already partially retrofitted, Jakob et al. [128] showed that improvements at the level of the building envelope can still be cost-effective. They also recommended the installation of PV systems due to quite favorable cost-effectiveness compared to other strategies. Similarly, Aguacil Moreno et al. [5] showed how the

integration of PV installations may determine a shorter payback time compared to a simple energy refurbishment. The reduction of the payback time due to PV installations could hence be an important trigger for large-scale, coordinated energy refurbishment interventions to the Swiss building stock.

However, the methods currently available for assessing the potential for energy refurbishment interventions only partially address the question of the solar potential in the urban environment [128] and/or they are limited to building- [128, 251] or neighborhood-scale analyses [250, 251].

#### 3.4.1.1 Federal incentive scheme

In 2010, the Swiss confederation introduced the "Building program" ("*Gebäudeprogramm, Programme bâtiments, Programma edifici*", [3]) in order to reduce the energy consumption and $CO_2$ emissions of the residential building stock. This program aimed at promoting energy refurbishment interventions for buildings built before 2000 through national-wide subsidies, and integration of renewable energy sources through canton-level incentives. In the first five years (2010-2014) of activity, 64180 energy refurbishment projects were subsidized.

This program been financed by the cantons and by the federal carbon tax, and the latter part is supposed to increase in the future [24]. The new Energy Act (EnG-LEne-LEne) as well as the revision of CO2 Act ($CO_2$-Gesetz, Loi sur le $CO_2$, Legge sul $CO_2$, Art. 34) strengthened the Building program (ENFV-OEneR-OPEn, Comments), by providing 1/3 of the tax income (capped to 450 MCHF/year) to the "Building program". Investments in building energy saving interventions can be deducted from the taxable income. Starting from 2020, also demolitions costs associated to energy-efficient housing will be fiscally-deductible and the tax deduction could be deferred up to 2 years [24].

Depite these measures, the building retrofit rate is still low (0.9% per year) and it has been claimed that such incentive scheme does not encourage a faster refurbishment rate than the normal one [293]. In this context, it can be argued that the renewable energy transition cannot "wait" for the refurbishment of the building envelopes to install photovoltaic systems, while BIPV could hopefully encourage the refurbishment of the urban building stock.

## 3.5 Synthesis and discussion

This chapter has briefly reviewed the main Swiss policy and regulatory framework at the intersection of solar energy, building energy refurbishment and urban planning. We summarize and discuss here some aspects of the review that are particular relevant for the definition of the thesis motivation, which will be formulated in Section 4.4.

The importance of solar energy in urban environments is attested by the presence of these aspects not only in energy-related legislation, but also in the spatial planning one. The fact that both the Energy Act and the Spatial Planning Act have successfully gone through a direct democracy procedure also implies a strong support from the Swiss people to these matters. The policy for urban inner development and densification (as opposed to greenfield development) is also important, as it testifies the relevance of the existing built environment in the planned urban development.

To this regard, Swiss legislation also provides a strong commitment towards the balance between the promotion of solar energy and the conservation of the natural and built environments. In particular, building integration aspects - for example, the need for a "compact shape" (RPV-OAT-OPT, Art. 32) - are

detailed at one of the highest sources of law. These aspects will be further discussed in Section 4.2.4, but we can already stress out the importance of considering such criteria in solar potential assessments.

In addition to the general considerations about electrification of heating and use photovoltaics (Chapter 1), we have seen the relevance of integrating building energy retrofitting with photovoltaic interventions also from a financial point of view in the Swiss context. Switzerland also encourages the use of solar energy and building energy refurbishment with a favorable regulatory and incentive framework, yet there are still some obstacles. We have seen how the facilitation framework for solar energy in buildings (notably, the building-permit waiver for "roof-adapted" solar systems) does not necessarily simply the procedure and is prone to conflicts. This causes a certain level of uncertainty in the approval process, which does not help the large-scale deployment of solar energy systems. We can also argue that the current incentive framework for solar energy and building energy refurbishment suffers from simplified allocation mechanisms, such as the waiting list. We have also seen that, despite the incentives, the refurbishment of the building stock has very low annual rates. This problem with allocation systems, which is common to many countries, will be further discussed in Section 4.3.4 and be part of the thesis target gaps listed in Section 4.4.

# 4 State of the art

This chapter provides an analysis of the state of the art in the core research areas investigated by this thesis. The literature review explores the latest research advancements in the assessment of the PV solar potential in urban areas and the subsequent use of this information in planning-support.

Unlike the literature review conducted in the previous chapters, this review aims more specifically at identifying the research gaps in the fields, some of which will be addressed Part II and Part III.

## 4.1 Urban-scale simulation of solar irradiation

Interest towards solar energy assessments has been rapidly growing and many models have been developed recently. Freitas et al. [88] provides an extensive review of both computational models and tools used in solar radiation models[1].

We conduct here a review on the solar radiation models that are available as a tool and their input/output data. In general, the larger the scale, the more simplified are the models applied and the less detailed are the input data. This is for example the case of regional-scale analysis conducted on the basis of low-resolution raster data. Similarly, the scale often influences the resolution of the sensor points, on which the output solar radiation is calculated. In this sense, this review is aimed at highlighting the trade-off between:

- analysis accuracy *vs* computational cost/time;
- data resolution *vs* broad applicability (in areas where high-resolution data might not be available);

Considering that analysis accuracy and data resolution both have a maximum reachable limit (due to computational power and/or sensor precision), we finally review the methods that have been used to account for the associated uncertainty (Section 4.1.5).

[1] As a reminder, in this section as elsewhere in the thesis, the word *model* is used to refer to very different concepts. In particular, it can apply either to mathematical and physical models (e.g., sky models and solar radiation models) or to geometrical models (e.g., 3D models, raster models). We will omit further specifications, as the context should make clear which usage applies.

### 4.1.1 Solar radiation models

The application of solar radiation models in urban environments is typically more complex than what has been presented in Section 2.2.6.1. In these conditions, the contribution of reflected solar radiation is usually higher than in an unobstructed situation and cannot, therefore, be neglected. A the same time, obstructions have also an opposite effect, reducing the quantity of visible sky (and thus the diffuse irradiance) and in some cases also obstructing the view to the sun (and thus the beam component).

Urban-scale analysis of solar potential requires a large amount of data to be simulated, which is challenging from different points of view. In terms of computational power, some models are very intense, especially when ray-tracing is involved. Alternative methods implementing cumulative sky models, daylight coefficients or radiosity algorithms have been used in order to reduce the computational time. In terms of memory, some calculations might also become very intense, unless appropriate strategies are implemented. To this end, CitySim implements a strategy in which the memory is periodically emptied by saving the data to the disk. Some authors discuss the trade-off between the large scale of the analysis and the accuracy of the simulation, in particular related to the need for including the diffuse component in arid climates [309] and the reflected component [248, 165, 191].

Freitas et al. [88] provides an extensive review of the main computational solar radiation models. We review here only those models that have been either only recently developed or extensively used in the past years, whereas in Table 4.1 we summarize the main features of a more restricted set of computational models, which are all available as a software tool or plug-in to other software, and have been either specifically developed or adapted for urban-scale assessments.

Some solar radiation models are extensions of GIS tools (like Solar Analyst [93], r.sun [248], v.sun [110]), while others are conceived for application on large 3D-city vector [165, 191] or voxel [110, 34] models. Liang et al. [165] proposed an algorithm mapping 3D vector models (triangular mesh) into 2D rasters allowing the implementation of fast GPU-based radiation models. However, this model is based on the simplified radiation model used in *r.sun* and does not include inter-reflections. Murshed et al. [191] coupled a comprehensive photovoltaic performance model with an advanced radiation model, also without considering the reflected component though. Isotropic sky models are used for the most popular GIS-based analysis tools [93, 248, e.g.]. Desthieux et al. [69] applied intead the Hay sky model [104], which was found to be more accurate than the Perez's one when using monthly average values, while Murshed et al. [191] used one of its variations, the HDKR model. An anisotropic model was also used by Catita et al. [49], which introduced the hyperpoint concept to simulate façade solar radiation on a raster model.

Advanced sky models and the inclusion reflected component from a 3D environment are present in more general-purpose lighting simulation tools, originally developed in the field of daylighting (Radiance-Daysim [244], Radiance-gendaylit [68] and Radiance-GenCumulativeSky [254]), as well as in the Simplified Radiosity Algorithm [252] used in CitySim [256].

Since Daysim uses a daylight coefficient approach, dividing the sky generated by gendaylit in discrete patches, it provides faster (but slightly less accurate) results compared to a standard simulation in Radiance-gendaylit [243], while providing (sub)hourly values, unlike Radiance-GenCumulativeSky, which provides only time-cumulated results. Patriarche and Dumortier [209] and Patriarche [210] conducted an experimental validation of three CitySim, an implementation of SRA [252] and Daysim (as well as of Heliodon [20]). They showed that CitySim and Daysim provides similar results, with a mean absolute difference of 1.5% from the reference measured values, while the former is about 60 times faster than the latter. Heliodon, while being as fast as CitySim, systematically understimates solar

*Table 4.1 – Non-exhaustive list of solar radiation models that have been applied to urban-scale assessments and their main characteristics. These models are all available as a publicly available software tool or plugin-in to other software.*

| Tool | Sky model(s) | Reflection | Geom. | Time | Studies |
|---|---|---|---|---|---|
| Simplified Radiosity Algorithm (SRA) [252] | Tregenza [302] and Perez All-weather [216] | Radiosity | 3D | Hour | [202, 183] |
| Radiance-GenCumulativeSky [254] | Tregenza [302] and Perez All-weather [216] | Backwards raytracing | 3D | Period | [218, 193] |
| Radiance-Daysim [244] | Tregenza [302] and Perez All-weather [216] | Backwards raytracing | 3D | Hour | [132, 62] |
| Radiance-gendaylit [68] | Tregenza [302] and Perez All-weather [216] | Backwards raytracing | 3D | Hour | [81] |
| v.sun [110] | Isotropic | N/A | 3D | Hour | [110] |
| SURFSUN3D [165, 166] | Isotropic | N/A | 3D | Hour | [165, 166] |
| Heliodon [20] | N/A | N/A | 3D | Hour | [21] |
| Solar Analyst [93] | Isotropic | N/A | 2.5D | Hour | [55] |
| r.sun [248] | Isotropic | Fixed contribution | 2.5D | Hour | [109] |

radiation due to the lack of reflected and diffuse solar radiation.

Based on this review, we consider that both Daysim and SRA (CitySim) provide adequate features (i.e. support to 3D geometry, inter-reflections and hourly resolution) for the scope of this work. The comparison of simulation time will be the object of further analysis in this thesis (Tables 11.3 and 11.12, while we will use Radiance-gendaylit as a ground truth to check the accuracy of the simulated value as part of a study on discretization settings Section 6.2. Although we acknowledge that the ground truth should be in principle an experimental observation, we consider that the use of a validated model has the advantage of being applied for a larger urban area and Radiance-gendaylit has been already to this scope ([254, 255].

### 4.1.2 Model inputs

Typical input data of urban-scale radiation models are sensor points, geometry, surface attributes, and weather data. Such input data come at different resolutions and different formats.

- *Sensor points* associated with their direction vectors (usually facing outwards with respect to the corresponding surface), on which the solar radiation is calculated. Sensor points and vectors can be also directly inferred by the input geometry, for example by using the center points of the surfaces or the pixels of a raster model.
- *Geometry*, defining the obstructive (and possibly reflective) field surrounding the sensor points. The geometry can be expressed in a 2.5D or 3D space, either as full geometric representation (3D coordinates of surface), its discrete 2.5D or 3D representation (pixel or voxels), or as simple obstruction angles (height and azimuth);
- *Surface attributes*, defining the material properties of the geometry;
- *Weather data*, including direct and diffuse solar radiation at multiple time-steps (usually each hour of the year). The radiation data can be either measured or being the result of statistical sampling based on several measured datasets, such as, for example, the Typical Meteorological Year [317]. When such data is not available or is not supported by the solar radiation model, the global solar radiation is computed on the basis of the sun angle (calculated from the latitude) and some parameters to account for the atmosphere attenuation [93, 248].

#### 4.1.2.1 Sensor points [2]

*Sensor points* associated with their direction vectors (usually facing outwards with respect to the corresponding surface), on which the solar radiation is calculated. Sensor points and vectors can be also directly inferred by the input geometry, for example by using the center points of the surfaces or the pixels of a raster model.

Sensor grids are used as input to simulation models for different uses, including noise propagation [289], solar radiation simulations [88, 34], visibility assessments [84] and computational fluid dynamics [56, part four]. The grids are produced by sampling 3D city models with 3D point-clouds using different discretization algorithms.

Unlike the level of detail (LOD), whose choice is usually limited by the available data and the type of analysis, the grid discretization depends on the scope and the target accuracy of the analysis. The finer the grid is, the more accurate the results are expected to be, at the cost though of longer simulation time. In the case of arrangement, the choice is mostly dictated by the type of assessment and expected output.

Based on the terminology derived from Computational Fluid Dynamics (CFD), we can distinguish between two types of arrangement:

- structured grids, in which "it is possible to define a curvilinear co-ordinate system that spans over the entire domain and hence the connectivity of the individual sub-domains is implicit" [197, 8.1];
- unstructured grids, in which "the connectivity of the individual sub-domains must be explicitly specified" (*ibid.*).

In CFD, both structured and unstructured grid arrangements are used, with the latter being usually preferred for complex geometry, in particular in the form of adaptive mesh resolution to maximize efficiency and accuracy [56, part four].

With regards to solar energy assessments, different discretization settings for grid spacing and arrangement are used in the literature. However, the choice is often not justified or is only based on reference values from the literature [in particular, 59]. Moreover, as can be seen in Table 4.2, there is no correlation between the LOD and the grid size, while intuitively the higher the LOD, the lower the grid spacing should be. Depending on the data input and modeling platform, methods based on either a structured or unstructured grid are used in the literature, without their choice being usually justified either by supporting arguments or by the specific analysis scope. There are two exceptions though. Waibel et al. [311] motivated the choice of (unstructured) meshing algorithms arguing that the density of the sensor points increases with the complexity of the geometry. However, it can be also argued that complex radiation and shading patterns can affect simple rectangular surfaces, for instance a façade in an urban canyon.

Yet, to the best of authors' knowledge, the influence of the sensor grid resolution and type has been mostly neglected in preceding studies. Only Alam et al. [11] and Bremer et al. [34] investigated this aspect, though using simplified solar potential calculations, neglecting for example reflected radiation.

[2] This section contains excerpts from a published journal paper [227]: Peronato, G., Rey, E., & Andersen, M. (2018). 3D model discretization in assessing urban solar potential: the effect of grid spacing on predicted solar irradiation. *Solar Energy*, 176, 334–349. https://doi.org/10.1016/j.solener.2018.10.011. The text is reproduced here as a courtesy of the publisher and with the agreement of the co-authors. G.P. contributed by conducting and writing the review.

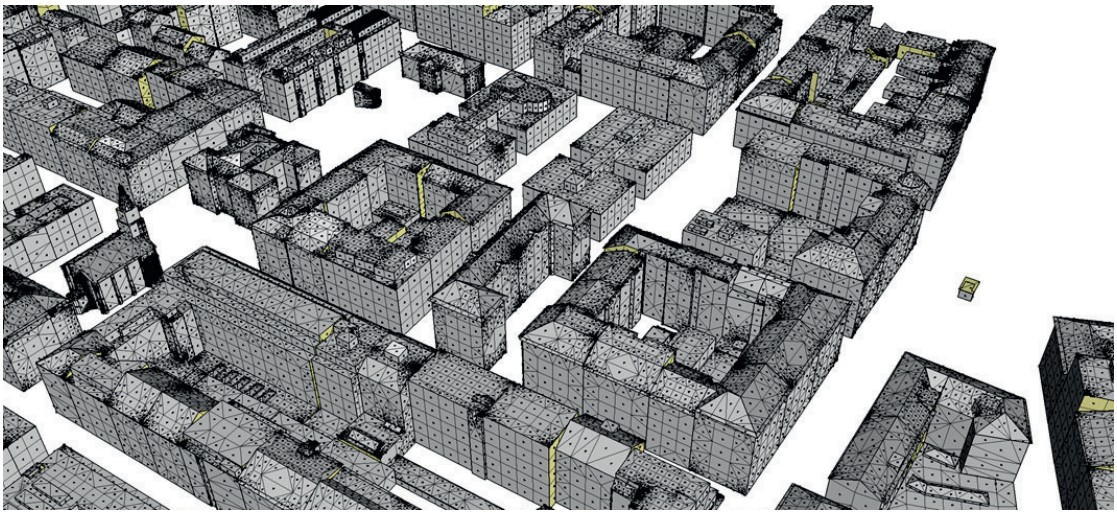

(a) Structured grid

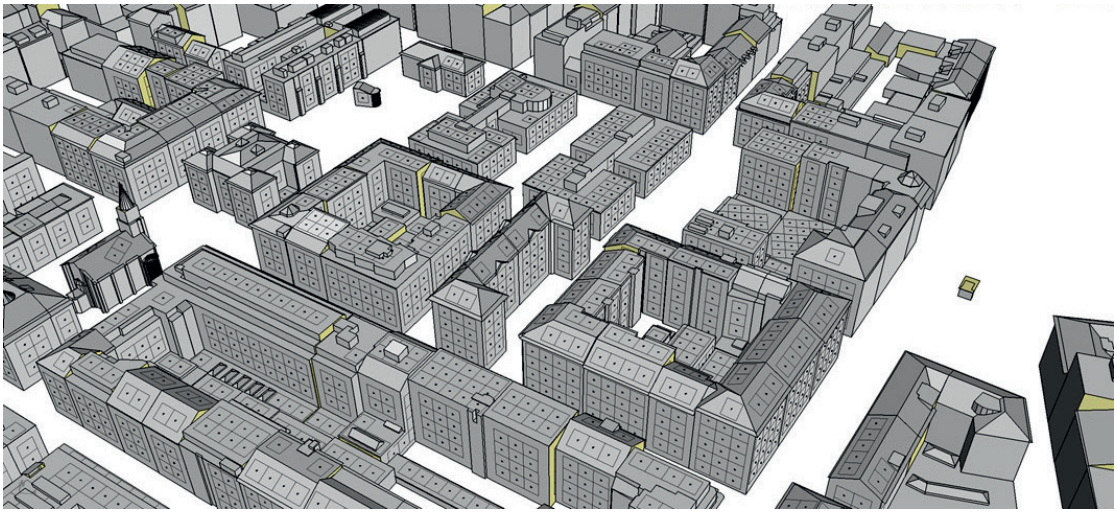

(b) Unstructured grid

*Figure 4.1 – Disposition of sensor points for the unstructured grid (above) and the structured grid (below). With the latter, the smallest surfaces do not have any sensor point.*
*Source: Peronato et al. [227] - SITG 3D model, extracted in June 2017*

Alam et al. [11] checked the sensitivity of the sky view factor to the meshing resolution of buildings, using different triangulation areas ranging from 5 $m^2$ to 0.01 $m^2$. They showed a significant influence only on shaded areas, for which the solar radiation is generally low. However, they did not come up with an optimal resolution for this kind of assessments, but rather stated that the quality of the meshing resolution is proportional to the accuracy of the result. Moreover, their method did not include inter-reflections nor the assessment of a structured grid.

Conversely, Bremer et al. [34] only analyzed a structured sensor grid and did not discussed unstructured grid arrangements. This sensor grid was in fact created using a texture-mapping algorithm, which necessarily works with regular grids as based on pixels, and was proved to provide a powerful visualization and an efficient data storage. They also implemented a structured voxel grid for representing

*Table 4.2 – Typical grid resolutions and arrangements, level of detail (LOD) and scale of analysis of the 3D models. Analysis focusing on single buildings are not included.*

| Reference study | Grid resolution | LOD | Grid arrangement | Scale |
|---|---|---|---|---|
| Compagnon [59] | 100 cm | LOD1 | Structured | Neighborhood |
| Montavon [184] | 100 cm | LOD1 | Structured | Neighborhood |
| Nault et al. [194] | 400 cm | LOD1 | Unstructured | Neighborhood |
| Jakubiec and Reinhart [132] | 150 cm | LOD2 | Unstructured | Urban |
| Peronato [218] | 100 cm | LOD1 | Unstructured | Neighborhood |
| Catita et al. [49] | 50 cm | LOD3 | Structured | Neighborhood |
| Wieland et al. [315] | 200 cm $^{o}$ | LOD2 | Structured | Neighborhood |
| Fath et al. [81] | 150 cm | LOD2 | Unstructured | Urban |
| Waibel et al. [311] | 210-430 cm $^{o+}$ | LOD1 | Unstructured | Neighborhood |
| Fonseca et al. [86] | 200 cm | LOD1 | Structured | Urban |
| Nault et al. [196] | 100 cm | LOD1 | Unstructured | Neighborhood |
| Costanzo et al. [62] | 150 cm | LOD1 | Unstructured | Neighborhood |
| Vulkan et al. [309] | 100 cm | LOD1 | Structured | Neighborhood |

$^{o}$Information retrieved from the authors, as not specified in the published paper
$^{+}$Minimum-maximum values, as mesh size varies during the optimization process

occlusions in their radiation model. They hence analyzed the impact of different resolutions (0.5, 1.0, 2.5, 5.0 and 10.0 m) of sensor grids, as well as of the occlusion voxels. They showed that the resolution of the sensor grid has a greater impact than the resolution of the occlusion geometry and significantly affects the accuracy of the results. Even if they applied a 1-m resolution for their case-study application, they did not suggest an optimal resolution, but rather showed the potential of using a multi-scale method for improving the computational performance.

#### 4.1.2.2 Geometry

*Geometry* is composed of the obstructive (and possibly reflective) surfaces surrounding the sensor points. Geometry can be expressed in a 2.5D or 3D space, either as full geometric representation (3D coordinates of surface), its discrete 2.5D or 3D representation (pixel or voxels), or as simple obstruction angles (height and azimuth). Different types of geometry can also be integrated in the same model, depending on the target resolution and analysis scope. For example, Bremer et al. [34] included voxels at different resolutions and polygons in the same model, and CitySim natively supports both close and far-field obstructions. The Table 4.3 provides a non-exhaustive list of the main types of geometry and applications, with references of some have been applied in recent studies.

For 3D geometry, the Level of Detail (LOD) (see Section 2.3) plays an important role as it affects the POA irradiation reaching the surfaces, by altering the available surface (e.g. a roof represented either as flat or gabled) as well as the representation of additional shading/reflecting surfaces (e.g. presence of chimneys). Since the Level of Detail plays also a role on the arrangement and choice of PV modules attached or integrated to the building envelope, we will examine directly this influence while dealing with the location potential for building-installed solar systems (Section 4.2.1).

#### 4.1.2.3 Attributes

*Attributes* are quantitative or qualitative information that are linked to the geometry. They provide additional information about some specific characteristics, such as, for example the reflective properties of the geometry.

*Table 4.3 – Geometry, with typical resolutions, used in a non-exhaustive list of previous works on solar potential assessments of existing urban areas.*

| Geometry | Space | Resolutions | Applications | Sample studies |
|---|---|---|---|---|
| Angles | 2.5D | 1-10° | Far-field obstructions | [98] |
| Pixels | 2.5D | 0.5-50m | Roofs, terrain, vegetation | [248] |
| Hyperpoints | 2.5D | 0.5-10m | Buildings, terrain, vegetation | [47, 49, 69, 309] |
| Voxels | 3D | 0.5-10 | Buildings, terrain, vegetation | [110, 34] |
| Mesh | 3D | 0.25-2m | Buildings, terrain, vegetation | [132, 253, 154, 165] |
| Polygons | 3D | N/A | Buildings | [78, 34, 191] |

*Table 4.4 – The table presents the reflective properties of surfaces.*

| Study | Roof | Facade | Ground | Vegetation |
|---|---|---|---|---|
| Fath et al. [81] | 20% | 30% | 20% | - |
| Compagnon [59] | - | 20% | - | - |
| Jakubiec and Reinhart [132] | from a database | 30% | 20% | 20% |
| Costanzo et al. [62] | 30% | 35% | 20% | - |
| IESNA [120][3] | 20% | 30% | 20% | 20% |

Attributes are typically assigned to vector geometry such as voxels, mesh and polygons. In the case of material properties, only few solar radiation models support them, including those based on Radiance, like Daysim [244] and the genCumulativeSky [254], and the Simplified Radiosity Algorithm [252].

In the case of Radiance-based algorithms, in most of the cases the *plastic* material is used, which is defined by five parameters: reflectivity (RGB values), specularity and roughness. Jakubiec and Reinhart [132] used Lambertian diffusers for building walls (30% reflectivity) and context (20% reflectivity), while a database of roofing materials was used for the absorptivity and reflectivity of roofs.

For the SRA algorithm implemented in CitySim [154], each surface is characterized by its short-wave reflectance.

#### 4.1.2.4 Weather

Standard weather data for solar radiation models include direct and diffuse data at either the horizontal plane or normal to the beam component. Weather files in the EnegyPlus format *.EPW provide the three distinct solar radiation values: Global Horizontal Irradiance (GHI or GlobHor), Diffuse horizontal irradiance (DHI or DiffHor) and Direct normal irradiance (DNI or BeamNor). In case that all these data are not available, empirical separation models are used to derive each radiation component based on sky condition predictors [99]. Because of the technical complexity of measuring DHI and DNI [101], most of the weather stations measure only GHI and empirical separation models are used to derive each radiation component . Gueymard and Ruiz-Arias [99] reviews the performance of these separation models.

Solar radiation data are based on datasets from ground measurements or from satellite images validated with ground measurement data [306]. In addition to radiation data, PV performance prediction models also use the air temperature and the wind speed data contained in the weather files. In the case of building performance simulation, air and ground temperatures, relative humidity, and wind speed from ground measurements are also used. When weather data is not available or is not supported

[3] Values for daylight simulation, limited to the visual spectrum.

*Table 4.5 – List of some popular weather file generators, with their main features and implementation for large-scale solar assessments.*

| Product | Weather scenarios | CC scenarios | Data source | Applications | Coverage |
|---|---|---|---|---|---|
| ASHRAE-IWEC [13] | No | No | Ground and empirical model (solar) | | 227 locations |
| ASHRAE-IWEC2 [14] | No | No | Ground and empirical model (solar) | | 3,012 locations |
| NREL-TMY3 [317] | No | No | Ground | US | |
| Meteonorm [245] | No | IPCC | Ground | Meteotest solar cadastres | World |
| SolarGis [282] | P90, P50, P10 | No | Satellite | World | |
| SolarAnywhere® [217] | No | No | Satellite | PVWatts | World |
| Classic PVGIS [249] | No | No | Ground (Europe) and satellite (Africa) | PVGIS | Europe and Africa |
| Climate-SAF PVGIS [187] | No | No | Satellite | PVGIS | World |

by the solar radiation model, the global solar radiation is computed on the basis of the sun angle (calculated from the latitude) and parameters to account for the atmosphere attenuation [93, 248].

In most of the case, weather data is provided in the form of a Typical Meteorological Year [317]. TMY files contain statistically sampled data from a set of measured data. Typical Meteorological Years (TMY2 and TMY3) are commonly used in energy simulation software [317]. Each file is formed by hourly values derived from multi-year measured values, processed so that each month is *typical* of the long-term climate. A typical month is selected according to the daily indices of 10 parameters, in which solar radiation (GHI and DNI) accounts for half of the weight. According to Vignola et al. [306], TMY data files should be used only for initial evaluation and present several limitations for solar assessments:

- they represent typical meteorological year and not solar year; in this sense, there are cases where data from solar radiation is far from the typical solar year because the TMY is weighted by 50% with non-solar meteorological values;
- TMY excludes on purpose extreme events, for example aerosols due to volcano activities blocking part of the solar radiation ;
- a large part of TMY and TMY2 data comes from modeled data, whereas TMY3 data have a limited range of measured data (1991 to 2005), which in 83% of the casse is limited to an even shorter extent (11.5 years) because of the removal of extreme events.

TMY-like data include the IWEC and IWEC2 datasets, which are commonly-used weather files in building simulation, as the former dataset is freely available from the EnergyPlus website. However the solar radiation is not measured but modeled from empirical models[4] and was shown to be severely biased for some locations in Northern Europe [173, Ch. 6].

P50 and P90 exceedance probabilities are a common method used in wind farm projects to determine the risk associated with an installation, and have been recently integrated also in the System Advisor Model (SAM) for solar assessments [71]. The output values calculated with these files represent the $50^{th}$ (respectively, $10^{th}$) percentile of the annual output of the solar system, meaning that there is a 50% (respectively, 90%) likelihood that the output exceeds the predicted values [71]. However, to the best of our knowledge, these or similar risk-based weather generators have not been integrated in urban-scale solar radiation assessments.

[4] http://weather.whiteboxtechnologies.com/faq, accessed on March 20, 2018

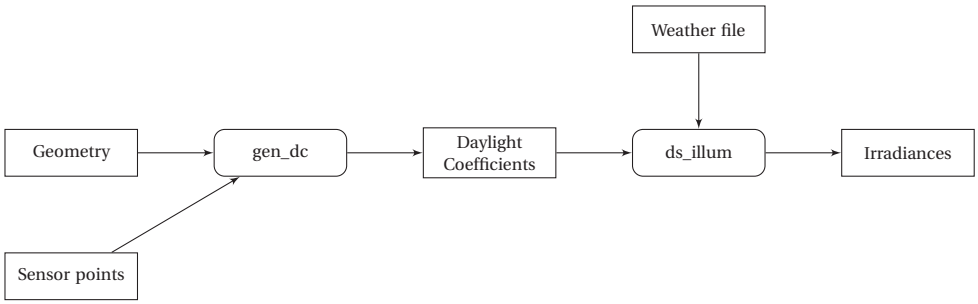


*Figure 4.2 – Main steps of a Daysim simulation.*

### 4.1.3 Output data

Output data computed by solar radiation models is irradiance expressed in kWh/m$^2$. In most of the cases, the irradiance is computed for each time step and can be subsequently be integrated over time and space. In some cases, the solar radiation models provide results that are already time-cumulated. This is for example the case of the *genCumulativeSky* model [254], in which the contribution of each sky patch is the time-cumulated solar radiation.

Most of the models provide results stored as simple text files. The fact of calculating hourly irradiance for a large number of locations results in very large datasets. In this sense, CitySim conveniently provides summary statistics for each surface (notably the time-cumulated irradiation) and, as an option, the results stored in a binary format, which helps the subsequent post-processing of the information.

Another feature of the output data is having the possibility of intermediate outputs, which then allow for variations of the same simulations. As can be seen in Figure 4.2, a Daysim simulation provides an intermediate output in the form of daylight coefficients. Since the weather information is used only for the last sub-program `ds_illum` (except for the latitude, which determines the number of daylight coefficients to be generated), the same daylight coefficients can be used to run multiple simulations with different weather conditions. This is particularly effective, as `ds_illum` is much faster to run than `gen_dc`.

### 4.1.4 Vegetation and solar energy

Vegetation deserves a special section[5], as it has some particular characteristics with respect to building and terrain geometry:

- its shape is dynamic over time as a consequence of natural growth and, for deciduous species, also periodically over seasons;
- it has a complex geometry composed of branches and leaves causing multiple light effects, often combining reflection, transmission and absorption;
- despite its natural origin, it has a distinctive status in the anthropic built environment, for differ-

[5]This section contains some excerpts from a published conference paper [221]: Peronato, G., Rey, E., & Andersen, M. (2016). 3D-modeling of vegetation from LiDAR point clouds and assessment of its impact on façade solar irradiation. In *ISPRS - International Archives of the Photogrammetry, Remote Sensing and Spatial Information Sciences* (Vol. XLII-2/W2, pp. 67–70). Athens. https://doi.org/10.5194/isprs-archives-XLII-2-W2-67-2016. The conference paper is published by Copernicus GmbH (Copernicus Publications) on behalf of the ISPRS under the Creative Commons Attribution 2.0 License. G.P. contributed by conducting and writing the review that is presented here.

ent reasons including but not limited to aesthetics (e.g. in gardens), comfort (e.g. as a shading device) and environmental awareness (e.g. as a device for pollution and $CO_2$ sequestration) reasons, and, as such, it is often placed close to buildings.

For such reasons, there is room for a potential conflict between vegetation and solar energy:

- they both depend on sun light and as such they might interfere by shading each other, more likely in the case of vegetation shading a solar module;
- they can be both be used to reduce carbon emissions: vegetation for compensation of emissions and PV substituting - once its own carbon content has been offset - a carbon-emitting energy source;
- they potentially can reduce the Urban Heat Island effect: vegetation is effectively used for such a scope thanks to its reflective and evo-transpirative properties; for PV there is potentially a cooling effect - with reference to traditional urban materials - at least for solar conversion efficiency higher than 10% [297], while Wang et al. [312] had opposite considerations;
- both vegetation [117] and PV [312] can reduce cooling loads in buildings, when used for shading purposes.

In the related field of daylight simulations, tree crowns are often modeled in 3D, while using use simple shapes to represent trees. For example, IESNA [120] suggests modeling trees as cones, spheres, or cylinders with a 20% reflectance. We can consider that this approach is possible also for our application, while it neglects most of the information available through *LiDAR* surveys.

In terms of materials, Jakubiec and Balakrishnan [131] reports an interesting debate occurred in Radiance-specialized on-line forums about the modeling technique to better represent the complexity light interactions of the tree crown: either using Radiance *trans* (i.e. semi-transparent) material or as *plastic* (opaque, Lambertian diffuser) with a certain percentage of void. Balakrishnan and Jakubiec [16] used latter the approach computing the gap percentage using HDR images and generating a random canopy model maintaining a visual similarity with the actual tree model. While these modeling methods are applicable also for urban solar potential studies, sensing the properties through HDR images is unfeasible for urban-scale applications.

Table 4.6 summarizes the methods used in the main studies focusing on vegetation effect on solar potential in urban environments. Previous studies have shown how vegetation influences solar irradiation on rooftops [300, 85], also taking into account the semi-transparent nature of tree canopies [301, 137, 172]. However, these studies use 2.5D raster models or 3D-cloud points, which limit the application to rooftops and not to façades, unless these are assumed contiguous to the roofs and a hyper-point approach is used [49]. Moreover, these studies did not include inter-reflections, which might significantly contribute to the total façade irradiation in urban environments. Jakubiec and Reinhart [132] included instead vegetation in a fully-3D space, but modeling both vegetation and terrain as part of the same triangulated mesh. More recent studies modeled the semi-transparency of trees from the LiDAR returns in the 3D space. However, Table 4.6 shows that the seasonal variability (which is connected to the classification between deciduous and evergreen vegetation) and the growth is not applied, unless with manual classification or surveys. If the growth is important for studies focusing on the future, the seasonal variability is crucial also at present times. We can though argue that considering the seasonal variability of vegetation as an uncertainty factor is acceptable for most applications of solar potential studies, such as the ones that will be targeted by this thesis (i.e., the ranking of urban locations).

*Table 4.6 – List of studies assessing the impact of vegetation on solar irradiation in urban areas. All these studies use LiDAR as the main data source.*

| Study | Geometry | Transparency | Variability | Growth |
|---|---|---|---|---|
| Levinson et al. [164] | 2.5D raster | - | - | asymptotic growth model on surveyed trees |
| Tooke et al. [300] | 2.5D raster | - | - | - |
| Tooke et al. [301] | 2.5D raster | Gap-probability model based on LiDAR returns | - | - |
| Jochem et al. [137] | 3D-cloud | Echo-ratio from LiDAR returns | - | - |
| Lukač et al. [172] | 3D-cloud+voxels | Leaf Area Index [124] based on manual classification | Seasonal | - |
| Fogl and Moudrý [85] | 2.5D raster | - | - | - |

### 4.1.5 Uncertainty analysis

Uncertainty analysis[6] is primordial when dealing with models, as in simulation-based assessments. Uncertainties can be defined as potential deficiencies due the lack of knowledge [AIAA as cited in 118]. Unacknowledged errors, such as the ones due to the applications of models or algorithms, can be also considered uncertainties because they are caused by a lack of knowledge (*ibid.*). Therefore, uncertainty analysis is used to test the model or input data against reference models or high-resolution data in order to retrieve the associated error.

The simulation of solar irradiation is based on different input data and mathematical models. Input data typically include a 3D representation of obstructions (e.g. buildings, trees, terrain), their material properties (e.g. transparency, reflectance), and measured or statistically-sampled irradiance values. Models are first applied for calculating irradiance values on tilted surfaces from horizontal and normal values, which are usually provided by meteorological stations. Prada et al. [235] showed that, in the context of building energy performance, the application of different radiation models produce a dispersion of simulation outcomes, hence an uncertainty in the predicted energy performance.

Other uncertainties occur with the models accounting for the shading and reflection from the context. As we have seen in Section 4.1.1, models developed for large-scale applications [248, 254, 255] typically rely on different simplifications of the physical reality to reduce the simulation time. For instance, the method by Šúri and Hofierka [248], which is conceived for regional-scale applications in a GIS environment, presents several simplifications in terms of reflected radiation and weather variability; the method by Robinson and Stone [254], while being based on physically-accurate backwards ray-tracing, implements sky patches accounting for both direct and diffuse contribution to simulate irradiation values cumulated over a certain period of time; Robinson and Stone [255] implemented instead a simplified radiosity algorithm (SRA) to include the contribution of reflected solar radiation by neighbor obstructions. All these methods have been tested against a reference model, which is assumed to be physically accurate, or against measured values. Robinson and Stone [254] and Robinson and Stone [255] used irradiance data simulated with Radiance sub-program *gendaylit* on an urban canyon, while Šúri and Hofierka [248] used measured horizontal global irradiation from a database.

[6] This section contains excerpts from a published journal paper [227]: Peronato, G., Rey, E., & Andersen, M. (2018). 3D model discretization in assessing urban solar potential: the effect of grid spacing on predicted solar irradiation. *Solar Energy*, 176, 334–349. https://doi.org/10.1016/j.solener.2018.10.011. The text is reproduced here as a courtesy of the publisher and with the agreement of the co-authors. G.P. contributed by conducting and writing the review that is presented here.

The choice of coarse discretization settings, even if detailed models are available, can help reduce the simulation time, at the cost of loss in accuracy though. In this sense, some studies focused on the error due to the use of low resolutions for sky subdivision and simulation time step [11] and resolution of 3D models [11, 34].

In some cases, an error has to be accounted due to the difficulty of obtaining accurate input data. 3D models at high Level of Detail (LOD) are often not available for large urban areas, as they are based on expensive aerial surveying and often followed by manual corrections, while in some cases they are possibly not the best choice for some specific applications, because they cause longer simulation time without significantly improving the results [29]. In this sense, Besuievsky et al. [23] investigated the effect of using 3D models with coarser LODs. Similarly, but with an application on simulation of building energy demand, previous work analyzed the effect of LOD [292, 198], semantic data quality [198] and spatial accuracy [314] on the simulation results. Biljecki et al. [28] investigated the propagation of measurement errors in 3D models at different LODs on the calculated solar irradiation.

The above-cited work use different methods on which the uncertainty can be assessed, depending on the model and data input. Uncertainty is thus defined:

- with reference to a ground-truth, which can be either measured [248] or assumed to represent more accurate results [23, 292, 198, 254, 255];
- with a probabilistic approach, to define confidence intervals out of aleatory uncertainty such as the one represented by weather [240] and positional error in 3D data [28, 314].

As we have seen also in Section 4.1.2.1, other studies have been tested the uncertainty related to the LOD of 3D model ([198]) and the discretization of the sensor grids ([11, 34], while using other solar radiation models than the one that will be used in this thesis (Daysim). It seems therefore relevant to test these factors against a reference model, as it will be done in Section 6.1 and Section 6.2.

### 4.1.6 Synthesis and discussion

In this section, we analyzed the state of the art of urban-scale simulation of solar irradiation. We reviewed the main models and gave an overview of the features and input data needed to perform urban-scale solar potential analysis. This had the main scope of introducing typical workflows and parameters used in similar analyses, to be implemented Chapter 11, as well as introducing the main aspects of uncertainty in current models. To this regard, sensitivity analyses towards the LOD and the discretization settings will be conducted in Chapter 6.

Based on this review, we have seen that Daysim and Citysim offer the support for 3D geometry, inter-reflections and hourly simulations, while using validated solar radiation models. Their use will be then implemented in the assessment workflow that will be presented in Chapter 11, also comparing their computational performance with regards to the specific task and 3D model Section 11.3.1.

We also stressed the importance of modeling the variability of weather and vegetation while reviewing existing models. Nonetheless, in most studies vegetation is considered as simple obstruction, without considering its complex geometry and seasonal variability. Also linking to what already seen in Section 2.3.3.2, we have seen how it is possible to accurately reconstruct its shape from LiDAR data, while the problem of the seasonal variability will be addressed with a specific decision-support workflow in Section 11.4.

## 4.2 Potential for building-installed solar systems

The suitability analysis is intended to classify building surfaces according to their aptness to install building-applied photovoltaic systems.

Fath et al. [81], based on earlier work by Quaschning [237], defined three solar potentials:

- **Theoretical potentia**l, i.e. the available solar potential on a region. We analyzed methods in the previous Section 4.1.
- **Technical potential**, which is composed of:
  - **location potential**, which defines the suitable area for installing PV modules;
  - **energy generation potential**, which defines the actual energy production based on the efficiency of the transformation of solar irradiation into electricity;
- **Economic potential**, which defines the share of the theoretical potential that is suitable for financing PV modules.

To this list, based on further analysis of the literature, we can identify this additional potential:

- **Integration potentia**l, which defines the share of the technical potential responding to architectural integration criteria.
- **Environmental potentia**l, which defines the share of the technical potential maximizing the environmental benefits, e.g. in terms of saved carbon emissions compared to alternative energy sources.

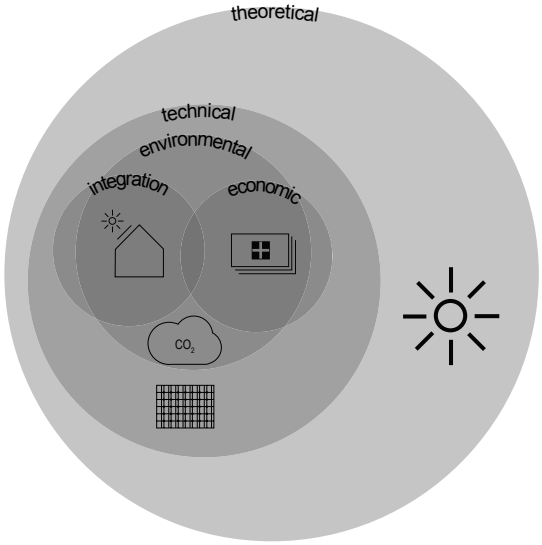


*Figure 4.3 – Relationship between the different solar potentials.*
*Icons CC SA-BY Till Teenk via* The Noun Project

The Figure 4.3 shows the intersection of the different potentials. It should be noted that only a part of the technical potential is both economically and architecturally suitable for installing PV modules, while this should be the target of any analysis investigating the comprehensive potential for building-applied solar systems.

As can be seen in Table 4.7, different levels of potentials have been investigated in the literature, but a

*Table 4.7 – The table presents the main focus of some sample literature studies with regards to the different solar potentials.*

| Study | Technical | | Environmental | Economic | Integration |
|---|---|---|---|---|---|
| | Location | Energy | | | |
| Fath et al. [81] | ✓ | ✓ | | ✓ | |
| López and Frontini [169] | | | | | ✓ |
| Orehounig et al. [203] | | | ✓ | | |
| Munari Probst and Roecker [188] | | | | | ✓ |
| Eicker et al. [78] | ✓ | ✓ | | | |
| Jakubiec and Reinhart [132] | ✓ | ✓ | | ✓ | |
| Murshed et al. [191] | ✓ | ✓ | | | |

comprehensive analysis is missing. The objective of this section is to describe the technical, economic and integration potentials, and review methods and indicators allowing the assessment of these potentials that can be applied at the urban scale. Considering that photovoltaics have lower carbon emissions than the Swiss grid for most of the time during the year (cf. Table 2.3), we will not review the PV environmental potential as we consider that this corresponds to the technical potential, i.e. all energy produced with photovoltaics is environmental-friendly and suitable to reduce the building carbon footprint.

### 4.2.1 Location potential

The location potential[7] identifies all the surfaces that are architecturally suitable for a BIPV installation. As pointed out by Fath et al. [81], "the LOD strongly influences available surface areas for photovoltaic installations" as, "with increasing LOD, the location potential can be expected to decrease". For instance, a LOD1 would generally provide higher irradiation results since all roof surfaces are considered flat, while in reality some parts are actually not optimally exposed.

At a city scale, the assessment of the solar potential is usually conducted by simulating a 3D model of the urban fabric [88]. However, the accuracy of the geometric representation of the urban fabric is variable, depending on the Level of Detail of the geometric model (Figure 2.6). In historical cities, such as the ones typical of Switzerland and other European countries, buildings usually present complex roof shapes, as well as overhangs and dormers, which limit the actual surface available for solar energy systems.

Since interiors modeled in LOD4 are not needed in solar potential assessments, LOD3 already provides a sufficiently accurate representation of the building. However, the availability of LOD3 models is mostly limited to small urban areas, probably because creating them on a large scale is laborious and requires extensive datasets, and because few applications can currently benefit from the added details [30]. Therefore, LOD1 and LOD2 models are normally used for solar potential assessments and reduction coefficient ratios are then applied to estimate the actual area of building surfaces that is

[7] This section contains few excerpts from a published conference paper [220]: Peronato, G., Bonjour, S., Stoeckli, J., Rey, E., & Andersen, M. (2016). Sensitivity of calculated solar irradiation to the level of detail: insights from the simulation of four sample buildings in urban areas. In *PLEA 2016 - Cities, Buildings, People: Towards Regenerative Environments, Proceedings of the 32nd International Conference on Passive and Low Energy Architecture; (Vol. 2)*. Los Angeles. The text is reproduced here as a courtesy of the conference organizers and with the agreement of the co-authors. G.P. contributed by conducting and writing the review that is presented here.

*Table 4.8 – List of location suitability criteria. Roofs are usually classified as flat if they have a tilt less than 10°[78].*

| Study | Flat roof | Tilted roof | Facade | Minimum area |
|---|---|---|---|---|
| Fath et al. [81] | 60% | 90% | 80% | 15 $m^2$ |
| Eicker et al. [78] | 29% | 60% | - | 20 $m^2$ |
| Jakubiec and Reinhart [132] | - | discarded if >60° | - | - |
| Murshed et al. [191] | Fixed inter-row distance | - | - | - |

available for the installation of solar energy systems (Table 4.8).

Although the solar potential of facades might be theoretically estimated at all levels of detail, only a few studies included such an analysis [45, 49, 59, 81, 241]. However, the potential of these surfaces should not be neglected. The IEA [119] estimated that about 27% of the solar energy potential of Switzerland comes from facade-mounted PV systems. A recent study in a University Campus in Lisbon [241] showed that the solar potential on facades is almost as large as the one on rooftops, because of their much larger surface area.

Similarly to roofs, the presence of balconies, windows and other building elements should be taken into account, but they are not defined in models with a LOD lower than 3. Karteris et al. [142] categorized some typical multi-family buildings in Greece and proposed some suitable facade photovoltaic installation strategies. The results from a simulation on sample buildings were then extrapolated through a GIS-based analysis to large urban areas at LOD0, showing their potential for such systems. However, the validation of the results obtained with such a method is missing. Moreover, it can be assumed that the integration of morphological analyses to estimate the WWR with simulation of more detailed geometric models (LOD 2) could lead to more accurate results.

The uncertainty due to Level of Detail (LOD) in environmental analyses, including simulation of solar irradiation, will be further discussed in Section 4.1.5.

### 4.2.2 Energy generation potential

The energy generation potential is directly linked to the results of Section 4.1. The electricity production is in fact mostly proportional to the POA irradiance, if we assume that the array is coplanar with the building surface, which is the case for most BIPV applications, as we did in this thesis (the use of tilted arrays on flat roofs will be analyzed in Section 8.2). Many urban-scale studies are limited to this first step, considering that the higher the solar irradiation, the greater the potential generated electricity. As pointed out by Jakubiec and Reinhart [132], "the PV performance is dependent on many factors which are unknown at the time of making a conceptual irradiation map such as module efficiency, panel orientation, wiring, and equipment and maintenance conditions."

Nonetheless, some previous studies analyzed the energy generation potential by coupling a solar radiation model with a PV module performance and, in some cases, to system and array performance models.

Table 4.9 shows a list of some precedent works that have taken into account the energy generation potential of PV modules. It can be seen that most of the studies use simpler models than those presented in Section 2.2.6. Moreover, the effect due to building integration is usually neglected by the

*Table 4.9 – List of models for PV energy generation potentials applied in urban-scale solar potential assessments.*

| Study | Module | System | Inverter |
|---|---|---|---|
| Fath et al. [81] | Fixed $\eta$ | Performance Ratio | - |
| Jakubiec and Reinhart [130] | Fixed $\eta$ with temperature coefficient | - | - |
| Freitas et al. [89] | Fixed $\eta$ with temperature coefficient | Mimumum current over a string | Fixed $\eta$ |
| Brito et al. [36] | Fixed $\eta$ with temperature coefficient | - | - |
| Chuprikova [57] | Empirical model for irradiance effect and temperature coefficient | - | - |
| Eicker et al. [78] | Fixed $\eta$ | Performance Ratio | - |
| Costanzo et al. [62] | Fixed $\eta$ with temperature coefficient | - | Fixed $\eta$ |
| Murshed et al. [191] | Fixed $\eta$ with temperature and optical losses coefficients | LBOS coefficient | - |

simplified temperature models.

It should be noted that these models are usually applied to conventional commercial modules, such as crystalline silicon modules. Emerging technologies, such as bifacial modules, are not included, while they could be implemented on solar radiation models including a reflection model (Table 4.1) as it is currently tested at the PV-array scale (Section 2.2.6.1).

### 4.2.3 Economic potential

Fath et al. [81] showed that in the city of Karlsruhe in Germany, the facades, despite representing more than 70% of the available surfaces and accounting for 41% of the total irradiation, provide only 13% of the economically-feasible solar energy production. The suitability on an installation is in fact also dependent on the financial feasibility, i.e. whether the energy generation is enough to provide an adequate return to the investor. The investor can be either the owner of the building or an Energy Service Company (ESCo) renting the roof space for a solar installation.

The PV-suitability of building surfaces is usually calculated by the achievement of a minimum solar irradiation threshold expressed in kWh/m$^2$ [59, 132], in kWh/kWp [170], or as a ratio of the maximum irradiation [86]. The threshold can be defined according to a rule-of-thumb economic assessment [19, 59] or a maximum payback time [81, 132]. The payback-time is usually calculated as the number of years necessary to get a positive Net Present Value [81, 132].

It is usually assumed that the investor corresponds to the building owner [81] and a maximum acceptable payback time is defined, regardless of the type of building ownership (e.g. private or institutional investor). However, Schalcher et al. [263] showed that different building owners do not have the same attitude regarding the building renovation interventions, because of the different constraints regarding, notably, single-family houses, co-owned buildings, and buildings for rental. Moreover, the investment costs should also be taken into account, as they may be relevant due to owners' budget restrictions or financing possibilities [128, p. 123]. It can be argued that similar considerations should be made also for PV installations, especially if they imply building renovations.

The regulatory framework (see Section 2.2.7) has also a large influence in the financial viability of solar installation. Germany and Italy, two countries with a very high share of PV energy production,

benefited from generous feed-in tariffs in the past under a net-metering scheme. In this framework, the return of investment is less subjected to variations of the financial context, as the feed-in tariff is usually guaranteed for a fixed amount of years. The investor is hence encouraged to maximize the annual solar energy yield, regardless of the actual fluctuations of the market electricity price over time. Conversely, under a net-billing scheme, the price of electricity sold is usually higher than the one injected into the grid. Depending on the contract with the energy utility company, these prices might also change during the day and be updated regularly to reflect the actual price of the electricity in the market. If self-consumption is allowed, from a financial point of view it becomes then particularly interesting to maximize the self-consumed energy. We will describe self-consumption-oriented strategies in Section 4.2.3.1

To summarize, we have seen that the conditions for financial profitability are changing depending on multiple factors, which are:

- the type and financial attitude of the investor;
- the general economic situation, e.g. the inflation and interest rate of alternative placements;
- the regulatory framework, e.g. the presence of a feed-in tariff or a self-consumption scheme.

Therefore, it is difficult to define a comprehensive economic PV potential at the urban scale, which should be rather defined on a case-by-case basis. However, we can highlight two main methods and their obstacles:

- a minimum threshold can be calculated by each investor to reflect their own conditions; however, the definition of this minimum threshold is subject to several assumptions about external conditions (e.g. the electricity cost and, in absence of a feed-in tariff, the price of sold electricity);
- in absence of a Feed-in tariff (FiT) and when self-consumption is allowed, the maximization of the self-consumed energy can be considered a proxy of the financial viability of the installation; however, the calculation of the self-consumption rate relies on the assessment of the electricity demand, which is highly dependent on building use and occupancy behavior.

#### 4.2.3.1 Self-consumption

Luthander et al. [175] provides an extensive literature review on self-consumption management. Self-consumption provides benefits to both the PV installation owner, by increasing the value of the electricity production, and to the grid manager, by avoiding for example high net load variance [175, 91]. It can be defined as the share of the electricity production that is directly consumed by the building on which the PV system is installed, that is:

$$\mathrm{SC} = \frac{C}{B+C}, \tag{4.1}$$

where $C$ is the absolute self-consumption and $B+C$ is the net generation (Figure 4.4)..

Directly related to the self-consumption is the self-sufficiency, which is the share of electricity consumption that is covered by on-site production, that is:

$$\mathrm{SS} = \frac{C}{A+C}, \tag{4.2}$$

where $C$ is the absolute self-consumption and $A+C$ is the net load (Figure 4.4).

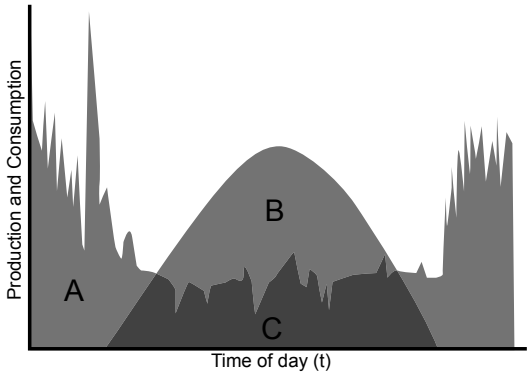


*Figure 4.4 – Schematic graph showing the net load (A + C), net generation (B + C) and absolute self-consumption (C) from a building solar installation.*
*Adapted from Luthander et al. [175]*

Both these indicators are defined by the instantaneous power consumption $L(t)$ and generation $P(t)$. The power generation utilized on-site (C) is also defined instantaneously ($M(t)$) and is expressed as follows:

$$M(t) = \min\{L(t), P(t)\}. \tag{4.3}$$

In this work we will use a hourly resolution ($t = hour$) and the indicators will be integrated over the year.

Self-consumption can be maximized by two means:

- Demand-Side Management, e.g. by shifting the electricity consumption of the building during daytime;
- storage, e.g. with a battery, possibly the one of an electric vehicle;

In addition to these methods, the optimized arrangement of PV modules can also improve the self-consumption, by choosing the locations that give the best match between the demand and production curves [174]. Freitas et al. [91] implemented genetic algorithms for the arrangement of the solar system to, among other scenarios, maximize the self-sufficiency and minimize the net-load variance on the electric grid. However, these algorithms heavily rely on computation and availability of high-resolution energy demand data, which make their applicability to the urban-scale unsuitable, unless similar trends are found across different urban areas.

### 4.2.4 Architectural integration potential

The architectural integration, i.e. the design issues of PV installation on building surfaces, are seen as a major factor for the acceptability of such systems by the population and the heritage protection services [108, 188]. Legal constraints may also deal with building-integration aspects. This is the case of Switzerland, where the legislation (OAT, 2014 Art. 32a) grants a waiver of building permission only for roof-integrated solar systems. It is hence crucial to include the architectural integration constraints in order to define the effective BIPV potential.

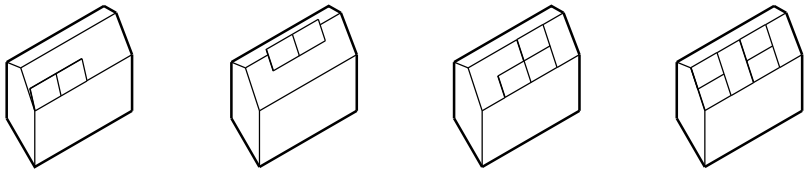

*Figure 4.5 – Four example or installations non respecting the SurHib [232] criteria (from left to right): coplanarity, respect of lines, shape and grouping.*

**Arrangement guidelines**

The architectural quality of a BIPV installation is particularly difficult to assess as it depends on several, mostly subjective, factors. To this end, some criteria have been established for assessing the coherence of the PV installation with the "global building design logic" [188], such as the ones proposed by the IEA PVPS Task 7 "Photovoltaics power systems in the built environment" [265] and the IEA-SHC Task 41 "Solar Energy and Architecture" [189].

Moreover, in the framework of the Swiss research project "Sustainable Renovation of Historical Buildings" (SuRHiB) [330], some architectural guidelines for the integration of solar technologies in historical roofs were developed on the basis of various existing cantonal guidelines [326]. A distinction was made between criteria, "focusing on shape and emplacement of the solar panels", and recommendations, dealing with more subjective aspects, e.g. the visual impact, and are hence conceived as non-mandatory suggestions for the designer. The criteria consist of:

- coplanarity, i.e. "solar panels should have the same orientation and the same inclination as the construction element"
- Respect of lines, i.e. solar panels "should respect the lines which provide the outline of the construction, particularly in the upper part"
- Shape, i.e. the use of a regular, rectangular shape better suits the shape of most buildings
- Grouping, i.e. scattered panels should be avoided
- Accuracy, i.e. "solar panels added to or integrated into a building must be perfectly connected or inserted into the construction element"

The application of the SuRHiB criteria was tested on eight roof typologies, facade, and installation in annex construction or in buildings with a decentralized plan [232] and ranked on a scale defining the level of feasibility of the intervention for each criterion. This method allows the planner to evaluate the criticality of the installation of solar panels for each type of installation. However, it does not suggest any integration strategy for the analyzed building typologies, so it cannot be used in combination with an energy production assessment.

In general, the integration guidelines, which have been applied by many public authorities in Switzerland, such as the Canton of Geneva ("respect of roof contours and lines parallelism", [281]), are mostly based on a qualitative evaluation that is made on a case-by-case basis by the designer or the building permission authority. In order to overcome the subjectivity of such criteria, [320] proposed a method based on saliency maps objectively quantifying the visual impact of solar installations. However, this method is suitable for architectural-scale design problems rather than urban planning assessments.

At a larger scale, the SuRHiB guidelines were applied as a criterion in a GIS-based multi-criteria assessment in the historic city center of Santiago de Compostela (EFFESUS project), the other criteria being

*Table 4.10 – Example of a calculation matrix using the LESO-QSV method [188].*

| Acceptability grid | | Zone sensitivity | | |
|---|---|---|---|---|
| | | Low | Medium | High |
| Field visibility | Low | 0 | 1.5 | 3 |
| | Medium | 1.5 | 3 | 6 |
| | High | 3 | 6 | 9 |

the level of protection of the buildings and the irradiation threshold [170]. Each rooftop intervention was classified as “allowed”, “partially allowed” or “not allowed” based on the aggregation of the criteria and recommendations. However, the authors did not mention the weighting scheme they used. Moreover, this method does not define the degree of suitability of different surfaces but rather assesses each building as a whole

In Switzerland, similar guidelines have been integrated in the federal legislation (see Section 3.1.2 and Figure 3.1) as a requisite for obtaining a building-permit waiver.

#### Sensitivity and visibility

There is a consensus on the fact that the visual acceptability of a type of integration depends on the sensitivity of the building it refers to [170] and/or of its surrounding area Bahjejian [15], Munari Probst and Roecker [188]. Different methods have been used in the literature to assess the sensitivity, based on the quality/historic relevance of each building [170], or on the type of urban areas [188].

Munari Probst and Roecker [188] defined “criticity” as an integrated indicator of sensitivity and visibility of a solar installation. This is calculated by constructing an evaluation matrix of the two criteria allowing a full compensation between the two (Table 4.10).

Florio et al. [84] developed an evaluation method for accounting for the visibility of solar systems at different scales of analysis.

### 4.2.5 Synthesis and discussion

In this section, we have analyzed the state of the art of methods for analyzing the different solar potentials at the urban scale. Based on this analysis, we can identify the following gaps:

- there is a lack of advanced energy generation (PV, system, inverters) models applied to urban-scale solar irradiation assessments; a part from some exceptions, we can notice a gap between the advanced solar radiation models that have been reviewed in the previous section Section 4.1.1 and the subsequent use of their output at high spatial (PV module) and temporal (hourly or higher) granularity for simulating the PV performance under real installation conditions;
- previous works focused on one or few potentials, while neglecting the integration of multiple potentials, e.g., taking into account both the financial and architectural integration constraints in a comprehensive method;
- also concerning the architectural integration, we have seen that the arrangement of PV modules is often used by public authorities as an evaluation criterion for the acceptability of the installation; we argue then that this criterion could be used also in urban scale analyses for better identifying suitable installation locations or arrangements.

## 4.3 Decision support for urban energy planning and subsidization

In this section[8], we will focus on the decision-making process related to solar energy and building energy refurbishment. We have seen that many works focused on the assessment methods, while the subsequent use of the information to take a decision is usually neglected.

Solar cadastres are meant to answer the most typical questions asked by building owners: "Is my building suitable for energy installations?"; "If yes, how much could I produce?". Energy planning tools are meant to answer a wider range of questions from a wider range of different stakeholders.

Finally, some of the stakeholders are often faced to the allocation of limited resources to encourage the deployment fo solar energy. Despite the huge potential of solar energy, its yield is often limited or slowed by practical limitations, related for example to regulation, funding and design constraints. Given a restricted number of resources, which can be intended for example as incentives but also as spatial locations, it is interesting to analyze the possible allocation methods. Therefore, we review some of the most typical allocation mechanisms.

We are also interested in allocation methods as a way to assign public incentives to boost the use of renewable energy. These public incentives are not necessarily monetary. Governments in fact can play a role through "subsidies, tax breaks, infrastructural allocation, preferential credit treatment, and permissions or licenses" [80].

### 4.3.1 Solar cadastres

A solar cadastres or solar map is "a GIS system providing the annual solar irradiation on building surfaces (roofs and/or facades), mostly accompanied by the output of solar thermal or photovoltaic systems, and connected to a website" [140].

Solar cadastres (or solar maps) are tools to provide decision-makers with information about the suitability of a given surface for the installation of solar power systems, such as photovoltaic or solar thermal. They are usually conceived as web-based mapping tools in which the solar potential is displayed as false-colors overlays on maps or ortho-photos of an urban area. Dean et al. [67], Jakubiec and Reinhart [132], Kanters et al. [140] provide an extensive review of solar cadastres in the United States and Europe. The long list of available solar cadastres indicates also the popularity of these instruments among many local authorities, which use them as part of their public investment strategies to encourage the use of solar energy (Section 2.4).

Most of the cadastres in the US listed by [132] are based on raster models using *r.sun* [248] or PVWatts [73] and they are targeted to roofs. A Daysim-based method [132] has been integrated in the Mapdwell solar cadastre [22], also targeted to roofs. Despite the earlier research on façade analysis (e.g., Carneiro et al. [46], Catita et al. [49]), the interest of solar cadastres is still mainly roofs, arguably for financial reasons. However the Swiss confederation recently released a country-wide solar cadastre (referred in this thesis as SFSC) including both façades and roofs. Despite the advanced 3D information (Appendix A.1.4) used for the analysis, the visualization is still 2D. Its features will be more extensively described in a comparison with this thesis proposed method in Section 13.3.

[8] This section contains some excerpts from a published journal paper [226]: Peronato, G., Rastogi, P., Rey, E., & Andersen, M. (2018). A toolkit for multi-scale mapping of the solar energy-generation potential of buildings in urban environments under uncertainty. *Solar Energy*, 173, 861–874. https://doi.org/10.1016/j.solener.2018.08.017. The text is reproduced here as a courtesy of the publisher and with the agreement of the co-authors. G.P. contributed by conducting and writing the review.

As shown by Kanters et al. [140], the suitability assessment of solar cadastres is generally based on minimum irradiation thresholds. In some cases, the choice of these thresholds is justified by financial assessments to guarantee the payback time of the installation [195, 132, 22]. Surfaces are often classified with different levels of suitability depending on their solar irradiation, such as “reasonable”, “good”, “very good” [140].

As we will see in Chapter 6, error, risk, and uncertainty vary depending on the selected threshold. However, solar cadastres generally have a deterministic approach, which neglects the uncertainty of the result and the concomitant risk in the decision. Thresholds are also sensitive to the geometric regularity of the arrangement of solar modules, an aspect that we will investigated in Section 11.3.3.3.

In addition to thresholds, another method to provide information about solar potential is to attribute to each building a solar score. The solar score is usually calculated by reference to a best-case installation, as in the Mapdwell solar maps [22], or by normalizing the data to the best and worst values in a given location, as in the SunNumber website [182]. This method facilitates comparisons between locations with non-homogeneous climate conditions as the score is relative to the specific conditions, allowing cross-country comparisons. However, the score still disregards other factors of uncertainty in the calculation which affect each building differently, such as vegetation modeling.

Solar cadastres focus on the potential of individual buildings, and in some cases differentiate the potential among the surfaces constituting the building envelope, while neglecting the aggregated potential of urban blocks or entire urban areas. They are targeted in fact to building owners, and often have an educational goal [67]. They are sometimes used as back-end planning tools by municipalities, though mostly limited to the evaluation of their own real estate properties [140] rather than planning purposes.

### 4.3.2 Online PV calculators

Online PV calculators are complementary tools to solar cadastres, which can be used both by building owners and solar energy professionals to have a quick estimate of the solar energy potential of a given solar energy installation. Unlike solar cadastres, they usually have a simplified modeling of shading geometry, using for example angle-based obstructions for the horizon, but allow the user to design a custom installation (e.g., by choosing the tilt and size of the array).

The most popular online PV calculators are PV-GIS [249], which is based on the *r.sun* model [248] (see also Section 4.1.1), and PVWatts, which is based on the homonym model developed at NREL [73] (see also Section 2.2.6.3).

PV-GIS originally provided radiation databases for Europe and Africa and only recently introduced a worldwide radiation database, while PVWatts natively supports the entire world but it is focused on the US market. There are also country-specific tools, which provide typical parameters for the local context. For example, the calculator of Swissolar [294] also estimates the investment cost, incentives and tax deductions for Switzerland.

### 4.3.3 Energy-planning tools

Compared to solar cadastres and PV calculators, energy-planning tools focus more explicitly on a wider range of stakeholders, particularly utility companies, and municipalities. Ouhajjou et al. [205] reviewed

some of these tools focusing on the integration of energy systems in urban environments (Table 4.11, 1-6).

Among these tools, Semergy [176] is particularly interesting as it is focused on the building energy refurbishment process. It provides a multi-objective optimization environment that helps choose the best renovation strategy. However, the tool is mostly intended to building-scale analyses, while the related city-planning tool (Ecocities) has been only recently developed. However, both software have only a partial support for PV integration strategies.

Ouhajjou et al. [204, 206, 207] proposed an ontology-based urban energy planning providing a classification of the PV-suitability of buildings from each stakeholder's perspective. However, this method then focuses on negotiation and consensus between the different stakeholders rather than the robustness of the single decision.

Fonseca et al. [86] developed a tool for the analysis and optimization of building energy systems, packaged as a ArcGis plugin. The tool, called City Energy Analyst, is still growing and expanding its features, which span from advanced energy modeling (including Life Cycle Analysis) to decision support, through multi-criteria assessment, 3D visualization and benchmarking. It recently included a module for PV simulation based on Daysim, while the platform is oriented towards the integration of multiple energy sources. Hong et al. [113] (CityBES) and Cerezo et al. [53] developed tools that are oriented to the city-scale building energy modeling, with a focus on retrofit and other energy interventions on existing buildings.

Ranalli et al. [239] coupled SAM technical-economical modeling. Through GIS spatial analysis, they created different scenarios (e.g. use of East-West-tilted roofs) to inform decision-makers on different planning policies to adopt. There is however a gap between the techno-economical analysis and the GIS analysis, which is limited on classifications based on tilt, azimuth, orientation rather than on modeling context-specific solar irradiation.

With the notable exceptions of CEA and CityBES, it seems that the reviewed tools are focused on techno-economical modeling or optimization, rather than on the integration between physical modeling and visualization-oriented decision-making. It seems thus that there is a double gap with, on the one hand, the most advanced solar radiation models seen in Section 4.1.1 and 3D geometry described in Section 2.3.3.2, and, on the other, with the user-friendly web interfaces of solar cadastres of (Section 4.3.1) and PV calculators (Section 4.3.2).

### 4.3.4 Allocation mechanisms

In the field of solar and building energy refurbishment subsidies[9], we find many of the mechanisms that were listed in Section 2.5.1

Funding for public policies encouraging renewable energy and building renovation is usually limited [116] and the demand cannot be completely satisfied. For solar energy, we can cite the cases of Switzerland [141] and Austria[157], which were forced to adopt waiting lists to face the high number of requests for feed-in tariff. These waiting lists are a consequence of a cap in the total amount of subsidies that can allocated.

[9] The DSIRE website website lists all incentive programs and policies promoting renewable energy and energy efficiency in the US: http://programs.dsireusa.org/system/program/tables [Last accessed on April 22, 2018]

*Table 4.11 – Non-exhaustive list of energy planning tools.*
*Table adapted and updated from Ouhajjou et al. [204]*

| | Study | Main focus | Scale |
|---|---|---|---|
| 1 | EnerGis [94] | Evaluation of building energy needs | City |
| 2 | SynCity [144] | Modeling of urban energy systems | City |
| 3 | UrbanSim [310] | Land-use scenarios development | City |
| 4 | CommunityViz [160] | Policy scenarios development | City |
| 5 | Semergy [176] | Automatic data retrieving + refurbishment decision support | Building |
| 6 | MEU [43, 213] | Optimization of energy flows based on CitySim [256] | Neighborhood/City |
| 7 | Ouhajjou et al. [204] | Ontology-based planning support for PV deployment | Neighborhood/City |
| 8 | City Energy Analyst (CEA) [86] | GIS-based optimization of building energy systems | Neighborhood/City |
| 9 | CityBES [113] | Building energy modeling supporting energy retrofit measures | Neighborhood/City |
| 10 | Cerezo et al. [53] | Building energy modeling supporting energy interventions (PV and demand side management) | Neighborhood/City |
| 11 | Ranalli et al. [239] | GIS-based decision support for solar potential | Neighborhood/City |

Alternative methods are also used, such as competitive bids and lotteries. For example, a former Oregon state incentive program for PV [10] used the former for small systems (5-10 kWp) and the latter for the larger systems.

In some cases, waiting lists are complemented by other allocation methods. A common pre-allocation method is to limit incentives only to interventions achieving a given threshold. This is for example the case for subsidies which require for PV a minimum peak-power installed (e.g. in Oregon, see footnote 10), and for building energy refurbishment a minimum intervention to be implemented (e.g. target U-value of the envelope [11]). This corresponds to a minimum cost to be paid by the participants to join the incentive program, i.e. their *willigness to pay*.

In some cases, this target level can be considered as *skill*, as it is not defined directly by a minimum design requirement but rather as the output of the design. This is for example the case of a maximum energy demand requirement or target energy label after the refurbishment (see for example the case of Neuchâtel in footnote 11), which can be reached by different design approaches, corresponding to different investments. The *skill* of the participant is to reach these requirements with the least investment. However, since post-occupancy evaluations are too difficult to implement, the evaluation is usually done through simplified assessments before submitting the building permit.

Similarly, the California Energy Commission assigns incentives and rebates for PV based on analysis using different performance models [153]: they use PVWatts [73] for existing buildings in their California Solar Initiative (CS) and the 5-parameter model [66], coupled with an inverter model, for the New Solar Homes Partnership (NSHP) program[12]

However, in most other cases, PV subsidies are generally allocated based on the total peak-power installed, with a minimum installation size being necessary to get access to the subsidizing scheme. This criterion does not need any calculation to be done, as it is based only on the size of the system. Moreover, the peak power is not necessarily the maximum power, as at lower temperatures or higher radiation intensities than the Standard Test Conditions the value can be exceeded [96, p. 89]. Access to subsidies is granted based on the willingness to pay, regardless on the actual production (or *skill*) of the

[10] http://programs.dsireusa.org/system/program/detail/3564 [Last accessed on April 22, 2018]

[11] The canton of Neuchâtel has different calculation systems based to assign incentives within the "Building Program" (Section 3.4.1.1): one based on standard maximum transmittance requirements for the envelope, and other two based on the global energy performance as defined CECB© and the Minergie© label systems.

[12] These models have been discussed in Section 2.2.6.3.

system. The rationale behind this is that people will anyway install panels in the best locations, while in reality it might not be always the case.

On the other had, as a limitation of performance-based allocation systems, we should cite that they do not consider the uncertainty associated with the model, which can determine a significant performance gap. Khoury et al. [147] showed for example that, in a representative sample of retrofitted multi-family houses in Switzerland, the achieved energy savings are 30 to 65% of the values estimated in the building permit requests. Chinazzo [54] showed that uncertainty in building performance simulations due to the use of different weather scenario is significant, while it does not influence the ranking of refurbishment strategies. However, this might not be the case when considering different locations and other uncertainty factors (as the ones listed in Section 4.1.5). If the ranking is affected, the fairness of the allocation system is jeopardized, unless the uncertainty is taken into account in the decision.

### 4.3.5 Synthesis and discussion

We have seen the importance for a comprehensive decision-support system for solar potential, which should combine the visualization and interactivity of solar cadastres with the complexity of decisions and the diversity of stakeholders involved. We have highlighted that current evaluation tools such as solar cadasters and allocation systems do not consider uncertainty in the assessment. We can argue that this factor might have an influence in the decision-making process.

We also have seen that most allocation systems for public incentives still rely on waiting lists and simplified methods to deal with the scarcity of funding resources. We argue that these methods are not optimal, as they do not target those investors that could make the most of the incentive. In this sense, we think that the use of decision-support systems for assigning public incentives could improve the efficiency of these mechanisms to boost solar energy and building energy efficiency interventions, as long as they take into account the uncertainty of the prediction model.

## 4.4 Motivation and targeted gap

The use of solar energy in the built environment has become a widespread topic. There are different reasons for that, among which we can cite:

- solar energy is available in every place on Earth;
- PV energy efficiency is constantly improving;
- the integration of renewable energy sources is becoming necessary to achieve building energy targets;
- PV is particularly suitable for building energy applications.

Because of this popularity and interest, there is a large corpus of research that has been developed in this interdisciplinary field. Only in the framework of the Chapter 4, we have reviewed almost 150 papers, some of them including in turn also extensive literature reviews.

This thesis wants to address the topic of solar energy potential in urban environments from the specific prospective of decision support. In this sense, we can identify the followings overall research gaps:

- research on solar potential assessment focused more on assessment methods and advanced models, rather than in the use of results as a support to decision-makers;

- decision-support systems such as solar cadastres are limited in the aggregation scale and granularity of the analysis;
- the uncertainty of the prediction models is usually not considered in the evaluation process.

In order to target these issues, there are different aspects that should be solved with regards to the topics reviewed in the state of the art. We present here below the goals of the thesis connected to the section-specific gaps.

#### Urban-scale simulation of solar irradiation

There is currently a gap between detailed simulation tools for single installations and those applied in large-scale analysis. This is in some cases motivated by the fact that the latter do not require the same level of detail as the former. However, we can argue that for building-installed solar systems, and in particular building-integrated ones, the level of detail of the analysis (in terms of geometry but also of predicted POA irradiance) should be as close as possible to reality.

The main barriers are hence due to:

- the lack of information available at the urban scale;
- the computational cost needed for large-scale simulations.

In both cases, this thesis aims at pushing the boundaries of the analysis in terms of granularity (spatial and temporal), while using the state-of-the-art models (Daysim), geodata (LOD2+ city models, high-resolution LiDAR point-clouds) and long-time weather data that are currently available in Switzerland. This will allow to run the analysis

- using a fully-3D city model for the analysis, including vertical discontinuities (e.g., overhangs) and 3D-reconstructed vegetation;
- integrating inter-reflections by backwards ray-tracing;
- using multiple simulations scenarios to account for variable and uncertain boundary conditions, such as vegetation and weather.

At the same time, this thesis will investigate the error that this method and data provide with regards to different ground-truths, such as, for example, hourly simulations with Radiance `gendaylit` and manually reconstructed 3D-models, which are not or are only hardly applicable at the urban scale.

#### Potential for building-installed solar systems

The need for a holistic indicator for the potential building-installed solar systems faces different problems, in particular the lack of data for urban-scale analysis. This is particularly true for financial indicators, which depend on the choices of the investor, and for the location potential, which depends on the Level of Detail (LOD) of the geometric model.

Acknowledging that an integrated solar potential is probably not a realistic goal, this thesis aims at bridging some of the individual potentials to reach a more comprehensive analysis. In particular, it aims at achieving a better integration of the *energy generation potential* with the *theoretical potential* constituted by the Plane of the Array Irradiance, by linking dynamic PV performance models to the results of the hourly irradiation simulations. Moreover, the thesis will also provide some novel methods in the single potentials analysis, such as:

- for the *architecture integration potential*, taking into account the arrangement of the PV modules will contribute to the design of an installation which is expected to pass some basic visual acceptability criteria;
- for the *economic potential*, the integration of a method to include the hourly self-consumption in the sizing of the system will provide a building-specific threshold, which can be considered a proxy of the financial and environmental viability of the installation.

**Decision support for urban energy planning and subsidization**

Allocation methods based on first-come-first-served principles are too simplistic and do not take advantage of the advancements in evaluation methods. Even if they are perceived as fair, their efficiency is scarce, as they do not target the aggregate welfare. Differently, we argue that the use of public money should be done through fair and efficient allocation methods, as long as effective evaluation systems are available.

With reference to the case of Switzerland that has been presented and discussed in Chapter 3, we can also raise some issues regarding the current system. Because of the uncertainty in the authorization process and consequent high-risk of litigation, we argue that the criteria defined by the Federal Spatial Planning Ordinance for roof-adapted installations (Section 3.1.2) are not a robust criterion for choosing suitable locations for installing PV systems. Similarly, incentives for building energy refurbishment have shown their limits, as it has been argued [293] that the same building refurbishment rate would occur without any incentive.

This thesis thus aims at providing a smart, need-based algorithms to detect which buildings or spatial locations would benefit more of a retrofit intervention. This could help local authorities to target investments where they are most needed as well as large building owners to prioritize the refurbishment of their building stock.

Often the evaluations made on the basis of simplified models and inputs are neglected or discounted. In this thesis, we want to couple the advanced simulation method presented above in an innovative planning-support system, targeting different decision makers and spatial resolutions. Moreover, we want to acknowledge uncertainty in evaluations, so as to provide robust decisions based on the multiple modeled scenarios.

To summarize, here are the specific goals with regards to decision-support:

- determine a robust ranking of spatial locations accounting for fundamental environmental uncertainties;
- show results using multiple indicators and spatial resolutions adapted to the different decision-makes;
- provide a 3D visualization interface making the most out of the 3D geodata used for the analysis.

# Part II
# Preliminary development and test applications

# 5 Towards an integrated analysis and assessment method

This chapter is meant to introduce Part II, which assembles several studies that were developed in the early phase of the PhD. These studies were conducted as preliminary investigations to define the content of the thesis and develop the method that will be presented in Chapter 11. The main goals of this Part II can be summarized as follows:

- show the importance of taking into account some uncertainty factors investigated by the thesis, such as:
  - Vegetation (Chapter 7);
  - Weather (Section 9.2);
  - Arrangement of PV modules (Chapter 8)
- define parameters that provide a good trade-off between accuracy and simulation time, as in the case of the sensor grid resolution (Section 6.2);
- select the most appropriate Level of Detail for the analysis (Section 6.1);
- test algorithms and workflows, in particular for 3D reconstruction, as for vegetation (Chapter 7);
- cross-compare analysis conducted at different granularities, datasets and levels of automation to assess the uncertainty related to the use of coarser yet automated procedures or datasets, as for the studies on the LOD (Section 6.1) and tilted arrays on flat roofs (Section 8.2);
- test extreme modeling scenarios defining the confidence intervals of the input data, as in the case of weather (Section 9.2) and vegetation (Chapter 7).

Chapter 9 contains two studies that conceptually follow one of the thesis main scopes, i.e., testing the robustness of solar potential assessments under different scenarios, as will be done in the thesis case-study application (Section 12.2.3), but are applied to a design decision, i.e., the choice between different design proposal, rather than a planning/policy one, i.e. the ranking of different urban locations.

The findings of the Part II that will be used in the core development of the thesis (Chapter 11) are listed at the end of each chapter and also summarized in the final chapter (Chapter 10).

The studies are ordered here starting from the analysis of fundamental modeling parameters to more applicative studies dealing with decision-support problems. This order does not follow the chronological sequence in which the studies were actually conducted during the PhD. For this reason, some studies contain different parameters and assumptions, due to their development at different stages of the PhD.

## 5.1 Characteristics of the preliminary analysis method

The different studies presented in Part II use partially-distinct methods, tools and datasets. However, we can identify some general characteristics that define a preliminary analysis method, that will be subsequently refined in Chapter 11:

- All studies are conducted with Radiance-based solar radiation models, which use backwards raytracing to account for inter-reflections and shading from the 3D geometry;
- The urban environment is represented through a vector 3D city model, either of new designs (Chapter 9) or existing buildings (all other chapters), at different LODs.

The main differences within these studies concern the Level of Detail (LOD) and the temporal granularity. Initial studies were conducted with either LOD1 or LOD2, because of their wider availability, and only later studies (Sections 6.2 and 8.2) used LOD2+ (i.e., including overhangs and rooftop superstructures), whose availability is still limited. Initial studies used time-cumulated analysis (normally, yearly), while subsequent studies used hourly resolution, so as to verify time-based error as in Section 6.2.2, or to include more advanced PV performance models or self-consumption models, which were though not applied here.

The studies also tested the suitability of the Rhino-Grasshopper 3D modeling environment to handle large geo-datasets. This platform, which is normally used with smaller-scale objects, was chosen for its powerful 3D and visual scripting features as well as for the easy integration with the simulation engines, trough existing open-source interfaces, such as Ladybug/Honeybee [259]. The final technical implementation of the modeling and simulation workflow will be only described in Section 11.2.4 and Section 11.3.4, but has been developed thanks to the studies of Part II, in particular the automation of a tile-based analysis (see Section 11.2.4).

Part II's studies focus on solar irradiation or feature a simplified PV performance model, i.e. with a fixed efficiency coefficient. The evaluation was normally conducted on a single indicator of solar potential, i.e. the annual solar irradiation normalized by footprint or floor surface. With the exception of the studies focusing on decision support (Chapter 9), this Part II is in fact mostly focused on the first development of a modeling workflow which will be further defined in Section 11.2. The final analysis method presented in Chapter 11 will include a wider simulation and decision-support framework, and will introduce novel visualization features.

# 6 Sensitivity of solar irradiation to modeling parameters

This chapter contains some preliminary analyses to the use of 3D city models in urban solar potential assessments. As discussed in Section 2.3.1, 3D city models are a virtual representation of reality that comes with various simplifications associated with the concept Level of Detail (LOD). The choice of a coarser LOD can be motivated by the difficulty of getting high-resolution data through remote sensing and photogrammetry techniques, but also by a precise intention of keeping the 3D model simple so as to facilitate its use in computer-based analysis.

Paradoxically, 3D models have to be discretized in order to be used in many environmental analyses. The discretization error is then added to the simplification associated to the original "continuous" 3D model. As for the choice of a low LOD, the choice of a low resolution might be aimed at facilitating the use of 3D models in computer-based analysis, in terms for example of computation time or memory handling. Similarly, ambient settings of a ray-tracing calculation also involve a balance between accuracy and computation time.

This chapter is aimed thus at evaluating the influence of the 3D model representation and discretization accuracy on solar potential assessments through sensitivity analyses. We will evaluate more specifically the impact of the LOD, of the discretization of city 3D models, and the main raytracing ambient settings on the predicted solar irradiation. In the analyses, we will calculate prediction error with reference to a ground truth, which will be either a finer LOD or a higher discretization resolution.

In solar potential assessments, solar irradiation is the main physical parameter influenced by the urban environment, notably in terms of shading and reflections. Also other micro-climatic parameters, such as for example temperature and wind, are influenced by the urban environment, but can be considered as less crucial for the PV performance and will not be investigated here. We will thus focus on solar irradiation and consider it a proxy for the photovoltaic potential.

To develop the studies presented in this chapter, we used 3D city models (of either single buildings or urban areas) from real case studies in Swiss cities. We argue in fact that alternative methods, such as procedural modeling used in related studies (e.g., [23, 28]), cannot adequately reproduce the specific morphological characteristics and variety of buildings in Swiss cities, especially the historical ones, in terms for example of roof shapes and super-structures. Moreover, these preliminary studies were also the occasion to test different 3D city models, of different LODs and sources, for the implementation in the final assessment workflow presented in Chapter 11.

## 6.1 Level of Detail

In this section[1], we investigated the sensitivity of solar irradiation to the Level of Detail (LOD) (see Section 2.3.1) of the 3D city model. We compared the results obtained in reference 3D models at LOD3 with those obtained using coarser LODs. The goal was to assess the confidence of results based on LODs lower than LOD3 and support the choice of the appropriate LOD for the final workflow implemented in this thesis.

### 6.1.1 Methodology

We selected four sample buildings (Figure 6.1) in the city of Neuchâtel from different construction periods and urban contexts that present varied roof shapes, types of façade and roof elements, as summarized in Table 6.1.

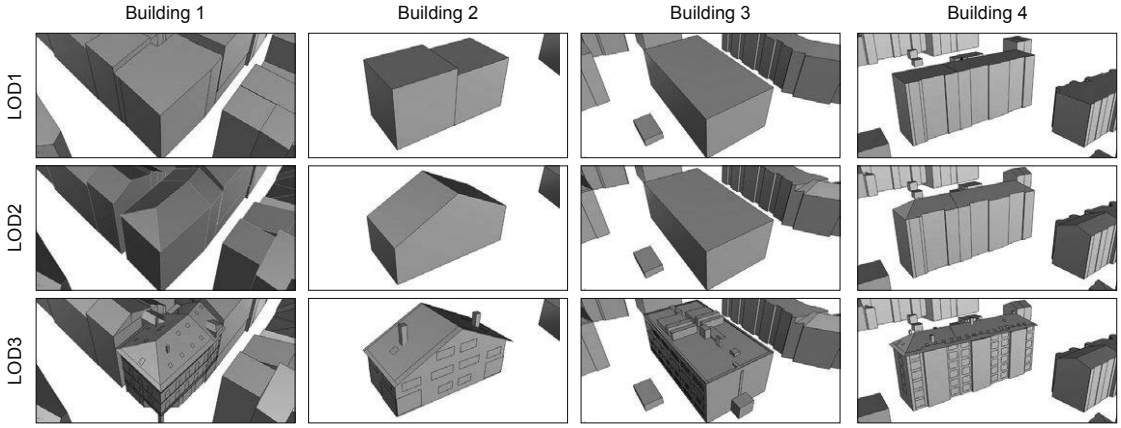


*Figure 6.1 – The case-study buildings at different LODs. See also Table 6.1.*
*Source: Peronato et al. [220]*

*Table 6.1 – Characteristics of the analyzed buildings. Their location is shown in Figure A.2.*

| Building | 1 | 2 | 3 | 4 |
|---|---|---|---|---|
| Period | 1961-70 | 1946-80 | 1986-90 | 1961-70 |
| Context | Historical center | Suburban | Urban | Urban |
| Main use | Residential | Residential | Offices | Residential |
| Roof type | Hip | Gable | Flat | Hip |
| Roof elements | Chimneys, Overhang, Windows, Dormers | Chimneys, Overhang | Chimneys | Chimneys, Overhang, Windows |
| Façade elements | Windows | Windows | Windows | Windows, Balconies |

[1] This study was carried out in the framework of two semester projects [31, 288] supervised by the author, which were later summarized in a conference paper. The following paragraphs contain excerpts from the original publication [220]: Peronato, G., Bonjour, S., Stoeckli, J., Rey, E., & Andersen, M. (2016). Sensitivity of calculated solar irradiation to the level of detail: insights from the simulation of four sample buildings in urban areas. In *PLEA 2016 - Cities, Buildings, People: Towards Regenerative Environments, Proceedings of the 32nd International Conference on Passive and Low Energy Architecture; (Vol. 2)*. Los Angeles. The text and figures are reproduced here as a courtesy of the conference organizers and with the agreement of the co-authors. G.P. contributed with the design and supervision of the project and writing of the paper. We follow here the same structure as the Chapter 11 to facilitate the comparison with the final workflow implemented in this thesis.

The total annual irradiation *Irrad* calculated as follows:

$$Irrad = \frac{\sum_{s=1}^{n} irrad_s \cdot area_s}{area_{footprint}}, \tag{6.1}$$

where $n$ is the total number of surfaces $s$ of the considered building and $irrad_s$ is the mean annual irradiation expressed in kWh/m$^2$ of a surface $s$. The results are normalized by the area of the building footprint so as to be able to compare the results of different buildings.

We then calculated the relative error *R.E.*, as a whole and separately for façades and roofs, assuming the LOD3 model as the ground truth:

$$R.E. = \frac{Irrad_{LOD_{1,2}} - Irrad_{LOD_3}}{Irrad_{LOD_3}}, \tag{6.2}$$

where a positive (respectively, negative) result means an overestimation (respectively, underestimation) of the total annual solar irradiation (*Irrad*) compared to the reference LOD3 model.

#### Modeling

We used 3D models of the case-study buildings at LOD1, LOD2 and LOD3 (Figure 6.1). The LOD3 model is considered here as the ground truth, i.e., a model representing the reality as much accurately as possible for what concerns the geometry of the urban canopy. The LOD1 (Appendix A.1.2) and LOD2 (Appendix A.1.3) models were automatically reconstructed in the software BuildingReconstruction [307] and their geometry visually checked and manually corrected in Rhinoceros. The LOD3 was manually 3D-modeled in Rhinoceros on the basis of the LOD2 model using photos and orthophotos as a reference for the added details.

A terrain mesh was created through Rhinoceros's MeshPatch command (Delaunay's triangulation) using the points of a Digital Terrain Model (DTM) at a 1-m distance resolution.

For the surrounding buildings, the automatically-reconstructed model was used at the same LOD as the simulated building, except for LOD3 for which the automatically-reconstructed LOD2 model of the context was used.

The materials were defined as Lambertian diffusers with 30% reflectivity for building surfaces and 10% for the ground, as suggested by the IES LM-83-12 approved method IESNA [120].

#### Simulation

The solar radiation simulation was conducted in Diva-for-Rhino [129], a graphical interface to the Radiance/Daysim [244] simulation engine, using its default Radiance parameters. In particular, the ambient bounces (`-ab`) parameter was set to 2, so that one reflection from the surrounding context is taken into account in the radiation model. A sensor grid was placed with the dedicated Diva-for-Rhino tool at a 1-m spacing, which was considered a suitable value for urban scale simulations [184].

### 6.1.2 Results

The results of the total annual solar irradiation (*Irrad*, Equation (6.2)) and Relative Error (*R.E.*, Equation (6.2)) have been plotted as a function of the minimum irradiation thresholds that have been considered appropriate for this study (400-1200 kWh/m$^2$), in both false-color maps (e.g., for building 1 in Figure 6.2) and line graphs (Figure 6.4 and Figure 6.3).

Figure 6.2 shows the irradiation of the building surfaces of building 1 for some notable thresholds. We can notice that no part of the façades can reach the 750 kWh/m$^2$ threshold in LOD1 and LOD2, while in LOD3 the limit is at 700 kWh/m$^2$, because of the effect of the overhangs. Starting from an 850 kWh/m$^2$ threshold, in LOD2 and LOD3 the part of the roof exposed to the North is considered as non-suitable, while in LOD1 the entire flat-modeled roof reaches that threshold. This determines an overestimation of the solar potential for LOD1 till a 1100 kWh/m$^2$ threshold, in which the shading from the surrounding buildings decrease the suitable area of the flat-modeled roof.

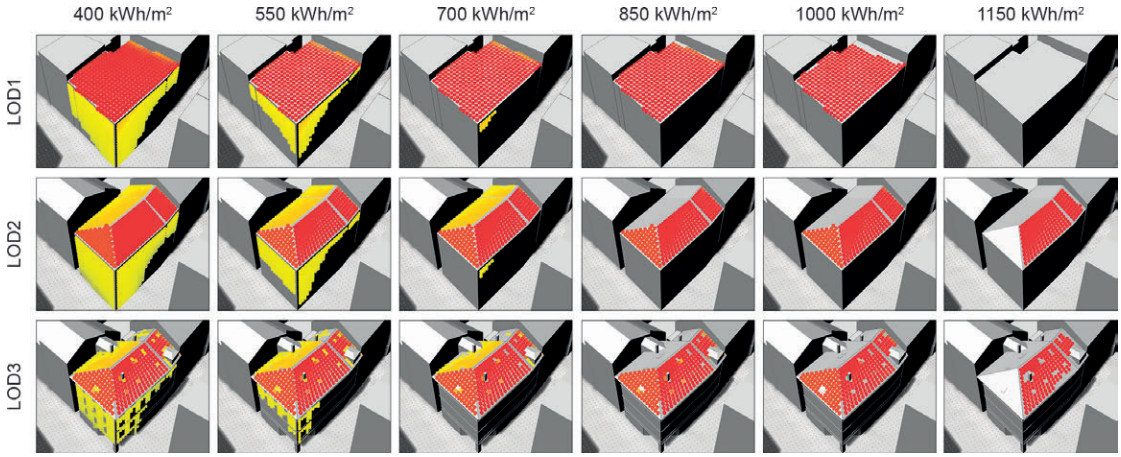


*Figure 6.2 – Annual total irradiation (Irrad, Equation* (6.1)*) for Building 1 at different minimum irradiation thresholds*
*Source: Peronato et al. [220]*

As can be seen in Figure 6.3, also for the other buildings the solar irradiation is often overestimated for LOD1 if we consider the entire building envelope. This is also the case of façades, where the losses are mainly due to the windows and balcony surfaces. Regarding the roofs, one would intuitively expect a general underestimation of the potential for buildings with a sloped roof (1, 2 and 4), as the roof surface is smaller than for LOD3 (and LOD2). On the contrary, we can see that the R.E. for roofs can be highly positive (building 3), slightly positive (buildings 1 and 2) or even negative (building 4), depending on the selected threshold. These differences are possibly due to the roof overhang, which is absent in building 3 and particularly larger in building 4. Moreover, in building 3, the presence of a large number of roof-top constructions considerably reduces the area available for solar systems.

For LOD2 models, the error is generally lower but, because of the lack of many architectural details, the solar irradiation is still overestimated. However, this is not the case for the higher thresholds of building 4, for which the irradiation gained on the large overhangs exceeds the losses due to roof-top chimneys and windows. If we look at the roofs, the situation is similar and for building 4 the solar irradiation is underestimated for all thresholds.

In building 3, for both LOD1 and LOD2 relative errors, we notice a drop of the curve for façades at a

threshold of 650 kWh/m$^2$. This is due to a vestibule which is present only in the LOD3 model (Figure 2). We decided in fact to consider this construction (including its roof) as part of the façade because it is attached to a façade that in LOD1 and LOD2 is sun exposed. The absence of the vestibule determines then an underestimation of the potential for the higher thresholds, due to the non-consideration of the irradiation gains on its rooftop.

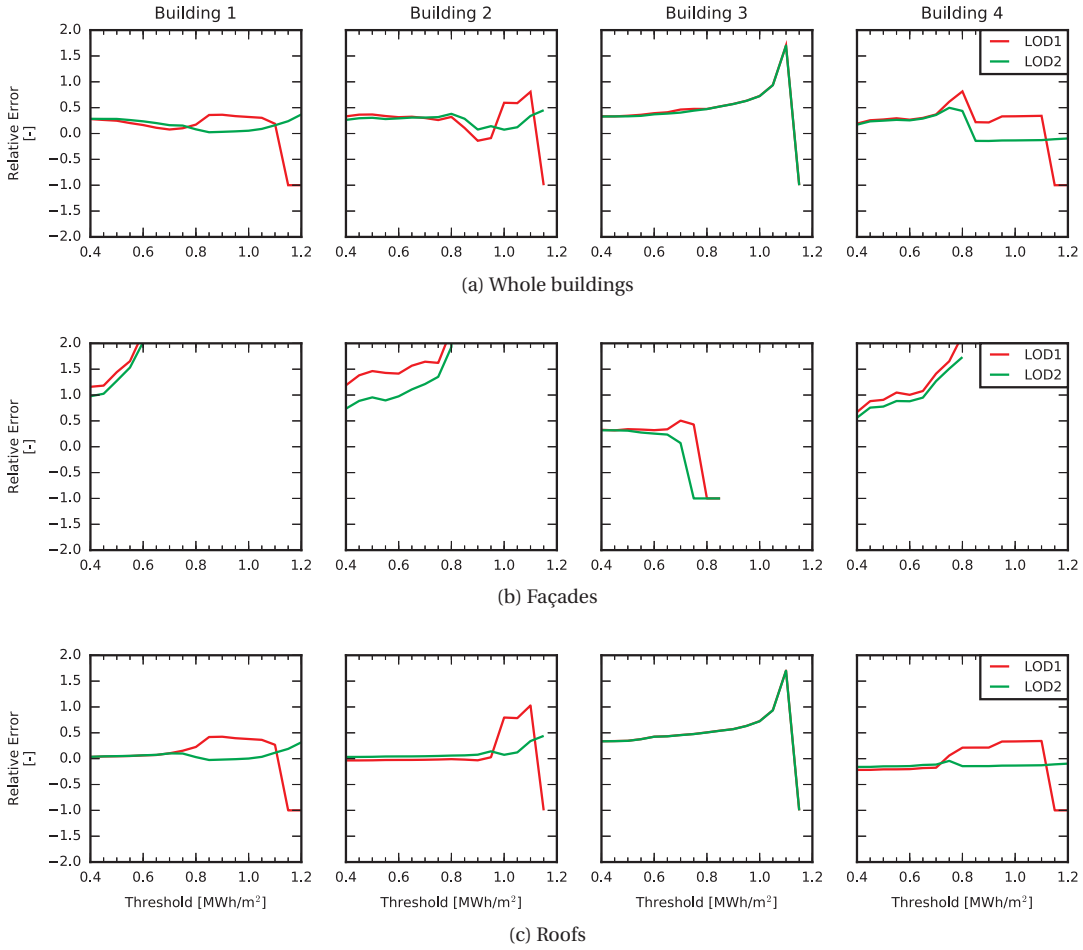


*Figure 6.3 – Relative Error (R.E., Equation* (6.2)*) for the case-study buildings at different minimum irradiation thresholds*
*Source: Peronato et al. [220]*

As can be seen in Figure 6.4, the irradiation curves are generally distinct, meaning that each LOD provides a different estimation of the LOD at all thresholds. Only for building 3, LOD1 and LOD2 provide similar irradiation values because the geometry of the building is identical as the roof is flat and the changes are only due to the different LOD of the contexts. We can also notice that the curve slopes are generally similar for lower thresholds if we consider the whole building and for all thresholds if we consider only the façades. This is because in these conditions the change in total irradiation is mostly due to windows and balconies, which are represented in either LOD1 nor LOD2.

In general, in absolute values (Figure 6.4) we can notice a greater difference between LOD2 and LOD3 curves at lower thresholds, as losses in façades have a great impact due to their larger surface. However, in relative values (Figure 6.3), this is not the case. The relative error is higher and with more varied

trends for high thresholds, usually corresponding to roof surfaces. This is because, due to the lower values of irradiation, a smaller variation represents a higher relative error. This could suggest that the effect of LOD increases the uncertainty of the effective energy yield in the present times, when only highly irradiated surfaces are considered as economically viable. At the same time, we can consider that the error due to the LOD at highly irradiated surfaces (i.e. roofs and upper part of the façades) can be more easily reduced, as an increasing number of 3D models include details such as overhangs and roof super-constructions, notably in Switzerland (Section 2.3.1).

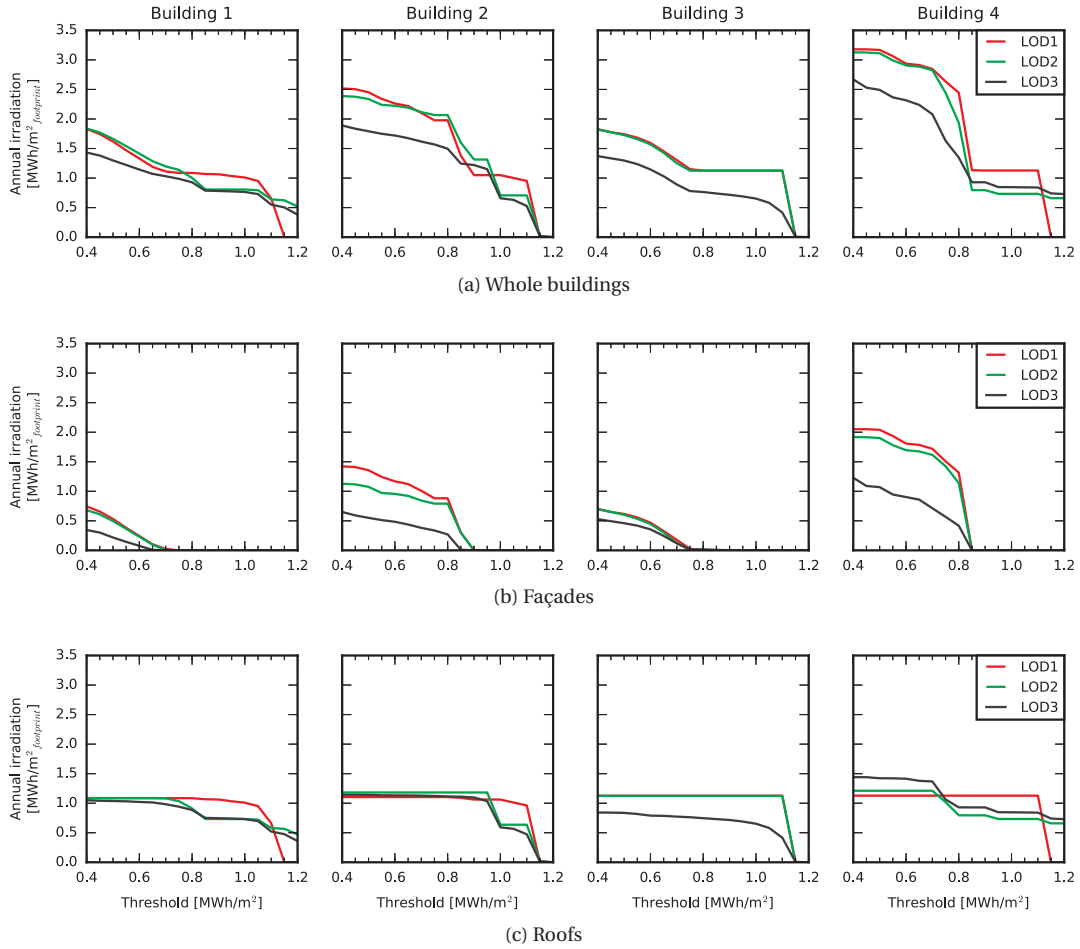


*Figure 6.4 – Annual total irradiation (Irrad, Equation* (6.1)*) for the case-study buildings at different minimum irradiation thresholds*
*Source: Peronato et al. [220]*

### 6.1.3 Contribution to the thesis development

As a reminder, this preliminary study presented some differences with the method that will be described in Chapter 11. In particular, it used automatically-reconstructed 3D models at LOD1 and LOD2, as opposed to the official 3D cadastres used in other sections of the thesis, which are released by GIS public authorities before a quality check. The study also used a meshing algorithm, as implemented in Diva-for-Rhino, which produce an unstructured sensor grid and we set a target distance of 1 m, minimum ambient bounces settings (`-ab 2`), and no vegetation. The influence of these settings will be

investigated in other sections of this chapter, i.e., Section 6.2 for the sensor grid and Section 6.2.2 for the ambient settings, or in Chapter 7 for vegetation.

We can highlight the following findings that contributed to the definition of the final methodology presented in Chapter 11:

- the importance of roof superstructures and overhangs, and hence the need for an LOD2.3 3D model including such details;
- the difficulty to predict the error due to the LOD, because of the high variance of results seen in the analyzed case studies.

## 6.2 Discretization settings

This work [2] addresses the question of the most appropriate grid characteristics for urban-scale solar potential assessments. In particular, it focuses on the grid resolution (i.e. the spacing between the sensor points) and spatial arrangement (i.e. whether sensor points are distributed according to a regular and constant spacing interval - structured grid - or as the faces of the mesh from which they are derived - unstructured grid).

As we will see in Figure 6.12, the computational cost of the simulations is correlated to the number of sensor points. For this reason, a lower resolution (i.e. greater spacing) grid is beneficial in terms of simulation time, but an acceptable accuracy should be guaranteed and the confidence intervals be known. Therefore, this work aims to quantify the error that has to be considered when using grid resolutions lower than 0.5 m, which we assumed to be the ground-truth. We also wanted to check whether the use of a structured or unstructured grid affects the simulated solar irradiation, as each grid-creation method presents a different spatial arrangement and quantity of sensor points.

In order to define some recommendations for solar potential analyses, we finally tried to answer the following questions while considering the specificity of the case study in an urban context:

1. At which resolution does the discretization error become acceptable?
2. Is solar irradiation over- or under-estimated when using low-resolution grids?
3. In which spatial and temporal conditions does the influence of grid resolution affect the results the most?

### 6.2.1 Methodology

The methodology of this work is composed of two main phases. The first phase consists in a simulation-based workflow (which is illustrated in Figure 6.5) to analyze the effect of different discretization settings on solar irradiation. This workflow is tested in an urban area of the city of Geneva, which will be presented in Section 6.2.1.1. The second phase is based on a similar workflow, but it is applied to a

[2] This section contains excerpts from a published journal article [227]: Peronato, G., Rey, E., & Andersen, M. (2018). 3D model discretization in assessing urban solar potential: the effect of grid spacing on predicted solar irradiation. *Solar Energy*, 176, 334–349. https://doi.org/10.1016/j.solener.2018.10.011. The text is reproduced here as a courtesy of the publisher and with the agreement of the co-authors. G.P.'s contribution included the design of the project, simulation and data analysis, and writing of the paper.

single building using more accurate simulations (i.e. using the actual sun positions instead of a daylight coefficient method) in order to check the accuracy of the previous results. The main steps of the first phase will be further explained in Sections 6.2.1.2 to 6.2.1.3 and 6.2.1.5, while the second phase will be detailed in Section 6.2.1.4.

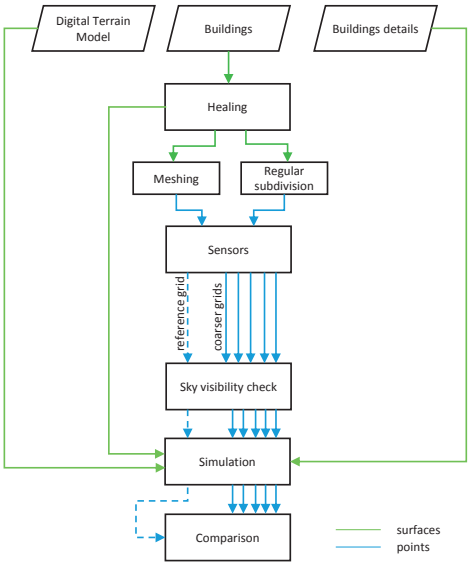


*Figure 6.5 – Schematic of the analysis workflow*
*Source: Peronato et al. [227]*

The core of the analysis is the comparison of solar irradiation values calculated with different discretization settings. We implemented a parametric analysis on 5 different resolution levels (0.5, 1, 2, 3 and 4 m) and 3 grid creation algorithms described in Section 6.2.1.2. Since the surface center point algorithm is independent on resolution, we thus studied in total $5 \cdot 2 + 1 = 11$ discretization settings.

In order to define the discretization error, we used the reference error with regards to the first resolution level, i.e. the grid with a spacing interval of 0.5 m, which provides the maximum number of sensor points for each surface. Unlike for the sensor grid resolution[3], we could not define a reference arrangement to be considered as the ground-truth. While the number of sensor points is greater for an unstructured grid, as can be seen in Fig. 4.1a, their arrangement is not homogeneous and might hence over-estimate the contribution of sensor points at the edges of the analyzed surface. For this reason, we did not focus on the effect of different grid arrangement types, but only on how results from a particular grid arrangement (structured or unstructured) are affected by the grid resolution.

### 6.2.1.1 Case study

The urban area we used in this study is a 350x350-m tile in the center of the city of Geneva. The tile includes 322 buildings, of which 109 fall within the analyzed inner urban area, while the others are part of a buffer zone of 50 m which is taken into account only as obstructing geometry. The Floor Area Ratio (FAR), which is a standard metric for urban measuring built density, of the selected tile, including the

[3]The terms “grid size”, “grid spacing” and “grid resolution” are used used as interchangeable synonyms in this work.

buffer zone of 50 m, is **3.1** and the median building height is **12 m**[4].

This tile includes a good variety of buildings shapes and sizes, while presenting a density value which is common for many inner areas of European and North-American cities. In terms of roof superstructures, the tile features flat, gable and hip roofs, as well as various types of architectural details (dormers, HVAC systems). In this sense, the 3D model of the Canton of Geneva at LOD 2.3 [5] provides a detailed representation of buildings, including their wide range of superstructures. Moreover, with the exception of a church, no building is enlisted in the heritage protection list, making the installation of BIPV systems possible, at least from a first legal assessment.

(a) Orthophoto (b) Plan

*Figure 6.6 – The analyzed buildings are located within the inner square and are tagged with their ID in Figure 6.6b.*
*Source: Orthophoto and building footprints from the SITG (June 2016). Originally published in Peronato et al. [227].*

#### 6.2.1.2 Modeling

The geodata, composed of a 3D model of buildings and a Digital Terrain Model at 0.5-m resolution, are first trimmed in ArcGIS and exported respectively as *.SHP and *.TIF. These files are then converted into *.DXF and *.XYZ files, using GDAL[6], specifically the *ogr2ogr* and *gdal_translate* libraries.

These files are hence imported in Rhino-Grasshopper respectively as points and curves. The point cloud is directly converted to a mesh, through a Delaunay triangulation. The curves of building geometry are subjected to the healing procedures described in Section 6.2.1.2, to ensure that the geometry is topologically correct and appropriate for the simulation.

Building surfaces and terrain are defined as Lambertian diffusers with 0.30 and 0.10 reflectivity respectively, as suggested by IESNA [120].

#### Creation of the sensor points

We implemented two different techniques for creating irradiance sensor points, based on the existing algorithm and a custom-made workflow. In both cases the output is a set of 3D points and vectors

[4] The floor area value for the FAR is calculated by considering the average building height and assuming a constant floor height of 3 m, while the plot area is considered as the entire surface of the 350x350 m tile, including hence both private plots and public space.
[5] For the LOD X.Y classification see Biljecki et al. [27].
[6] Version 2.1.0, 2016/04/25 (http://www.gdal.org/, last accessed on March 2017)

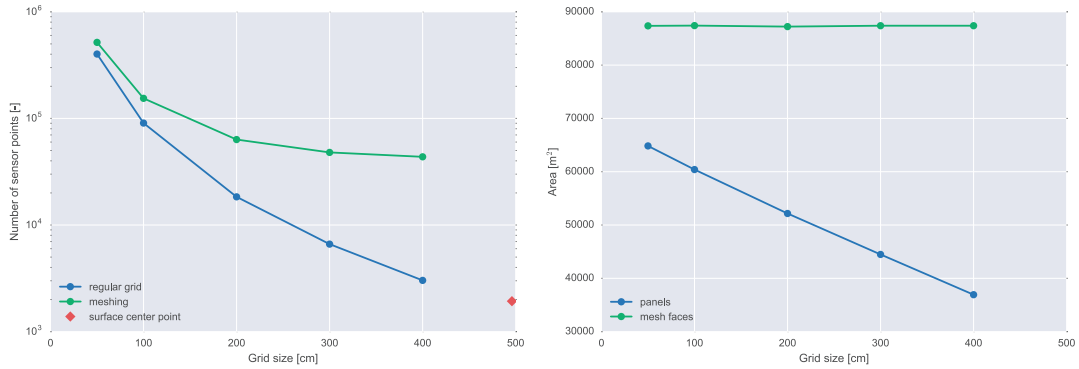


*Figure 6.7 – Characteristics of the two grid types in terms of number of sensor points (a) and mesh face area (b). The number of sensor points when placed at the surfaces' centers (red marker) has been arbitrarily plotted with $x = 480$. Only surfaces with at least one sensor at 4-m spacing are considered. As the spacing interval (grid size) increases, we observe a much greater decrease in the number of sensor points than for the mesh points.*
*Source: Peronato et al. [227]*

which are used as input for the simulation. The two algorithms produce a much different quantity (Figure 6.7a) and distribution (Section 4.1.2.1) of sensor points on surfaces.

**Structured grid** This grid is created with the algorithm that will be described in Algorithm 11.1, as included on the thesis final method presented in the Chapter 11.

**Unstructured grid** The *Generate test points*[7] component included in Honeybee [259] was used to create the sensor points. This component first creates a mesh with a target minimum and maximum face edge length which is equal to the set spacing interval. However, the density of mesh faces is not constant and, as can be seen in Fig. 6.7a, is generally higher close to the polygon edges, but it allows a complete coverage of buildings surfaces. The center point of each mesh face and the corresponding normal vectors are then used as sensor points for the simulation, as done by previous studies [e.g. 11].

**Surface center point** In this special case, a single sensor point is fixed in the geometric center of each surface. Considering that in our 3D model a surface usually corresponds to a semantic surface (e.g. a wall, a roof face), this grid arrangement provides the least defined grid (e.g. composed by a single point), while it is supposed to represent the average behavior of that surface considering that is located in its center. For this reason, this method is commonly used for simulations of solar irradiation intended for the assessment of building thermal performance.

In order to reduce the calculation time, we also checked whether each point actually sees the sky. This is done trough a Radiance simulation using a constant diffuse sky. Only points seeing the sky have been included in the simulation. It should be noted that roof superstructures such as dormers were not included in this check. For this reason, points distributed on a roof surface, in reality might be covered by a dormer or other superstructures. This was chosen in order to assure the comparability of results (i.e. the same grid) with 3D models at LOD2, which do not include such details.

[7] Version 0.0.59, January 26, 2016

#### Geometry healing

Compared to the dataset used for the case-study application presented in Chapter 12 (Appendix A.1.5), the Geneva SITG 3D cadastre (Appendix A.1.6) presented more topological errors that needed to be corrected, such as non-planar curves and inwards oriented normals.

We tested the curves imported from the DXF files for planarity. The vertices of the curves not passing the test are projected to the best-fitting plane. New planar curves can be created out of the projected points and all curves are thus converted to surfaces.

We adopted a simulation-based approach to check whether the building surfaces are correctly oriented, i.e. outwards with respect to the center of the building, which is described in Algorithm 6.1.

- Create a grid at a 10-m resolution using a meshing grid
- Run a Radiance simulation with an uniform sky on the grid
- Flip surfaces having more than 95% sensor points with less than 5% of the maximum illuminance value obtained in the area

**Algorithm 6.1:** Radiance-based algorithm to correct the wrong orientation of building surfaces (facing inwards)

Unfortunately, Algorithm 6.1 fails to reverse some inwards-oriented surfaces, such as those that are partially adjacent to other surfaces, because the ratio of their sensor points than can see the sky is usually below the set threshold (95%). Even if these surfaces (yellow-colored. in Section 4.1.2.1) cannot be included in the simulations, we assume that this does not affect the assessment process, as it is unlikely that such surfaces will be used for installing BIPV systems.

#### Weather

We used a weather file containing data of a typical meteorological year (TMY) for Geneva made by ASHRAE IWEC and available from EnergyPlus website[8].

#### 6.2.1.3 Simulation

Simulations are conducted in Daysim [244], using Honeybee as the graphical interface [259]. Data analysis, i.e. the comparison of simulation results using different grids, is conducted using Python scripting, while relying on Rhino-Grasshopper for the visualization of spatial false-color maps.

The Radiance parameters are listed in Table 6.2. In particular, the number of admissible ambient bounces (-ab parameter) is set to 2, which means that during the ray-tracing, one reflection of each ray from the context is taken into account. This is considered an acceptable simplification for urban-scale simulations. However, the influence of these parameters will be checked in a sensitivity analysis (Section 6.2.2.2)

[8] https://energyplus.net/weather-location/europe_wmo_region_6/CHE/CHE_Geneva.067000_IWEC, last accessed on March 2017.

*Table 6.2 – Radiance parameters used in this work: ambient bounces* -ab*, ambient resolution* -ab*, ambient divisions* -ad*, ambient super-samples* -as*, ambient accuracy* -aa*.. Other settings for* -ab *and* -ar *parameters have been tested in Section 6.2.2.2.*

| -ab | -ar | -ad | -as | -aa |
|---|---|---|---|---|
| 2 | 300 | 1000 | 500 | 0.1 |

#### 6.2.1.4 Comparative analysis against Radiance-based simulations

In order to test the accuracy of the simulations, we run a simulation using Radiance's *gendaylit* and *rtrace* on each daylit hour of the year. Since the computational cost for an annual simulation in Radiance is much greater than in Daysim, the validation in Radiance was limited to one sample building (ID 54 in Fig. 6.6b), which has some typical characteristics of this urban area: gable roof with a dormer, one façade facing a courtyard and another one facing the street, while other two façades are adjacent to the contiguous buildings.

We used the same geometry and material definitions used in the simulation in Daysim. Daysim and Radiance share in fact the same data format (**.rad*). However, for this comparative analysis, we included in the simulation only the sensor points belonging to the selected building.

We thus analyzed the results for the four surfaces of the building displayed in Fig. 6.8, so as to evaluate the accuracy of the simulations in Daysim compared to Radiance with regards to the specific purposes of this paper at both different spatial (whole building or single surfaces) and temporal (annual and hourly time time-steps) granularities.

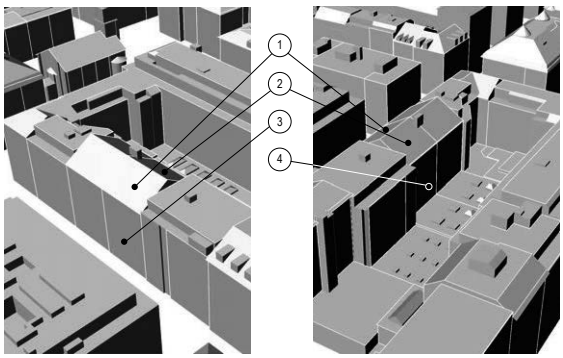


*Figure 6.8 – Legend for surfaces of the case-study building used in Section 6.2.1.4.*
*Source: Peronato et al. [227]*

#### 6.2.1.5 Evaluation

Using the simulation output (hourly irradiance value for each sensor node), the yearly solar irradiation of each surface normalized by surface area was computed. We then obtained the suitable surface and irradiation as a function of different irradiation thresholds using the following equations:

$$SuitArea = \sum_{s=1}^{n} A_s \cdot t_s \qquad \text{with } t_s = \begin{cases} 1, & \text{if } i_s \geq threshold, \\ 0, & \text{otherwise.} \end{cases} \tag{6.3}$$

$$SuitIrr = \frac{\sum_{s=1}^{n} i_s \cdot A_s \cdot t_s}{\sum_{s=1}^{n} A_s \cdot t_s} \qquad \text{with } t_s = \begin{cases} 1, & \text{if } i_s \geq threshold, \\ 0, & \text{otherwise.} \end{cases} \tag{6.4}$$

where $A_s$ and $i_s$ are respectively the face area [m$^2$] and the annual solar irradiation [kWh/m$^2$] corresponding to each sensor point $s$, and $n$ is the total number of sensor points.

We used these suitability metrics as only highly-irradiated surfaces are usually selected for installing solar systems as more economically-viable. It should be noted that thresholds are decreasing along with the decrease in cost of solar panels and increase of their efficiency.

On the basis of the previous equations, we calculated the metrics that we used to evaluate the uncertainty of a grid at spacing interval $g = x$ [m] with regards to the reference grid at a spacing interval of $g = 0.5$ [m]:

$$AreaRatio = \frac{SuitArea_{g=x}}{SuitArea_{g=0.5}} \tag{6.5}$$

$$IrrRatio = \frac{SuitIrr_{g=x}}{SuitIrr_{g=0.5}} \tag{6.6}$$

$$IrrDiff = SuitIrr_{g=x} - SuitIrr_{g=0.5} \tag{6.7}$$

Similarly, we calculated also the Root Mean Square Error (RMSE) and Relative Root Mean Square Error (RRMSE) for each surface $s$:

$$RMSE = \sqrt{\frac{1}{n} \sum_{s=1}^{n} (SuitIrr_{s,g=x} - SuitIrr_{s,g=0.5})^2} \tag{6.8}$$

$$RRMSE = \frac{\sqrt{\frac{1}{n} \sum_{s=1}^{n} (SuitIrr_{s,g=x} - SuitIrr_{s,g=0.5})^2}}{\frac{1}{n} \sum_{s=1}^{n} SuitIrr_{s,g=x}} \tag{6.9}$$

It should be noted that we considered in this analysis only surfaces that have at least one sensor at each grid spacing, in order to compare a consistent set of surfaces. The considered surfaces are rendered with gradient false colors in Figure 6.13.

### 6.2.2 Preliminary sensitivity analyses

In this section, we present the results of preliminary sensitivity analyses to test the effectiveness of the methodology. The goal of this section is twofold: testing the sensitivity of simulations to some Radiance parameters used in the Daysim simulations and testing the results of Daysim against "pure" Radiance-

based simulations (i.e. using *gendaylit* without daylight coefficients). As explained in Section 6.2.1.4, Daysim considers discrete sun positions (65 for the considered location), unlike the *gendaylit* which considers the actual sun position for each hour. This simplification is expected to influence the results, especially for highly obstructed surfaces.

We conducted a test in a case-study building, i.e. a building of the analyzed tile which is considered to be representative of the urban conditions of the area and represented in Fig. 6.8.

#### 6.2.2.1 Comparison with Radiance

The ratios of irradiance values calculated in Radiance and Daysim are first presented for each hour of the year. In Fig. 6.9, we can see that the frequency increases along with the increasing grid spacing. This means that the accuracy of Daysim simulations is decreasing with increasing grid spacing. Because of the discrete sun positions, a sparser sensor points distribution is more likely prone to errors due to the discrete sun positions (65), while for lower spacing intervals each surface is represented by more sensor nodes, the error being then more easily compensated.

In Fig. 6.9 we can also see that the South-facing façade (surface 3) is the most affected by the simplifications of Daysim, and this is especially visible in winter where we can see a frequent overestimation of hourly values, especially starting from a grid spacing equal to 3 m. Conversely, on the North-façade oriented towards the courtyard (surface 4) the irradiation is generally - constantly in the case of a grid spacing equal to 3 or 4 m - overestimated.

The annual results presented in Fig. 6.10 show that trends for Daysim and Radiance results are similar and the curves mostly coincident. However, starting from a grid spacing equal to 4 m, there is an underestimation in Daysim results compared to Radiance ones. This is probably caused by irradiation on the South-façade being most of the time underestimated.

We also notice that the error calculated by both simulation engines is negligible till a 2-m spacing interval, as the two curves are mostly coincident. Similarly, in the graphs of hourly results, the range of variation for grid at 1 m and at 2 m is very similar and always contained between 0.5 and 1.5, while being significantly wider for coarser grids.

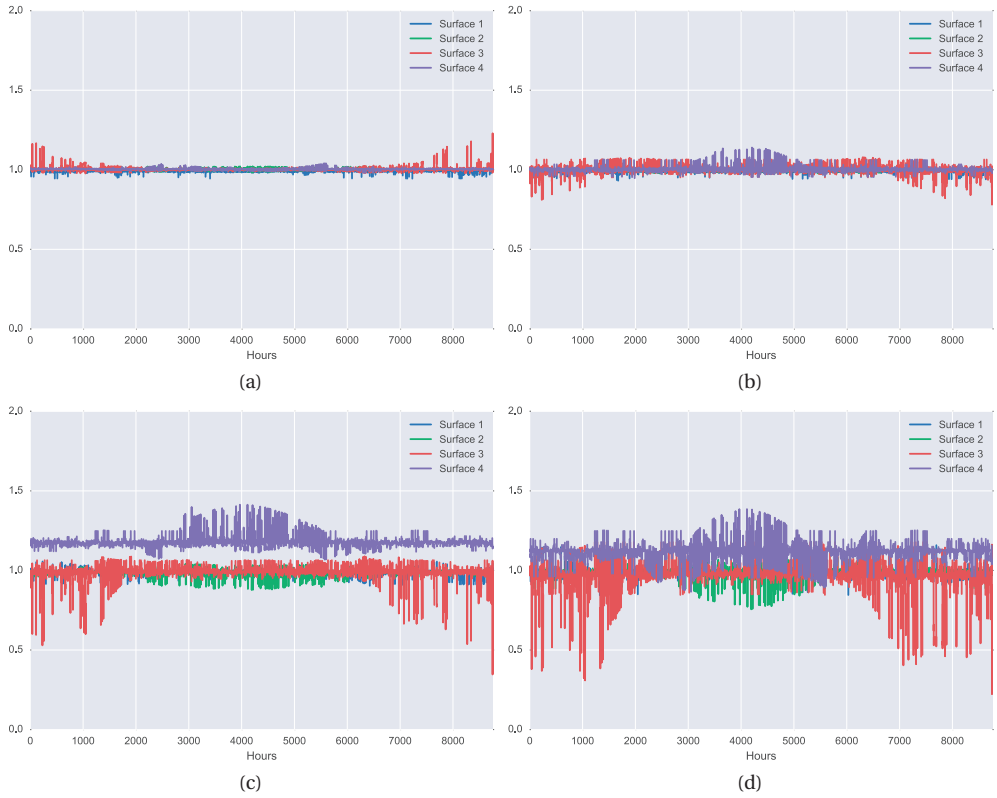


*Figure 6.9 – Ratio of hourly solar irradiance values calculated in Radiance to those calculated in Daysim at different grid sizes: a) = 1 m, b) = 2 m, c) = 3m, d) = 4 m). See Fig. 6.8 for reference to surface numbers. Starting at a spacing interval of 3 m, we can notice significant discrepancies between results in Daysim and Radiance.*
*Source: Peronato et al. [227]*

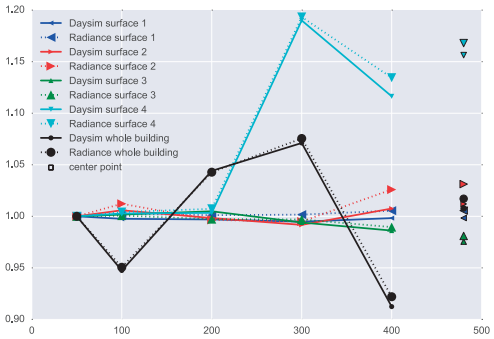


*Figure 6.10 – Ratio of suitable solar irradiation (see Eq. 6.6) with spacing $g = x$ [m] to suitable solar irradiation with $g = 0.5$ [m] with threshold $t = 0$ [kWh/m$^2$] for different simulations run with Daysim and Radiance on a structured grid. See Figure 6.8 for reference to surface numbers. Please note that, for better visualization, results for sensor points placed at the surfaces' centers (unfilled markers) have been arbitrarily plotted with $x = 4.8$ [m]. We can see that the trend is similar for simulations run with Radiance and Daysim.*
*Source: Peronato et al. [227]*

#### 6.2.2.2 Sensitivity to ambient bounces and accuracy

We tested simulations in Daysim at increasing grid spacing using different Radiance parameter for ambient accuracy `-aa` and ambient bounces `-ab`, which are listed in Table 6.3.

As can be seen in Fig. 6.11a, the choice of the parameter influences the received solar irradiation. By setting *-aa* to 0, we notice a reduction of about 10%. However, this reduction is consistent at all spacing intervals. Similarly, we notice an increase of annual solar irradiation by using higher *-ab* parameters than the default one of *-ab* 2. This is expected because the augmentation of number of bounces augments the quantity of reflected solar radiation that is taken into account. However, the increase is not significant and, as for *-aa*, is consistent at all spacing intervals.

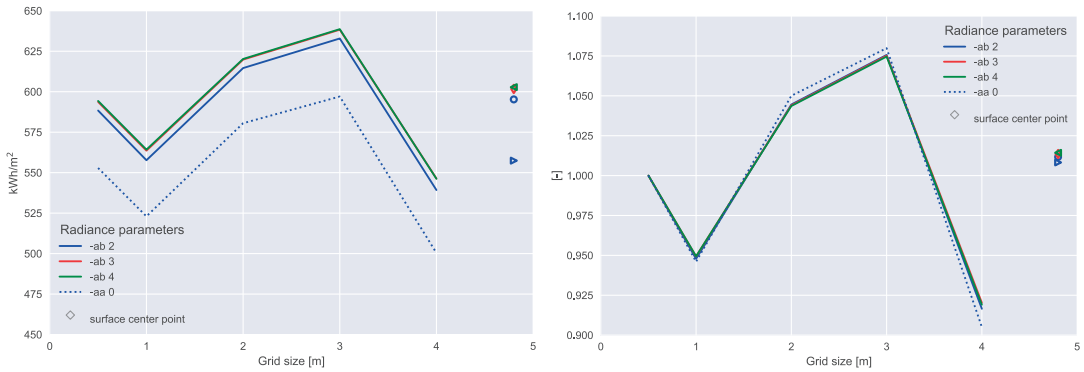


(a) (b)

*Figure 6.11 – Suitable solar irradiation (a, see Eq. 6.4) and ratio of suitable solar irradiation (b, see Eq. 6.6) with spacing $g = x$ [m] to suitable solar irradiation with $g = 0.5$ [m] for threshold $t = 0$ [kWh/m$^2$] (b). Please note that, for better visualization, the results for sensor points placed at the surfaces' centers (unfilled markers) have been arbitrarily plotted with $x = 4.80$ m. As expected, the higher the ambient bounces, the higher the irradiation; conversely, with an ambient accuracy set to 0, the irradiation is significantly lower than with the default parameter of 0.1. However, for both parameters, we notice similar trends regarding the effect of the grid spacing.*
*Source: Peronato et al. [227]*

*Table 6.3 – Tested Radiance parameters (the other parameters are the same as in Tab. 6.2), and grid size. Ambient bounces* -ab *parameter varies from 2 (i.e., 1 bounce onto the 3D scene before reaching the sky vault) to 4 (i.e., 3 bounces). Ambient accuracy* -aa *parameter varies from 0.1 (i.e., low error interpolation) to 0 (i.e., no interpolation). The row* Dist. *indicates the spacing of the grid, where* c *is a single sensor point at the center of the surface.*

| | | | | | | | | | | | | | | | | | | | | | | | |
|---|---|---|---|---|---|---|---|---|---|---|---|---|---|---|---|---|---|---|---|---|---|---|---|
| `-ab` | 2 | 2 | 2 | 2 | 2 | 2 | 3 | 3 | 3 | 3 | 3 | 3 | 4 | 4 | 4 | 4 | 4 | 4 | 2 | 2 | 2 | 2 | 2 | 2 |
| `-aa` | .1 | .1 | .1 | .1 | .1 | .1 | .1 | .1 | .1 | .1 | .1 | .1 | .1 | .1 | .1 | .1 | .1 | .1 | 0 | 0 | 0 | 0 | 0 | 0 |
| Dist. | .5 | 1 | 2 | 3 | 4 | c | .5 | 1 | 2 | 3 | 4 | c | .5 | 1 | 2 | 3 | 4 | c | .5 | 1 | 2 | 3 | 4 | c |

### 6.2.3 Results

We present here the results of the analysis at different spatial resolutions, starting from annual results calculated on the entire urban sector down to a more detailed analysis per surface, through both comprehensive plots and spatial maps. Fig. 6.13 shows a perspective view of the analyzed 3D model of the urban area with some error metrics visualized as false-colors on the building surfaces.

Figure 6.12 shows the computation time for the Daysim `gen_dc -dir` command, which is the most computational-intensive part of the simulation, as it performs the raytracing for the different sun positions (65 for the considered location).The raytracing for the diffuse component (`gen_dc -dif`) is faster and can be run in parallel, while the other Daysim subprograms have negligible computational time. We can see that the time needed to perform the simulation logarithmically decreases with the grid size, indicating that use of coarser grid is highly beneficial in terms of computational cost. Moreover, also the absolute time needed to simulate the tile at a 0.5-m resolution (above 16 hours) is considerable in case of large-scale applications.

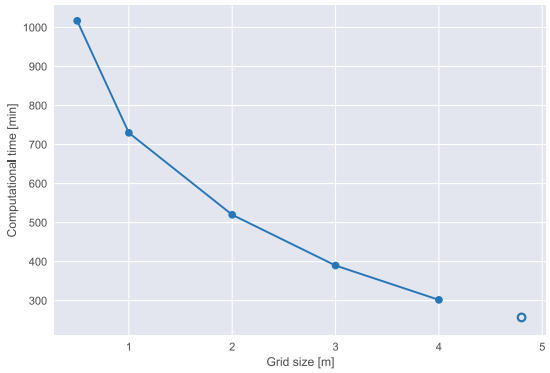


*Figure 6.12 – Computation time (in minutes) at the different structured grid resolutions with spacing $g = x$ [m] for the Daysim `gen_dc -dir` command. Please note that, for better visualization, the result for sensor points placed at the surfaces' centers (unfilled marker) has been arbitrarily plotted with $x = 4.8$ [m]. The test has been conducted on a desktop computer equipped with an Intel© Core ™ i7-4790K CPU and a clock speed of 4.0 GHz.*
*Source: Peronato et al. [227]*

#### 6.2.3.1 Urban-scale analysis

As can be seen in Figs. 6.14 and 6.15, the use of a structured or unstructured grid has a huge impact on the results. This is because the unstructured grid keeps the area almost stable at all spacing intervals, as mesh faces cover the whole building envelope, while the panelization process determines a decrease of the available area (Fig. 6.7b). Consequently, this causes also a significant decrease in the number of sensor points, which does not occur in the case of an unstructured grid (Fig. 6.7a).

By normalizing the results of the structured grid by the area available at $t = 0$ [kWh/m$^2$], a decrease for most of the thresholds can be noticed, but with a much smaller magnitude (Fig. 6.14c). We can assume such normalized results are more realistic, as they consider only the actual panel surfaces. It can be also noticed that the surface decreases more steeply for high thresholds, because of the losses of highly irradiated surfaces that are available at $t = 0$ [kWh/m$^2$].

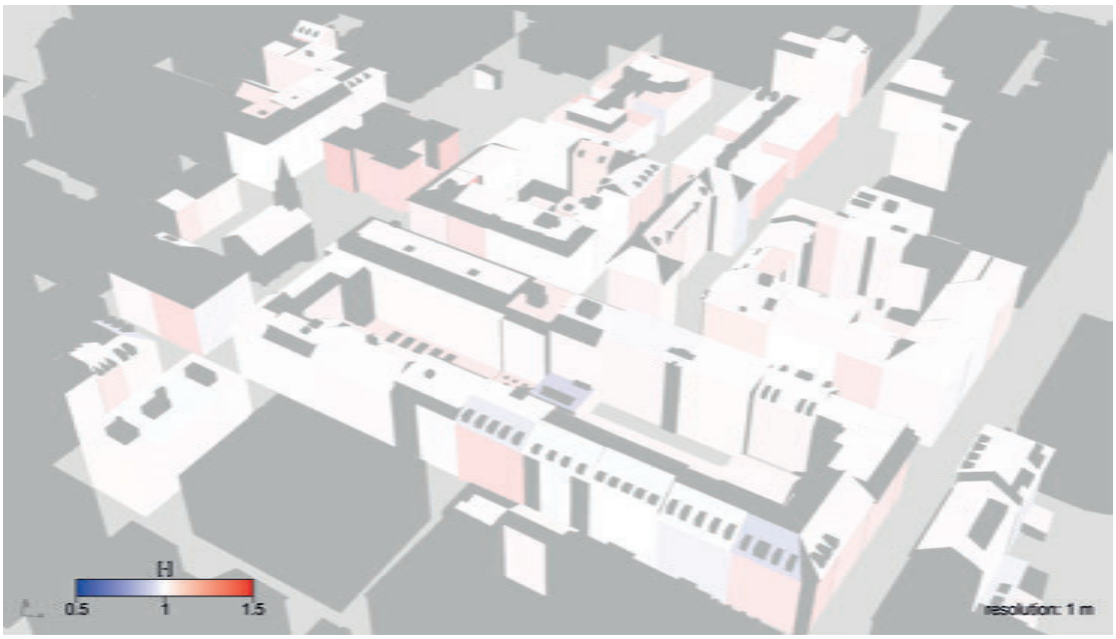


(a)

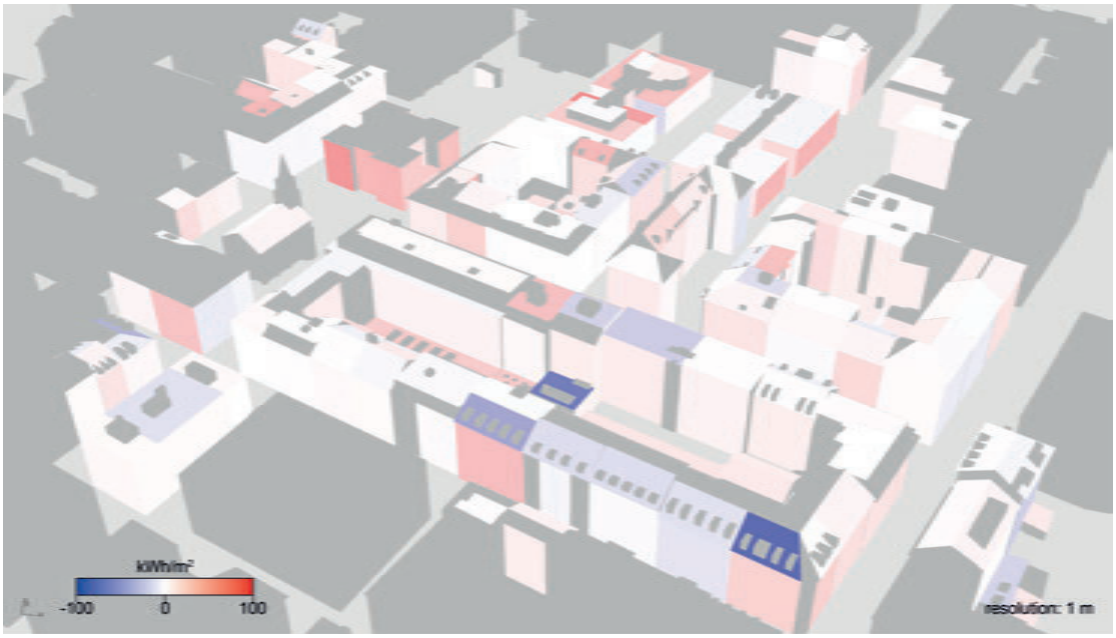


(b)

*Figure 6.13 – Ratio of suitable solar irradiation (a, see Eq. 6.6) and difference of suitable solar irradiation (b, see Eq. 6.7) at resolution $g = x$ [m] (indicated in the bottom-right corner) and at reference resolution $g = 0.5$ [m] with threshold $t = 0$ [kWh/m$^2$] on a structured grid. An animation presenting the results for the different resolutions can be seen using Adobe Acrobat or Adobe Reader. The animation frames are plotted in Appendix A.4.1 and Appendix A.4.2. The false-color maps are based on data extracted from the Système d'information du territoire à Genève (SITG), as of June 2016*
*Source: Peronato et al. [227]*

However, with respect to the suitable irradiation (Fig. 6.15b) lower thresholds present more losses. For both area and irradiation, decreasing curves along with the increasing grid size can be observed. This means that we tend to underestimate the available irradiation and the suitable area, if the 0.5-m grid is considered as the reference. However, this is not always the case if the analysis is limited only to low thresholds (in terms of area) and high thresholds (in terms of irradiation). In this case, the variation is negligible and in some cases even positive. Moreover, the surface reduction caused by coarser resolutions is more significant for high thresholds, while, on the contrary, in terms of irradiation low thresholds are more affected.

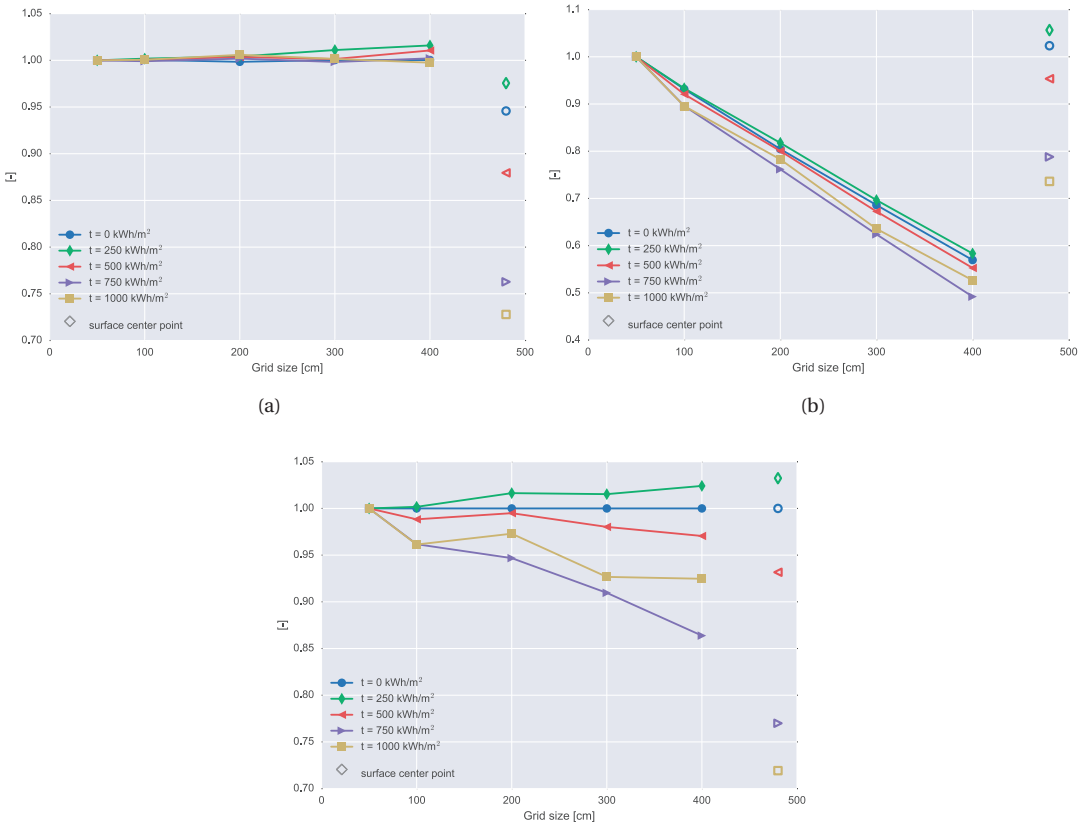


*Figure 6.14 – Ratio of suitable surface (see Eq. 6.5) at spacing $g = x$ [m] to suitable surface with resolution $g = 0.5$ [m] for different thresholds $t$ [kWh/m$^2$]. Subfigure a) shows results for an unstructured grid, clearly the least sensitive to resolution, b) for a structured grid and c) for a structured grid normalized by $t = 0$ [kWh/m$^2$]. Please note that, for better visualization, the results for sensor points placed at the surfaces' centers (unfilled markers) have been arbitrarily plotted with $x = 4.8$ [m] and that the y-scale is not constant across the three graphs. In the case of the structured grid (b), the suitable surface is inversely correlated with the grid spacing (cf. Fig 6.7b).*
*Source: Peronato et al. [227]*

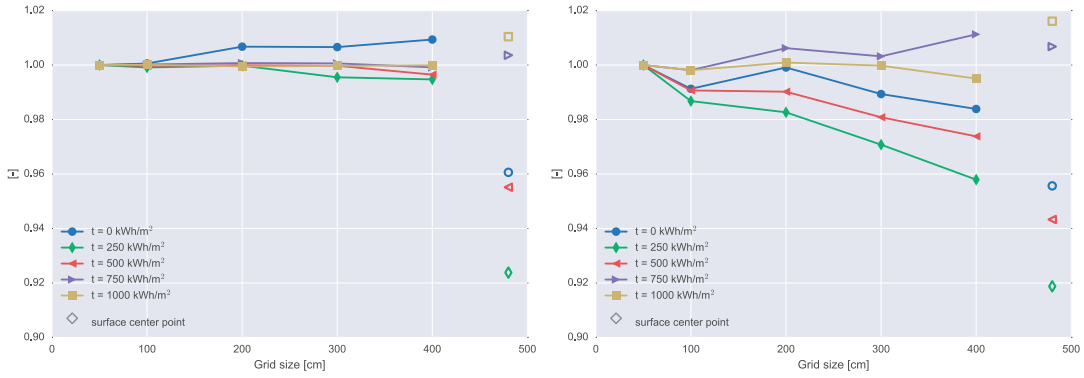


(a) (b)

*Figure 6.15 – Ratio of solar irradiation (see Eq. 6.6) with resolution $g = x$ [m] to annual solar irradiation with $g = 0.5$ [m] for different thresholds $t$ [kWh/m$^2$]. Subfigure a) shows results for an unstructured grid, b) for a structured grid. The results for sensor points placed at the surfaces' centers (unfilled markers) have been arbitrarily plotted with $x = 4.8$ [m].*
*Source: Peronato et al. [227]*

#### 6.2.3.2 Comprehensive surface analysis

If we consider the RRMSE (Figs. 6.16c and 6.16d) calculated on each surface, we find higher error values that the one seen in the previous section for the ratio of available solar irradiation. The maximum RRMSE is still low, though: 7% for $g = 400$ and $t = 0$, corresponding to a RMSE of 45 kWh/m$^2$, for a structured grid. Unlike for the ratio of available solar irradiation, for a structured grid we can see that the error increases at all thresholds with a linear trend with decrease of the resolution, while for an unstructured grid it is stable for all resolutions lower than 1 m. The trend of the structured grid could be due to specificities of the algorithm: with increase of spacing, the offset from the border of the surfaces also increases, causing losses in the upper part of the façade.

If we analyze the difference in irradiation for each surface *IrrDiff* (see Eq. 6.7 with threshold $t = 0$ [kWh/m$^2$] for a structured grid) plotted in Fig. 6.17, we can notice an increase of the median and upper quartile. This means that the annual irradiation per surface is more likely to be overestimated with regards to the 0.5-m grid.

By looking at the distribution of the variation in suitable solar irradiation (Fig. 6.18), we can also see that the negative solution space gets larger while increasing the grid size (from subfigures a to e). This could explain why the cumulative results (Fig. 6.15) show a decreasing trend, while the results per surface (Fig. 6.17) have an increasing trend: by increasing the grid spacing, surfaces with a strong negative variation (> 100 kWh/m$^2$ in Fig. 6.18) occur more frequently.

We should consider that these results are for a structured grid and a threshold $t = 0$, which is a worst-case scenario as already noticed in Section 6.2.3.2.

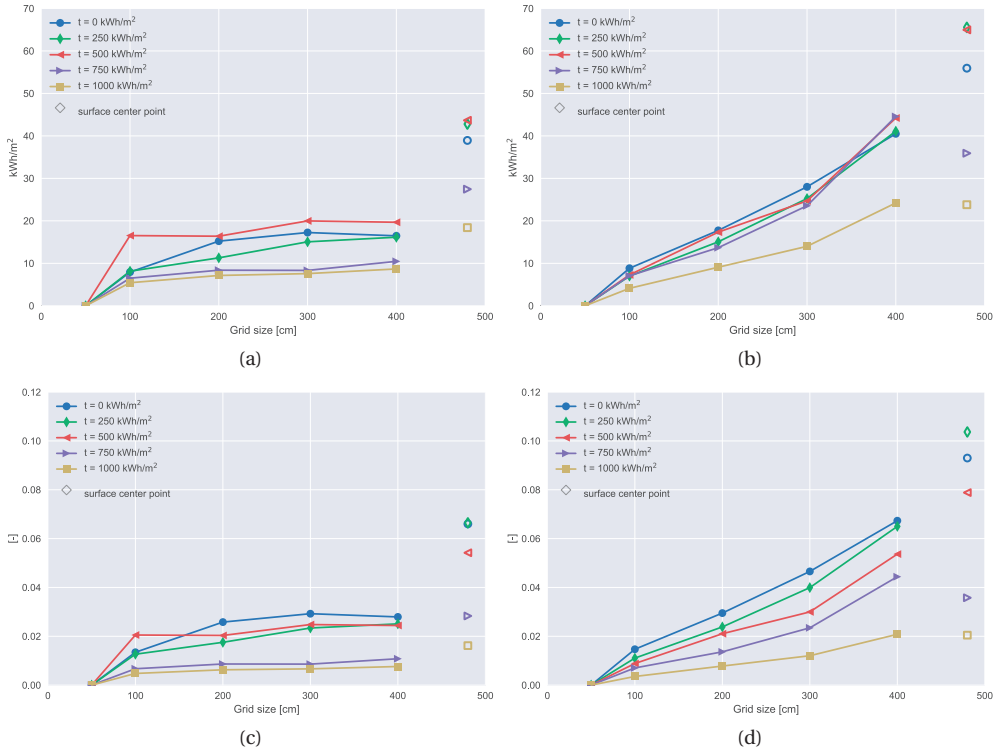


*Figure 6.16 – In the first row, Root Mean Square Error (see Eq. 6.8), and, in the second row, Relative Root Mean Square Error (see Eq. 6.9) for resolution $g = x$ [m] and reference values calculated at $g = 0.5$ [m], for different thresholds $t$. Subfigures a) and c) show results for an unstructured grid, b) and d) for a structured grid. The results for sensor points placed at the surfaces' centers (unfilled markers) have been arbitrarily plotted with $x = 4.8$ [m]. Results for the unstructured grid present a mostly-stable error, while for the structured grid it is increasing with the grid spacing.*
*Source: Peronato et al. [227]*

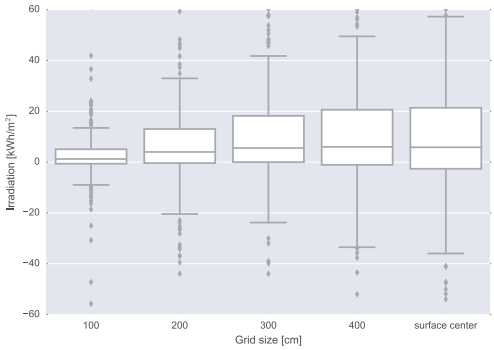


*Figure 6.17 – Difference of suitable annual solar irradiation (see Eq. 6.7) with threshold $t = 0$ [kWh/m$^2$] for a structured grid. This corresponds to a worst-case scenario both for arrangement and threshold. Please note that some data points are outside the y-limits. Surface irradiation is generally overestimated using coarser grids, while there is an increasing number of surfaces whose irradiation is highly-underestimated. The median difference is stable starting from a 3-m resolution.*
*Source: Peronato et al. [227]*

#### 6.2.3.3 Spatial surface analysis

In Fig. 6.13b we clearly see some roof surfaces with constructions presenting a strong decrease in irradiation. This happens for example when in low-definition grids the sensor points are shaded by the construction, while in the reference grid other well-exposed sensor points counter balanced the results. Those surfaces present a strong decrease, while overall most of the surfaces slightly increase their irradiation, in particular those South-facing and the façades. This seems to confirm the results that we have seen in Fig. 6.17.

By looking at Fig. 6.18, we can see that the difference in solar irradiation is generally greater on façades than on rooftops. Similarly, North-facing façades present a smaller variation compared to the other orientations. This corresponds to the expectations, as vertical and North-facing surfaces have a less favorable solar exposition than roofs. If we exclude North-facing surfaces, we cannot see any significant variation due the orientation. Nevertheless, the points corresponding to flat roofs have the greatest variation (both negative and positive) at all resolutions.

We can see in Fig. 6.18b, that the distribution of range of values is very similar to that of Fig. 6.18a, and always under 100 kW/m$^2$, except for one data point, which is located on a vertical surface. Starting from 6.18c the difference in values become more significant and in many cases this is higher than 100 kW/m$^2$.

As already seen in Fig. 6.17, most of the surfaces present an increase of solar irradiation. However, the extremes can be observed in the lower part of the plots of Fig. 6.18, in particular with low-resolution grids. Again, these results explain why we observe a general decrease in solar radiation at the urban level - i.e. a limited number of surfaces with huge losses -, and an increase at the surface level - i.e. the majority of surfaces presenting a positive variation.

### 6.2.4 Discussion

The scope of this work was the investigation of the impact of 3D model discretization on the calculated solar irradiation. In the previous sections, we have analyzed the results using different metrics and analysis targets. In the light of these results, we will discuss here the significance of these findings for solar assessments in urban environments and compare them to prior works. We will finally list the shortcomings related to the methodology and the improvements and extensions to be planned in future work.

#### 6.2.4.1 Significance of findings

We have seen that the results vary across different thresholds and orientation (azimuth and tilt angle). This means that the significance of the findings for solar energy assessments depends on the specific conditions in which solar modules are installed.

Thresholds represent a typical assessment method for evaluating the PV-suitability of surfaces (Section 4.2.3). A minimum annual irradiation is needed in fact for the economic viability of a (BI)PV installation. However, the viability thresholds are expected to lower in the upcoming years, due to lower prices of photovoltaics as well as of increasing efficiency. We can hence consider that lower thresholds represent a benchmark for future assessments. In this sense, the results show that the uncertainty of the actual solar yield of building surfaces will have an increasing importance in the

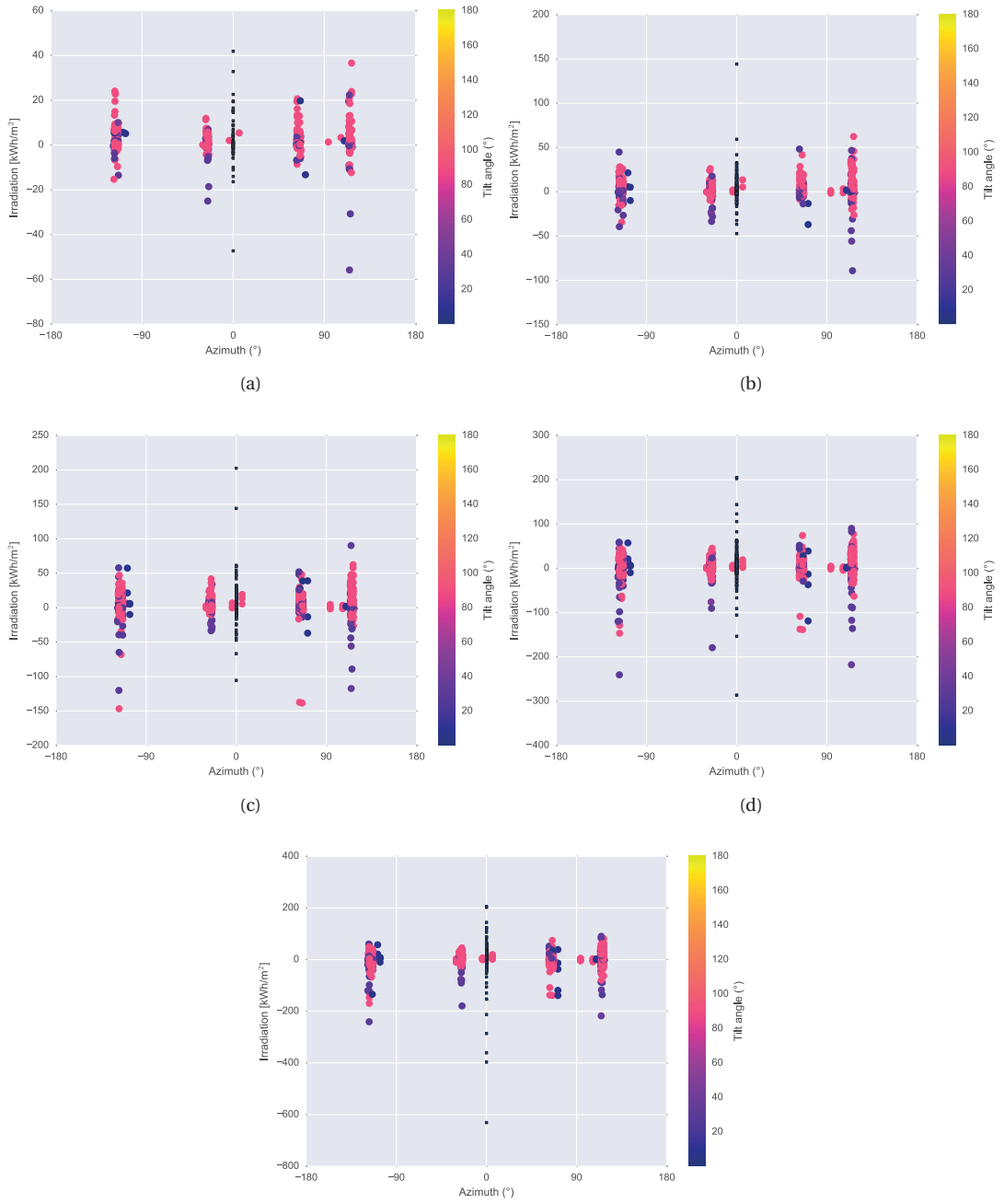


*Figure 6.18 – Difference of suitable solar irradiation (see Equation (6.7)), depending on orientation (x-axis) and tilt angle (colors), with threshold $t = 0$, for a structured grid at increasing spacing: a) 1 m, b) 2 m, c) 3 m, d) 4 m, e) surface center. North is at azimuth = 0°. Some data points in Fig. Figure 6.18e are outside the y-limits. The squared data points represent horizontal surfaces (i.e. they do not have an azimuth) and have been arbitrarily set to $x = 0°$. Horizontal surfaces present the highest error values (both positive and negative). Among tilted surfaces, South-facing surfaces present as expected higher absolute error values. With increasing grid spacing, we can notice an increasing number of highly-underestimated irradiation at all orientation and tilts.*
*Source: Peronato et al. [227]*

future, as the difference in the results increases when considering lower thresholds. Conversely, for typical urban-scale assessments at present conditions only considering surfaces with more than 1000 kWh/m$^2$ per year, a low resolution is sufficient for having a good accuracy.

The orientation is related to the threshold. Vertical and North-exposed surfaces do not attain higher thresholds. In terms of vertical angle, façades have a higher relative variation with regards to the 0.5 m resolution grid. For this reason, we can assume that they also need smaller grid spacing in order to achieve good accuracy. However, a smaller grid spacing on façades is probably excessive, unless a higher LOD (including for example windows and balconies) is used.

In terms of tilt angle, roofs present greater difference with regards to the reference grid because they also have higher irradiation values. At all resolutions, flat roofs present significant variations, probably because of the presence of many roof superconstructions, whose shading effect is correctly represented only at very high resolutions.

In general, the error values found in this work are relatively small (e.g. 0.07 RRMSE for a 4-m spacing). We acknowledge that other uncertainty factors, such as, for example, the Level of Detail and reflective properties of surfaces, might have a higher impact than the ones analyzed in this work. However, we should consider that the grid size (as well as the ambient parameters) are freely set by the user and coarser settings are only determined by the need of reducing the computational cost. Differently, some other parameters rely on the quality of information that is available at the urban scale. In this sense, the use of standard reflective values is normally acknowledged in the literature (e.g. in Jakubiec and Reinhart [132], Fath et al. [81]), as this information is hardly obtainable for each single building.

#### 6.2.4.2 Comparison to relevant prior art

Similarly to what will be observed in Chapter 7 regarding the effect of vegetation on solar irradiation, also in this study we noticed that results are highly influenced by the analysis granularity. At the scale of the analyzed urban level, the difference between different grid resolutions is mostly negligible, while at the surface level we noticed a large variation in the results, which intuitively increases with the coarser grids. This is because, at the large scale, underestimations partially compensate overestimations of solar irradiation. On the contrary, at the surface level, the behavior of the grid at the different scales is unpredictable, as depends, among other factors, on the shape of the surface and the presence of obstructions.

As Alam et al. [11], we also noticed that shaded areas are those more impacted by the effect of resolution, at least in relative terms. As in their work, we saw that solar irradiation per building is not constantly over-estimated or under-estimated, but it depends on the specific building situation.

As both Alam et al. [11] and Bremer et al. [34] already noticed, we also confirmed that the accuracy of results decreases when using coarser grids. However, in terms of calculated relative errors, we have found smaller values than those obtained by Bremer et al. [34] (in their case, 10% of mean solar irradiation for a 1-m sensor grid resolution). This difference might be due to the different characteristics of the urban areas and calculation methods (e.g. in their case the obstructions are defined as voxels and the model does not account for reflected radiation).

#### 6.2.4.3 Limitations

The possibility of generalizing the results to other urban areas is hard to assess. We can assume that parameters that might influence the results are built density, building typology (including roof type), street aspect ratio and the presence of roof-top constructions. The characteristics of the analyzed area are common in many historical cities in Europe and we can thus expect similar results. Moreover, due to the specific characteristics, such as high built density and presence of roof-top constructions, we can expect that the findings of this study could represent a worst-case scenario. Similarly, the calculated irradiation ratio and RRMSE should be directly comparable to other locations with similar characteristics. However, the absolute difference and the RMSE calculated in this paper is clearly climate-dependent, therefore we cannot extrapolate this information to other contexts, unless it is normalized by the local mean irradiance.

Concerning the limitations of the model, the 3D model we used provides a quite accurate representation of reality, as it includes the actual roof shape as well as rooftop superstructures, but, as in LOD2 specifications, windows and balconies are not modeled. For this reason the area which is here considered as available for installing solar PV is probably overestimated. However, since we analyzed the surface-normalized values and considering that windows are usually homogeneously distributed on the façades, we can assume that the results are not significantly affected.

With regards to the method for testing the sensitivity of the results, we here used a simple parametric analysis focusing on the resolution of the sensor grid and its arrangement. Therefore, we generally used standard values for the other simulation-specific parameters, such as, for instance, the reflectivity of the materials and the number of inter-reflections. However, these and other parameters might have a combined effect with the grid resolution and arrangement, which was not investigated in this work.

### 6.2.5 Conclusions

This study analyzed the impact of the sensor grid resolution and its spatial arrangement on solar irradiation. The scope of this work was twofold:

1. defining the grid resolution allowing the best trade-off between accuracy and the number of sensor points (i.e. a proxy of computational cost) for urban-scale assessments
2. assessing the error that has to be considered, with regards to reference parameters, while using coarser resolutions.

We highlighted the importance of the grid arrangement and - to some extent - its resolution in the calculated solar irradiation. Results show that a structured grid is much more affected by resolution, as the number of sensor points substantially decreases along with the space interval. However, the decrease of sensor points potentially determines also a saving in the simulation time and allows an early evaluation of PV-suitable surfaces by excluding those that are too small.

We have also seen the importance of the scale at which results are analyzed. Sensitivity to the resolution augments with analysis at higher granularity. However, the median irradiation difference with the reference grid is not significantly varying between the thresholds.

The results of the comparison with Radiance show that the method proposed in this paper is more robust when using small spacing intervals, as it is less subjected to errors due to the simulation engine.

The results of the validation showed also the error up to a 2-m spacing interval is negligible, even at higher spatial or temporal granularities. In this sense, we can conclude that the results showed in this paper are also accurate till a 2-m resolution, while they could be biased due to simplifications in the simulation tool at coarser resolutions. We also noticed that the results are more affected by the simplifications of the simulation engine when analyzing hourly values (especially in winter) and surfaces, especially the inner and North-facing (azimuth ~ 25°) ones.

On the basis of the results and considering the limitations discussed in the previous section, we can finally provide some answers to the initial research questions.

*At which resolution does the error become acceptable?* All considered resolutions (0.5 to 4 m) provided acceptable deviations from the reference results (0.5 m). However, for structured grids with resolutions higher than 2 m, the error due to the simulation engine significantly affects the results and should be hence avoided. The choice can also be motivated by the fact the size of the long-side of a PV modules is generally smaller than 2 m (the median value from the CEC database [51] is 1.65 m).

*Are solar irradiation and PV-suitable area over- or under-estimated when using low-resolution grids?* When analyzing the results for the entire urban area, irradiation is slightly underestimated using coarser grids. However, if the results are analyzed per surface, most of them have overestimated results in terms of solar irradiation. This is likely caused by the significant losses due to shading of roof-top constructions, which determine a underestimation of some specific surfaces affecting also the entire urban area.

*In which spatial and temporal conditions does the influence of grid resolution affect the results the most?* Results are mostly affected during winter, which represent though a marginal part of the yearly solar irradiation. In relative terms, façades are more affected by resolution, while in absolute terms roofs show a stronger effect. In particular, roofs with over-constructions are in some cases highly affected by using a coarser grid ($< -100$ kWh/m$^2$·year).

Even accounting for the specificities of the analyzed urban area (in terms for example of morphology, architectural details and built density), we argue that the results of this study can be used to suggest an indicative spacing interval that provides a good trade-off between computational cost and accuracy of the results. Moreover, the same methodology can be also applied to a new location to check whether the proposed spacing interval is also optimal in other conditions.

### 6.2.6 Contribution to the thesis development

We presented here a preliminary study that helped the definition of the thesis final method that will be presented in Chapter 11. Because of its earlier development, we should remind that this study included though some differences with the final method. Apart from the different location (Geneva instead of Neuchâtel), it was based on 3D models with a different origin (SITG 3D model of Geneva Appendix A.1.6) but including a similar LOD as the SITN 3D cadastre of Neuchâtel (Appendix A.1.5) and did not include vegetation.

Due to the the large number of surfaces with a wrong normals orientation, a different healing procedure was necessary for the building geometry dataset (Algorithm 6.1), as opposed to the simpler procedure that will be described in Section 11.2.1.1. The study also had a lower number of ambient bounces (2) than the final method (3). As we have seen in Section 6.2.2, the limited number of ambient bounces

did not impact the findings on the grid resolution, while having a significant impact on the absolute irradiation value.

We summarize here below the main findings that contributed to the thesis development:

- The study provided a Grasshopper-based algorithm for the creation of a structured grid, which will be implemented in the final method (Algorithm 11.1); compared to the method used in Section 8.1, it preserves the distance between points constant across different surfaces. This algorithm determines a consistent reduction of sensor points to be simulated (and thus a saving of simulation time), while allowing the assessment of the geometric regularity (Section 8.1) and of the actual number of panels fitting a given building surface.
- The study suggested the use of a structured grid with a 2-m spacing for the simulation in Daysim. Based on these findings, we considered that this resolution provided a good balance between accuracy and simulation time compared to the reference 0.5-m grid and also a good match with the reference simulations conducted in Radiance. In this sense, the study also provided the validation of Daysim against the reference simulation engine Radiance, for our application.
- We have also seen the significant gain in solar radiation obtained by considering inter-reflections with `-ab 3` compared to `-ab 2`). The increase was less significant when adding an additional bounce (`-ab 4`), at the expense, though, of longer simulation time. For this reason, we will use `-ab 3` in the final simulation workflow (Section 11.3.1).

# 7 Modeling of vegetation from LiDAR data

This chapter includes a series of studies that conducted to the definition of the software workflow and modeling scenarios that will be implemented in the final thesis method (Section 11.2.2).

As shown in Section 4.1.4, LiDAR data provide convenient information for segmenting and reconstructing vegetation, while these are rarely used in 3D solar radiation studies nor in the related daylight analyses. The following sections will present a fully-3D modeling and simulation workflow that will be developed in this thesis. They will also show a scenario-based method to deal with the varied characteristics of vegetation. These characteristics, in particular the seasonal change of deciduous vegetation, are difficult to sense in urban environments where a large range of tree species are present, unless surveys at different seasons are conducted.

## 7.1 Preliminary study on façades

This study [1] assessed the sensitivity of solar irradiation to vegetation modeling. The analysis was conducted with limited datasets and a limited scope. In particular, it considered only on façade solar irradiation. This for two reasons: first, the analysis was based on a LOD1 model, which does not provide the actual shape of the roofs; second, we assumed that the effect of vegetation is much larger on façades than on roofs, at least in relative terms, because trees are usually smaller than a typical building, whose roof cannot hence be shaded.

### 7.1.1 Methodology

The processed datasets consist of (a) vegetation 3D-points from a LiDAR dataset (7-14 p/m$^2$), (b) a Digital Terrain Model (0.5 m resolution) and (c) a 3D vector model of buildings (LOD1). The workflow is composed of two main phases, as detailed below. Tiled data (350x350 m grid with a 50 m overlap on each side) produced in a GIS platform is imported and processed within the Rhinoceros CAD

[1] This section contains excerpts and figures from a published conference paper [221]: Peronato, G., Rey, E., & Andersen, M. (2016). 3D-modeling of vegetation from LiDAR point clouds and assessment of its impact on façade solar irradiation. In *ISPRS - International Archives of the Photogrammetry, Remote Sensing and Spatial Information Sciences* (Vol. XLII-2/W2, pp. 67–70). Athens. https://doi.org/10.5194/isprs-archives-XLII-2-W2-67-2016. The conference paper is published by Copernicus GmbH (Copernicus Publications) on behalf of the ISPRS under the Creative Commons Attribution 2.0 License and is reproduced here with the agreement of the co-authors. G.P.'s contribution included the design of the project, simulation and data analysis, and writing of the paper.

environment through the Grasshopper visual programming platform, coupled with different plug-ins and external programs.

Three tiles extracted from the city of Neuchâtel (46°59'N 6°56'E, 430 m asl), whose main morphological characteristics are listed in Table 7.1, comprise the case study for this paper.


*Figure 7.1 – The three selected urban areas (interior square = 250 m) with in colors the segmented tree crowns, in white the filtered points.*
*Source: Peronato et al. [221]*

*Table 7.1 – Green and built volume, calculated in a raster 2.5D model. The tiles IDs refer to Figure 7.1.*

| Tile | 204 | 235 | 238 |
|---|---|---|---|
| Vegetation [$m^3$] | 55222 | 91814 | 108560 |
| Buildings [$m^3$] | 455099 | 161460 | 192226 |
| Ratio [-] | 0.12 | 0.57 | 0.56 |

The tree segmentation and shape reconstruction phases are based respectively on voxel and convex-hull algorithms, which have been already used in the literature for ITCD [e.g. 313, 100]. A convex hull describes the biggest volume including the vegetation points, so it is particularly suitable to produce a scenario representing the maximum tree obstruction. The choice of these algorithms is also motivated by the fact that they are included in existing Grasshopper plugins or can be easily integrated in the workflow through coupling with external programs.

The LiDAR vegetation points are first processed using the Volvox plugin [2] for Grasshopper (see Fig. 7.1). The points are divided into several point clouds using a voxel topology of 50 cm, which is within the optimal size range suggested by Wang, Weinacker, and Koch [313] for LiDAR data of density between 5 and 12 p/$m^2$. To filter out the noise due to vegetation points, only clouds with more than 50 points are kept. Finally, the point clouds are processed in the QHull engine [18] to produce the convex hulls representing the trees.

The terrain mesh is created through a Delaunay triangulation using the DTM data. An evenly-spaced sensor grid of 1x1 m is created on all building surfaces. Building surfaces and terrain are defined as Lambertian diffusers with 0.30 and 0.10 reflectivity respectively, as suggested by IESNA [120], while for vegetation the following scenarios are used:

- 0 - Trees are not included, to model an extreme situation with trees without leaves and trunk.
- 1 - Trees are modeled with a translucent material, with 0.553 reflectivity and 0.19 transmissivity.

[2] http://www.grasshopper3d.com/group/volvox [Last accessed on June 5, 2016]

This settings are suggested by Radiance main developer Greg Ward, as cited by Jakubiec and Balakrishnan [131].

- 2 - Trees are modeled with an opaque material with 0.20 reflectivity, as suggested by by IESNA [120].

It should be noted that the time for simulating scenario 2 is significantly longer (up to 10 times) than the one for the other two. Also, because ambient bounces are limited to 2, only direct solar radiation passes through the vegetation canopy.

An annual simulation of solar radiation is conducted in Radiance/Daysim [244], through the Ladybug/Honeybee interface [259]. The simulation inputs are the sensor grid, the geometry (buildings, vegetation and terrain meshes) and the material definitions. During the ray-tracing, one reflection of each ray is taken into account by setting the number of permissible ambient bounces (`-ab 2`).

### 7.1.2 Results

As can be seen in Figure 7.2, the maximum annual variation (scenario 1 - scenario 2) for all tiles is of about 860 kWh/m$^2$. This corresponds to the maximum irradiation that can be achieved on façades, and that can be completely lost due to the obstruction of vegetation (scenario 1). Minimum values are also similar and negative for all façades. This is probably due to the reflection of trees on North-exposed façades. The upper and lower quartile boundaries show that the variation in this range is much smaller. We also notice that while the lower and median quartiles have similar values, the upper quartile significantly changes depending on the characteristics of the tile.

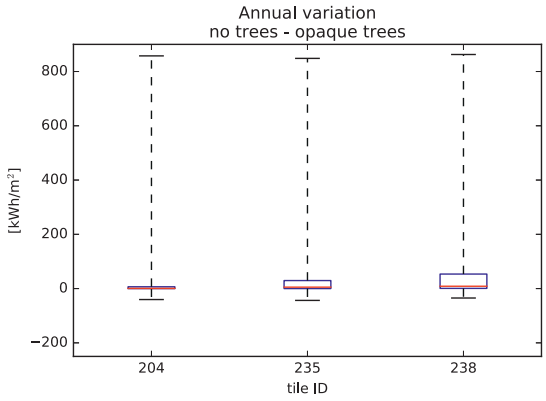


*Figure 7.2 – Absolute variation of annual solar irradiation per sensor point. The tile IDs refer to Figure 7.1.*
*Source: Peronato et al. [221]*

If we look at the results of single buildings, for example those of tile 204 in Figure 7.3b, we can see that the variation between buildings is very high, and in some cases can be much higher than the variation of the whole tile. In our findings, exposed buildings are more sensitive to the vegetation effects. This can be seen in the results of building 23, which has large South-exposed façades.

If we look at the monthly values (Figure 7.4a), we see a similar seasonal trend for all scenarios. In particular, scenario 1 is always between the curves of the other two scenarios. In relative terms, the

difference between scenario 0 and 2 (Figure 7.4b) shows a different trend, with peaks in winter and in summer.

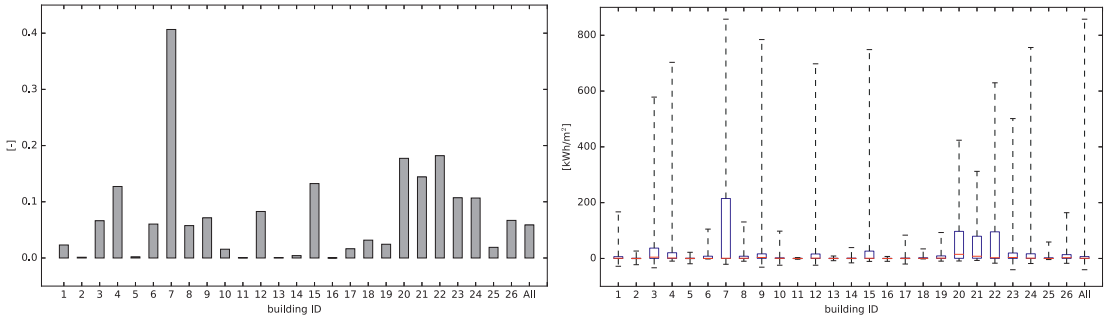


(a) Relative values per building

(b) Absolute values per sensor point

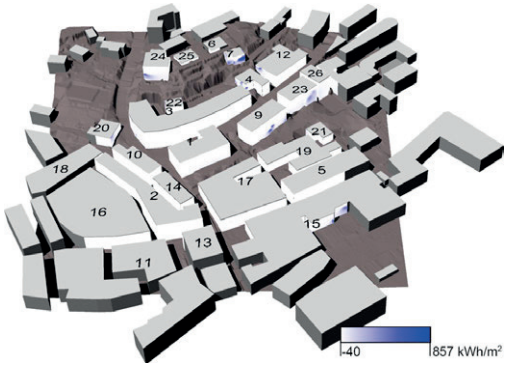


(c) Absolute values per sensor point in false colors.
Vegetation is considered but not shown

*Figure 7.3 – Difference of annual solar irradiation between scenario 0 and scenario 2 (tile 204)*
*Source: Peronato et al. [221]*

### 7.1.3 Conclusion

The results of the analyzed tiles fall within the ranges of relative variation of solar irradiation due to vegetation (3-20%) obtained by previous studies focusing on rooftops [164, 85]. In absolute values, the results are not directly comparable, because of the different climatic conditions as well as by the fact that our analysis was targeted to façades.

By using a higher level of spatial granularity than previous studies, we also showed that the value for the entire tile is not representative of the conditions of the different buildings and building surfaces belonging to it, at least in our case study, which has an irregular distribution of buildings and vegetation. In this sense, the method could have an useful application also for building owners, who would be able to evaluate the risk of irradiation loss due to vegetation in the different parts of the building envelope. The high spatial variability also suggests that the results cannot be extrapolated to different urban areas (e.g. many suburban developments where there is a regular arrangement of buildings and trees) nor climates. However, by increasing the number of simulated tiles, we would be able to check whether some geometric indicators such as the vegetation volume can predict the uncertainty on the calculated irradiation. This would help reduce the number of simulations of tree scenarios to only the tiles and/or

the building in which vegetation has a significant impact.

Although the absolute reduction of irradiation on façades found in the case-study application is rather low (median annual reduction of 1-9 kWh/m$^2$), in relative terms the results are comparable to those obtained by precedent studies on rooftops [164, 85]. Moreover, by augmenting the granularity of the analysis at the building scale, we have seen that the reduction can be very significant (up to 40% for a single building), depending on the solar exposure and the presence of obstructing vegetation.

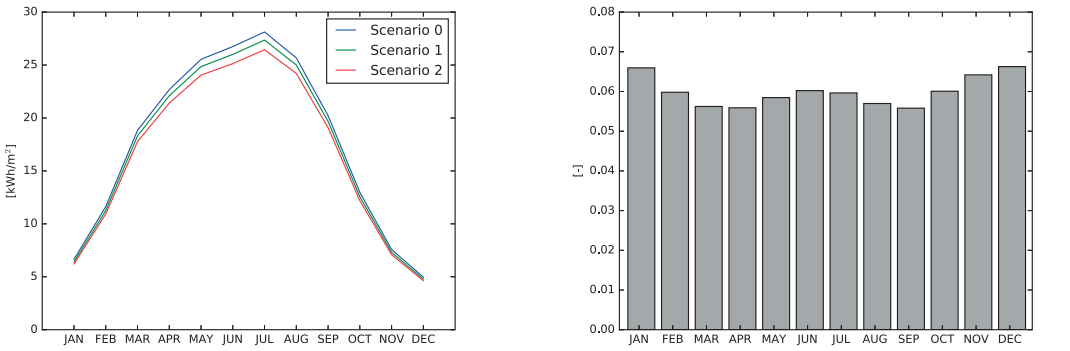


(a) Absolute values for the three scenarios

(b) Relative difference between scenario 0 and scenario 2

*Figure 7.4 – Monthly solar irradiation (tile 204)*
*Source: Peronato et al. [221]*

### 7.1.4 Contribution to the thesis development

As a reminder, this study was conducted as a preliminary exploration to the use of LiDAR reconstructed vegetation in solar studies. For this reason, it presents some differences with the final thesis method presented in Chapter 11. In particular, it is based on a LOD1 3D model (Appendix A.1.1) of Neuchâtel, as opposed to a LOD3 model of the same city (Appendix A.1.5), and of a 1x1-m grid, as opposed to a 2x2-m irradiation grid. The analysis was limited to façade solar irradiation, as the LOD1 model was considered inaccurate for assessing the results of rooftops (see Section 6.1), and it used a ConvexHull to reconstruct the shape of the vegetation based on the popular software qHull, insted of its generalization alpha-shape, that was implemented in the final workflow using MATLAB (Section 11.2.2).

We highlight here below the findings that contributed to the definition of the final method presented in Chapter 11:

- The 3D-representation of vegetation through the ConvexHull is not always very accurate, mostly due to the errors in the segmentation phase when considering contiguous trees (see Figure 7.1). We can also notice that the resulting shape is a worst-case scenario, because, by definition, the actual tree shape is always contained into the hull and in some cases it might be significantly smaller. As already mentioned in Section 2.3.3.2, alpha-shapes allow the integration of the segmentation phase as well as of shape-control parameters giving a more realistic representation of the tree shape. For these reasons, alpha-shapes will be used in the final thesis implementation presented in Section 11.2.2.
- Regarding the semi-transparent nature of trees, we have seen that the results of scenario 1 are

always within the values of scenario 0 and scenario 2, while, in absence of measurements, we do not know whether the actual results would be closer to scenario 0 or 2. Therefore, we can argue that, in absence of measured values, these extreme scenarios (o and 2) provide a better description of the uncertainty that has to be considered while assessing the solar potential of an urban area. Moreover, the lower simulation time makes these scenarios more suitable for large-scale assessments.

## 7.2 Random vegetation input

This study [3] was aimed at improving the decision-making based on multiple modeling scenarios for vegetation, as the ones presented in Chapter 7. The hypothesis behind this study was that random sampling would give a better understanding of the effect of vegetation on solar potential by simulating the actual distribution of evergreen and deciduous vegetation in an urban location. We consider here, as in the final methodology (Section 11.2.2), only two vegetation scenarios: 'no trees' or 'opaque' (corresponding to scenario 0 and 2 in Section 7.1.1).

The random vegetation input is composed by sampling each of these scenarios with equal probability at each time step using Algorithm 7.1, which is also illustrated in Figure 7.5. The proportion of sensors blocked or not blocked by vegetation (obstructed vs unobstructed) is determined by taking an evenly-spaced sample from a standard uniform distribution, i.e., $P(op) \sim \mathscr{U}(0,1)$ and $P(nt) = 1 - P(op)$ ($op$ → opaque, $nt$ → notrees). The proportions of obstructed and unobstructed sensors in the 'synthetic simulation' resulting from Algorithm 11.9 corresponds to $P(op)$ and $P(nt)$.

We produced randomly-sampled DC production from the vegetation scenarios with the method described in Algorithm 7.1 and Figure 7.5. We show the results of 450 vegetation scenarios: 50 randomly-sampled combinations for 9 different increasing ratios of 'no trees' and 'opaque' scenarios (from 0.1 to 0.9). The ratios are a proxy for partial-obstruction, as if each tree was either completely obstructing a panel at some time or not.

Figure 7.6 shows that the randomly-sampled data does not provide any additional information compared to the extreme min/max scenarios. In fact the box-plots are symmetrical with respect to the median, i.e., the first and third quartiles are always positioned at the same distance from the extremes. This implies that the distribution of the output is completely governed by the sampling distribution of ratios. Testing with other distributions confirmed this.

These findings contributed to the definition of the final method presented in Chapter 11 and applied to the case study in Chapter 12, which is based on the two extreme scenarios 'no trees' and 'opaque', without random sampling. In particular, we developed a method to compare different urban locations based on these scenarios, which will be introduced in Section 11.4.3.

[3] This study was conducted for the test-case application presented in Chapter 12 with a methodology very similar to the one presented in Chapter 11. The following paragraphs contain excerpts from the original publication [226]: Peronato, G., Rastogi, P., Rey, E., & Andersen, M. (2018). A toolkit for multi-scale mapping of the solar energy-generation potential of buildings in urban environments under uncertainty. Solar Energy, 173, 861–874. https://doi.org/10.1016/j.solener.2018.08.017. The text and the figures are reproduced here as a courtesy of the publisher and with the agreement of the co-authors. G.P. contributed to the development of the algorithm and the writing (with P.R.). The numerical results are slightly different than in the original publication, because of the different parameters used.

**Data:** $h$-by-$p$ matrix of hourly electricity for the two vegetation scenarios, where $h$ are the hours and $p$ the sensor points.
**Result:** $h$-by-$p$matrix of hourly electricity with random sampling of the two vegetation scenarios.

1. generate $n$ generations of $p$-long mask array filled with 0s, corresponding to 'off';
2. for each generation $g$, fill the first $g/n \cdot p$ elements of the mask array with 1s, corresponding to 'on';
3. shuffle the mask array $m$;
4. apply the mask $m$ to one vegetation scenario $s$ and the inverted matrix $\neg m$ to the other vegetation scenario;
5. sum the two resulting masked vegetation matrices.

**Algorithm 7.1:** Sampling algorithm to create the random vegetation scenarios from a standard uniform distribution of 'no trees' and 'opaque' scenarios. The algorithm is illustrated in Figure 7.5.

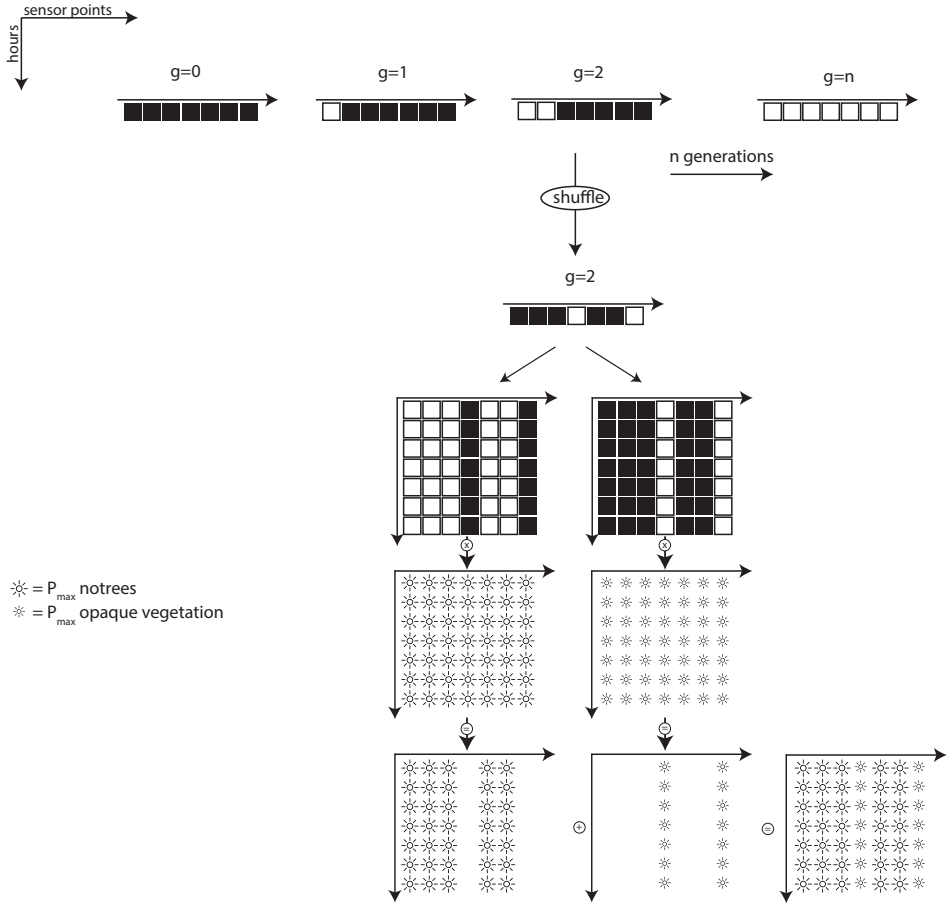


*Figure 7.5 – Illustration of the Algorithm 7.1 used to create the random vegetation scenarios from a standard uniform distribution of 'notrees' and 'opaque' scenarios.*
*Source: Peronato et al. [226]*

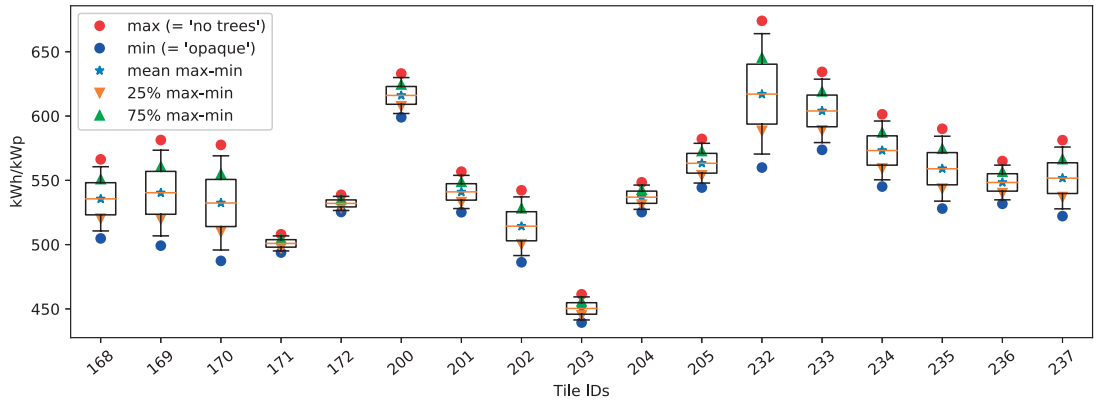


*Figure 7.6 – Boxplot of simulation outputs from randomly-sampled vegetation scenarios. The ratios of obstructed:unobstructed sensors were sampled as described in Algorithm 7.1, i.e., from a uniform distribution. The dataset is the same used in Chapter 12. The location of the tiles are shown in Figure 12.5.*

# 8 Arrangement of PV modules on buildings

As we have seen in the state of the art (Section 4.2), the potential of building-installed solar systems responds to both architectural-integration and performance criteria, which have a direct influence on the location and arrangement of solar systems. Some of these criteria are difficult to evaluate at the urban scale, as they rely on the evaluation of many decision-makers, in particular the building owners, that are likely to have different attitudes and priorities (e.g., between aesthetics and return of investment).

This section contains two studies investigating the impact of arrangement strategies on the energy yield of solar systems from two different perspectives and applications. The first study (Section 8.1) deals with the architectural integration potential of BAPV or BIPV modules installed at the same tilt of the surface they belong to. More specifically, it presents a method to assess the geometric regularity of these installation. The second study (Section 8.2) deals instead on the economic and environmental potential of tilted arrays installed on flat roofs. It aims at finding the installation conditions (tilt angle and spacing) of tilted arrays maximizing relevant financial and environmental indicators, so as to have a more realistic indication of the solar potential of flat roofs.

## 8.1 Geometric regularity of building-attached solar installations

This study[1] presents an algorithm introducing a geometric-regularity criterion aimed at the early assessment of solar enegy-generation potential in urban contexts.

We consider here only solar systems installed at the same tilt of the building surface, such as BIPV and some BAPV systems. As we have seen in the state of the art (Section 4.2.4), the arrangement of the modules on the building surfaces plays a role in the acceptability of the installation and some regularity criteria have been introduced in the federal and cantonal legislation.

[1] This section contains excerpts from a published conference paper [219]: Peronato, G., Rey, E., & Andersen, M. (2015). Sampling of building surfaces towards an early assessment of BIPV potential in urban contexts. In *Proceedings of PLEA2015 Architecture in (R)Evolution*. Bologna. Retrieved from https://infoscience.epfl.ch/record/209966/files/PLEA2015_Peronato_final.pdf. The text and figures are reproduced here as a courtesy of the conference organizers and with the agreement of the co-authors. G.P.'s contribution involved the design of the study, simulation, data analysis and writing. We follow here the same structure as in Chapter 11 to facilitate the comparison with the final workflow implemented in this thesis.

### 8.1.1 Methodology

The sampling algorithm is based on a geometric-regularity criterion. Its definition is inspired by a selection of design guidelines provided by the Canton of Geneva [281], such as "regrouping the [PV] elements", "adopting preferably a rectangular shape" and "respecting building contours and the parallelism of lines" (translation ours). Two approaches towards geometric regularity are evaluated and compared with a standard calculation method based only on a solar irradiation threshold.

In the first approach, which we refer to as the *conservative approach*, the parts of the façade that, despite achieving the irradiation threshold, prevent a regular disposition of solar panels on that surface are discarded. Conversely, the *aggressive approach* takes into account also those parts of the façade that, despite not achieving the irradiation threshold, allow a regular disposition of solar cells on that surface.

This concept is implemented in an algorithm (Algorithm 8.1 and Figure 8.1) that analyzes the grid of points created on each building surface to be used as sensors in the simulation of solar radiation. These points are organized in parallel horizontal lines so that their belonging to a particular line can be used in the sampling algorithm to determine if the geometric-regularity objective is fulfilled.

- In the **conservative approach**, a sensor $p_{b,s,l}$ is considered suitable for BIPV installation only if all the sensors on the line $l_{b,s}$ achieve the irradiation threshold.
- In the **aggressive approach**, if a certain number ($n_{min}$) of sensor points $p_{b,s,l}$ of the line $l_{b,s}$ achieve the irradiation threshold, all the sensor points on the line $l_{b,s}$ are considered suitable for a BIPV installation.

**Algorithm 8.1:** Description of the geometric regularity approaches. See also the graphical representation in Figure 8.1.

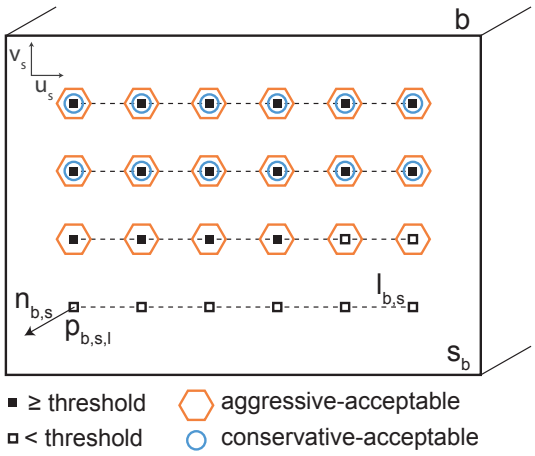


*Figure 8.1 – Graphical representation of the selection of sensor points (Algorithm 8.1) based on irradiation threshold and regularity.*
*Source: Peronato et al. [219]*

As can be seen in Figure 8.1, by using the aggressive approach, two points not achieving the threshold are considered acceptable. The minimum number of sensor points ($n_{min}$) for a line to be considered

suitable can be freely fixed by the user. The smaller its value is, the greater is possibly the number of sensor points that will be considered suitable despite not achieving the irradiation threshold. In this work, the most extreme scenario, i.e. $n_{min} = 1$, was chosen in order to show the maximum possible increment in energy production that can be obtained by this approach. However, if the choice of the irradiation threshold is determined by an economic or environmental minimum payback time, the decision-maker should accept the risk of the non-viability of the installation. If such viability is determinant for the project and the geometric regularity is still considered an important factor, the conservative approach should be chosen instead.

#### Modeling

The Algorithm 11.7 is tested in three buildings from an automatically-reconstructed 3D city model. The 3D model of Neuchâtel (see details in Appendix A.1.3) is created using the software BuildingReconstruction [307]. This modeling workflow is implemented in Grasshopper through its standard components.

The distance between points, in both $u$ and $v$ directions, was set to 1 m, as it is considered a standard value for urban-scale solar simulations (see Table 4.2).

#### Simulation

The simulation was run through Diva-for-Grasshopper using the GenCumulativeSky algorithm [254] (see also Section 4.1.1), which provides the annual cumulative solar irradiation for each sensor point, expressed in kWh/m$^2$.

The simulation results were processed through Algorithm 8.1 and converted into electricity using fixed PV efficiency ratios: 15% for roof and 8% for façade surfaces, considered among the standard values for, respectively, polycrystalline silicon- and cadmium telluride-based modules [105, para. 1.4.2]. The latter is considered a more suitable technology for façade installation, due to the higher probability of having partial shading on some cells, which would more highly affect the performance of polycrystalline modules [146], as well as because of the wide range of possible installations as thin-film (e.g. on shading devices or integrated in glazing).

#### Evaluation

The irradiation results, expressed in kWh/m$^2$ of exposed surface, were transformed in kWh by multiplying the value of each point by the sensor point mean area, calculated by dividing the area of each surface $s_b$ by the number of sensor points $p_{b,s,l}$. The obtained values were then converted to energy production using the above-mentioned PV-efficiency coefficients and finally normalized in kWh/m$^2$ of footprint surface in order to compare buildings of different sizes with the same reference scale

### 8.1.2 Results

Figure 8.3 shows that the use of the conservative and aggressive approaches determine, respectively, a reduction and an increment in the energy production with respect to the normal calculation method (i.e. the one without geometry sampling) for all selected irradiation thresholds, except for those from 1175 to 1250 kWh/m$^2$ as no sensor point is within this range. Moreover, the difference in energy production

can significantly vary depending on the chosen threshold and geometric-regularity approach.

In general, the loss in energy production due to the conservative approach is greater than the possible increment due to the aggressive approach. However, this is not the case for a threshold of 1150 kWh/m$^2$, which brings about a 134% increment for the aggressive approach and only a 71% reduction for the conservative approach. In this case, only scattered roof parts of buildings A and B achieve the irradiation threshold and are hence discarded using the conservative approach, while a much larger surface gets considered if the normal and aggressive approaches are implemented, as can be observed in the fourth column of Figure 8.2.

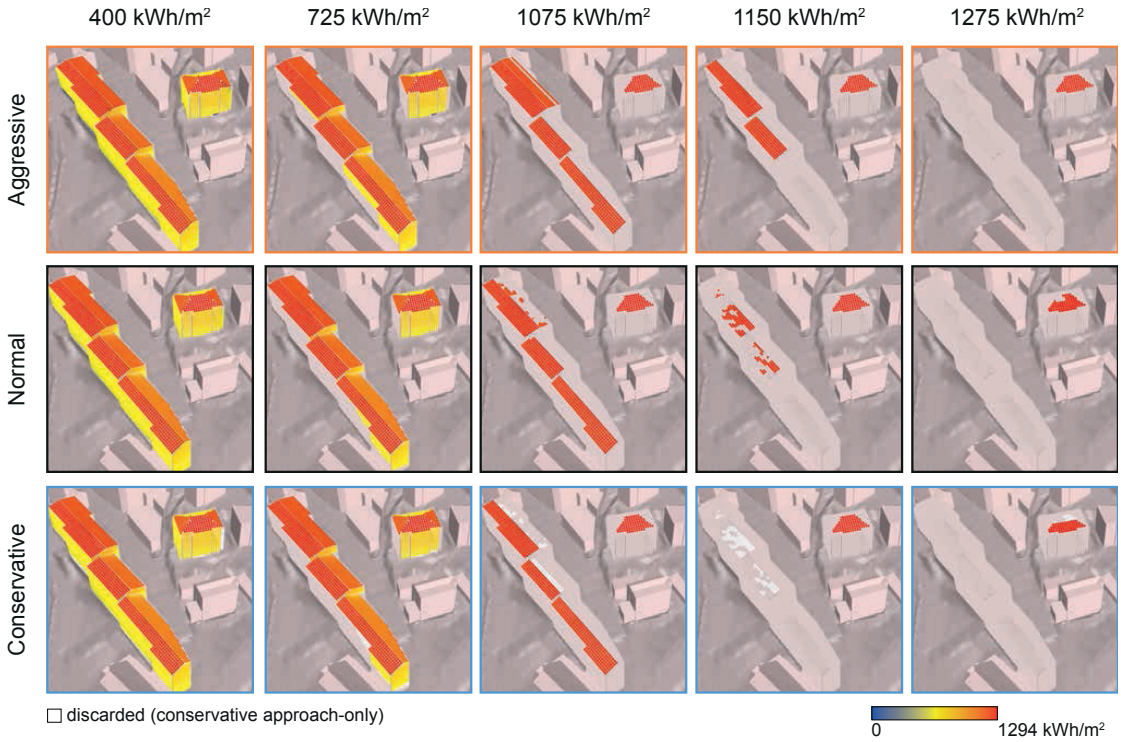


*Figure 8.2 – Suitable surfaces as defined by the proposed approaches (Figure 8.1) for different irradiation thresholds*
*Source: Peronato et al. [219]*

### 8.1.3 Contribution to the thesis development

As a reminder, this was a preliminary study to assess the impact of geometric regularity approaches to the solar irradiation, and, due to its limited scope and early development in the thesis work, presents several differences with the final analysis method that will be described in Chapter 11. In particular, it implements the GenCumulativeSky [254] model (see section 4.1.1) as integrated in the DIVA-for-Grasshopper interface, with minimum ambient bounces settings (`-ab 2`), as opposed to Daysim with `-ab 3` used in the final workflow. The study is based on a 3D model reconstructed from a DSM (Appendix A.1.3) at a LOD2, and therefore it does not include roof superstructures as in the final 3D model at LOD2.3.

The study contributed to the definition of the final method presented in Chapter 11 by showing the effect of a geometric regularity approach in a threshold-based calculation of solar energy potential.

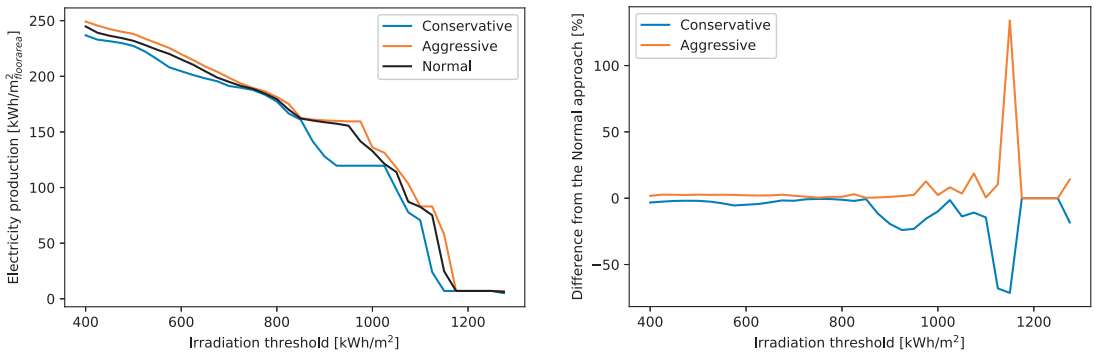


(a) Energy production for each approach

(b) Difference with the normal approach

*Figure 8.3 – Absolute (a) and relative (b) energy production values for the considered approaches at different minimum irradiation thresholds*
*Source: Adapted from Peronato et al. [219]*

To this end, it helped define a data-tree structure in Grasshopper ($\{b;s;l\}$) that stores the information regarding the line $l$ to which each sensor belongs to and allows hence the application of a geometric-regularity approach. This data structure was also used in the final implementation of the Algorithm 11.7. The study also provided the first version of the Algorithm 11.1 to create a structured grid, while missing the steps 3-4 of ensuring a constant distance between the sensor nodes.

## 8.2 Performance of tilted solar arrays

In this study[2], we investigated the potential for Building-Applied Photovoltaics (BAPV) systems installed as tilted arrays on flat roofs as they are still a very common solution. In fact, these systems are generally cheaper than Building-Integrated Photovoltaics (BIPV), while providing optimal installation conditions, due to flexible orientation and tilt angle, and good ventilation.

When assessing the photovoltaic potential of a city, a large variety of installation conditions of roof BAPV arrays exists, such as size, azimuth and simple/double orientation (e.g. S or E-W), and tilt angle. However, in solar cadastres the assessment is commonly done assuming that PV panels are installed horizontally, as in the Swiss Federal Solar Cadastre (SFSC) (see Section 13.3), or by adjusting the results considering a fixed tilt and spacing [22]. Yet, even if a horizontal array would maximize the number of installed panels, such an installation is not technically feasible, because of lack of water drainage and dust self-cleaning. On the other hand, optimal tilt angle and spacing will depend on the specific building and surrounding conditions (in terms of size, shading, inter-reflections), regulatory framework (e.g. self-consumption, incentives) and optimization objectives (e.g. financial or environmental).

[2] This study was conducted in the framework of a semester project [162] co-supervised by the author and later summarized in a conference paper [225]. This section contain excerpts from the conference paper: Peronato, G., Aguacil Moreno, S., Legrain, A., Vitali, S., Rey, E., & Andersen, M. (2018). *Assessing the photovoltaic potential of flat roofs: insights from the analysis of optimised array arrangements.* To be presented at PLEA 2018, Hong Kong, China. The text is reproduced here as a courtesy of the conference organizers and with the agreement of the co-authors. G.P.'s contribution was the design of the project, its supervision (with S.A.M.) and the writing. After describing the study-specific methodology, we follow the same structure as the Chapter 11 to facilitate the comparison with the final workflow implemented in this thesis.

### 8.2.1 Methodology

We compared different tilted installation strategies, maximizing either the financial or the environmental benefits, to simplified horizontal assessments on three flat roofs in a dense urban area (Figure 8.4). The analysis was conducted on three case-study buildings that are presented in Table 8.1.

We implemented a parametric study to test the effect of different tilt angles (5-26°, with a 1° step) and distance of arrays (0-195 cm, with a 15-cm step) on the chosen indicators for the two considered orientations. Unlike typical approaches defining the inter-array distance based on a maximum number of shaded hour in the winter solstice [6], our method avoids the arbitrary choice of such a parameter and allows the inclusion of indirect radiation to find the optima for each indicator.

*Table 8.1 – Characteristics of the analyzed flat-roof buildings. Their location is plotted in Figure A.2 and an aerial view can be seen in Figure 8.4.*

| Building | A | B | C |
|---|---|---|---|
| Roof area [$m^2$] | 459 | 591 | 207 |
| Floor area [$m^2$] | 1353 | 3014 | 880 |
| Orientation | South-East | South-East | South-East |
| Type of obstructions | Vegetation | Stairwell, chimneys | Stairwell, chimneys |


*Figure 8.4 – Aerial view of the three case studies buildings.*
*Image: ©2014 SITN*

#### Modeling

We used a 3D model of the three buildings and their surroundings (Neuchatel - LOD2.3), including vegetation and terrain, as described in Section 11.2.

We studied two typical orientations of PV panels: South-facing to maximize per-panel production and East-West double-oriented to maximize the size of the installation while matching the building load-curve.

#### Simulation

The parametric study was conducted in Grasshopper coupled with Daysim, through the Honeybee interface, to simulate hourly solar irradiances on tilted panels, as described in Section 11.3.1. The PV yield was calculated using a fixed efficiency of 19.7% and an annual degradation rate of 0.55%, corresponding to a high-tier polycrystalline module available on the market at real installation conditions.

#### Evaluation

We selected three possible installation strategies corresponding to three different approaches installers may take in current practice. The first indicator ("energy cost") exemplifies the approach of an energy utility company that wants to minimize the Levelized Cost of Electricity (LCOE). The second approach ("profit") is aimed at maximizing the profit of an investor, considering the cost of both self-consumed and grid-injected electricity, calculated as the Net Present Value (NPV) on a 25-year period. The third indicator ("$CO_2$ avoidance") considers the environmental impact of the installation by maximizing the avoided carbon intensity with respect to an alternative energy source. Financial parameters refer to current (2017) Swiss local and federal legal framework, with one-time power-based subsidies for <100kWp installations, and a feed-in rate varying depending on the size of the installation, but always lower than the electricity-buying price, which makes self-consumption particularly interesting. Estimated income-tax deductions and interest rate (5%) are also included in the financial model.

For the environmental model, we assumed a substitution of the imports from the German grid (conservative value of 300 $gCO_2$/kWh [299]) and estimated the carbon footprint of solar panels as 70 $gCO_2$/kWh, which is consistent with LCA studies (Table 2.3).

### 8.2.2 Results

If we consider the "profit" indicator (Table 8.2), S-oriented arrays provide the best results for buildings A and B, while an EW orientation gives the best results for building C, as it maximizes the number of panels on its smaller roof surface (hence benefiting from peak-power subsidies).

Table 8.3 shows that the electricity yield with optimized tilted arrays is always lower or equal to the one calculated assuming flat panels (simplified method). Similar values are reached when using the "$CO_2$ avoidance" approach as well as when considering building C, as in both cases the number of installed panels is maximized by using an EW orientation.

Despite the peak-power subsidies and self-consumption benefits, financial-based strategies ("energy cost" and "profit") favor smaller size, higher-yield South-facing installations for buildings A and B. However, for building C, due to the smaller available roof surface, the array size should be maximized for economy-of-scale reasons, and hence installed facing East-West. Horizontal installations can approximate only the "$CO_2$ avoidance" indicator. Differently, for the financial indicators, there is no generalizable tilted-to-horizontal ratios, as the roof size, coupled with the incentive/feed-in framework, plays also an important role.

### 8.2.3 Contribution to the thesis development

This study was aimed at finding a conversion ratio from the simulated PV potential on horizontal sensor nodes to the actual production of tilted arrays. To this end, it used similar tools and data than in

*Table 8.2 – Arrangements maximizing the "profit" indicator for the analyzed buildings and orientations*

| Building | A | | B | | C | |
|---|---|---|---|---|---|---|
| Array orientation | S | EW | S | EW | S | EW |
| NPV [kCHF] | 15.5 | 1.2 | 26.7 | 19.1 | 9.8 | 10.5 |
| Tilt angle [°] | 26 | 5 | 26 | 5 | 5 | 7 |
| Spacing [cm] | 165 | 195 | 165 | 80 | 15 | 0 |
| Power [kWp] | 29.0 | 36.9 | 27.6 | 51.1 | 18.6 | 21.7 |
| N. of panels [-] | 84 | 107 | 80 | 148 | 54 | 63 |
| Yield [MWh/y] | 24.1 | 27.6 | 25.2 | 41.9 | 15.6 | 17.8 |

*Table 8.3 – Yield ratios of tilted arrays to horizontal arrays for the analyzed buildings and indicators*

| Building | A | B | C |
|---|---|---|---|
| "Energy cost" | 0.74 | 0.73 | 0.93 |
| "Profit" | 0.44 | 0.38 | 0.93 |
| "$CO_2$ avoidance" | 0.99 | 1.03 | 0.96 |

the final workflow presented in Chapter 11 (same modeling workflow, Daysim simulation for hourly irradiances), while using a fixed coefficient ratio, as opposed to the PVLIB model implemented in the final thesis workflow. It also used only 2 ambient bounces (`-ab 2`), as this was considered as appropriate for simulations on roofs only.

The results from the tested buildings showed that tilted arrays provide 38 to 103% of the energy yield on a hypothetical horizontal installation depending on the roof and indicators. Based on this limited number of case studies, it is not possible to draw general conclusions on the best arrangement for PV arrays on flat roofs.

We can speculate that there is a maximum size of buildings for which it is worth to have almost horizontal modules, as it is the case of building C, which is the smallest of the three buildings and have values of about 0.95 for all indicators (Table 8.3). Similarly, we have noticed, that similar values are reached for the environmental indicator, which is stable for all three analyzed buildings.

Based on these findings, we can consider that almost-flat PV modules maximize the energy production and thus also the $CO_2$ avoidance indicator. In the case of small buildings, there might be an interest for this arrangement also for financial indicators. At the same time, a minimum tilt of about 5° should allow adequate water drainage. For these reasons, for the thesis final method (Section 11.3.3.3), we opted for a 0.90 reduction coefficient ratio for flat roofs, considering a minimum tilt and some free space for panel inspection.

# 9 Assessing the performance robustness of urban design variants

This section contains the outcomes of two studies that have a partially-different scope from the rest of the thesis. The authors were asked to evaluate the performance of urban designs from student studio projects at EPFL. Therefore, these studies deal with the evaluation of design proposals of new neighborhoods rather than of existing buildings as in the other sections of this thesis. However, since the research problem involved a similar decision-making framework, these studies contributed to the development of the final thesis method and we think that they are a relevant contribution to this Part II.

Because of their peculiarity, the concept of Level of Detail (LOD) cannot always be applied to these studies. Although most of the projects look like a LOD1 3D model (i.e., a *shoe-box* model), we do not know whether this depends on the early stage of the design process, in which the actual roof shape has not been decided yet, or it is due to a precise choice of having flat roofs.

The goal of these studies was to show that the evaluation, expressed as a ranking, of the urban design is highly dependent on some parameters fixed by the user, which depend on their attitude towards the payback time of the investment and towards the risk connected to weather. To this end, we assessed the robustness of the ranking to the change of the irradiation threshold and the radiation scenario.

## 9.1 Evaluation under varying evaluation conditions

This study[1] evaluated 8 student projects (represented in Figure 9.3) for the "Gare-Lac" area in the city of Yverdon-les-Bains (Switzerland). The original publication [195] contained an analysis of both its active and passive solar potential. We will report here only the active solar potential study which was conducted by the author. They are completed and re-structured so as to be consistent with the method structure presented in Chapter 11.

[1] This section contains some excerpts translated from a book chapter originally published in French [195]: Nault, E., Peronato, G., & Andersen, M. (2015). Forme urbaine et potentiel solaire. In E. Rey (Ed.), *Urban Recovery*. Lausanne: Presses Polytechniques et Universitaires Romandes (PPUR). The text is reproduced here as a courtesy of the publisher and with the agreeement of the co-authors. G.P. contributed to the design, simulation, data analysis and writing of the part of chapter related to active solar potential that is presented here.

### 9.1.1 Methodology

In this work, we consider both Solar Thermal (ST) and Photovoltaics (PV) potential, calculated as described in Algorithm 9.1. ST is considered here as a viable alternative to the combined use of PV and heat pump for the production of Domestic Hot Water (DHW). The solar thermal is actually determined by the estimation by the demand, which is here limited to the 50% of the DHW need during the heating season in order to prevent an oversizing of the system.

- Sort sensor points by cumulative thermal energy production over winter time;
- Consider for ST those sensor points that provide the Domestic Hot Water (DHW) sizing demand, which is calculated as follows:

$$DHW_{sizing} = A_{th,u} \cdot (DHW_{needs_u}/3.6) \cdot \frac{8}{12} \cdot 0.5, \qquad [\mathrm{kWh/m^2}] \quad (9.1)$$

  where $A_{th,u}$ is the floor area for a building use $u$, and $DHW_{needs_u}$ are the DHW thermal energy needs [MWh/m$^2$] shown in Table 11.9 (e.g. 75 MWh/m$^2$ for use $u$ as multi-family housing);
- Consider all other sensor points for Photovoltaics (PV).

**Algorithm 9.1:** Calculation of the Solar Thermal (ST) and Photovoltaics (PV) potential

The suitable irradiation is calculated using Equation (6.4). We considered thresholds $t$ in the range [400;1200] kWh/m$^2$ at 100 kWh/m$^2$ steps for PV. No threshold was used for ST calculation. A target irradiation threshold was obtained with a simple financial calculation based on the Net Present Value (NPV):

$$NPV = \sum_{y=0}^{n} \frac{C_y}{(1+r)^n}, \qquad (9.2)$$

where $C$ are the cash-flows for the year $y$ and $r$ in the interest rate. The calculation considers an initial investment $C_{y=0} = -500$ CHF/m$^2$ generating a positive cashflow at every year $y$ through the electricity that can be sold (or self-consumed) at 0.20 CHF/kWh, which is depreciated by an interest rate $r = 2\%$. Considering a payback time of 20 years, the NPV becomes positive at $y = 20$ if we consider an irradiation of 1020 kWh/m$^2$. We can then assume that a 1020 kWh/m$^2$ minimum threshold would provide a 20-year payback. This is a conservative estimation as many modules would actually exceed the target irradiation value. However, we do not consider the operation and maintenance costs of the installation and the time of use, which has as an influence in the actual energy financial value, as the electricity injected into the grid is expected to have a lower remuneration price than the self-consumed one.

The calculation of the energy production (thermal energy for ST and electricity for PV ) used a fixed energy conversion efficiency of 0.70 for ST and of 0.15 for PV (0.08 when installed on façade, assuming the use of thin-film technologies to provide more flexible architectural integration, also in windows and balconies).

#### Modeling

We used the 3D models of the student projects at a supposed LOD2 and of the surrounding buildings at LOD1, while the terrain was modeled as a flat surface. The surface area for housing, respectively for services, was determined on the basis of the student drawings and the figures are listed in Section 9.1.1.

All building surfaces were modeled with a 0.30 reflectance, respectively 0.10 for the ground surface..

A typical weather file was obtained in Meteonorm [246] for Yverdon-les-Bains using the latest available radiation data (2000s).

*Table 9.1 – Characteristics of the analyzed projects and DHW sizing needs as calculated in Equation* (9.1)

| Project | Housing floor area [$m^2$] | Commercial floor area [$m^2$] | DHW sizing demand [MWh] |
|---|---|---|---|
| **CPH** | 111492.0 | 66722.0 | 928.7 |
| **LYN** | 255448.0 | 63862.0 | 1921.8 |
| **AMS** | 167210.7 | 72724.3 | 1330.5 |
| **LLN** | 132476.4 | 88317.6 | 1124.4 |
| **MIL** | 117997.5 | 39332.5 | 910.5 |
| **BER** | 265766.0 | 34674.0 | 1925.9 |
| **BCN** | 187024.3 | 86923.7 | 1500.0 |
| **DUB** | 185477.5 | 89752.5 | 1495.8 |

#### Simulation

Simulations for solar radiation were conducted using Radiance and the GenCumulativeSky model [254] through the Diva-for-Grasshopper interface. We considered two different time periods: the whole year and the heating season only (15 September-15 May).

#### Indicators

The considered indicators and rankings are based on energy generation (or surface of solar collectors) normalized by the footprint (or conditioned floor) surface area. It should be noted that this analysis targets thus installations that provide the most energy for a given surface area, but not necessarily the ones that make better use of the generated energy to respond to the demand of the buildings.

### 9.1.2 Results

As shown in Figure 9.1a, LLN is ranked first for solar thermal potential, thanks to the sloped South-facing roof. Conversely, CPH's potential is jeopardized by the terraced buildings, which are shading it and decrease hence the solar irradiation on its envelope. Excluding these two extreme cases, the other projects present similar results.

When analyzing the PV solar potential, using a 1020 kWh/$m^2$ threshold, we obtain similar results for most of the projects. For the same above-mentioned reasons, CPH is also the project with the lowest performance. On the other hand, LLN, which had the best performance for ST potential, is now ranked second-last for PV potential. This is because the most favorable surfaces in terms of solar exposure, i.e. the South-facing roof faces, have been extensively used for solar thermal and only a small share of the other surfaces achieves the threshold fixed for photovoltaics.

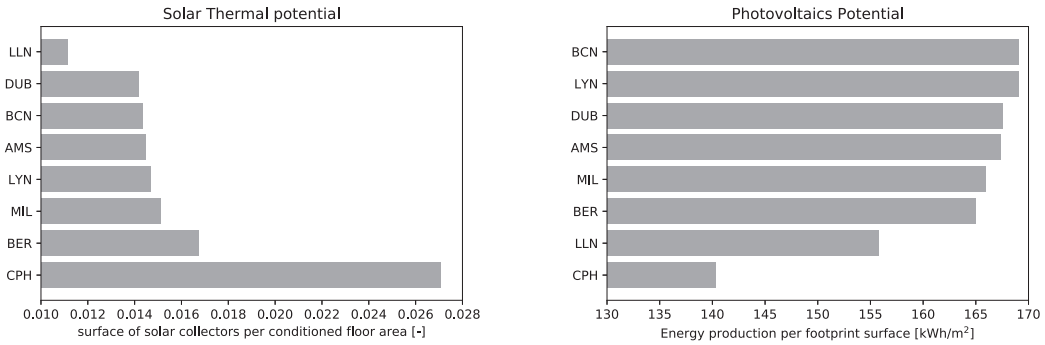


(a) Solar Thermal

(b) Photovoltaics - threshold = 1020 kWh/m$^2$

*Figure 9.1 – Solar energy production*

The choice of the solar irradiation threshold is based on a simplified financial analysis neglecting factors such as the possible electricity price increase or the improvement of solar cells efficiency (or decrease of their cost). Moreover, it considers a standard payback time, which might not be appropriate for some investors. For these reasons, the comparison of results obtained with different thresholds becomes relevant.

The sensitivity analysis shows that the projects' ranking is significantly influenced by the choice of the irradiation threshold. While the ranking is almost stable till a 900 kWh/m$^2$ threshold, the situation becomes more instable for the upper thresholds because of the smaller difference between the results Figure 9.2. This is due to the fact that with thresholds lower than 900 kWh/m$^2$, PV-suitable surfaces are almost all located on roofs and that figures are normalized by the footprint surface area, which usually corresponds to the roof area.

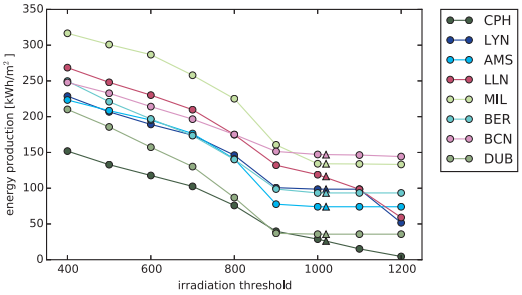


*Figure 9.2 – Sensitivity analysis at different irradiation thresholds [kWh/m$^2$]*

At the upper thresholds, we can easily identify some poorly-performing projects: for example, CPH is always ranked last or second-last, and BER is also ranked among the last positions. Conversely, the best-performing projects are more difficult to identify. While MIL is always first ranked for lower thresholds, this is no more the case starting from a 900 kWh/m$^2$ threshold. However, as can be seen in Table 9.2, its performance is only 2% lower the one of the first-ranked project (i.e., BCN). For this reason, we can consider that MIL should be still be considered the best project at all thresholds.

*Table 9.2 – PV energy potential normalized by the maximum value for each threshold*

| | 400 | 500 | 600 | 700 | 800 | 900 | 1000 | 1020 | 1100 | 1200 | Mean |
|---|---|---|---|---|---|---|---|---|---|---|---|
| **CPH** | 0.78 | 0.76 | 0.75 | 0.78 | 0.78 | 0.84 | 0.84 | 0.83 | 0.77 | 0.79 | 0.79 |
| **LYN** | 0.86 | 0.83 | 0.81 | 0.84 | 0.84 | 0.88 | 1.00 | 1.00 | 1.00 | 0.97 | 0.90 |
| **AMS** | 0.91 | 0.91 | 0.90 | 0.93 | 0.91 | 0.88 | 0.99 | 0.99 | 0.99 | 1.00 | 0.94 |
| **LLN** | 0.91 | 0.89 | 0.88 | 0.90 | 0.88 | 0.92 | 0.94 | 0.92 | 0.81 | 0.60 | 0.87 |
| **MIL** | 1.00 | 1.00 | 1.00 | 1.00 | 1.00 | 1.00 | 0.98 | 0.98 | 0.98 | 1.00 | 0.99 |
| **BER** | 0.89 | 0.86 | 0.83 | 0.84 | 0.80 | 0.85 | 0.97 | 0.98 | 0.98 | 0.82 | 0.88 |
| **BCN** | 0.78 | 0.77 | 0.74 | 0.76 | 0.77 | 0.90 | 1.00 | 1.00 | 0.99 | 0.85 | 0.85 |
| **DUB** | 0.99 | 0.96 | 0.91 | 0.91 | 0.86 | 0.87 | 0.99 | 0.99 | 0.99 | 1.00 | 0.95 |

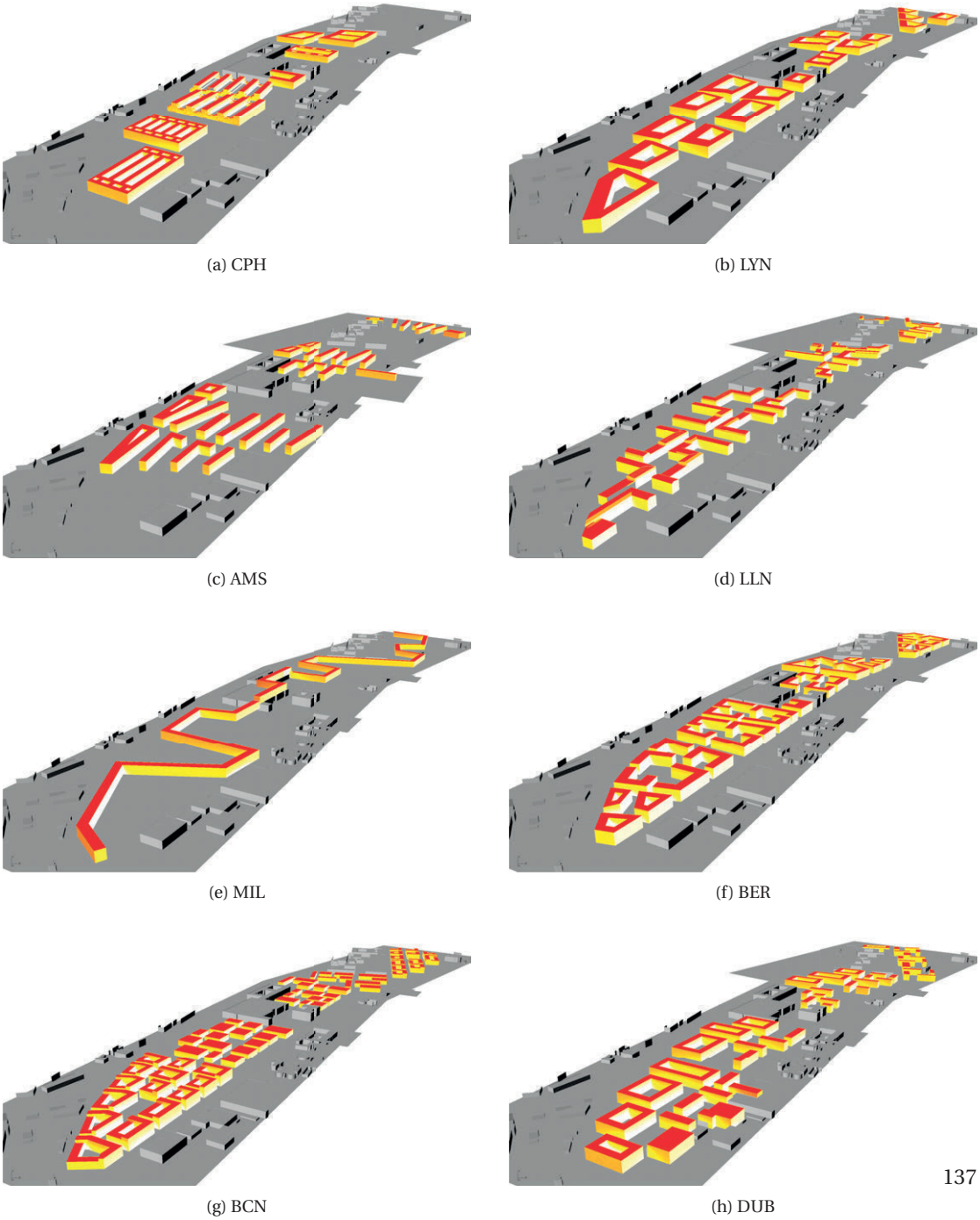

(a) CPH (b) LYN

(c) AMS (d) LLN

(e) MIL (f) BER

(g) BCN (h) DUB



*Figure 9.3 – 3D models of the projects*

## 9.2 Evaluation at different weather scenarios

This project[2] evaluated 9 student projects (represented in Figure 9.4) for a brown-field area redevelopment in the city of Crissier (Switzerland). The original publication [223] built up on the findings of the previous study (Section 9.1) to show that the ranking of projects is not only varying depending on the given threshold (i.e., on the financial viability parameters set by the decision-maker) but also on the considered weather scenario.

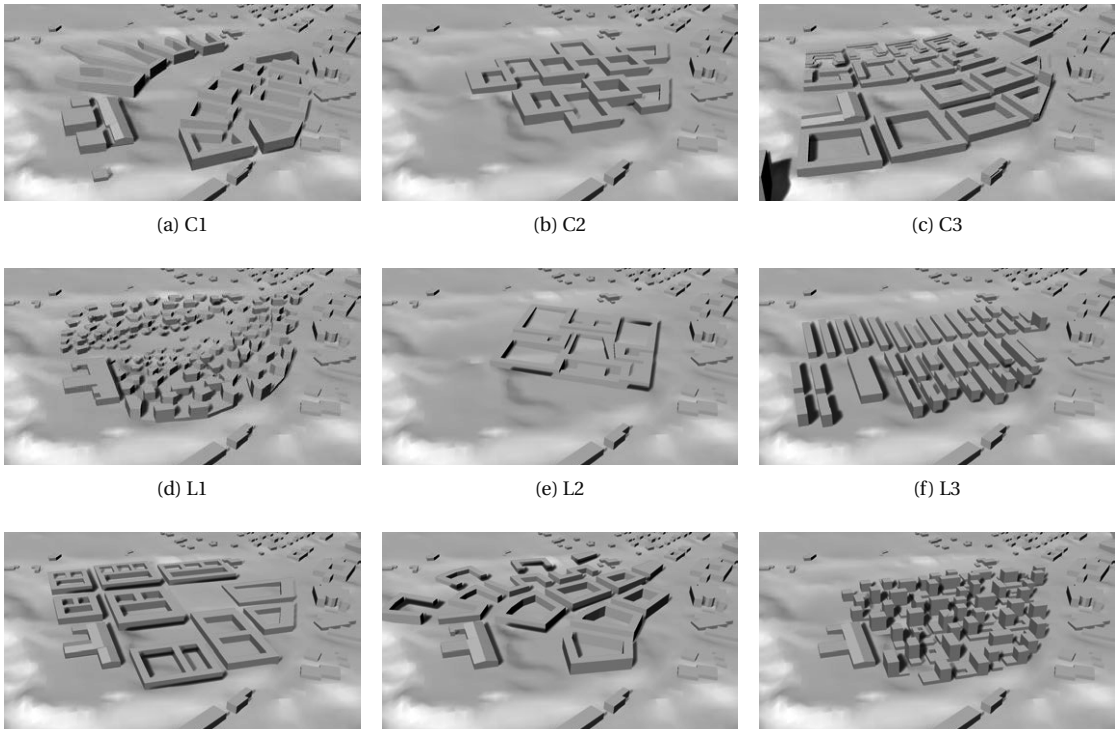

(a) C1 (b) C2 (c) C3

(d) L1 (e) L2 (f) L3

(g) R1 (h) R2 (i) R3

*Figure 9.4 – 3D models of the projects*
*Source: Peronato et al. [223]*

### 9.2.1 Methodology

In this work, we used annual solar irradiation as a proxy for PV potential. We use the concept of stability, which corresponds here to the maximal frequency of a ranking [17], to assess the robustness of each project with regards to the varying irradiation threshold at the chosen radiation scenario.

[2]This section contains some excerpts translated from a book chapter originally published in French [195]: Peronato, G., Rastogi, P., & Andersen, M. (2017). Robustesse de l'évaluation du potentiel solaire de formes urbaines différenciées. In E. Rey (Ed.), *Suburban polarity*. Lausanne: Presses Polytechniques et Universitaires Romandes (PPUR). The text is reproduced here as a courtesy of the publisher and with the agreeement of the co-authors. G.P. contributed to the design (with P.R.), simulation, data analysis and writing of the chapter.

#### Modeling

The 3D model of the projects is obtained from the students' original drawings, while for the context we used a LOD1 model (Appendix A.1.1) of the buildings and a DTM. Building surfaces are modeled with a 0.20 reflectance, and the terrain with a 0.10 reflectance.

The weather scenarios are produced from recorded data at the Geneva-Cointrin weather station (GVA)[3] for the period 1981-2014. Unlike in the method described in Algorithm 11.2, the concatenated months are here the $q$-th months of the dataset, where for "low rad" $q = 0$, for "mid rad" $q = 50\%$ and for "high rad" $q = 100\%$. The two extremes years "low rad" and "high rad" are hence formed by the months with respectively the lowest and higher solar radiation in the considered period. This method provides extreme weather scenarios which are not likely to occur, but rather represent a conservative decision framework.

#### Simulation

The annual hourly simulations are conducted in Daysim, using the Honeybee interface for Grasshopper, considering one reflection from the context (`-ab 2`).

### 9.2.2 Results

The following paragraph describe the results with the goal of finding the best performing project. Unlike in a planning decision where the ranking indicates the priority of interventions, here we are interested in finding the top-ranked project, as only project to be selected and built.

#### Ranking at different thresholds

Figure 9.5 shows the ranking variation as a function of the irradiation threshold. We can notice that the ranking becomes very sensitive to the selected irradiation threshold starting from a 200 kWh/m$^2$ threshold. Similarly, we can also notice a great variability in ranking and a decrease of stability. This is because, starting from this threshold, the share of surfaces achieving it is more variable across the projects, because of their different exposition conditions. R2 is well ranked at the lower thresholds thanks to its many exposed façades, while it looses positions along with the increasing of the thresholds, up to being ranked last at the highest threshold.

We can also notice that starting from a 200 kWh/m$^2$ the ranking of the three radiation scenarios does not follow the same trend. This means that some projects are more sensitive to a particular radiation scenario than other projects. This is the case, for example, of C1 as of a 600 kWh/m$^2$ threshold, for winch the low-rad and mid-rad scenarios loose positions more rapidly than the high-rad scenario. This means that its relative performance is more robust facing to high-irradiation conditions, for which it is systematically top-ranked. Conversely, R1 improves the ranking starting from the low-rad scenario and gets to the top positions between 800 and 900 kWh/m$^2$. This is probably due to that fact that, unlike its highly-shaded façades, its roof is well exposed: for this reason, its potential is larger under low radiation conditions and high thresholds, at which only the roofs are considered.

Figure 9.6 shows the performance of the projects at four sample thresholds. We can notice that at

[3] More information can be found in this information sheet: https://www.meteoswiss.admin.ch/product/input/smn-stations/docs/GVE.pdf [Last accessed: August 13, 2018].

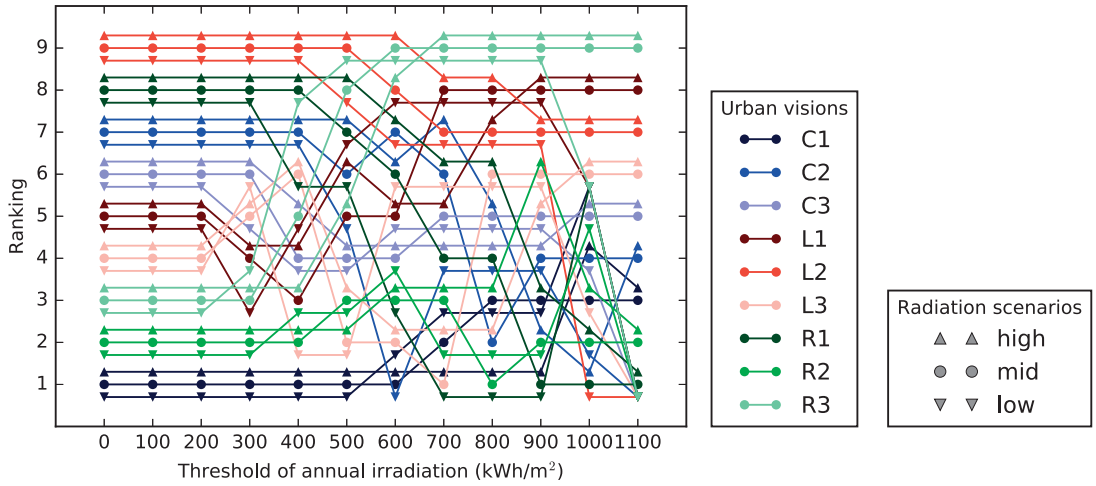


*Figure 9.5 – Ranking of the nine projects and two radiation scenarios as a function of the irradiation threshold*

specific thresholds some projects are ranked better than other even at higher radiation scenarios. This is for example the case of the 0 kWh/m$^2$ threshold, in which the mid-rad scenario is ranked better than the high-rad scenario of almost all other projects. This suggests a better relative performance of project C1.

### Stability of ranking

Table 9.3 shows that C1 has the highest ranking stability among the considered projects. It is the project bearing the most frequent the same rank: in particular, it is ranked first on for half of the considered thresholds. Although the stability value is not high in absolute terms, this gives us an indication of the robustness of the assessment of this project when considering multiple irradiation thresholds. Moreover, the good rank at the other considered thresholds suggests that the project has a good solar potential under other conditions too. Conversely, all other projects have a stability lower than 50%. It is hence difficult to provide a robust ranking for these projects as, according to the parameters selected for the viability evaluation, their relative performance can change.

### Weather uncertainty

Figure 9.7 shows the uncertainty level (expressed here as the difference between the high-rad and low-rad scenarios) at different irradiation thresholds. We can notice that project C1, although almost always top-ranked in the ranking of Table 9.3, is also the one that is the most sensitive at the weather variability and has hence the greatest uncertainty. Conversely, L2 is always at the bottom positions of the ranking, but stands out here for the lowest uncertainty (up to a 800 kWh/m$^2$ threshold). At the 900 kWh/m$^2$ threshold, we find a minimum uncertainty for all projects as, at this threshold, only roofs are usually considered and, as all projects have flat roofs, the normalized irradiation is almost the same. For the higher thresholds, uncertainty increases again because of the low-rad scenario, which has a null potential for all visions.

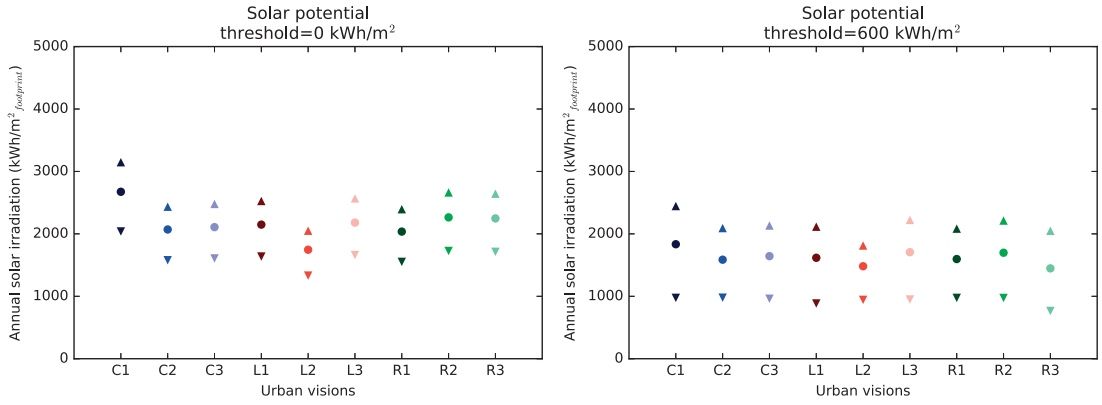


(a) threshold = 0 kWh/m$^2$




(b) threshold = 600 kWh/m$^2$

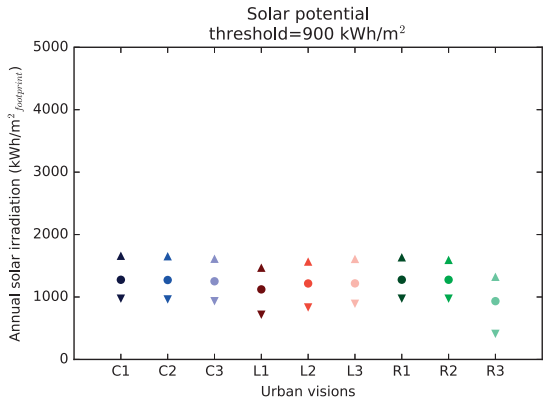


(c) threshold = 900 kWh/m$^2$

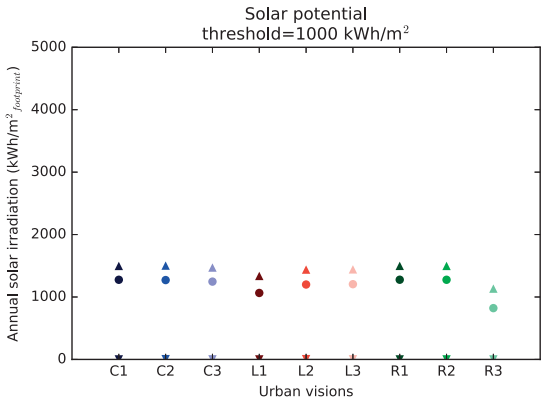


(d) threshold = 1000 kWh/m$^2$

*Figure 9.6 – Comparison of the total solar irradiation of the analyzed projects for the three radiation scenarios (see fig. 9.5 for the marker legend) at different irradiation thresholds*

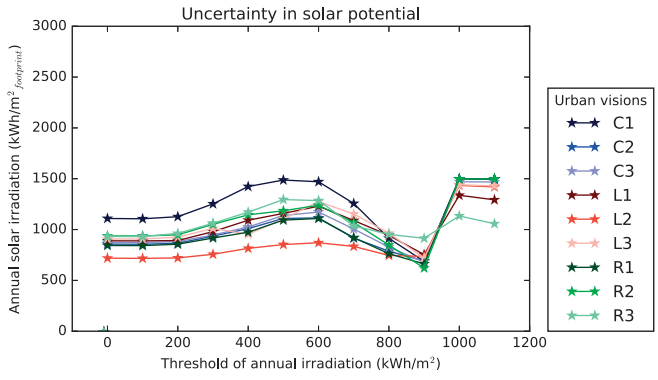


*Figure 9.7 – Weather uncertainty for each project expressed as the difference between the high-rad and low-rad scenarios*

### Overall ranking

An overall ranking can be established by choosing the most frequent rank at the different irradiation thresholds (Table 9.3, last row). Nonetheless, the low stability for some scenarios (< 0.5) suggests that

*Table 9.3 – Ranking using the projects solar irradiation (mean of the three radiation scenarios) as a fonction of irradiation threshold. Stabilty is here defined as the maximum frequency of a rank in one column. The last row shows the most frequent rank for a project at the considered thresholds (in case of same rank, the lowest one is chosen).*

| | Projects | | | | | | | | |
|---|---|---|---|---|---|---|---|---|---|
| Threshold [kWh/m$^2$] | C1 | C2 | C3 | L1 | L2 | L3 | R1 | R2 | R3 |
| 0 | 1.00 | 7.00 | 6.00 | 5.00 | 9.00 | 4.00 | 8.00 | 2.00 | 3.00 |
| 100 | 1.00 | 7.00 | 6.00 | 5.00 | 9.00 | 4.00 | 8.00 | 2.00 | 3.00 |
| 200 | 1.00 | 7.00 | 6.00 | 5.00 | 9.00 | 4.00 | 8.00 | 2.00 | 3.00 |
| 300 | 1.00 | 7.00 | 5.67 | 3.67 | 9.00 | 5.33 | 8.00 | 2.00 | 3.33 |
| 400 | 1.00 | 7.00 | 4.33 | 4.00 | 9.00 | 4.67 | 7.33 | 2.33 | 5.33 |
| 500 | 1.00 | 6.00 | 4.00 | 6.00 | 8.67 | 2.33 | 7.00 | 2.67 | 7.33 |
| 600 | 1.33 | 4.67 | 4.33 | 6.00 | 8.00 | 3.33 | 5.33 | 3.33 | 8.67 |
| 700 | 2.00 | 5.67 | 4.67 | 7.00 | 7.33 | 3.00 | 3.67 | 2.67 | 9.00 |
| 800 | 2.33 | 3.67 | 4.67 | 7.67 | 7.33 | 4.67 | 3.67 | 2.00 | 9.00 |
| 900 | 2.33 | 3.33 | 4.67 | 8.00 | 7.00 | 5.67 | 1.67 | 3.33 | 9.00 |
| 1000 | 4.33 | 2.33 | 4.67 | 7.33 | 5.00 | 5.00 | 3.00 | 3.33 | 8.00 |
| 1100 | 2.33 | 3.00 | 3.67 | 5.67 | 5.00 | 4.33 | 1.00 | 1.67 | 6.33 |
| Stability | 0.50 | 0.42 | 0.33 | 0.25 | 0.42 | 0.25 | 0.33 | 0.42 | 0.25 |
| Ranking | 1.00 | 7.00 | 4.67 | 5.00 | 9.00 | 4.00 | 8.00 | 2.00 | 9.00 |

this ranking is not much robust. If the top-ranked project and more stable (C1) is not selected for some reasons, the choice between the other projects should be done at a specific threshold. Moreover, we have seen that the C1 project is also the one with the greatest uncertainty due to weather (up to a 800 kWh/m$^2$ threshold), which is also a factor to consider. This could suggest to limit the PV installation in the locations where this minimum irradiation threshold is achieved, that is mainly on the roof.

## 9.3 Conclusion

As specified in the chapter introduction, the studies presented here were based on a different methodology and scope than the rest of the thesis. They also used simplified indicators of the photovoltaic solar potential. In particular, in the second study, the analysis was limited to the annual solar irradiation, which was considered as a proxy for the photovoltaic potential. Moreover, the weather scenarios that were presented here represent extreme situations that are not likely to happen, as they concatenate months with the lowest or highest GHI from a 30-year dataset. To this regard, in the final method, we developed a refined system to make sure that the cumulative GHI of the concatenated months corresponds to the annual GHI of an actual recorded year (Algorithm 11.2).

Both studies highlighted the influence of the selected irradiation threshold on the ranking of the projects. This is something that is commonly neglected in existing solar cadastres, in which the minimum irradiation threshold is defined on the basis of general assumptions (see Section 4.3.1). On the contrary, these studies considered that the financial conditions of the decision-maker were not known. This is a common case in the early phase of urban master-planning, when some crucial characteristics of the new neighborhoods (e.g. building typology and density) are defined before their assignment to the building developers. In this case, we argue that the stability of the solar potential rank at different irradiation thresholds can be considered an indicator of the robustness of the given evaluation for multiple investors. However, because of the different application of the thesis, in the next chapters we will consider that the decision-maker is the user of our evaluation method, and as such they are free to set their specific minimum threshold. In alternative, the threshold is automatically

set based on the energy needs of the building (Section 11.3.3.2).

The second study has also shown that the ranking is influenced by the weather scenario. This means that the we can have distinct rankings depending on the weather conditions that we consider. Choosing a design variant that has a stable ranking under different weather scenarios provides thus a more robust choice against weather variability. A similar analysis will be conducted in Section 12.2.3.3 in the framework of the case-study application, comparing, instead of design projects, different urban locations at various thresholds and under different weather scenarios.

# 10 Summary of preliminary findings

This short chapter summarizes the findings of the Part II of the thesis, in particular the recommendations that are directly used for the development of the method that will be presented in Chapter 11. Section 11.2.

As explained in Section 5.1, these studies were used as preliminary test applications of the final modeling method that will be described in Chapter 11. In this sense, from a methodological point of view, these studies showed the application of Radiance-based solar radiation models to 3D city models with a high Level of Detail (LOD2+ and LOD2+). They also showed the feasibility of a Grasshopper+Rhino-based 3D modeling workflow to process the geometry and handle large geo-datasets as tiles.

Throughout the studies of Part II, we have developed a 3D-modeling workflow in which PV modules are simulated on all building surfaces, while the final size of the system can be decided by considering only those achieving a minimum irradiation threshold. As seen in Section 4.2.3, a minimum irradiation threshold is considered as a criterion for the financial viability of the installation. For this reason, most of the studies of this Part II investigated the effect of modeling parameters at different minimum irradiation thresholds, showing that there are sometimes different behaviors. For example, the root mean square error due to coarser sensor grid resolution is lower at high thresholds (Section 6.2).

Chapter 7 presented a method for the segmentation and 3D-reconstruction of vegetation canopy from LiDAR point-clouds, which will be further expanded in Section 11.2.2. The introduction of a random distribution of opaque obstruction (Section 7.2) did not improve the understanding of the effect of vegetation with regards to simple extreme scenarios, which will be then used also in the final method (Section 11.2.2).

In terms of algorithm development, in Section 6.2 we first introduced a Grasshopper-based workflow to provide regular arrangement of solar modules, which will be further defined in Algorithm 11.1. The arrangement of the PV modules was also the common topic of the two studies described in Chapter 8. Section 8.1 proposed a algorithm (Algorithm 8.1) to deal with geometric regularity requirements, notably the shape compactness (see Section 4.2.4). Section 8.2 investigated the effect of different array design so as to find a common utilization ratios of flat roofs. However, it showed that there is a high variability of results depending on the goal of the investor and the characteristics of the roofs, notably the size. Among the studied buildings, only the strategy minimizing the carbon impact showed a quite stable utilization of the rooftop, corresponding to a maximization of the annual generation by panels tilted with a minimum angle. As we dealt with a large urban area with varied buildings and investor attitudes, we will use this approach also in the final method presented in Section 11.3.3.3.

The studies also defined some recommendations that will be implemented in Chapter 11:

- the use of a 3D city model including rooftop over-constructions and overhangs, as it allows to reduce the error due to the Level of Detail, which is particularly significant at high irradiation thresholds, when rooftops are the target surfaces (see Section 6.1);
- the use of a 2-m spacing between sensor nodes, as this resolution corresponds to a good balance between the accuracy (<3% relative RMSE) of the prediction and the interpolation error due to the Daysim model (see Section 6.2);
- the use of 3 ambient bounces, as this is also a good trade-off between computational cost and accuracy: an additional bounce, did not show significant increase solar irradiation (see Section 6.2 and in particular Section 6.2.2.2).

In terms of quantitative results, the studies showed the influence of different error or uncertainty factors. The findings are of course relative to the conditions in which these studies were carried out, but can give some indications for future investigations.

- the error due to the use of coarser grid linearly increases with the resolution but is limited to 7% of relative RMSE for a 4-m spaced sensor grid
- the effect of opaque vegetation on façades is in the range of 3-20% at the urban tile level compared to an unobstructed scenario, while it is higher if we increase the spatial and temporal granularity (see Chapter 7). It should be noted that the effect of vegetation will be further investigated in Section 12.2.3, with a wider sample of urban tiles and analyzing the entire building envelope, including roofs.

Chapter 9 focused on decision support and showed the influence of different modeling parameters (minimum irradiation threshold and radiation scenario) on the the ranking of different design projects. We have seen that even one of the simplest approaches to decision making such as ranking different (design) options is affected by these modeling parameters. Only if we size the installation to cover most of the surfaces including façades (i.e., low irradiation threshold), the ranking is stable, while if targeting only the best-exposed surfaces (i.e., high irradiation threshold), it is subjected to changes. For this reason, we argue that the stability of the ranking is a factor that should be taken into account in the choice of a variant, at least as much as its performance. To this end, Section 11.4 will introduce a score-based method to consider different scenarios in the calculation of a ranking.

# Part III
# Core development and verification

# 11 A comprehensive assessment and decision-support method

This chapter presents a method bridging a typical problem of spatial decision making - the ranking of multiple locations - with the modeling and simulation of PV energy generation and building energy retrofit potential. The method is based on advanced geodata and weather measurements that are commonly available in Switzerland. The case-specific figures and examples presented in this chapter refer to the case-study application, which is a sector of the city of Neuchâtel, in Switzerland. The case study will be more extensively introduced in Chapter 12.

The developed method aims at supporting ranking decisions under uncertainty. We will in fact consider multiple modeling scenarios that will be fed to different preference and ranking aggregation models. At the same time, the method is also targeted to multiple stakeholders. For this reason, we will present different indicators and spatial aggregation scales that are appropriate to specific stakeholders.

## 11.1 Overview

The analysis is based on a workflow consisting of five main steps: the modeling of geometry and of weather data (Section 11.2), the simulation of the energy indicators (Section 11.3), the inclusion of the indicators in a comprehensive decision-support method (Section 11.4) and finally the visualization of the outputs in a 3D-mapping system (Section 11.5). The entire workflow is represented in Figure 11.1. It will be used for the case-study application that will be presented in Chapter 12.

It should be noted that this workflow has been developed throughout the PhD. In this sense, earlier applications described in Part II present some different input data, software and parameters, which have been described in the corresponding *Methodology* sections.

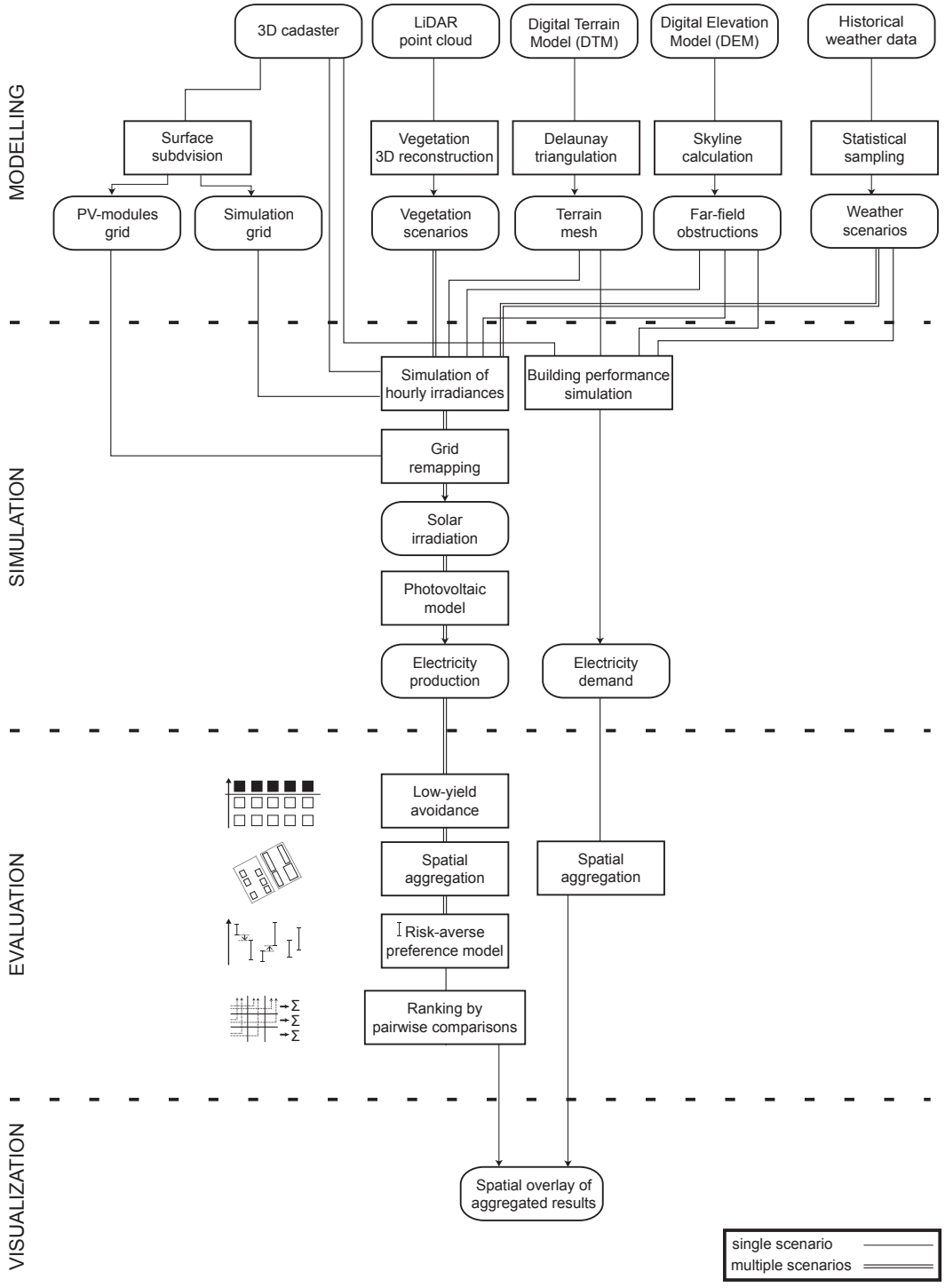


*Figure 11.1 – A flowchart representing the different steps of the workflow.*
*Source: adapted from Peronato et al. [226]*

## 11.2 Modeling

In this section, we describe the modeling of the input data that are used in the simulation. Such data include both geometry and weather information, which have to be processed before they can be used as input of the simulation.

### 11.2.1 Geometry

The geometry input data consist of a fully-3D vector model, in which surfaces are represented either as polygons (building surfaces) or triangular meshes (terrain, vegetation). Following the results of Section 6.2, we also implemented an algorithm to create a structured sensor grid on the building surfaces, which will be used as input for the simulation of the solar irradiances. Therefore, we describe here below the main components of the 3D city model, i.e. buildings, terrain, vegetation, as well as the sensor point grid.

#### 11.2.1.1 Buildings

For the target analysis area, two 3D cadastres were available at the beginning of 2017. The country-wide 3D model by Swisstopo (Appendix A.1.4) and a recent 3D cadastre by the Canton of Neuchâtel (Appendix A.1.5), which both include roof overhangs. As we have shown in Section 6.1, the Level of Detail (LOD) highly influences the accuracy of solar potential analyses. In relative terms, the highest error was found at high minimum irradiation threshold (i.e., on roofs), mainly because of the absence of super-constructions such as dormers and staircases. As can be seen in Figure 11.2, the SITN 3D cadastre provides an accurate representation of many rooftop super-constructions, as well as some façade details represented in the official cadastral footprints, was hence preferred for this analysis. However, it should be considered that the representation of façades is still much simplified with regards to rooftops, affecting hence the overall reliability of the results including façades, as it will be also discussed in the thesis conclusions (Section 14.3.2.1).

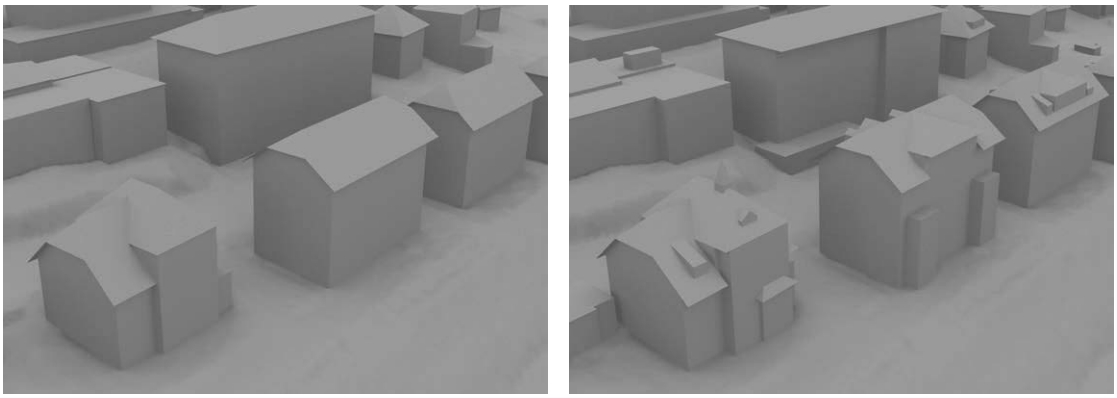

(a) swissBUILDINGS3D 2.0 (Appendix A.1.4) (b) SITN 3D cadastre - (Appendix A.1.5)

*Figure 11.2 – Comparison of the 3D city models from the Swiss confederation (a) and the Canton of Neuchâtel (b). Although they can be considered at the same LOD 2.3 using the classification by Biljecki et al. [30], the SITN 3D cadastre on the right is clearly more accurate, representing also small rooftop super-constructions and some façade details.*
*Data source: Buildings - Swisstopo (left) and SITN (right); terrain - SITN DTM 1 m*

The SITN 3D cadastre consists of several multi-patch geometry *.SHP files, one for each of the following semantics: buildings' roofs, buildings' façades, buildings' footprints, super-structures' roofs, super-structures' façades, other constructions' roofs, other constructions' façades. The other constructions are in general small buildings that are not classified as such in the cadastre (e.g. a garage). The super-structures include architectural details, such as dormers or stair-cases, located on the buildings' rooftops.

The curves of the building geometry were transformed into NURBS surfaces in Grasshopper using either the automatic conversion of Grasshopper (for roofs and footprints) or its "boundary surface" component (for super-structures and façades). The dataset is of good quality and does not need particular healing procedures, except fo the following actions:

- buildings' roofs facing downwards were flipped;
- buildings' roofs failing conversion to surface were converted using Grasshopper "boundary surface" component.

#### 11.2.1.2 Sensor points [1]

As shown in the literature review (Section 4.1.2.1), we can identify two main types of arrangements of sensor points: structured or unstructured grids. A regular arrangement of sensor points in a structure grid is needed to predict the geometric regularity of the installation and therefore its acceptability (see Section 8.1). With the exception of the *dxgridmaker* program included in the STADIC tool [48], which is, however, limited to horizontal surfaces, no out-of-the-box solutions exist for creating a structured and evenly-spaced sensor grid adapted for simulations in the Radiance/Daysim platform.

The structured grid is hence produced using a custom Grasshopper workflow (Algorithm 11.1) based on the one presented in Peronato et al. [219] (which has been applied in the same study described also in Chapter 8) to keep the spacing interval constant across different surfaces.

1. All surfaces are rebuilt while rotated along the x,y axis, so that their u-v axes are oriented accordingly:
2. Each surface is divided in equal segments along the u-v axes of the surfaces:
3. The point grids of each surface are scaled up so that the distance between each point corresponds to the target spacing interval;
4. Points that fall outside the corresponding surface because of the scaling procedure are discarded. It should be noted that this algorithm determines that the sensor points are centered on the corresponding façade, i.e. with an offset with respect to its boundaries.

**Algorithm 11.1:** Creation of sensor points as a structured grid

Because of the division in equal segments conducted with the *Divide Surface* Grasshopper component, the spacing between each point is constant within one surface and direction but not always correspondent to the target spacing interval. For this reason, we introduced in Algorithm 11.1 two further steps

[1] This section contains some adapted excerpts from a published journal article [227]: Peronato, G., Rey, E., & Andersen, M. (2018). 3D model discretization in assessing urban solar potential: the effect of grid spacing on predicted solar irradiation. *Solar Energy*, 176, 334–349. https://doi.org/10.1016/j.solener.2018.10.011. The text is reproduced here as a courtesy of the publisher and with the agreement of the co-authors. G.P. contributed by developing the original concept and its implementation in Grasshopper as well as with the writing.

to ensure a constant distance interval between the sensor points.

For each tile, sensor points are arranged on the buildings included in the 250x250-m tile. The two following sensor grids will be used in this work:

- **grid1**, a structured grid with a 2-m spacing. The arrangement and resolution was set following the sensitivity analysis described in Section 6.2.
- **grid2**, a structured grid with a spacing which corresponds to the size of the PV module. In this work, we used a commercial module whose size is 1.30 x 0.88 m.

#### 11.2.1.3 Terrain

The terrain is modeled with a Digital Terrain Model (DTM) at 1.0-m resolution provided by the SITN. This could also be obtained by resampling the LiDAR data to a raster grid.

A Delaunay algorithm, as implemented in Rhino "Meshpatch" command, was used to convert the DTM points to a mesh. Subsequently, we used Rhino "ReduceMesh" command (in a Python routine based on the Rhinoscript syntax) to simplify the mesh by merging all coplanar contiguous faces into a single face. This corresponds to a loss-less conversion to a Triangulated Irregular Network . For thermal simulations, the simplification involved a lossy conversion (95% reduction, 1/10 accuracy) so as to more significantly reduce the number of faces of the mesh and, consequently, the simulation time.

#### 11.2.1.4 Far-field obstructions

The skyline representing far-field obstruction is calculated at a 1° resolution using ArcGis' skyline tool in an automated workflow which is illustrated in Figure 11.3. We used as input data a subset of the Digital Terrain Model at 25-m resolution from Swisstopo, limited to the main topographic features in the area (Jura mountains at West, Alps at South and East), as can be seen in Figure 11.4a. The 3D point on which the skyline is calculated is located at the center of each tile at a 3-m height from the level of the ground.

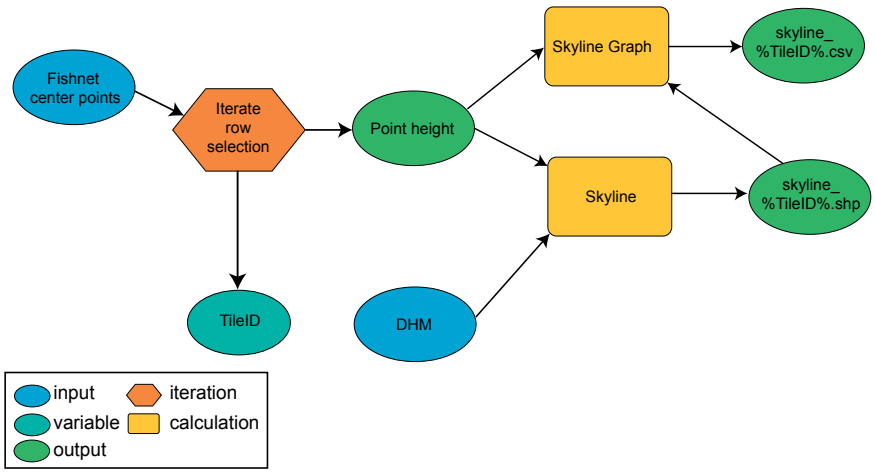


*Figure 11.3 – ArcGis workflow for calculating the skyline for each tile. The shape and colors correspond to ArcGis ModelBuilder default values. The sample outputs for tile 101 are plotted in Figure 11.4a (*.shp) and Figure 11.4b (*.csv).*

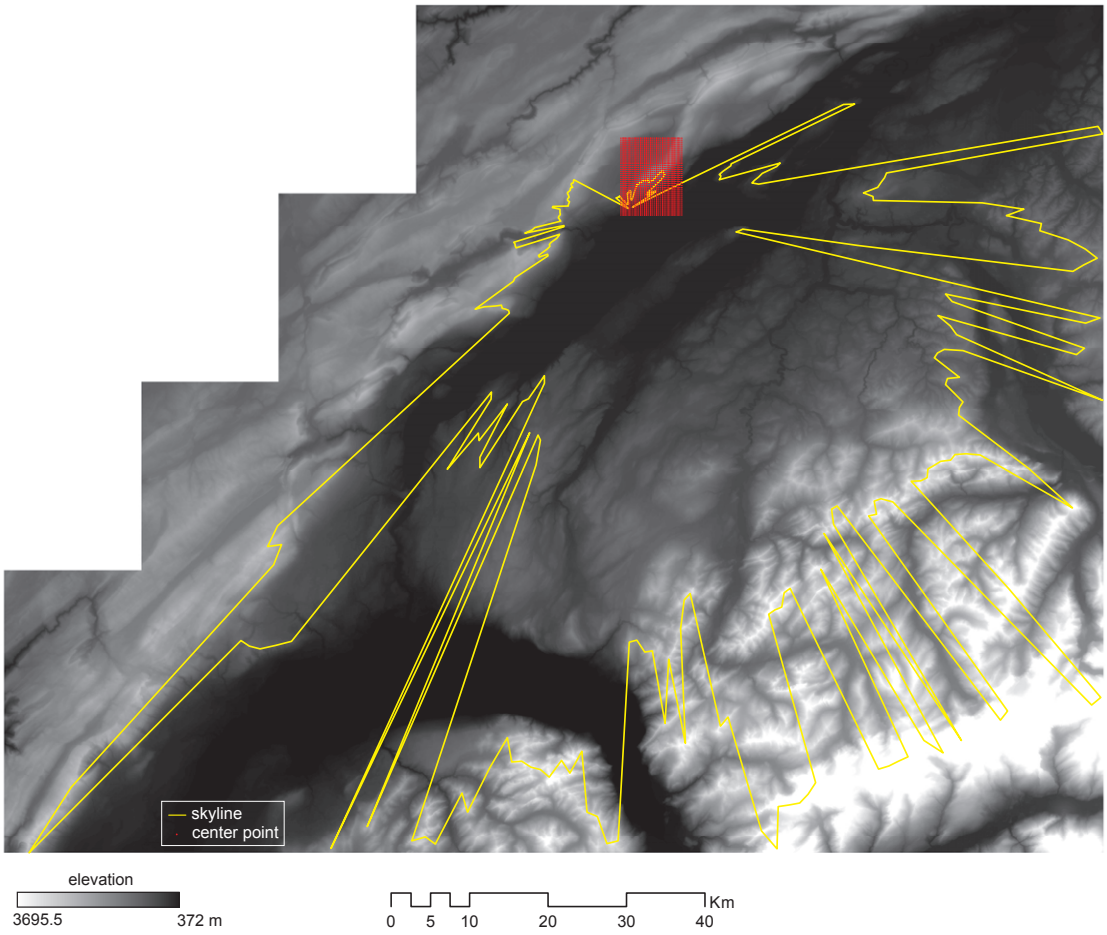


(a) Map

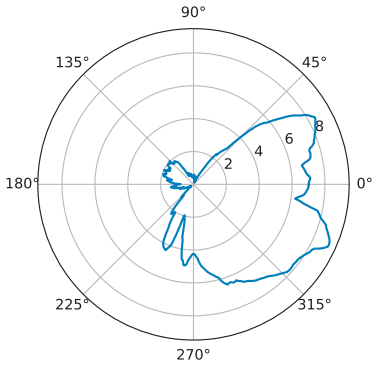


(b) Polar plot

*Figure 11.4 – Outputs of the ArcGis workflow showing the 2D-representation of the skyline (a) and the corresponding obstruction angles (b) for tile 101. Subfigue (a) also shows the center points for all tiles and the Digital Terrain Model at 25-m resolution used for the calculation.*
*Data source: Swisstop DHM25*

### 11.2.2 Vegetation

The vegetation was modeled using alpha-shapes. These allow a more realistic shape than their particular case of ConvexHulls (see Section 2.3.3.2), which were applied in the preliminary application presented in Section 7.1. We used the MATLAB function *alphaShape* with the parameters listed in Table 11.1. The thresholds allow a segmentation of the cloud points in different regions, corresponding to single trees or group of close trees.

The MATLAB-based workflow was developed with the help of Matthew Parkan, including some scripts from his library Forestry toolbox [208]. The input data for the alpha-shape algorithm consist of the LiDAR points classified as high vegetation (LiDAR class = 5) from the latest available dataset from the Canton of Neuchâtel. This dataset is part of an airborne laser scanning (ALS) conducted between March and May 2016 and has a resolution of about 30 pts/m$^2$.

The mesh generated by the alpha-shape algorithm is then modeled using an opaque material as we have seen in Section 7.1.1, using Radiance *plastic* material with a 0.20 reflectivity. In the application of the evaluation workflow, this corresponds to the 'opaque' scenario. We will also consider another scenario without vegetation called 'no trees' . The 'no trees' scenarios is also the one used in the thermal simulations, as explained in Section 11.3.2.1.

*Table 11.1 – Parameters of the MATLAB function* alphaShape

| Radius [m] | HoleThreshold [m$^3$] | Region Threshold [m$^3$] |
|---|---|---|
| 1.5 | 10 | 5 |

### 11.2.3 Weather

Weather data used in this work is composed of both recorded and modeled data. We produced weather files for simulation in Daysim, PVLIB and CitySim. The weather data was obtained for the NEU weather station[2]. This station does not provide all indicators needed for the simulation, notably DNI, DHI, ground temperature and nebulosity. For this reason, we used some models (i.e., Reindl [242] and Meteonorm [246] proprietary algorithm) to retrieve the missing weather parameters (Table 11.2).

We used two types of weather scenarios: typical weather and extreme weather scenarios (in particular the 'low rad' scenario), whose characteristics and generation method will be explained in the following sections.

#### 11.2.3.1 Typical weather

The typical weatherfile was produced using the software Meteonorm [246], based on the latest dataset for solar radiation (1991-2010) and temperature (2000-2009) for the station NEU. This weather file is produced using the proprietary algorithm from Meteonorm (version 7.1.11.24422). This method aims to create a file that represents typical conditions for four meteorological parameters - dry bulb temperature, dew point temperature, wind speed, and direct and diffuse solar radiation. The weight of each value in the selection procedure reflects the influence that each parameter has on the selection process.

[2]More information can be found in this information sheet: https://www.meteoswiss.admin.ch/product/input/smn-stations/docs/NEU.pdf [Last accessed: June 26, 2018].

*Table 11.2 – Weather parameters and data sources*

| | Scenarios | | Typical | | |
|---|---|---|---|---|---|
| | Daysim | PVLIB | Daysim | PVLIB | CitySim |
| GHI | Meteosuisse | | Meteonorm | | Meteonorm |
| DNI | Meteosuisse* | | Meteonorm | | Meteonorm |
| DHI | Meteosuisse* | | Meteonorm | | Meteonorm |
| Air temperature | | Meteosuisse | | Meteonorm | Meteonorm |
| Ground temperature | | | | | Meteonorm |
| Wind speed | | Meteosuisse | | Meteonorm | Meteonorm |
| Wind direction | | | | | Meteonorm |
| Precipitation | | | | | Meteonorm |
| Nebulosity | | | | | Meteonorm |

*Modeled from GHI using the Reindl model [242]

The choice of parameters makes these files suitable for both solar and building energy modeling simulations. We chose such a method to have a consistent weather file (i.e., including all weather parameters) to be used for all simulations included in this thesis.

#### 11.2.3.2 Extreme weather [3]

Unlike typical weather file such as the Typical Meteorological Year (TMY), which represent median weather conditions, we created custom weather scenarios in order to have a more conservative estimation of solar radiation. Using Meteosuisse dataset, we extracted mean hourly values for global solar radiation (GHI), air temperature, relative humidity, wind speed and wind direction from the period 1981-2017.

The DNI and DHI solar radiation values were obtained from GHI by applying the Reindl diffuse model as implemented in Daysim subprogram `gen_reindl`. We used GHI as the indicator for the creation of the time series with the method explained in Algorithm 11.2, considering that it is the most influencing parameter for the performance of the solar panel. We also assume that temperature is to a large extent correlated to the global solar radiation.

Algorithm 11.2 is based on the concept of $q$-th quantile year and of $q$-th quantile months. We created in fact a composite year by concatenating $q$-th quantile months while making sure that the resulting year presents at least (respectively the maximum when $q \geq 0.5$) the same yearly GHI as the $q$-th quantile year. This method is conceptually similar to $Px$ years [50] (where $x = 1 - q$), which defines scenarios where there is a $x$ probability of having higher GHI than the simulated scenario.

The weather parameters other than GHI (wind speed, wind direction, relative humidity, DNI and DHI) corresponding to the same time as the selected months are included in the created scenario year.

Figure 11.5 presents two $q$-th quantile years where $q = 0$ (i.e., 1987, the year with the lowest GHI) and $q = 100$ (i.e., 2011, the year with the highest GHI) and four scenario years created with Algorithm 11.2 for $q = [0, 10, 90, 100]$, considering $n = 13$ neighbors and a $t = 1\%$ tolerance with respect to the corresponding $q$-th year.

[3] This section is the fruit of a collaboration with Parag Rastogi and contains some excerpts from a joint publication [226]: Peronato, G., Rastogi, P., Rey, E., & Andersen, M. (2018). A toolkit for multi-scale mapping of the solar energy-generation potential of buildings in urban environments under uncertainty. *Solar Energy*, 173, 861–874. https://doi.org/10.1016/j.solener.2018.08.017 The text is reproduced in this thesis as a courtesy of the publisher and with the agreement of the co-authors. G.P. and P.R. equally contributed to the conceptual development, coding, and writing.

As we can see in Figure 11.5, the $q0$ and $q100$ scenario years (2011 and 2017) are not always within the boundaries of the 0-th and 100-th quantile years, while the monthly differences are compensated throughout the year, as they have an equivalent annual sum. We can in fact notice that the $q0$ and $q100$ scenario years are composed of months that are usually quite far (up to a $n$ distance) from the corresponding $q$-th quantile months, which are represented by the end of the whiskers of the boxplot.

In the case-study application (Chapter 12), we will use the $q10$ year as the 'low rad' scenario, providing a conservative (whereas not as extreme as a $q0$ would be) scenario for the application of the low-yield preference model (Section 11.4.4).

1. Create a $y \cdot m$ matrix, where each column $m$ contains all the months (e.g., all Januaries) from the different years $y$ of the dataset, excluding leap days
2. Sort the matrix by ascending monthly GHI
3. Find the months that - once concatenated to form a January-to-December year - present at least (or, at most, for $q \geq 0.5$) the same yearly GHI as the $q$-th quantile year $Y$ of the dataset by applying the following heuristic:
   (a) Start from the q-th months as a first approximation
   (b) Check whether $\text{GHI}(y)/\text{GHI}(Y) \leq t$ ; if not, continue
   (c) Substitute some months with those from the $n$-th nearest neighbor years
   (d) Create a new fictitious year $y$ concatenating the newly-selected months
   (e) Check whether $\text{GHI}(y)/\text{GHI}(Y) \leq t$ ; if not, repeat steps (c) and (d)

**Algorithm 11.2:** Creation of weather scenarios. Step 3 resembles a genetic algorithm with a population of one per generation.

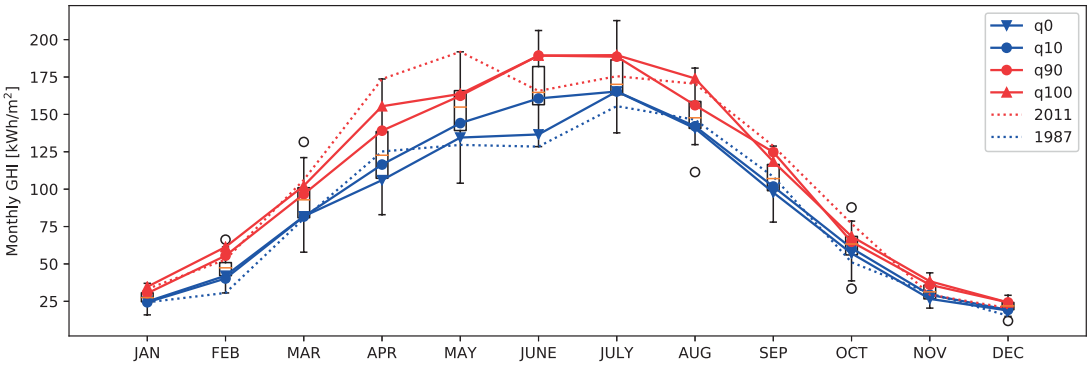


*Figure 11.5 – Plot of monthly cumulative GHI of different years. The boxplots show the variation of the monthly GHI over the period 1981-2018. The dotted lines show real years, 1987 and 2011, respectively with the lowest and highest GHI in the considered period. The other curves show the weather scenarios created applying the Algorithm 11.2 at different quantiles $q$.*

### 11.2.4 Technical implementation

The core of the modeling part is conducted in a Windows environment (8-core CPU with a 4.00-GHz clock-speed and a 24-GB RAM) as part of a Rhino-Grasshopper 3D algorithmic workflow. More

specifically, the workflow uses the following software packages:

- ArcGis ArcMap 10.5, for tiling datasets and calculating the skyline
- Ogr2Ogr (as included in GDAL 2.2.1), for converting GIS files (*.SHP) to CAD geometry (*.DXF)
- MATLAB R2017B, for modeling vegetation from the LiDAR dataset using the Digital Forestry Toolbox [208];
- Rhinoceros 5.14 64-bit, through its Python interface and the Rhinoscript syntax, for meshing point data and conversion between different formats (from *.OBJ to *.3DM and from *.XYZ to *.3DM mesh)
- Grasshopper3D 0.9.0076, for processing all the geometry and the 3D cadastre, using the following plugins:
  - the Ladybug+Honeybee suite (v. 0.59) [259] to compile the simulation input files for DaySim;
  - a custom version of the GHCitySim plug-in (v. 0.2.2), developed by the author [222], to compile the simulation input files for CitySim;
- Meteonorm 7.1 for creating typical weather files;
- Python (with the modules `pandas`, `numpy` and `pyepw`) and Daysim's subprogram `gen_reindl` for creating the weather scenarios based on recorded data from Meteoswiss.

The geometry is imported in Rhino-Grasshopper as native Rhino geometry (*.3DM), after conversion from the original format. For example, the *.SHP datasets of the 3D cadastre were converted to *.DXF using the Ogr2Ogr program from the GDAL library and finally to *.3DM using a custom Python script based on the Rhinoscript syntax.

To facilitate the processing of the geometry by reducing the memory needs, we used a tiling approach implemented as an ArcGis ModelBuilder workflow (Figure 11.6). All geometry datasets are divided in squared tiles of size of 250 m with a buffer of 50 m overlapping the adjacent tiles. The buffer zone is included for shading and inter-reflections calculations only. The tile size and overlap characteristics are similar to the optimal ones found by Romero Rodríguez et al. [257] (200 m with 100 m buffer) for a case study in Ludwigsburg in Germany, providing an uncertainty lower than 1%. Each tile is processed in a Grasshopper `for` loop (i.e., by "animating" a *slider* component over the tiles) creating the input files for the simulations. Each tile requires a few minutes to be processed by Grasshopper.

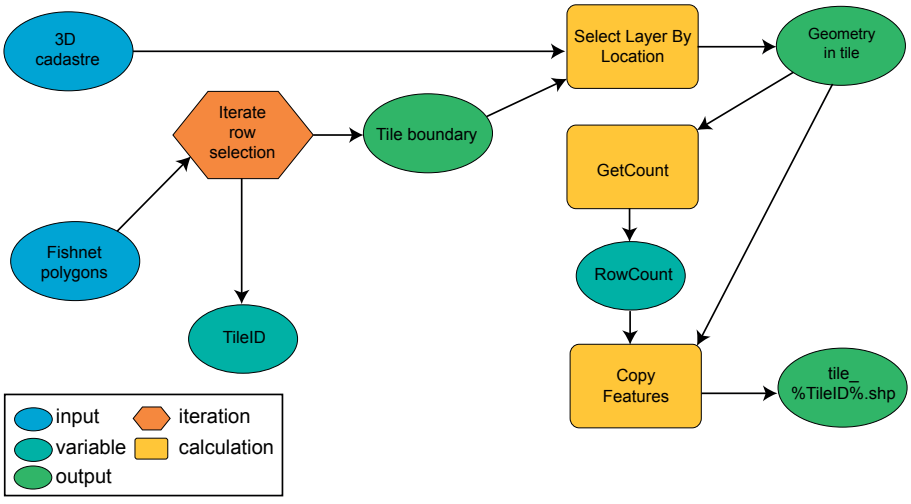


*Figure 11.6 – ArcGis workflow for tiling the data. The shape and colors correspond to ArcGis ModelBuilder default values.*

## 11.3 Simulation

The simulation workflow couples two different software (Daysim and CitySim) for the estimation of the solar irradiances and the photovoltaic yield. It also implements the CitySim software to simulate the building energy needs, which are used to size the solar system and to estimate the energy saving potential after the building retrofit.

### 11.3.1 Solar irradiance

As we have seen in the literature review (Section 4.1.1), both CitySim and Daysim have been used and validated for urban-scale applications. An initial modeling and simulation workflow [224] tested the use of CitySim for the simulation of hourly solar irradiances. However, in this preliminary test application to two buildings in Neuchâtel (Figure 11.7), we realized that CitySim was not suitable for simulating a high-resolution sensor grid, as its computational performance was greatly harmed by the high number of polygons in the scene. Unlike Daysim, which reads the sensor points as a separate input than the geometry, the radiosity algorithm included in CitySim performs a view-factor calculation from the center of each polygon in the scene. This is probably why, in the test application shown in Table 11.3, Daysim was found 2 times faster than CitySim. For this reason, we decided to perform the simulation of solar irradiances using Daysim.

*Table 11.3 – Comparison of the simulation time for two buildings in Neuchâtel. The 9808 sensor points for the CitySim simulations are the center points of each polygon, while in DaySim only the center of the 1934 PV modules (in false colors in Figure 11.7) are considered.*

| | Daysim | | CitySimPro |
|---|---|---|---|
| | `gen_dc -dir` | `gen_dc- dif` | `-I` |
| Calculation time | 19 min | 2 min | 37 min |
| Sensor points | 1934 | | 9808 |

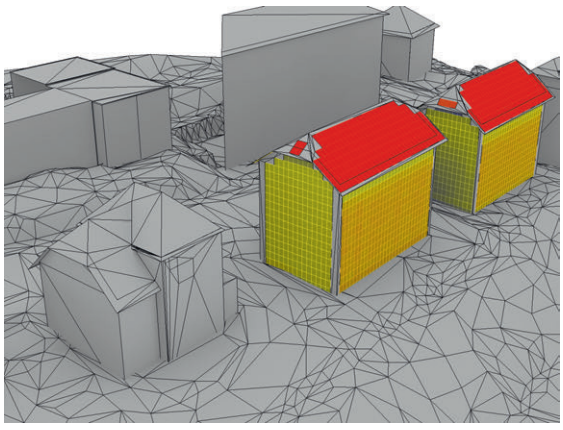

*Figure 11.7 – Render of the 3D model used for the simulations of Table 11.3 with the face boundaries highlighted. The irradiance is simulated only on the sensors placed on the envelope of the two buildings in the foreground on the right, the rest of the geometry acting as shading/reflecting context only.*

In Daysim, we used the Radiance parameters indicated in Table 11.4. As we have seen in Section 6.2.2,

the use of 3 bounces provides a significant increase of reflected radiation compared to 2 bounces, while the increase is smaller for a higher value, at the expense of a much longer simulation times. For this reasons, we considered that 3 bounces was the optimal parameter for this application.

Daysim supports horizon obstructions to the diffuse component in its subprogram `ds_illum` through an angle-based representation of the skyline at a 10° azimuth resolution. In our application, we averaged out the values calculated in Section 11.2.1.4 and we also included the obstruction of the direct component by a change in `ds_illum`'s source code implemented by Jan Wienold and described in Appendix A.2.4.

All surfaces were modeled with a *plastic* material in Radiance, i.e. as a Lambertian material. Each surface was assigned a standard solar reflectance indicated in Table 11.5, which is consistent with values found in the literature (Table 4.4).

The simulation of solar irradiances was conducted using the *grid1* (see Section 11.3.2.1), which corresponds to a 2-m structured grid with a 2-m spacing. The results were then remapped to the denser *grid2* (*ibid.*), whose spacing corresponds to the one of an actual PV module. The value of each node of *grid2* was interpolated from *grid1* using an Inverse Distance Weighting (IDW) algorithm considering the euclidean distance in the $x$, $y$ plane from the 3 closest points having the same normal.

*Table 11.4 – Radiance parameters used in this work. Other settings for `-ab` and `-aa` parameters have been tested in Section 6.2.2.*

| `-ab` | `-ar` | `-ad` | `-as` | `-aa` |
|---|---|---|---|---|
| 3 | 300 | 1000 | 500 | .1 |

*Table 11.5 – Solar reflectance values used in this work.*

| Roof | Façade | Vegetation | Terrain |
|---|---|---|---|
| 0.2 | 0.3 | 0.2 | 0.1 |

## 11.3.2 Building energy demand

Building energy demand is composed of building thermal loads to provide heating and other electricity needs for appliances, ventilation and electric lighting. In this work, we did not consider the use of air conditioning, while cooling loads could be also calculated in a similar way. The final energy demand we have considered is electricity, as we assume the use of a heat pump to be implemented in the buildings after the envelope retrofit.

### 11.3.2.1 Energy needs for space heating

The building energy needs for space heating at the current building status are calculated in CitySim. The final energy (electricity demand) for heating is calculated by assuming the use of a heat pump with a conservative fixed COP of 2.8. We also estimated the energy need for space heating after renovation

assuming that it will be equal to the target value $Q_{H,li}$ defined by the norm SIA 380/1:2016 [278] [4] Therefore, the hourly heating power $P_{\text{refurbished}}$ after refurbishment is defined as follows:

$$P_{\text{refurbished}} = P_{\text{refurbished}} \cdot \frac{Q_{H,li}}{Q_{\text{current}}}, \tag{11.2}$$

where $P_{\text{current}}$ is the hourly heating power [Wh] before renovation as simulated in CitySim, and $Q_{\text{current}}$ is its sum over the entire year (i.e. annual energy needs) normalized by the floor area [kWh/m$^2$]. We assume that the refurbishment of the building envelope the hourly profile of the building energy needs for space heating will not change, except for the magnitude. However, this assumption does not consider the change in inertia of the building and efficiency of building systems after refurbishment, as will also be discussed in Section 14.3.2.

The CitySim model involves a simplified representation of the building thermal behavior and their occupants. Each building is considered as a single thermal zone. The external building envelope of the building (divided into ground-floor, walls and roofs) and close shading surfaces are the only geometrically-described entities, while far-field obstructions, envelope thermal properties and internal loads are described by some numerical parameters. In the following paragraphs, we describe the main components of the thermal model.

#### Building envelope properties

The choice of the thermal envelope characteristics was based on the year of construction. We used the same wall typological construction typologies proposed and calibrated by Perez [213] for the City of Neuchâtel. The building walls were modeled as a CitySim `<composite>` with the layers defined by their thickness, conductivity, specific heat capacity and density as listed in Perez [213, Appendix A.2.2], while ground floors and roofs were modeled only by a single layer and its conductivity. The corresponding U-values of walls, ground floors and roofs are listed in Table 11.6. The short-wave reflectance properties are listed in Table 11.5 and are hence consistent with those of the solar radiation model.

Windows were defined by four parameters: U-value, Window-to-wall ratio (WWR), g-value and opening ratio.The opening ratio was set fixed at 0.9 for all buildings (i.e., a fully operable window with a 10% of surface occupied by the frame), while the g-value was fixed at 0.47 (to 0.49 for buildings built after 2000) as proposed by [213, Table 3.7]). The Window-to-wall ratio (WWR) was set depending on the year of construction, adapting the values taken from Perez [213], and those found in the analysis of five building archetypes presented in the thesis by Sergi Aguacil [4]. These values are clearly only indicative, especially because they do no take into consideration the different building orientations.

#### Internal loads

We considered only the internal loads related to people, using an estimated occupation based on the use of the building (housing or non-residential) and its floor area, as calculated in Algorithm 11.4. The

[4] The target energy need for space heating for renovated buildings from the SIA 380/1:2016 [278] $Q_{H,li}$ [kWh/m$^2$] is calculated as follows:

$$Q_{H,li} = r \cdot t \cdot [Q_{H,li0} + \Delta Q_{H,li} \cdot (A_{th}/A_E)], \tag{11.1}$$

where $r$ is the renovation factor set to $r = 1.5$ for refurbishment projects, $t$ is the renovation factor set to $t = 1$ for Neuchâtel, $A_{th}$ is the floor area as calculated in Algorithm 11.4, and $A_E$ is the area of the surfaces of the thermal envelope excluding the adiabatic surfaces as described in Algorithm 11.3.

main parameters are listed in Table 11.7 and the considered occupancy schedules derived from the SIA 2024:2015 [277] norm are shown in Figure 11.8.

*Table 11.6 – Construction-period-based parameters for thermal model. BGAUP lists categories from the Swiss Federal Register of Buildings and Dwellings (RegBL). The occupancy values are from the SIA 380/1:2016 [278, Table 27]. The infiltration and the U-Values are as estimated by Perez [213, Tables 3.4, 3.7, 3.8 and 3.10, Appendix A.2.2]. Wall U-values after 2010 correspond to the SIA 380/1:2009 limit values [278, Table 2]. The last line shows default (conservative) values used when the period of construction is not available.*

| | GBAUP | WWR | Infiltration rate | U-Value [W/m$^2$K] | | | |
|---|---|---|---|---|---|---|---|
| | | [-] | [$n_{nat}$] | Wall | Roof | Ground floor | Windows |
| Before 1919 | 8011 | 0.15 | 0.7 | 0.94 | 0.7 | 1.6 | 2.3 |
| 1919-1945 | 8012 | 0.15 | 0.7 | 0.94 | 0.7 | 1.6 | 2.3 |
| 1946-1960 | 8013 | 0.25 | 0.6 | 1.35 | 0.65 | 1.5 | 2.3 |
| 1961-1970 | 8014 | 0.25 | 0.55 | 1.03 | 0.60 | 1.3 | 2.3 |
| 1971-1980 | 8015 | 0.25 | 0.5 | 0.88 | 0.43 | 1.1 | 2.3 |
| 1981-1985 | 8016 | 0.25 | 0.4 | 0.90 | 0.31 | 0.68 | 2.3 |
| 1986-1990 | 8017 | 0.25 | 0.4 | 0.90 | 0.31 | 0.49 | 2.3 |
| 1991-1995 | 8018 | 0.25 | 0.35 | 0.69 | 0.25 | 0.49 | 2.3 |
| 1996-2000 | 8019 | 0.25 | 0.35 | 0.69 | 0.25 | 0.49 | 2.3 |
| 2001-2005 | 8020 | 0.35 | 0.30 | 0.51 | 0.25 | 0.35 | 1.7 |
| 2006-2010 | 8021 | 0.35 | 0.30 | 0.51 | 0.22 | 0.35 | 1.7 |
| 2011-2015 | 8022 | 0.35 | 0.30 | 0.25 | 0.22 | 0.25 | 1.7 |
| After 2015 | 8023 | 0.35 | 0.30 | 0.25 | 0.22 | 0.25 | 1.7 |
| N/A | - | 0.30 | 0.70 | 1.03 | 0.7 | 1.5 | 2.3 |

*Table 11.7 – Usage-based parameters for thermal model. GKAT, GANZWG list categories from the Swiss Federal Register of Buildings and Dwellings (RegBL).*

| | $Q_{H,li0}$ [kWh/m$^2$] | $\Delta Q_{li}$ [kWh/m$^2$] | Building usage (GKAT) | Number of dwellings (GANZWHG) | Occupancy [p/m$^2$] |
|---|---|---|---|---|---|
| Multi-family | 13 | 15 | 1021, 1025, 1030 | > 1 | 0.025 |
| Single-Family | 16 | 15 | 1021, 1025, 1030 | = 1 | 0.017 |
| Non-residential | 13 | 15 | all other categories | N/A | 0.050 |

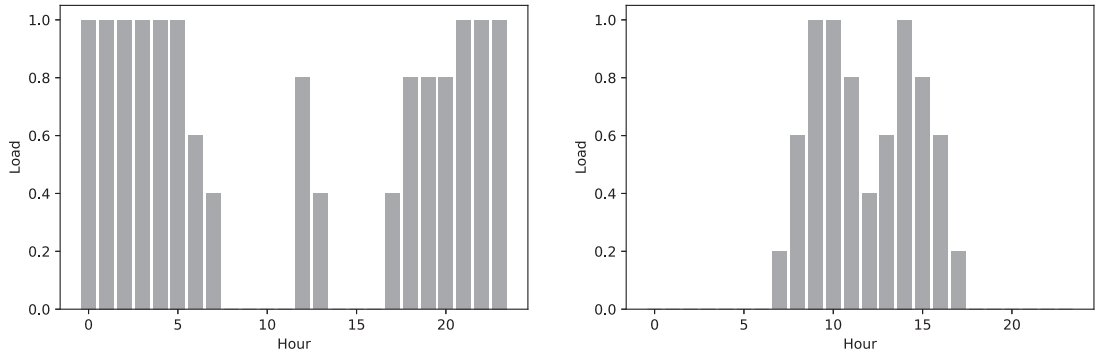


(a) Residential (b) Other

*Figure 11.8 – Load schedule for occupation. The residential schedule corresponds to single- and multi-family housing from SIA 2024:2015 [277, p. 32], while for other building usages we assume the occupancy profile of an office from SIA 2024:2015 [277, p 38].*

### Geometric model

The geometric model includes two family of surfaces:

- geometry included in the heat-transfer and radiation model: all building surfaces located within in the 250x250-m tile;
- geometry included only in the radiation model (shading and reflection only): roof overhangs, terrain and building surfaces located in the 50-m buffer zone;

The geometric model is prepared for the thermal simulation through the steps listed in Algorithm 11.3. However, the internal geometric properties of the building cannot always be directly calculated by the CitySim solver, notably when the building geometry does not form a closed volume. The building floor area and volume are hence computed using the steps described in Algorithm 11.4 and assigned as a numerical input to the thermal model.

1. Each surface is intersected with every other surface in the dataset and the resulting intersections are removed from the model. The intersections correspond to building surfaces adjoining other building surfaces, e.g., buildings with a common wall. Since CitySim cannot model inter-building thermal exchanges, we remove these surfaces from the simulation, which results in considering them as adiabatic.
2. The original polygons are meshed using Grasshopper *Meshing simple* smoothing settings. Non-planar surfaces are triangulated into a minimum number of triangles. Mesh faces smaller than 0.10 $m^2$ are removed
3. Roof surfaces are duplicated and flipped (i.e. set with downwards-facing normals) and included in the shading and reflective geometry with a 0.30 reflectance value so as to model the effect of overhangs on building façades

**Algorithm 11.3:** Preparation of geometry for thermal simulation

1. The fooptrint is triangulated in a mesh with $m$ faces $f$ of 2-m side and area $a \simeq 4$ [$m^2$];
2. Raytracing is performed from the center of each mesh face upwards to the intersection with the roof surface so as to compute the distance $h$ [m];
3. The volume $V$ is hence defined by the following equation:

$$V_{th} = k_V \cdot \sum_{n=1}^{m} a_f \cdot h_f \tag{11.3}$$

   where $k_V = 0.9$ is the actual volume coefficient proposed by Perez [213, p. 59].
4. The floor area $A$ is defined as follows:

$$A_{th} = k_A \cdot \frac{h}{H} \tag{11.4}$$

   where $k_A = 0.8$ is the actual floor area coefficient proposed by Perez [213, p. 58] and $H = 3$ [m] is considered as the typical floor height.

**Algorithm 11.4:** Calculation of building volume and area

#### Far-field obstructions

Far-field obstructions (calculated in Section 11.2.1.4) are added to the CitySim model as obstructed horizon angles with a 1° azimuth resolution.

### 11.3.2.2 Other electricity needs

In addition to the energy needs for space heating, we considered the electricity demand for appliances, electric lighting and ventilation, as well as the energy need for Domestic Hot Water (DHW) provided by a heat pump with fixed COP of 2.8.

The hourly electricity demand was calculated in the Algorithm 11.5 by distributing the annual energy demand set by the norm SIA 2024:2015 [277] into an hourly profile according to schedules fixed or estimated through the same norm. For electric lighting, we included an approach similar to the one developed by Burger and Hall [38] so as to exclude the hours for which it is not needed because the space is daylit. The Figure 11.11 shows the hourly power density $P_h$ at each hour of the year as calculated with the Equation (11.6).

For appliances, we used the schedule provided by the norm SIA 2024:2015 (Figure 11.10), whereas for ventilation and Domestic Hot Water (DHW) we used the load schedule of occupation (Figure 11.8) also provided by the SIA norms. We assumed that the need for ventilation is directly correlated to the presence of building users. The maximum hourly power is obtained using Equation (11.5) with $l = 1$ and the hourly load using Equation (11.6).

1. Custom lighting schedules (Figure 11.9) are created considering the criteria from the norm SIA 2024:2015 [277] . For example, the residential usage assumes a profile providing 4 and 3 hours of full load during respectively daytime (7 am - 6 pm) and nighttime (6 pm - 7 am), while distributing these loads according to the occupation profile.
2. Subsequently, a simplified daylight criterion is introduced. As proposed by Hall and Burger [102, 38], it is assumed that electric lighting is not used when the Global Horizontal Irradiance (GHI) is larger than 200 kWh/m$^2$, i.e. in these hours we force a null load power ($l = 0$) regardless of the load profile.
3. The maximum load power is then defined as:

$$P_{\max} = \frac{D}{\sum_{h=1}^{8760}(L_h \cdot l_h)}, \tag{11.5}$$

   where $D$ is the annual electricity demand from Table 11.8 (respectively for DHW, Table 11.9 multiplied by a 2.8 COP), $L$ is the relative load for each hour $h$ from Figure 11.9, and $l$ is the daylight parameter ($l = 0$ if GHI > 200W/m$^2$, else $l = 1$).
4. The hourly power at each hour $h$ is then obtained by the following equation:

$$P_h = P_{\max} \cdot L_h \cdot l_h. \tag{11.6}$$

**Algorithm 11.5:** Hourly load curve demand for electric lighting. For appliances and ventilation, only steps 3 and 4 are used and $l = 1$. The Python implementation is shown in Appendix A.2.2.

*Table 11.8 – Annual electricity demand from SIA 2024:2015 [277] expressed in [kWh/m$^2$]*

| Use | Single-family | | | Multi-family | | | Office | | |
|---|---|---|---|---|---|---|---|---|---|
| Scenario | Std | Tgt | Exist | Std | Tgt | Exist | Std | Tgt | Exist |
| Appliances | 14 | 7 | 18 | 14 | 7 | 18 | 14 | 6 | 29 |
| Lighting | 4 | 2 | 4 | 4 | 2 | 4 | 19 | 5 | 19 |
| Ventilation | 0.7 | 0.4 | 0 | 1.2 | 0.7 | 0 | 2.1 | 1.3 | 3.4 |

*Table 11.9 – Annual thermal energy demand for Domestic Hot Water (DHW) from SIA 380/1:2009 SIA [276, Tab. 23] (values in [MJ/m$^2$]) and SIA 380/1:2016 SIA [278, Tab. 27] (values in [kWh/m$^2$])*

| Use | Single-family | Multi-family | Office and shops |
|---|---|---|---|
| DHW needs [MJ] | 75 | 50 | 25 |
| DHW needs [kWh/m$^2$] | 21 | 14 | 7 |

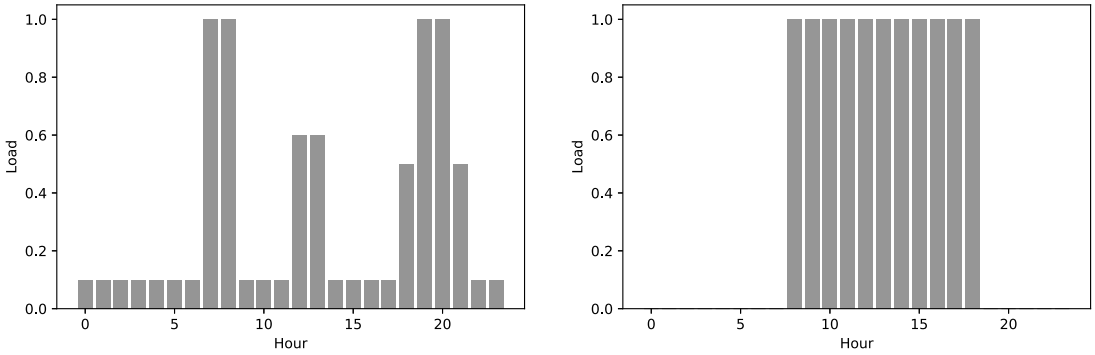


(a) Single- and multi-family housing

(b) Office

*Figure 11.9 – Load schedule for electric lighting. The sum of the loads fulfills the criteria of the SIA 2024:2015 norm [277, p.32 and p. 38], i.e., for residential, 4 full-load hours from 7 am to 6 pm and 3 full-load hours from 6 pm to 7 am, and, for office, 11 full-load hours from 7 am to 6 pm.*

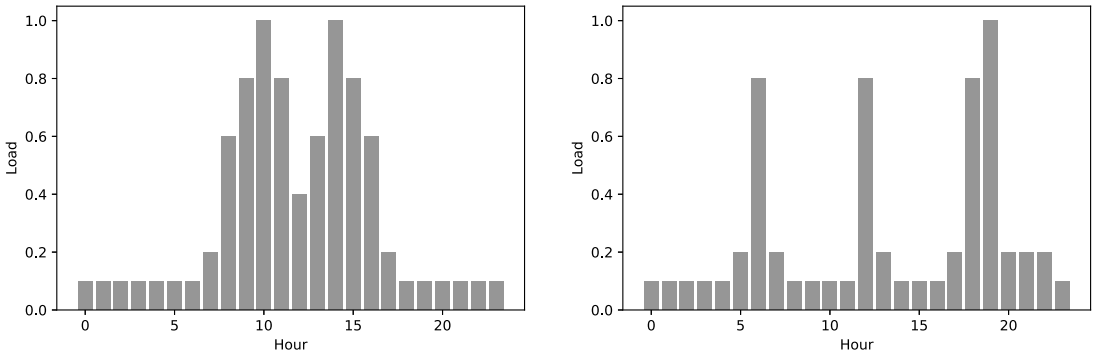


(a) Single- and multi-family housing

(b) Office

*Figure 11.10 – Load schedule for appliances from SIA 2024:2015 [277]*

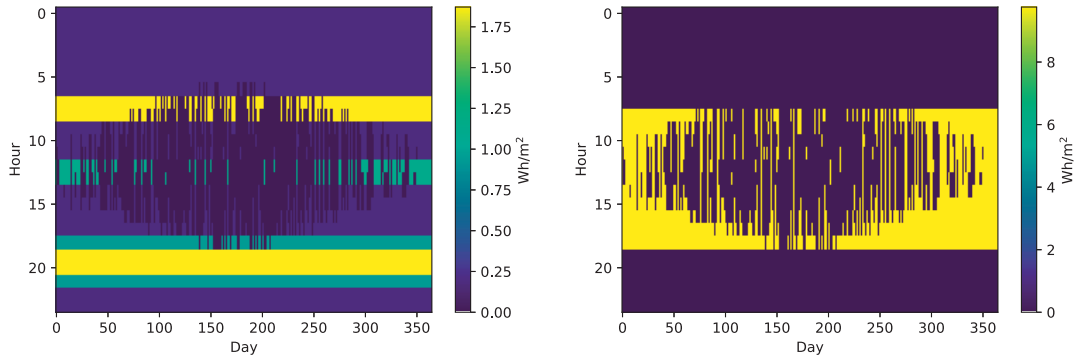


(a) Single- and multi-family housing

(b) Office

*Figure 11.11 – Power density for electric lighting expressed in [W/m$^2$], as calculated in Equation* (11.6)*. The daylight parameter is calculated based on the typical weather file for Neuchâtel. The sum of each hourly value gives the annual electricity demand defined by SIA 2024:2015 and listed in Table 11.8.*

### 11.3.3 Photovoltaic yield

The photovoltaic yield is calculated by applying state-of-the-art PV performance models discussed in Section 2.2.6.3 on the hourly irradiances simulated in Daysim. The estimation is completed by heuristics for the arrangement of the PV modules and the sizing of the solar system, which will be presented in Sections 11.3.3.2 and 11.3.3.3.

#### 11.3.3.1 Simulation of power

The simulation of PV performance at installation conditions was conducted using the models provided by the PVLIB-Python library [111].

We used the De Soto model [66] to obtain the parameters for the Single Diode model (see Section 2.2.6.3), as implemented respectively in `pvsystem.calcparams_desoto()` and `pvsystem.singlediode()`. We considered the module parameters for the De Soto model listed in Table 11.10. These values were either measured on or estimated for a 185Wp module from a Swiss manufacturer by researchers at SUPSI BIPV center, and adapted, in terms of voltage and current at the maximum power point, to a 190Wp module of the same type and manufacturer.

The De Soto model also requires the cell temperature, which was calculated using Sandia PV Array Performance Model [150], as implemented in PVLib function `pvsystem.sapm_celltemp()`, and the POA irradiance, which was simulated in Daysim. The cell temperature model is defined by the POA irradiance (which was simulated in Daysim), the wind speed, dry bulb temperature (which were taken from the weather file), and a `model` parameter describing the type of installation. The `model` parameter was set to '`insulated_back_polymerback`', which provides the most conservative temperature estimation adapted to building-integrated applications.

The output DC hourly maximum power calculated with the De Soto model is transformed to AC power with a simple fixed coefficient, i.e. a Performance Ratio $PR = 0.85$. Partial shading of the array or of the module is not considered. We assume that for the purpose of our application, without a determined arrangement of the strings and sizing of the inverters, this simplification is acceptable. It will be tested

*Table 11.10 – Characteristics at STC of the commercial 185Wp BIPV module used in this work. The main parameters of the De Soto model were provided by SUPSI's BIPV center.*

| Parameter | | | Source |
|---|---|---|---|
| Current at maximum power point [A] | $I_{mp}$ | 8.5 | Manufacturer |
| Voltage at maximum power point [V] | $V_{mp}$ | 21.8 | Manufacturer |
| Current at short circuit [A] | $I_{sc}$ | 9 | Manufacturer |
| Open-circuit voltage [V] | $V_{oc}$ | 26.3 | Manufacturer |
| Short-circuit current temperature coefficient [%/C] | $\alpha_{sc}$ | +0.046 | Manufacturer |
| Parameters for the De Soto model | | | |
| Product of the usual diode ideality factor [-], number of cells in series [-], and cell thermal voltage [V] | a | 1.2 | SUPSI |
| Photocurrent [A] | $I_L$ | 9 | SUPSI |
| Diode reverse saturation current [A] | $I_o$ | 1.02e-10 | SUPSI |
| Series resistance [Ω] | $R_s$ | 0.18 | SUPSI |
| Shunt resistance [Ω] | $R_{sh}$ | 2200 | SUPSI |
| Short-circuit current temperature coefficient [A/C] | $alpha_{sc}$ | 0.00414 | $\alpha_{sc}/100 \cdot I_{sc}$ |
| Energy bandgap [eV] | EgRef | 1.121 | Reference from [72] |
| Temperature dependence of the energy bandgap [1/K] | dEgdT | -0.0002677 | Reference from [72] |

against measured values in Section 13.2.

#### 11.3.3.2 Sizing of the system

The sizing of the solar system is determined by two methods:

- a minimum electricity generation threshold (expressed in kWh/kWp); this can be determined with a simple financial calculation, as we will see in Section 12.2.1;
- a sizing heuristic balancing the Self-Consumption (SC) and Self-Sufficiency (SS) of the building (see Section 4.2.3.1), which is detailed here below.

Both methods assume a business model targeted to single buildings, rather than solar communities or energy utility companies, and do not consider the impact on the grid. The relevance and limitations of these two methods for some particular users will be further discussed in Section 14.3.2.2.

**Sizing heuristic**

The goal of this heuristic is to avoid the system potential oversizing when all available building surfaces are covered with PV modules, which is the standard output of the arrangement algorithms if no minimum threshold is selected, while maximizing the self-sufficiency and self-consumption of each building. This is similar to the method proposed by Aguacil Moreno et al. [6], which implements, though, the selection of modules based on minimum irradiation thresholds. This method assumes

In our implementation, we used an algorithm (Algorithm 11.6) to find the equilibrium between self-sufficiency and self-consumption by sorting the modules and progressively discarding those with the lowest annual yield up to meeting the goal. It should be noted that this algorithm is far from being optimal. It is based in fact on the total annual PV yield, while the SC and SS indicators are calculated on an hourly basis. In this sense, we might exclude some modules that provide a good self-consumption, while having a relatively-poor annual performance. This might be the case, for example, of façade-installed modules, which have a better match of the demand and production curves in winter compared to tilted modules, while having a lower annual cumulative yield. However, we

argue that this method provides a first sizing of the system, with the advantage of beging very fast to compute compared to optimization algorithms.

**Data:** Hourly AC production and electricity demand
**Result:** List of PV modules
**while** $SC < SS$ **do**
  discard PV module with the lowest annual yield;
**end**

**Algorithm 11.6:** Algorithm to size the solar system

#### 11.3.3.3 Arrangement of the modules

For the simulation of the photovoltaic yield, PV modules were assumed to be placed on all surfaces with a non-null sky-view factor, regardless on the actual suitability for installation. In particular, it should be noted that the geometric model used in this work not include windows nor small roof super-constructions as chimneys. For this reason, we used the reduction coefficient ratios listed in Table 11.11. In particular, for flat roofs, we assumed that modules would be installed almost flat (5° minimum tilt angle for water drainage), so as to maximize the energy production and minimize (at least, under business-as-usual energy mix scenarios, in which high-carbon electricity is imported from Germany) the carbon content of the produced electricity (see Section 8.2). Based on the findings from the same preliminary study (though limited to few case studies), this approach is supposed to be robust to different roof shapes and load curves, while it should be noted that it does not maximize the self-consumption, but rather the annual energy production.

The arrangement of the PV modules also included the consideration of the geometric regularity of the installation, which was discussed in Section 4.2.4 and tested in Section 8.1. As a result of the structured grid determined by the Algorithm 11.1, the PV modules were arranged in rows along the $u$ axis of each $u \cdot v$ surface, as can be seen in Figure 11.12. This allows the application of a regularity algorithm shown for each row $r$. We decided to implement the conservative approach illustrated in Figure 8.1. To this end, the Algorithm 11.7 considers only the rows $r$ in which each module achieves a given threshold. The threshold can be either set by the user or calculated as a result of the heuristic for sizing the system presented in Section 11.3.3.2.

If a single module does not achieve the threshold, then all modules belonging to that row are discarded, resulting in a total power as in the following equation:

$$P_r = c_r \cdot \sum_{m=1}^{n} (P_m \cdot t_m) \qquad \texttt{with } t_m = \begin{cases} 1, & \texttt{if } P_m \geq \textit{threshold}, \\ 0, & \texttt{otherwise}. \end{cases}$$
$$c_r = \begin{cases} 1, & \text{if } \sum_{m=1}^{n} (P_m \cdot t_m) = \sum_{m=1}^{n} (P_m), \\ 0, & \texttt{otherwise}. \end{cases} \tag{11.7}$$

where $P_r$ is the power of a row $r$ composed of $n$ modules $m$, each one with a power $P_m$.

**Algorithm 11.7:** Algorithm for the regular arrangement of PV modules.

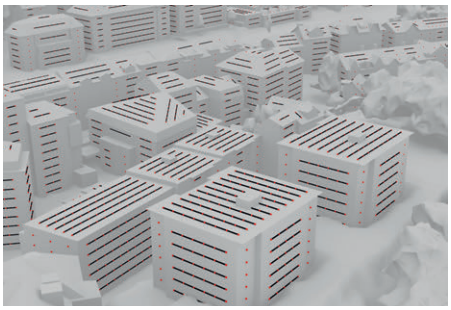

*Figure 11.12 – The image shows the alignment of sensor nodes (red spheres, here with a 2-m spacing) along rows following the application of the regularity algorithm (11.7.)*
*Source: SITN Cadastre, LiDAR 2016 and DTM 1.0 m*

### 11.3.4 Technical implementation

The simulation input files are post-processed in Python to be run in an Unix environment. In the case-study application (Chapter 12), the simulations for the case-study are run in a Linux machine (48-core CPU with a 1.355-GHz clock-speed and a 125-GB RAM). This allows the simulations to be run in parallel for multiple tiles. We use the following simulation engines:

- Daysim (version 4.0-2012 using RADIANCE 4.1a with Photon Map Extension, compiled at Fraunhofer ISE), for the simulation of hourly irradiances; a custom version of Daysim subprogram `ds_illum` modified by Jan Wienold including the shading of the direct sun contribution from the horizon is used, as documented in Appendix A.2.4.
- CitySim Pro 64bit (Build 20/07/2017), for the simulation of building energy needs for space heating.
- PVLIB version 0.4.1, for the simulation of the photovoltaic yield.

PVLIB is run sequentially after the interpolation of the hourly irradiances calculated in Daysim from *grid1* to *grid2* (see Section 11.3.1). The PV performance models are applied in a `for` loop to each sensor node (corresponding to a PV module) of *grid2*.

Table 11.12 shows the time necessary to perform the main steps of the simulations. We can notice that the inclusion of the vegetation significantly increases the duration of the simulation. It should be considered that simulation time needed to run PVLIB is mostly due to the rudimentary loop-based Python implementation, which has room for significant improvements in terms of speed.

The simulation of multiple weather scenarios is conducted using the same workflow, but running Daysim subprogram `ds_illum` on the previously calculated daylight coefficients, as explained in Section 4.1.3. This subprogram takes only a few minutes to calculate the irradiances based on the new weather file.

*Table 11.11 – Criteria for identifying types of sensor points through their normal vector and applied reduction coefficient ratios. Window-to-wall ratio (WWR) values are listed in Table 11.6.*

| | Flat roof | Façade | Tilted roof |
|---|---|---|---|
| Normal vector | $v_x = v_y = v_z = 0$ | $v_z < -0.01 \vee v_z > 0.01$ | `else` |
| Reduction ratios | 0.9 | 1 – WWR | 1.0 |

*Table 11.12 – Duration (in hours) of the main steps of the simulation of a tile. The example refers to tile 170 in Neuchâtel (see Figure 12.6). This tile contains 7'655 sensors simulated in Daysim, which are mapped to 33'584 sensors simulated in PVLIB, and 53 buildings simulated in CitySim. The total computation time excludes the one of `gen_dc -dif`, which can be run in parallel to `gen_dc -dir`.*

| Scenario | Daysim | | CitySim | PVLIB | Total |
|---|---|---|---|---|---|
| | `gen_dc -dir` | `gen_dc -dif` | | | |
| 'opaque trees' | 14.4 h | 2.3 h | - | 1.2 h | |
| 'no trees' | 4.9 h | 0.9 h | 25.5 h | 1.2 h | |
| Total | 19.3 h | 3.2 h | 25.5 h | 2.4 h | 47.3 h |

## 11.4 Evaluation

This section[5] presents the evaluation method used in this work to support the decision under uncertainty. We first describe the indicators and spatial divisions used. We then propose two different methods to deal with the considered uncertainty factors, i.e. vegetation and weather. This is made possible by the use of extreme modeling scenarios calculated in the previous sections.

### 11.4.1 Indicators

To evaluate the value of a solar power installation, we need to calculate the energy produced by it and the relation of this production to the energy consumed by the buildings on which these installations are located. Thus, we split the quantities into two categories: 'generation' / 'consumption' and 'efficiency' / 'displacement' .

We consider the following three energy 'generation' or 'consumption' outputs from simulating a building and its solar photovoltaic system:

**Gross electric energy production** – the cumulative energy produced every hour, assuming that the rate of production is constant during that hour [Wh]. In this work, we consider DC electricity production as a proxy for AC electricity production, which is the relevant quantity assessing the performance of the solar system. However, the energy 'efficiency' or 'displaced' measures described here below should be calculated with AC electricity.

**Space conditioning need** – hourly energy demand for space heating or cooling in a building [Wh]. Since our case studies are in Switzerland, space cooling need is not considered in this thesis.

**Electric energy demand** – hourly energy demand for lighting, appliances, domestic hot water and space heating in a building.

Along with these simulation outputs, we considered the following 'energy efficiency' or 'energy displacement' measures:

[5] This section contains some excerpts from a published paper [226]: Peronato, G., Rastogi, P., Rey, E., & Andersen, M. (2018). A toolkit for multi-scale mapping of the solar energy-generation potential of buildings in urban environments under uncertainty. *Solar Energy*, 173, 861–874. https://doi.org/10.1016/j.solener.2018.08.017. The text and figures are reproduced in this thesis as a courtesy of the publisher and with the agreement of the co-authors. G.P. contributed to the conceptual idea of the ranking systems, coding and development of indicators (with P.R.), and writing (with P.R.).

**Building energy displaced** – the amount of local (building) electricity energy demand that is displaced by the gross electric energy production, assuming complete self-consumption [Wh].

**Energy saving potential** – the amount of space heating/cooling energy savings if a building were renovated to some current standard [Wh].

**Building retrofit energy potential** – sum of annual energy saving potential and gross electric AC energy generation potential [Wh].

These quantities are often normalized to compare different buildings, set-ups, plots, technologies, etc., on an equal footing. Depending on the goals of the analysis, different normalization factors may be applied to these quantities:

**Peak power installed** – the nominal peak power production of a PV installation [Wp].

**Conditioned floor area** – conditioned floor area of a building [$m^2$].

**Building footprint area** – area occupied by a building at ground level [$m^2$].

The following indicators are retained for this analysis.

The **PVPot** indicator considers only the PV generation potential. It corresponds to the Gross electric energy production normalized by the Peak Power installed.

$$\text{PVPot} = \frac{E_{AC}}{P}, \tag{11.8}$$

where $E_{AC}$ is the AC electricity production from PV [kWh] and $P$ is the peak power installed [kW].

The **RenPot** indicator considers only the energy displacement from energy saving measures. It corresponds to the energy saving potential normalized by the conditioned floor area.

$$\text{RenPot} = \frac{\frac{Q_{current} - Q_{H,li}}{\text{COP}}}{A_{th}}, \tag{11.9}$$

where $Q_{current}$ and $Q_{H,li}$ are the heating energy needs before and after retrofit [kWh], COP is a fixed coefficient of performance for a heat pump of 2.8 [-], $A_{th}$ is the conditioned floor area [$m^2$].

The **RenPotPV** indicator considers the energy displacement both from energy saving measures and energy generation. It is therefore a comprehensive indicator of the building retrofit energy potential normalized by the conditioned floor area.

$$\text{RenPotPV} = \frac{\frac{Q_{current} - Q_{H,li}}{\text{COP}} + E_{AC}}{A_{th}}, \tag{11.10}$$

where $Q_{current}$ and $Q_{H,li}$ are the annual heating energy needs before and after retrofit [kWh], COP is a fixed coefficient of performance for a heat pump of 2.8 [-], $E_{AC}$ is the annual AC electricity production from PV [kWh], $A_{th}$ is the conditioned floor area [$m^2$].

### 11.4.2 Spatial aggregation

This work considers a typical problem of spatial decision making: the evaluation of multiple locations to find the most suitable one(s) for some given goals and constraints. The simulation of PV production is conducted at the panel level, and these quantities are aggregated at different spatial divisions to be meaningful for different decision makers. For example, an owner of a housing estate may be interested in finding the optimal roof location from a collection of buildings in a relatively small area, while a municipality might be interested in subsidizing the retrofit of the buildings with the highest energy saving potential.

Spatial divisions could be based on ground conditions such as planning laws and decisions, constructions, or abstractions such as Cartesian coordinates. Here below are the spatial divisions considered in this work:

**Surfaces** – as defined in the 3D cadastre, excluding surfaces of super-structures (i.e., architectural details such as dormers and other roof-top protrusions) and other constructions not classified as buildings.

**Buildings** – as defined in the 3D cadastre.

**Planning zones** – homogeneous urban areas, as defined in the local planning tools.

**Tiles/grids** – a Cartesian subdivision of the space into squares of equal areas.

### 11.4.3 Ranking from risk-averse comparisons

Most methods for solving spatial-decision problems assume that complete information is available, so that decision-makers know the outcome of their choice precisely. However, in real-world applications, this is often not the case. In spatial decision problems, uncertainty can be related to errors in position or attributes [178, 7.2.2.2], or the preferences of decision-makers [177, 8.1.2]. We will focus here on attribute errors and will only consider decisions based on a single criterion.

Methods to account for uncertainty can be categorized as either direct methods, which include uncertainty directly in the preference model (e.g., by the use of probabilistic and fuzzy decision types), or indirect methods, which quantify the uncertainty by sampling different inputs. Typical indirect approaches to quantifying uncertainty are sensitivity and error propagation analyses. The main difference is that while the latter work by propagating perturbations or variations of the inputs through the model, the former incorporate the error/uncertainty associated with each parameter in the model itself [177, 8.2]. Indirect methods can be used to test the robustness of a decision to the variation of some parameters, while direct methods are aimed at making the preference model robust to such variations.

As shown by Malczewski [177, 8.2], an alternative $A_i$ is preferred to $A_k$ if the lowest value of the $i$'th criterion outcome $(V_i - \sigma_{V_i})$ is greater than the highest value of the $k$'th outcome $(V_k + \sigma_{V_k})$, i.e.,

$$A_i > A_K \quad \text{if, and only if,} \quad (V_i - \sigma_{V_i}) \geq (V_i - \sigma_{V_k}). \tag{11.11}$$

By this criterion, an alternative may not be selected over another when there is an overlap of the range of the chosen outputs, as shown in Fig. 11.13. We call this *risk-averse* decision-making, and discuss it further in Section 11.4.3.1.

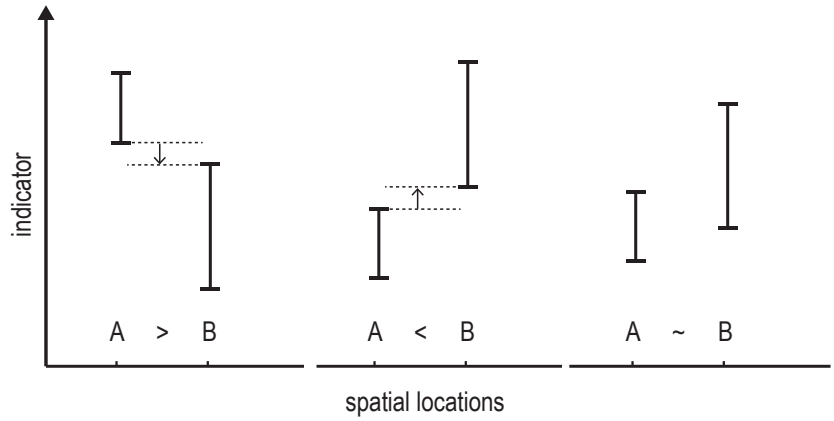


*Figure 11.13 – Risk-averse preference model, adapted from Malczewski [177]. In the left-most case, A is* always *better than B, while the opposite is true in the central case. A risk-averse decision-maker would be unable to make a decision in the right-most case since there is overlap.*
*Source: Peronato et al. [226]*

#### 11.4.3.1 Preference model

We demonstrate here an approach which is based on the comparison of summary statistics accounting for their confidence intervals. This method is meant to systematize decision-making about how to select one spatial location over another under uncertainty. Based on the outcome of this preference model, we show an aggregation of its outcome into a ranking.

The proposed method is appropriate for epistemic sources of uncertainty such as vegetation. Remote-sensing data cannot properly characterize the transmission factor of the vegetation canopy and its seasonal variations. Therefore, we expect that the actual transparency level at any given time of year is somewhere between a fully-opaque tree canopy and a fully-transparent one. The extremes correspond to unrealistic boundary (environmental) conditions, but nevertheless have some advantages: they can be modelled easily and allow risk-averse decision-making.

To avoid risk completely, we should make the choice between two locations based on opposite extreme scenarios, as we cannot conclusively exclude the scenario that these two locations have opposite vegetation characteristics. That is, one zone has sparse, deciduous vegetation and the other has dense, evergreen vegetation. This leaves us with three possible outcomes of a comparison:

$$\texttt{if } max(A) < min(B) \texttt{ then } A < B,$$

$$\texttt{elif } min(A) > max(B) \texttt{ then } A > B,$$

$$\texttt{else } A \sim B,$$

where $max(\cdot)$ corresponds to the 'no trees' scenario and $min(\cdot)$ to the 'opaque trees' scenario. This model is represented in Figure 11.13.

We used the method where each plot is compared to every other to determine winners and losers in a comprehensive pairwise match-up. Each comparison is carried out using ranges of outputs from a

small set of annual simulations using extreme input conditions, which is a crude estimate of the range of annual sum of energy production values. The results of each match-up can be stored as all-or-none scores, i.e., +1 for a win, 0 for a tie, and -1 for a loss; or scaled scores, where each difference between two plots is stored as a fraction of the largest difference in a given group, e.g., 0.7 for a 'large win' or 0.25 for a 'small win'. Each of these scoring systems may be thought of as representing different attitudes to risk: the all-or-none system is more risk-averse since inconsistent performers are less likely to stand out over a large number of match-ups. However, using the all-or-none principle implies the same risks as a first-past-the-post electoral system, i.e., the plot that has the highest number of wins is first, regardless of the number of wins as a proportion of the total match-ups or magnitude of these wins.

#### 11.4.3.2 Ranking aggregation

There are three main methods to aggregate results from comparisons into a ranking: permutation-based, matrix factorisation, and score-based probabilistic methods [167]. Permutation methods are computationally expensive, while matrix factorisation and score-based methods provide an efficient way to obtain a ranking from pairwise comparisons [82].

We used a score-based method, as it provides decision-makers with an intuitive and easy system to compute rankings from multiple pairwise comparisons. Specifically, we applied Copeland's method [233, p. 122], which tracks the number of victories or defeats from each pairwise comparison. In pairwise comparisons with expert answers, the decision matrix might be incoherent, since human experts may show inconsistency over time. As the outcomes in our method are derived from objective comparisons of the bootstrapped summary statistics of time series, the decision matrix is perfectly coherent. When the production from two plots is compared, the conditions under which each is tested are comparable.

These comparisons are symmetric, i.e. if $x > y$, then $y < x$. In this sense, the score calculated when comparing location $x$ to $y$ ($\pm 1$) has to be the additive inverse of the score calculated when comparing location $y$ to $x$ ($\mp 1$). Whenever a comparison yields no winner, because the variation in a summary statistic due to uncertain boundary conditions is larger than the difference between the two locations, the assigned score is 0.

As we discussed in the preference model above, for some risk attitudes, identifying the winner of each comparison is not enough to identify the best candidate. It is also necessary to quantify how much better (or worse) a location is compared to its opposing ones. To enable this comparison, we integrated a fuzzy logic system for both our preference models. This system is based on calculating *fractional wins*, i.e., the difference between two choices divided by a normalisation factor. The normalisation factor *norm* is

$$norm = |max(min(E_A - E_B)) - (min(max(E_A - E_B))|, \tag{11.12}$$

i.e., the difference between the highest production using the min-radiation scenario (e.g., opaque vegetation) and the lowest production using the max-radiation scenario (e.g., no vegetation). This method results in a normalisation factor *norm* which is applied to the assigned *score*, so that the highest score $\pm 1$ is only assigned to the victory/defeat with the largest margin.

The preference model is described in Algorithm 11.8 and incorporated in a Python function included in Appendix A.2.3.

`if` $max(A) < min(B)$ `then` $score = \frac{max(A)-min(B)}{norm}$

`elif` $min(A) > max(B)$ `then` $score = \frac{min(A)-max(B)}{norm}$

`else` $score = 0$

where *norm* is defined in Equation (11.12).

**Algorithm 11.8:** Risk-averse preference model. This model is implemented in a Python script listed in Appendix A.2.3.

### 11.4.4 Ranking with low-yield avoidance

The challenge of any climate-based simulation is to understand micro-climatic conditions, i.e., the local conditions experienced by a solar panel, while only having data about the conditions at the regional or global scale, i.e., smooth meso-scale data. In our analysis, we ignore the spatial variation of wind and temperature at the microclimatic scale. That is, we assume that the effect of the urban microclimate on temperature and wind speed is experienced uniformly by each plot/tile. We model the changes in solar availability on a panel due to obstructions but not the localized wind speed and temperature. For this reason, we cannot apply the previously-described preference model to weather scenarios. That is, the meso-climatic variations (and the uncertainty about those variations) apply equally to all urban locations belonging to the same micro-climate. However, decision-makers might be interested in avoiding the risk of installing solar modules in locations that under-perform with respect to a benchmark.

We propose a method based on two weather scenarios, one with 'typical' and one with low radiation availability, as described in Algorithm 11.9 and Figure 11.14. It is then obtained. Subsequently, the ranking is obtained by applying the risk-averse preference model on the resulting yield conducted using the two vegetation scenarios.

Simulation with the 'low rad' weather scenario is used to discard locations that fall below a certain threshold $t$ and an estimate of the annual yield is then calculated using the typical weather results (Figure 11.14).

$$P = \sum_{m=1}^{n} (P_m \cdot t_m) \qquad \texttt{with } t_m = \begin{cases} 1, & \texttt{if } P_{lowrad,m} \geq t, \\ 0, & \texttt{otherwise.} \end{cases} \tag{11.13}$$

where $P$ is the cumulated power of of $n$ modules $m$, each one with a power $P_m$ under a typical weather scenario and a power $P_{lowrad,m}$ under a 'low rad' weather scenario, and $t$ is the selected minimum threshold.

**Algorithm 11.9:** Low-yield avoidance model (see also the schematic drawing in Figure 11.14). This model is implemented in a Python script listed in Appendix A.2.1.

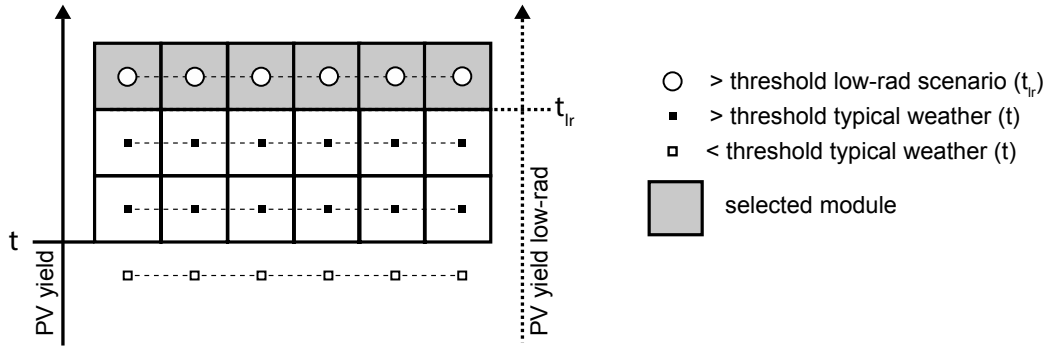


*Figure 11.14 – Schematic drawing of the low-yield avoidance method (Algorithm 11.9). The PV yield is calculated using typical weather, while the selection of the PV modules is based on threshold calculated using a 'low rad' weather scenario.*

Although irradiation thresholds are not unequivocal, we think that they are a useful instrument to define the suitability of a surface, considering the attitude to the payback time: in general, if we neglect economy-of-scale considerations, the higher the threshold, the shorter the payback time of the solar system will be, as only the top-producing PV modules are retained. In this sense, we should consider the minimum acceptable threshold as a variable, which can be selected by the decision maker depending on their preferences. However, it should be noted that the higher the threshold, the smaller the installation and hence the higher is the share of the cost of installation on the final cost, which is then not proportional to the size. Therefore, this method might underestimate the actual payback time for high thresholds.

### 11.4.5 Suggested applications

Table 11.13 shows some possible uses of the proposed indicators and spatial aggregation for different stakeholders and decision-makers. In the context of this thesis, we only give some recommendations, while the actual relevance and usefulness of the proposed indicators and spatial aggregations for different decision-makers should be directly tested with the final users. In addition to the users we specifically target in this thesis (e.g., local planning authorities, large building owners, and ESCos), we also suggest the possible relevance for building owners, which are the main users of traditional solar cadastres (Section 4.3.1, as well as grid managers, which will be highly affected by the large-scale deployment of photovoltaics. The sizing heuristic is suggested here only to local authorities, while we consider that the other decision-makers can make informed financial decisions to size the system using for example a minimum threshold. Similarly, the different spatial aggregation are considered relevant for planning authorities and grid managers, as all other stakeholders will mostly look at the building scale only. Single building owners and planning authorities might also be interested on smaller aggregation scales (building surface and single PV module) to check the energy generation of single surfaces as well as the visual impact of the installation.

### 11.4.6 Technical implementation

The evaluation consists of a series of Python scripts parsing and processing the simulation results (i.e. hourly electricity production per module and building energy needs for space heating) and the

*Table 11.13 – The table shows some suggested uses of the features of the evaluation method for different decision-makers. The "ranking" column indicates whether the ranking of spatial locations is considered as a sufficient and relevant information or the absolute values are still needed. ESCos are considered both for energy saving interventions and solar installations (solar contracting).*

| Stakeholder | Sizing (Section 11.3.3.2) | Indicator(s) (Section 11.4.1) | Aggregation (Section 11.4.2) | Ranking | Suggested use |
|---|---|---|---|---|---|
| Building owner | Threshold | PVPot<br>RenPot<br>RenPotPV | Building<br>Surface<br>PV module | No | Check the energy potential of their own building and the arrangement of solar modules |
| Building portfolio owner/manager | Threshold | PVPot<br>RenPot<br>RenPotPV | Building | Yes | Prioritize energy saving interventions and PV installations |
| Local planning authorities | Heuristic | PVPot<br>RenPot<br>RenPotPV | Building<br>Zone<br>Grid<br>PV module | Yes | Prioritize incentives and planning interventions |
| ESCo | Threshold | PVPot<br>RenPot<br>RenPotPV | Building | Yes | Identify possible customers |
| Electricity grid manager | Threshold | PVPot | PVPot<br>Building<br>Zone<br>Grid | No | Test the effect of different PV penetrations on the grid |

geometry, and exporting the results in the target visualization format. The core Python functions implementing the evaluation process are listed in Appendix A.2.1. To perform the evaluation, the user has to set the following parameters:

- **Tiles**, lis of tile IDs to be processed;
- **Scale**, string defining the spatial division of the analysis (see Section 11.4.2). In this implementation, we can choose between "tile", "zone", and "building". It is also possible to visualize the PV potential results per "surface" or "module";
- **Threshold**, either a number with a minimum threshold (expressed in kWh/kWp) or the string "auto" for using the balanced threshold calculated by the Algorithm 11.6 (see Section 11.3.3.2);
- **Regularity**, boolean to activate the regularity algorithm (Algorithm 11.7)
- **Low-yield avoidance**, boolean to activate the low-yield avoidance algorithm (Algorithm 11.9)
- **Indicator**, string corresponding to the selected indicator (see Section 11.4), e.g. "kWhkWp", "RenPot" or "RenPotPV"

Depending on the scale of the analysis and the number of tiles, the evaluation can take from few seconds to a few minutes. If the simulation results and the geometry have been already loaded into the memory, the computation time is significantly shorter.

## 11.5 Visualization

The evaluation method presented in the previous section is only the first step of the decision-making process. It is in fact completed by a 3D visualization platform, which allows decision-makers to see and interact with the results. Unlike traditional solar cadastres which are mostly targeted to owners of single buildings (see Section 4.3.1), this platform is addressed to stakeholders dealing with a number of

buildings in the same area. In this sense, we consider that the user is primarily interested in comparing spatial locations, rather than knowing the actual potential of each single location (which is though still possible by clicking on a specific object). Moreover, thanks to decision-support methods presented in the previous section, we can achieve a robust ranking of the urban locations.

In this work, we target decision-makers including both public and private stakeholders such as planners working for the municipality, owners of real estates composed of several buildings in the same urban area, or ESCos interested in investing in the area. The goal is to provide them with a simple but effective system to autonomously navigate the results of the evaluation at the different spatial aggregation scales. To this end, the visualization strategy is based on a 3D representation of the analyzed geometry at multiple resolutions using semi-transparent overlays displaying the results on the different indicators.

### 11.5.1 Concept

Figure 11.15 illustrates the main features or the visualization interface and Figure 11.16 some screenshots of its current implementation. The results are displayed through semi-transparent false-color overlays displaying the normalized score. By clicking on an object, the user has access to descriptive data about the indicators and the ranking. The map also displays a decision plot, which conveys four levels of information:

- the mean energy performance of the vegetation scenarios, through the bar height;
- the difference of energy performance between the two vegetation scenarios, through the error bar;
- the ranking, through the position of the indicator bar (1$^{st}$ ranked at left);
- the normalized score, through the false-color of the bar.

The descriptive data is usually displayed as a call-out balloon upon click of the user. Other elements (text, graphs) can be inserted as image overlays. In the sample implementation of Figure 11.16, the plot and the color key and added as overlays.

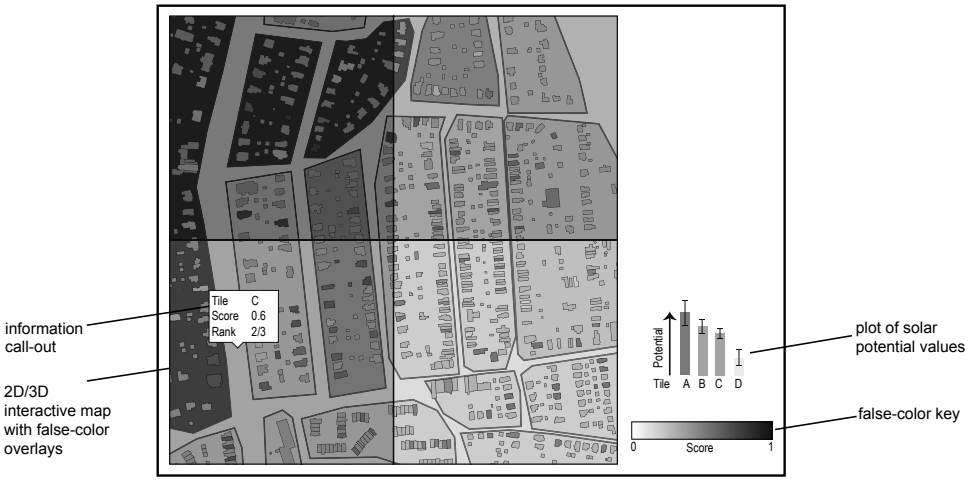


*Figure 11.15 – Schematic concept of the visualization interface as implemented in this thesis.*

We argue that the false-color overlays at different resolution scales could provide relevant information to the targeted stakeholders. In particular, the overlays can highlight homogeneous areas (e.g., similar score for buildings contained in the same zone) or non-homogeneous areas (e.g., a building with a high score in a low-score zone, or the opposite). This could suggest different strategies to the decision-makers, such as joint retrofit interventions within areas with a similar score, or the concentration of electricity production in buildings with higher potential than their neighbors.

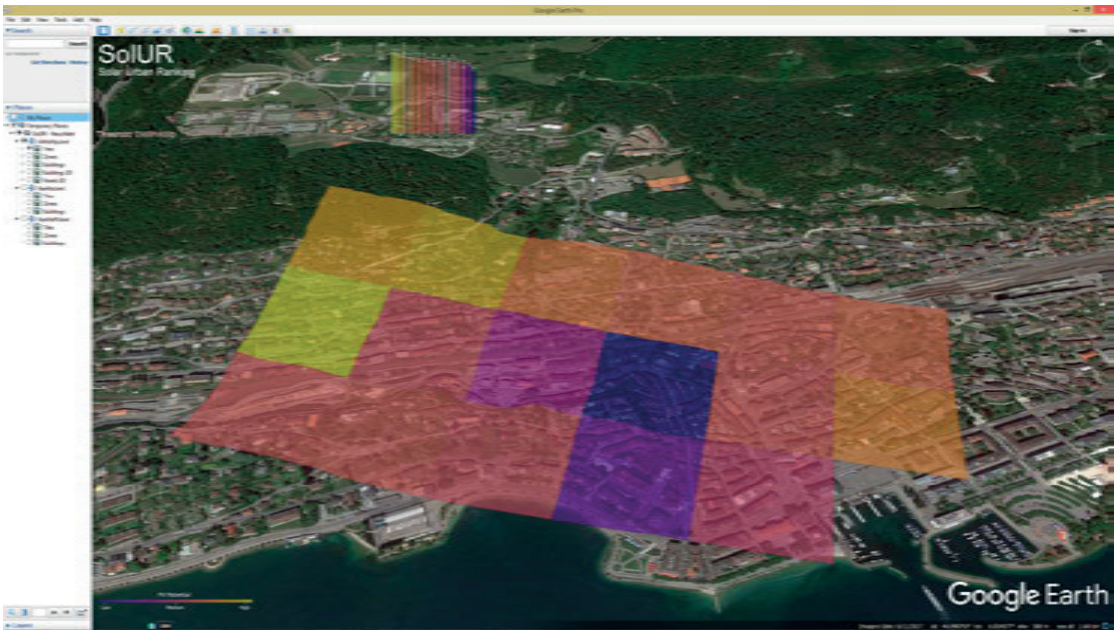


*Figure 11.16 – Current implementation of the visualization concept in Google Earth Pro. The animation presenting the different spatial aggregation scales can be seen using Adobe Acrobat or Adobe Reader or, as separate frames, in Appendix A.4.3.*
*Background image: ©2018 LandSat-Copernicus and Google*

### 11.5.2 Technical implementation

Figure 11.16 shows a series of screen-shots of the current implementation of the visualization concept presented in Section 11.5.1, through the use of KML files in Google Earth. These KML files are compiled by the evaluation scripts presented in Section 11.4. The KML files resulting from an evaluation can be overwritten and automatically reloaded into the 3D mapping software. For example, the user can run two analyses at different thresholds and visualize the updated results in almost-real time.

KML, formerly Keyhole Markup Language, is a XML-like markup language for geoinformation developed by Google and now adopted and maintained by the Open Geospatial Consortium. KML was originally developed for use in Google mapping tools, but since the OGC implementation has become a widely-used format for representation of geodata also in other platforms, such as the open-source software CesiumJS [65]. To this end, KML files provide an XML representation of 2D and 3D polygons including style attributes and description data. As a standard feature in geo-visualization, most KML viewers allow the display of different layers of information superimposed, which is useful for the implementation of the visualization concept.

In our implementation, the geometry is described as a `<polygon>` (defined by its outer boundary

only) and is linked to a <style> object with a false color. The false-color gradient is mapped to the Normalized Score (for “tile”, “building”, and “zone” spatial divisions) or the gross electricity production normalized by the peak power (for building surface- or PV module-based visualizations). The visualization of PV modules requires a very high number of <polygon> objects and, due to I/O limits, is hence possible only for small areas (e.g., one single tile). This limitation could be overcome by incorporating the PV modules’ false colors as raster texture in each surface.

## 11.6 Synthesis and discussion

This chapter has proposed a method targeting the research gaps that were highlighted in Section 4.4. This method was implemented as a semi-automated workflow dealing with the modeling, simulation, evaluation and visualization of solar potential.

With regards to the solar radiation models, we proposed to couple existing state-of-the-art raytracing models, which were applied to 3D geometric models with a high level of detail and fine ambient and discretization settings. The chapter also described a workflow that integrates the analysis of building-integrated solar potential at different levels, mainly the technical and location ones, but including also some aspects of the architectural integration potential (regularity) and of economic potential (self-consumption). It also proposed a novel integration of the analysis with decision-making and visualization techniques. In particular, we have seen a solution to implement the use of extreme modeling scenarios in the decision making. The outcome is a solar potential score that can be used in allocation problems as well as the indicator in the proposed 3D visualization interface.

The workflow was described here with the purpose of presenting the modeling parameters, some of which had been investigated in Part II, and illustrate the modeling scenarios that will be used in the next chapter. It also described the workflow from a technical point of view, so as to act as a reference for future similar implementations. The next chapter will focus on the applicability of the workflow in a real case study. In addition to giving some context-specific indicators for solar energy planning, it willl show how the proposed modeling scenarios have an influence in the decision and highlight hence its added value. For a complete overview of the method, the reader is hence referred to Section 12.2.4.2 for the general findings that were the outcome of the application of this method.

# 12 Case-study application: Neuchâtel

This chapter presents a case-study application of the methodology presented in Chapter 11 to the city of Neuchâtel. The case study was selected in the framework of the umbrella project [247] this thesis belongs to, as Neuchâtel was considered as representative of the middle-sized city of the Swiss plateau.

We first describe the general characteristics of the city, in terms for example of built and vegetation morphology, and planning policy and bylaws. Second, we present the results of the analysis conducted with the methodology presented in Chapter 11 and discuss the results, in terms of case-specific planning implications and general findings.

The surface of the city of Neuchâtel being particularly large (18.05 $km^2$), for the application of the method itself we will consider here only a smaller area, which is highlighted in Figure 12.1.

## 12.1 Presentation of the case study

The city of Neuchâtel is composed of about 5'000 buildings. We analyze here only a subset of the building stock composed of 1'383 buildings comprised in an area of about 1.06 $Km^2$, in which the historic center is about at the middle. We chose this area for the variety of building uses (Figure 12.3) and construction periods (Figure 12.2). Moreover, as can be seen in Figure 12.1, some morphological characteristics are constant across the entire built area, such as:

- the prevalent arrangement of buildings along the lakeside, i.e., generally with the main façade facing South-East;
- the railway line separating the downtown area with mixed-use buildings of different sizes and the uphill residential neighborhoods, mostly constituted of single-family housing;
- most of the buildings are isolated, while in the denser downtown area we can see a more a predominant contiguous built canopy as well as some courtyard blocks.

The selected area shown in Figure 12.1 presents thus a sample of these characteristics. Nonetheless, it should be noted that, unlike in many cities in Europe or North-America, buildings shapes and distributions are varied, and no uniform blocks can be identified, not even in residential, low-density neighborhoods. In some cases, Figure 12.2 highlights some buildings belonging to the same development project, but these are usually composed of up to three buildings.

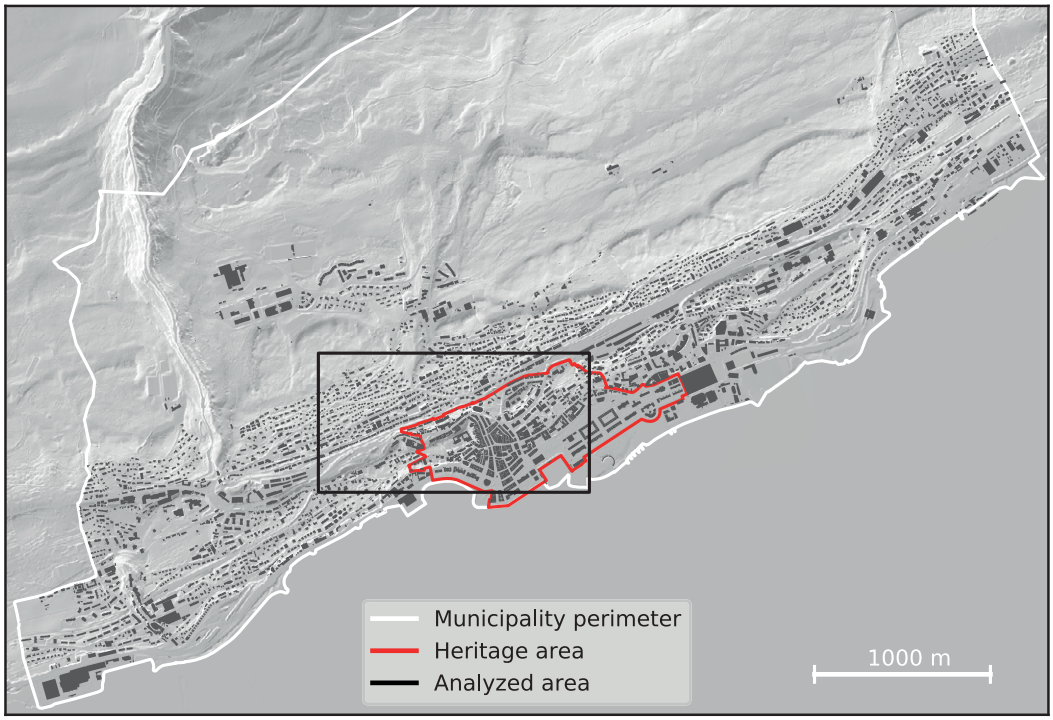


*Figure 12.1 – The buildings of the city of Neuchâtel; please note that the Chaumont et La Combe D'Enges areas, in the North-West of the municipality perimeter, are not included in this map.*
*Data source: SITN Cadastre 2017 and Swisstopo SwissBOUNDARIES3D 2018*
*Background: Swisstopo SwissALTI$^{3D}$*

### Characteristics of buildings

We present here an analysis of the building characteristics of the area conducted on the basis of the available geo-databases, in particular the SITN cadastre, the Swiss Federal Register of Buildings and Dwellings (RegBL) and the Survey of Architectural Quality (*Récensement Architectural du Canton de Neuchâtel (RACN)*). It should be noted that these databases do not have a full intersection and thus only a subset of the building stock is listed in all databases.

As can be seen in Figure 12.2, in the analyzed area, the building construction period is particularly old, with more than 80% of the buildings being built before 1970. This figure is consistent with the entire building stock of Neuchâtel included in the Swiss Federal Register of Buildings and Dwellings (RegBL). Since many buildings in the historical city center do not have the period of construction (plotted in grey in Figure 12.2), we can assume that the share of older buildings is even larger.

According to Perez [213], who conducted a calibration study for their thermal model using measured data, the construction period with the worst performance, i.e. with the highest U-value (= 1.35 W/m$^2$K), is 1946-1960. Buildings built before the 2$^{nd}$ world war benefit of better thermal envelopes than buildings built in the immediate post-war period, due to the massive masonry construction. Starting from the 1970s, with the oil crisis, the attention to the thermal aspects of the construction increases. Unfortunately, the RegBL for Neuchâtel does not provide the fields corresponding to the year and period

of latest refurbishment, so it is not possible to map the buildings that have been renovated. However, considering that the estimated yearly refurbishment rate is 0.9%[1] and that the refurbishment incentives of the Buildings Program (see Section 3.4.1) started in 2010, we can estimate that about 15-20% of the residential building stock have had a refurbishment intervention.

As can be seen in Figure 12.3, in terms of building uses, 60% of buildings are residential. This figure is lower than for the entire city building stock (81%), as the city center consists of many commercial buildings. As expected, single-family housing is mostly concentrated in the low-density neighborhoods North of the railway, while we find large multi-family housing along the railway line as well as in the downtown area.

In terms of heritage protection, a large part of the analyzed area falls within the perimeter of areas classed in the ISOS inventory with an A or is listed in the first category of the RACN. This is quite obvious since in this area of the city we find the historical center, the castle as well as the lake-side parks. Most of the buildings in the low-density urban areas are not listed or are even classified as "unsettling" in the RACN. There are however some notable exceptions of single buildings or even blocks of buildings, such as the ones facing the railway line, which are listed in the ISOS inventory because of their "rare length and homogeneity."

The protected buildings do not comply with the requirements for the building permit waiver defined by the Federal Planning Ordinance (see Section 3.1.2). However, this does not prevent the installation of solar systems, only it requires a more careful integration, which is then subjected to an evaluation of the authorities granting the building permit. The case study presented in Section 13.2 is an excellent example of successful integration of solar systems in a building classed in the ISOS inventory with an A.

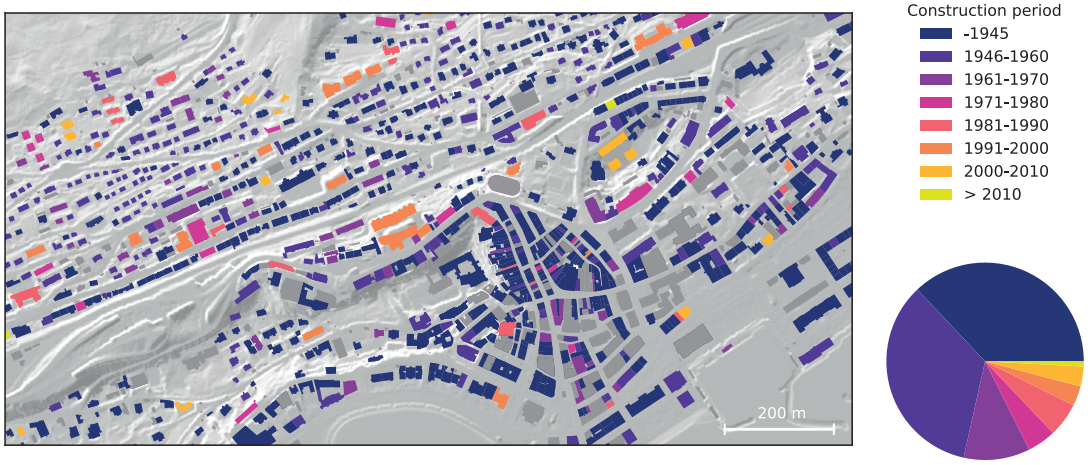


*Figure 12.2 – Map and pie chart showing the building construction period. More than three quarters of the building stock was built before 1970,*
*Data source: RegBL and SITN. Background: Swisstopo SwissALTI$^{3D}$ - Footprints: SITN Cadastre*

[1] http://www.sia.ch/fr/themes/energie/modernisation-du-parc-immobilier-suisse/, Last accessed on August 20, 2018

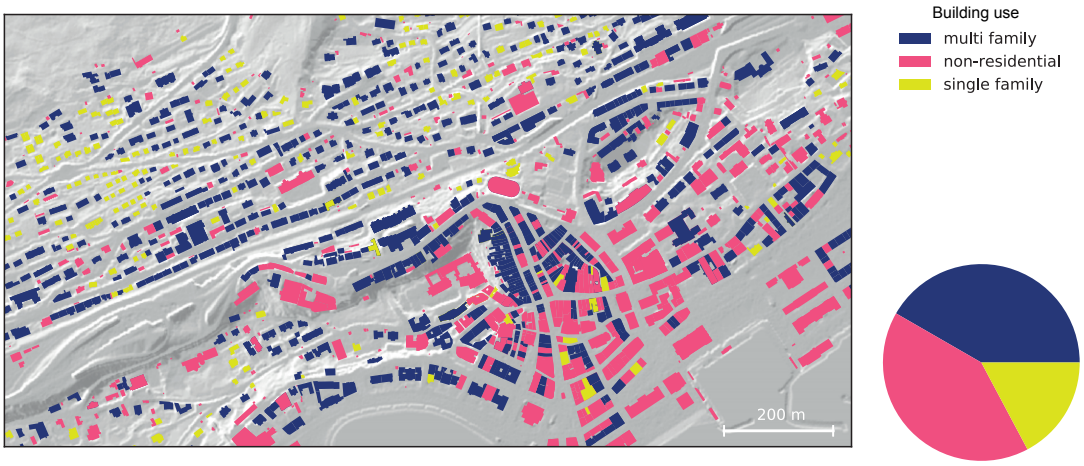


*Figure 12.3 – Map and pie chart showing the building uses. Non-residential buildings are mostly located just around the inner central area. As expected, single-family buildings are mostly located in low-density urban areas.*
*Data source: RegBL and SITN. Background: Swisstopo SwissALTI$^{3D}$ - Footprints: SITN Cadastre*

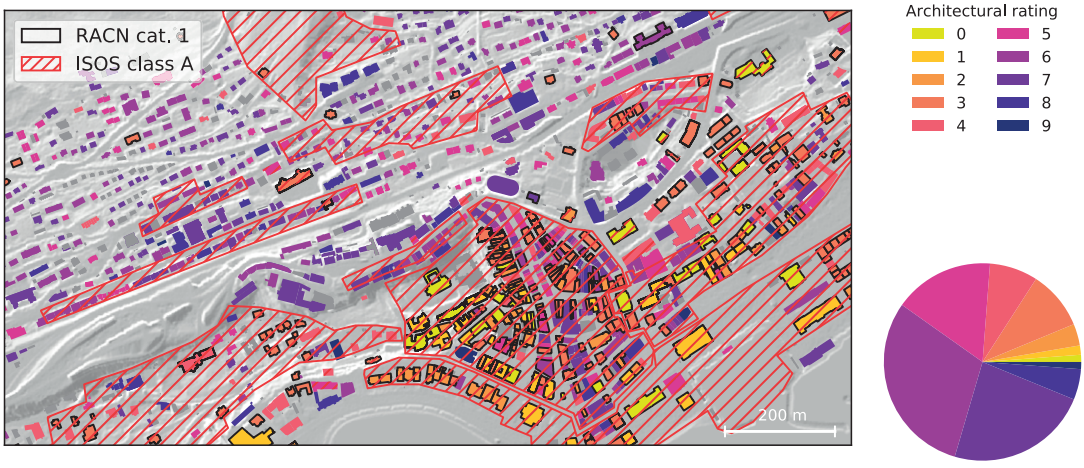


*Figure 12.4 – Evaluation of building architectural quality (see Table 12.1) and heritage protection at the federal (ISOS) and cantonal level (RACN category 1). The protected buildings do not qualify for the building permit waiver for solar installations allowed by the Federal Planning Ordinance (see Section 3.1.2).*
*Data source: RegBL, RACN, ISOS. Background: Swisstopo SwissALTI$^{3D}$ - Footprints: SITN Cadastre*

*Table 12.1 – Evaluation table of building architectural quality in the Canton of Neuchâtel. Buildings listed in the first category do not comply with the requirements for the federal building-permit waiver for solar systems presented in Section 3.1.2.*
*Source:*
*https://sitn.ne.ch/web/dictionnaire/patrimoine_architectural/complete/PA1_recensement_architectural.pdf , own translation*
*Last accessed on August 23, 2018*

| Category | Rating | Description |
|---|---|---|
| 1 | 0 | Remarkable |
| | 1 | Interesting from multiple perspectives |
| | 2 | Clearly interesting |
| | 3 | Probably interesting |
| 2 | 4 | Typical |
| | 5 | Pictoresque |
| | 6 | Neuter or banal |
| 3 | 7 | Uninteresting |
| | 8 | Unsettling |
| | 9 | Strongly unsettling |

### Vegetation and built density

Figure 12.5 shows the distribution of vegetation and built volume in the analyzed area. As expected, the vegetation volume is higher in low-density areas, such as in the residential area over the railway line (tiles 232,233 and 234) and close to the castle park and by the lake (tile 168, 169 and 170).Tile 232 has almost three times the vegetation volume as the median tile and about 1/6 of its built volume, but this is because almost half of its area is covered by forest.

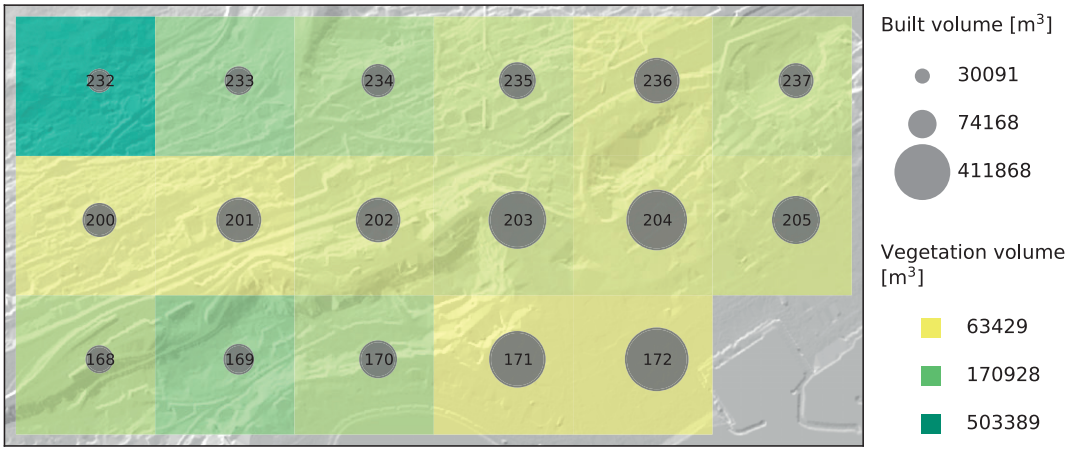


*Figure 12.5 – Vegetation and built volume per tile calculated from the DSM and DTM. The tile ID is plotted at the center of each tile. As in all tile analysis, tile 173 in the bottom-right corner is not considered because of its limited number of buildings. Upper-left tiles correspond to low-density urban areas with a strong presence of vegetation.*
*Background: Swisstopo SwissALTI$^{3D}$*

Table 12.2 shows that tile 170 has a much larger variation of irradiation due to vegetation than tile

203. This can be intuitively expected by the large presence of vegetation, which can be appreciated qualitatively in Figure 12.6 and quantitatively in Table 12.2. As expected, façades are more affected by vegetation than roofs, but the effect on the whole building envelope is also relevant (-16% for tile 170), because of the larger share of both sensors nodes and irradiation on façades than on roofs.

If we consider the impact of inter-reflections (i.e., `-ab 3` compared to `-ab 1` for the diffuse and `-ab` for the direct contribution), we notice an opposite situation. The reflected component has a clearly stronger impact for the denser tile 203, especially on façades, for which it contributes up to +18%.

*Table 12.2 – Effect of vegetation on tile 170 and 203 (Figure 12.6)*

| Tile 170 | Whole building | Façades | Roofs |
|---|---|---|---|
| Share of irradiation | 100% | 70% | 30% |
| Share of sensor nodes | 100% | 67% | 33% |
| Variation of irradiation due to opaque vegetation | -16% | -17% | -14% |
| Variation of irradiation due to inter-reflections (-ab 3) | +8% | +9% | +7% |
| Tile 203 | | | |
| Share of irradiation | 100% | 39% | 61% |
| Share of sensor nodes | 100% | 69% | 31% |
| Variation of irradiation with opaque vegetation | -4% | -6% | -3% |
| Variation of irradiation due to inter-reflections (-ab 3) | + 9% | + 18% | + 3% |

(a) Tile 170 (b) Tile 203

*Figure 12.6 – Orthogonal view of 3D-reconstructed vegetation overlapped to an orthophoto for the tiles analyzed in Table 12.2. Their location is shown in Figure A.2.*
*Background image: Swisstopo CITIMAGE 2014 obtained via the SITN*

The influence of vegetation on the analyzed urban tiles (considering the PV electricity production) can be also seen in Figure 12.22c. Where we see a median influence of vegetation of -9% and a maximum value of -16%, corresponding to tile 232.

## 12.2 Results

This section presents the results of the evaluation of the solar potential of the analyzed buildings. We first describe the sizing of the solar systems in Section 12.2.1 and then apply the evaluation models presented in Section 11.4 based on the PV systems sized using Algorithm 11.6. The analysis is run for multiple relevant indicators and spatial aggregation scales. In Section 12.2.3, we compare the results obtained with the proposed ranking method with those of a state-of-the-art method not accounting for the uncertainty.

### 12.2.1 Sizing of the solar systems

As shown in Section 11.3, the solar systems are sized using two different methods: a minimum yearly AC production or a heuristic balancing the self-consumption and self-sufficiency of the system (Algorithm 11.6). The effect of the sizing can be seen in Figures 12.7 and 12.8: in high-density urban areas, the solar systems are not down-sized by the heuristic, as the self-sufficiency ratio is lower than the self-consumption. On the contrary, when a minimum threshold is applied, most of the systems are sized down, selecting only the best-performing modules (Figures 12.7b and 12.8c).

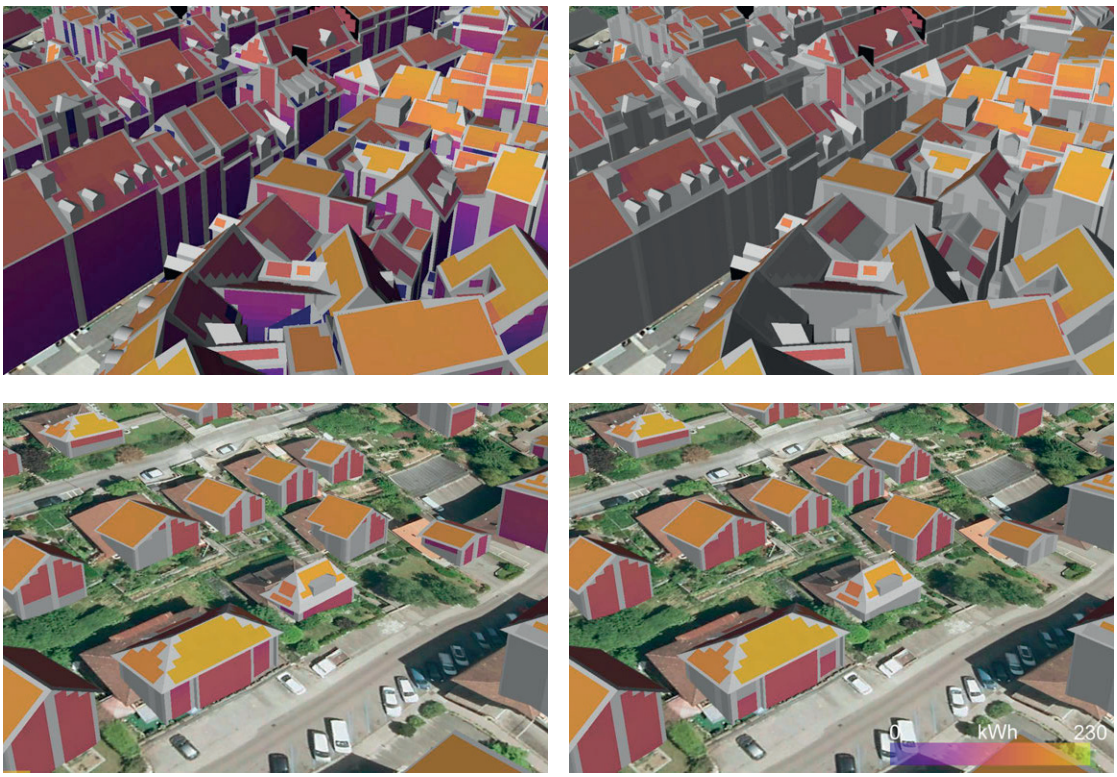


(a) Heuristic (balance of SC and SS)

(b) Minimum threshold (650 kWh/kWp)

*Figure 12.7 – False-color visualization of the PV modules' annual electricity generation. The solar systems are sized by the two methods presented in Section 12.2.1: we can notice a significant difference in the first row showing the denser city center, where the sizing heuristic (a) selects also the façade-mounted modules, while these modules do not achieve the minimum threshold (650 kWh/kWp = 120 kWh per module) used in (b).*

*Sources: Imagery - Swisstopo CITIMAGE 2014 obtained via then SITN - 3D model: SITN Cadastre*

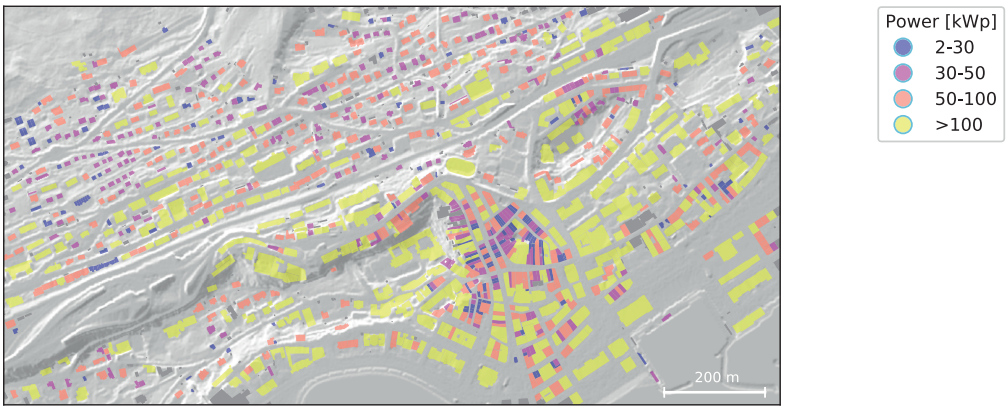


(a) All modules (unsized)

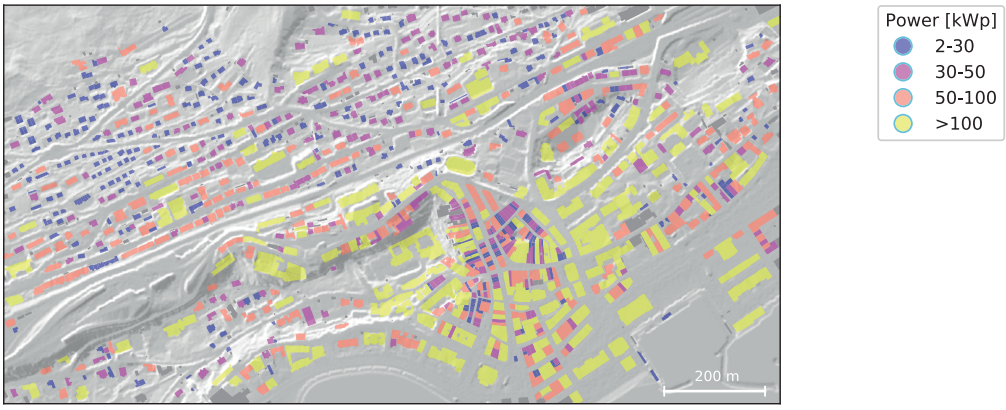


(b) Heuristic (SS-SC balance)

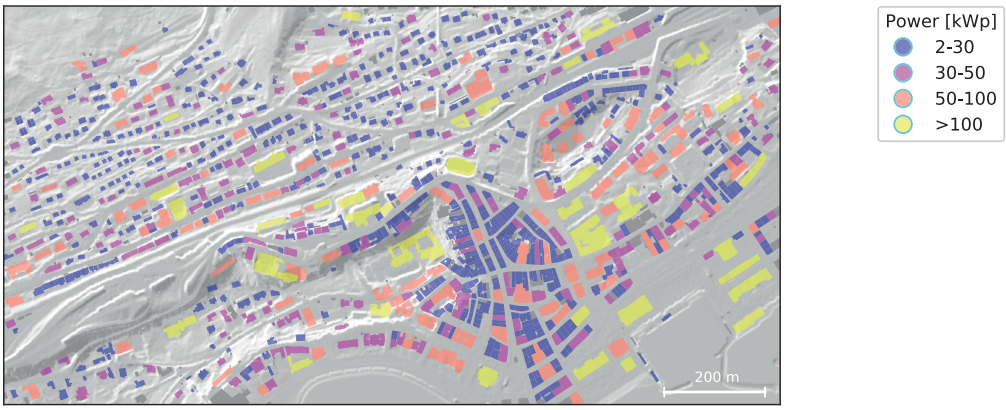


(c) Minimum threshold (650 kWh/kWp)

*Figure 12.8 – Power of the building solar systems before (a) and after (b, c) applying the different sizing methods presented in Section 12.2.1.*
*Background: Swisstopo SwissALTI$^{3D}$ - Footprints: SITN Cadastre*

#### 12.2.1.1 Minimum threshold

Here we present a sample financial simulation, similar to the one already applied in Section 9.1, to calculate a minimum PV yield threshold, which can be used to size the PV system. Unlike the heuristic presented in the previous section, this method is based on location- and time-specific financial parameters, in particular the cost of electricity (for self-consumption or injection into the grid) and of the PV installation. The cost of the installation and the tax deduction were calculated on the basis of the data from Swissolar online calculator. We considered also the federal incentives and the local incentive from the municipality of Neuchâtel, which together account for almost 50% of the investment. We conducted then the discounted cash flows on 25-year period, assuming a linear degradation up to 85% of the initial performance of the PV modules, 1% of the investment for annual maintenance costs and 3% of interest rate.

It should be noted that the cost of the system is dependent on the size of the system. We considered here a gross cost of 1883 CHF/kWp, which corresponds to the installation cost for 30 kWp system according to the Swissolar online calculator [294]. A smaller (respectively, larger) system would have a higher (respectively, lower) unitary cost. The Self-Consumption (SC) influences the viability of the system, as the self-consumed electricity has a higher financial value than the surplus electricity injected into the grid. For example, in the present conditions in Neuchâtel, the self-consumed electricity has about two times the value of the injected one and this difference is expected to increase in the future. We assumed a conservative Self-Consumption (SC) of 10%, which should be achieved in most of the situations, while the actual value would depend on the size of the system and the demand curve.

The simulation of the NPV for a sample installation shown in Table 12.3 defines a minimum PV yield threshold of 650 kWh/kWp for a module to achieve a 20-year payback. It should be considered that PV modules composing the installation would probably have a higher electricity production than the minimum threshold, increasing hence the financial viability of the system.

*Table 12.3 – Main parameters for calculating the minimum PV yield threshold, expressed as kWh/kWp or kWh/module, to get a 20-year payback of the installation (i.e., positive NPV).*

| | | Source/Assumptions |
|---|---|---|
| Power installed | 30 kWp | |
| Degradation after 25 years | 20% | Technical sheet of the module presented in Table 11.10 |
| Gross investment | - 56'480 CHF | Swissolar [294] |
| Local incentives | 10'000 CHF | 500 (capped to 10'000) CHF/kWp* |
| Federal incentives | 15'400 CHF | EV-RU-RU for integrated installations (Table 3.3) |
| Tax saving | 7'907 CHF | Swissolar [294] |
| Net investment | -26'729 CHF | |
| Annual savings from SC | 482 CHF | 0.24 CHF/kWh** |
| Annual remuneration from the grid | 2078 CHF | 0.11 CHF/kWh** |
| Annual maintenance costs | -565 CHF | 1% of investment Swissolar [294] |
| Interest rate | 3% | |
| Payback time | 20 years | |
| NPV 25 years | 3'914 CHF | |
| PV yield | 650 kWh/kWp | |
| | 120 kWh/module | |

* Municipality of Neuchâtel, Arrêté concernant l'utilisation du fonds communal pour l'énergie, 29.01.2018
** Viteos, 2018 rates

#### 12.2.1.2 Heuristic

Figure 12.9 shows the spatial distribution of the threshold obtained with the heuristic, i.e., the minimum annual AC electricity production that is required for PV module to be considered in the installation. As can be seen most of the buildings in the historic center have a lower or null threshold, meaning that all simulated modules (whose number is limited because of the low available exposed building surface area) have to be considered to provide a minimum self-sufficiency level.

Single-familiy buildings in low-density areas present higher thresholds to limit the size of the solar installation. Large buildings and buildings in the historical center present mostly a null threshold, as their self-sufficiency is lower than the self-consumption even when their surfaces are fully covered by PV modules (cf. Figure 12.11). Figure 12.10b shows that these buildings have a lower SS value (median of 0.25) and higher SC value (median of 0.39) than the whole dataset of buildings, which have an equilibrium between these two indicators at about 0.32 (Figure 12.10a). It should be noted that most of these buildings with SC > SS have walls shared with other buildings, which contributes to increasing their self-consumption in two ways: by reducing the heat losses and hence the building energy needs, and by limiting the number of panels that can be installed. Conversely, small-size buildings located in low-density residential areas are often isolated, i.e., they have four façades on which solar modules can be installed and this can lead to an over-sized system unless a sizing heuristic, as the one proposed here, is applied.

The most self-sufficient buildings are usually of small size and located in low-density residential areas, and these buildings are also the ones with the lowest self-consumption. It should be noted that for such buildings, the SC and SS values correspond to the equilibrium found by the sizing heuristic.

In terms of annual coverage (Figure 12.11c), most of the buildings cover about 100% of their electricity demand, i.e., they are (almost) net-zero buildings, and some (mostly small residential buildings) have even a net-positive energy balance. However, some large buildings, as well as most of the buildings located in the historical center, cover less than half of their annual electricity demand with solar energy.

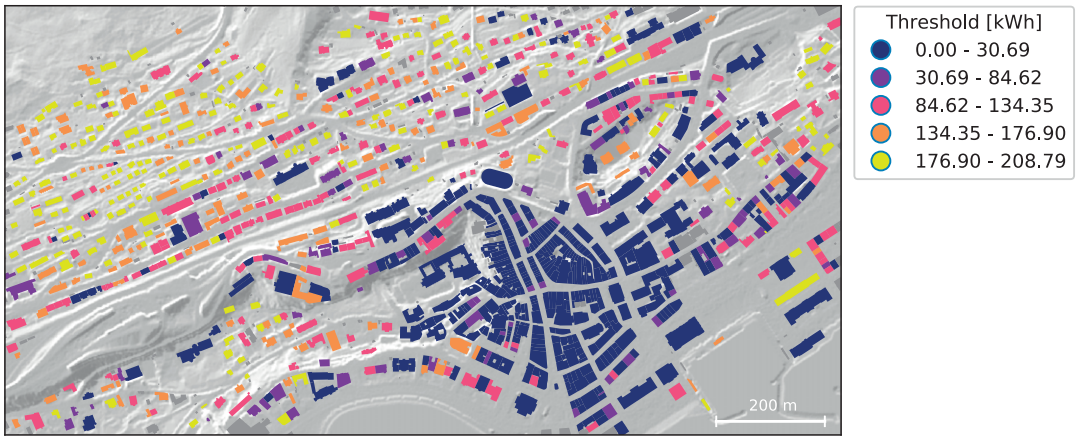


*Figure 12.9 – Minimum electricity threshold per module for each building, as determined by the sizing heuristic (Algorithm 11.6). Buildings in the central areas have a low or null threshold, indicating that even considering all PV modules, Self-Consumption (SC) is greater than Self-Sufficiency (SS). The SC and SS values of these buildings are displayed in Figure 12.10b. Conversely, buildings in low-density areas present higher thresholds, meaning that some modules are discarded to reach a balance between the two indicators.*
*Background: Swisstopo SwissALTI$^{3D}$ - Footprints: SITN Cadastre*

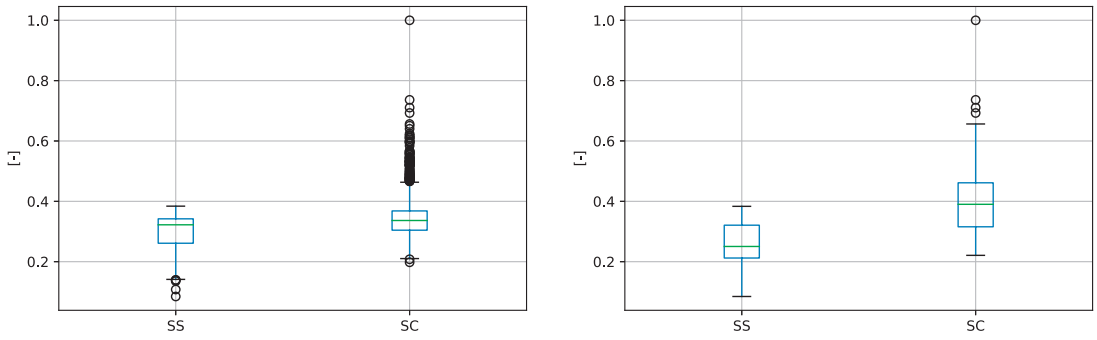


(a) All buildings

(b) Buildings with SC > SS

*Figure 12.10 – The distribution of Self-Consumption (SC) and Self-Sufficiency (SS) ratios as regulated by the sizing heuristic. For buildings where SC > SS, all PV modules are considered (0-threshold in Figure 12.9) resulting in a higher self-consumption.*

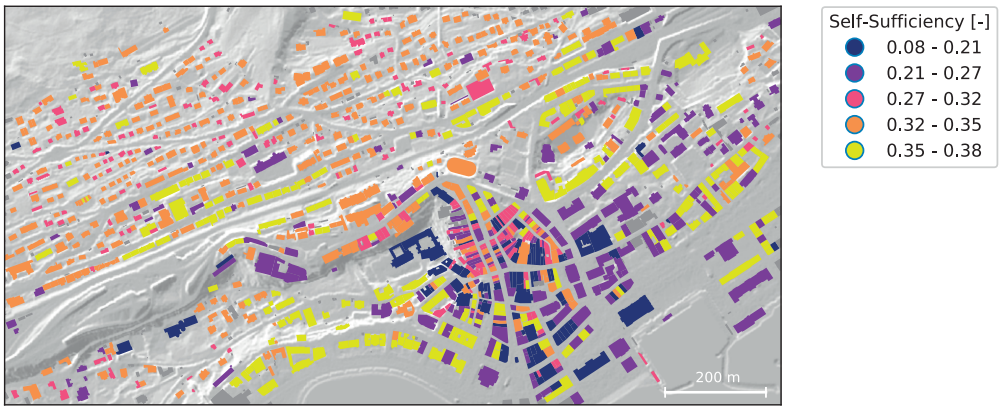


(a) Self-sufficiency

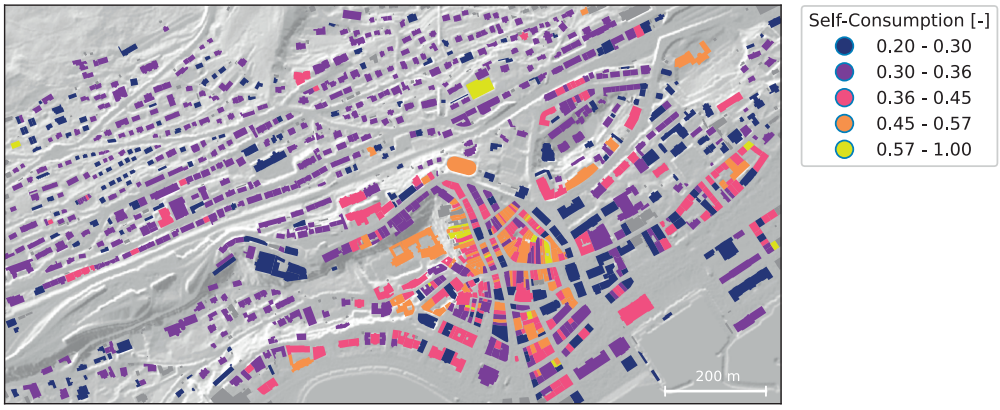


(b) Self-consumption


(c) Coverage ratio

*Figure 12.11 – The distribution of SC and SS ratios as regulated by the sizing heuristic and the resulting annual coverage ratio of building energy demand. Buildings in central area have low hourly self-sufficiency and hence also low annual coverage ratio, despite all available surfaces being considered for solar installations (see Figure 12.9).*
*Background: Swisstopo SwissALTI$^{3D}$ - Footprints: SITN Cadastre*

### 12.2.2 Evaluation

The evaluation is conducted using the three indicators (Figures 12.16 to 12.18) and the three aggregation scales (tile, zone and building, subfigures a to c) and a grid interpolation (Figure 12.19).

We show here the results with solar systems sized using the heuristic balancing self-consumption and self-sufficiency ratios. This determines a minimum production per panel that varies across buildings, as shown in Figure 12.9, and the preservation of the geometric regularity of the system (Algorithm 11.7). The sizing effect to the total power installed is shown in Figure 12.13 and a visual example of the application of the geometric algorithm is shown in Figure 12.14. Both building energy needs and the PV yield used for sizing the system were calculated under a typical weather scenario.

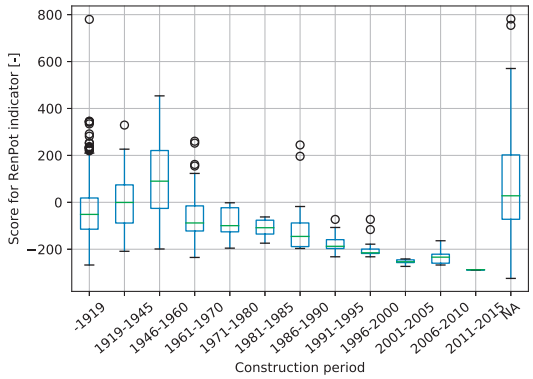


*Figure 12.12 – Boxplot showing the score calculated for the building retrofit potential indicator (Equation* (11.9)*) for each building construction period. Buildings with a negative value already achieve the target energy need for space heating set by the SIA 380/1:2016 norm [278] (see Section 11.3.2.1). As expected, we can notice an improvement of the performance along time starting in 1961, which becomes consistent after 1991.*

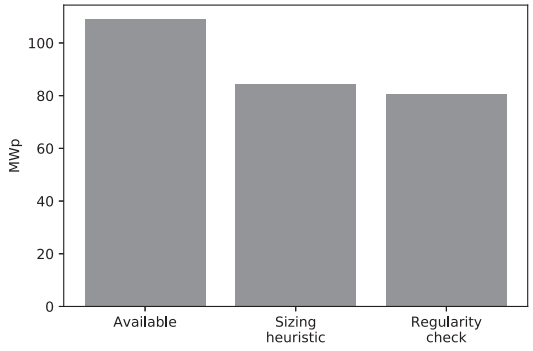


*Figure 12.13 – The bar plot shows the power installed in the analyzed area, after sizing with a balanced SC and SS (Algorithm 11.6), and checking the regularity of the installation (Algorithm 11.7). The power installed has been weighted using the parameters shown in Table 4.8.*

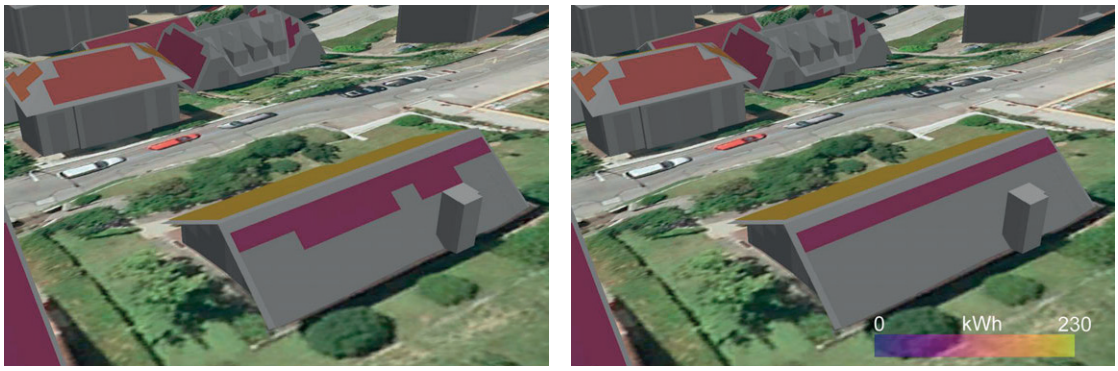


(a) Without regularity check (b) With regularity check

*Figure 12.14 – Effect of the geometric regularity to a solar installation sized using a minimum a threshold of 580 kWh/kWp. In the foreground roof face, we can notice that the bottom row of the installation is fragmented into more chunks in (a) and is hence discarded in (b).*
*Sources: Imagery - Swisstopo CITIMAGE 2014 obtained via the SITN - 3D model: SITN Cadastre*

As can be seen comparing Section 12.2.2 with Figure 12.16c, the heuristic penalizes the buildings in the central areas, as all solar modules are used, also those with a low annual energy yield. However, when applying a minimum threshold as in Section 12.2.2, buildings in the central areas can also have a high solar potential, as only their best-exposed surfaces are used. In particular, some roofs in the West-side of the main central street have a South-facing roof that provide optimal results, as can be also seen in Figure 12.7 (top images).

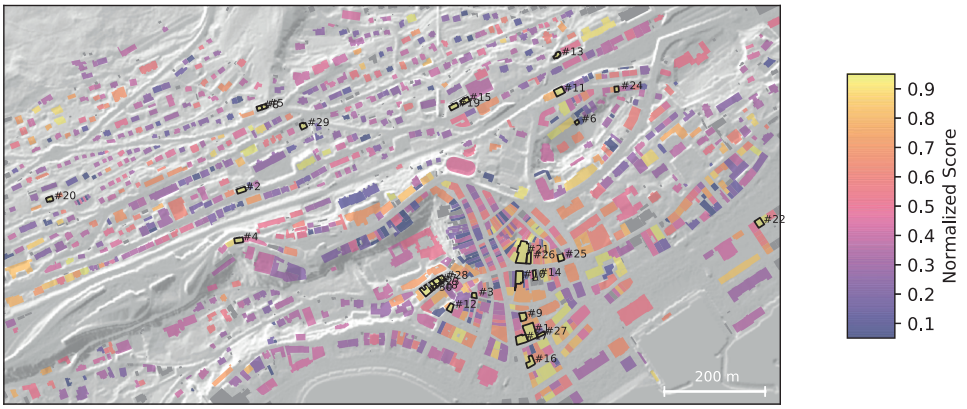


*Figure 12.15 – Normalized score for the PV potential indicator (eq.* (11.8)*) using a minimum threshold of 650 kWh/kWp. The top-ranked buildings are highlighted with a black outline (# identifies the rank): they are located across the city, but a cluster can be seen in the central area. Results are more extensively described and discussed in Section 12.2.2.*
*Background: Swisstopo SwissALTI$^{3D}$ - Footprints: SITN Cadastre*

If we look at the results using the heuristic, as expected, the three best-performing tiles (200, 232 and 233) are located in the low-density area. These results are consistent for all three indicators. In these tiles, we can also find a large concentration of top-ranked buildings and zones, especially for the PV

potential indicator.

Conversely, the dense historical center is the worst performing and contains the last-ranked tile (203) for the PV potential, because of the high shading and limited availability of surfaces for solar systems. This is also confirmed by the heat map shown in Figure 12.19a, in which the only two zones with a low score for the PV potential are located in the historical center. As already noticed in the previous section, despite all surfaces being used for solar systems (corresponding to a null threshold in Figure 12.9), the coverage ratio (Figure 12.11c) and self-sufficiency (Figure 12.11a) of the buildings are very low. However, for the building retrofit potential indicator (Figure 12.17), the inner historical center is well performing, because of the compact urban fabric which limits thermal losses and relatively low transmittance of the envelope of buildings built before the Second World War.

Figure 12.19 shows a heat spot (located approximately at the intersection of tiles 200, 201, 232, 233) which is consistent for all indicators. This is also confirmed by the high number of top-ranked buildings as well as of two contiguous zones ranked #8 and #9 for the *RenPotPV* indicator (Figure 12.18). The other heat spots belong to areas with just a few sparse buildings and are hence probably not much representative.

In general, the greater the aggregation scale, the clearer are some general spatial tendencies, such as the different performance of low-density versus denser urban areas. Differently, the finer the analysis granularity, the more difficult is to find a spatial justification of the performance, because this depends on context-specific (e.g. the presence of shading elements nearby) or non-spatial reasons (e.g. envelope insulation, building use). This becomes clear by looking at the maps of buildings (Figures 12.16c, 12.17c and 12.18c), where the top-ranked ones are often spread across the entire urban area rather than concentrated in a particular spatial location. Similarly, the heat maps of Figure 12.19 also show a varied situation, with local high-potential zones being located just beside low-potential zones. This is particularly true for indicators integrating the retrofit potential (*RenPot* and *RenPotPV*), which is highly dependent on the quality of the building envelope rather than on spatial conditions. Excepted for the inner town center, periods of construction are fairly location-independent and thus mixed in the analyzed urban area Figure 12.2.

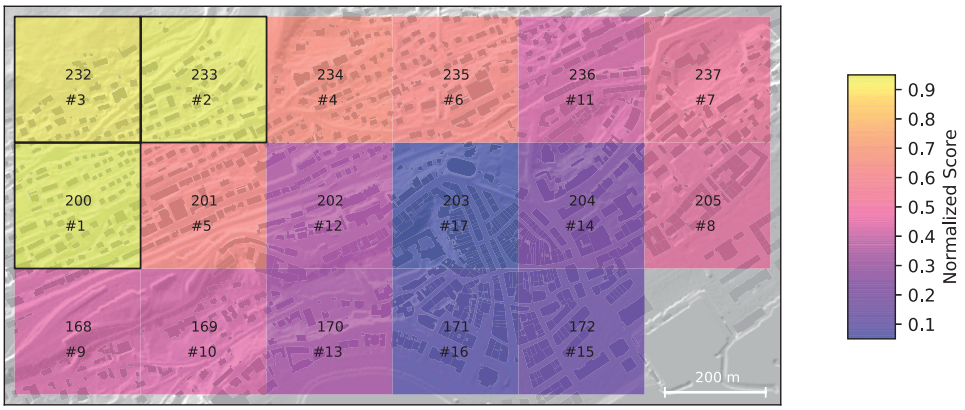


(a) Tile

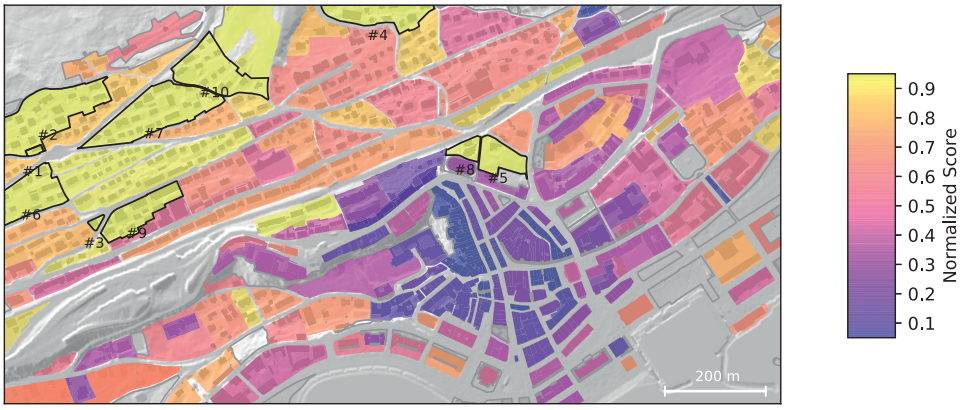


(b) Zone


(c) Building

*Figure 12.16 – Normalized score for the PV potential indicator (eq.* (11.8)*) using a SC-SS-balanced threshold. The top-ranked spatial locations are highlighted with a black outline; # identifies the rank. High-potential areas are mainly located in the low-density urban areas. Results are more extensively described and discussed in Section 12.2.2.*
*Background: Swisstopo SwissALTI$^{3D}$ - Footprints: SITN Cadastre*

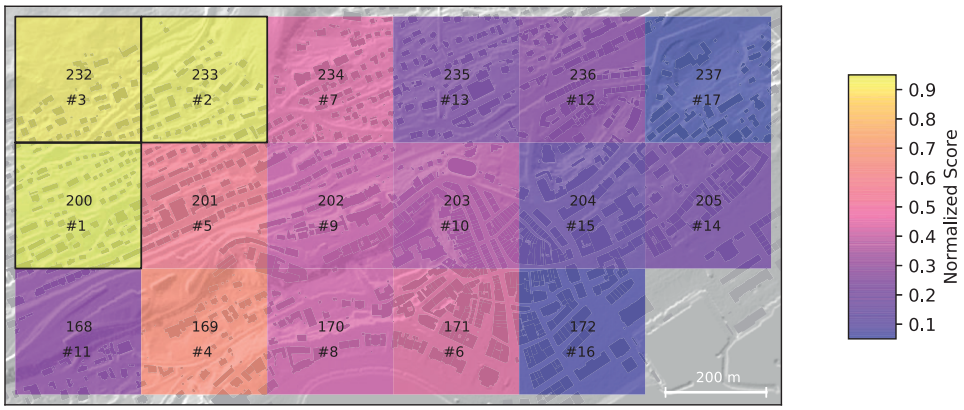


(a) Tile

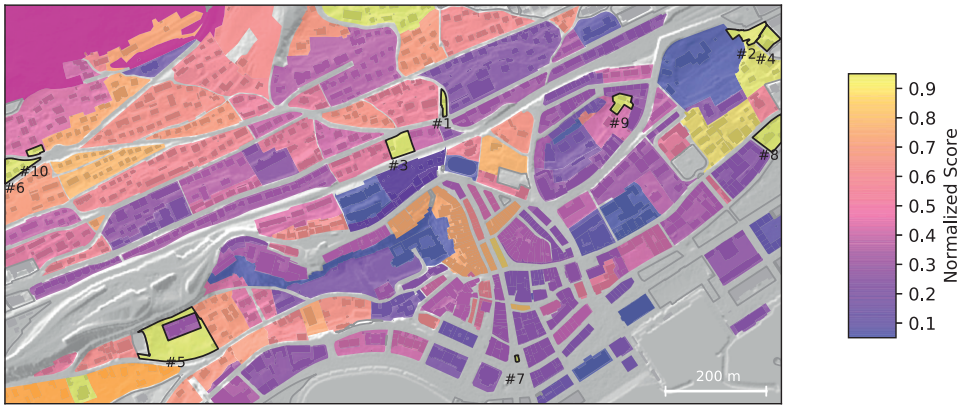


(b) Zone


(c) Building

*Figure 12.17 – Normalized score for the building retrofit potential indicator (eq.* (11.9)*). The top-ranked spatial locations are highlighted with a black outline; # identifies the rank. At the zone- and building-scale, high-potential locations are quite evenly spread across the city. Results are more extensively described and discussed in Section 12.2.2.*
*Background: Swisstopo SwissALTI$^{3D}$ - Footprints: SITN Cadastre*

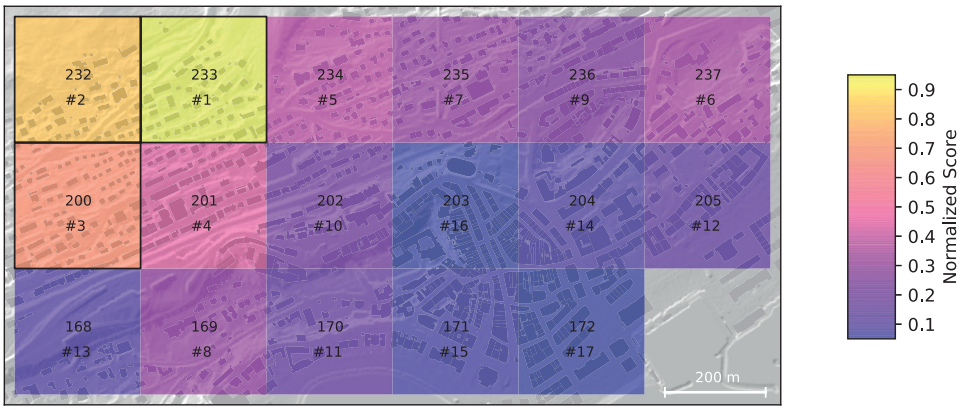


(a) Tile

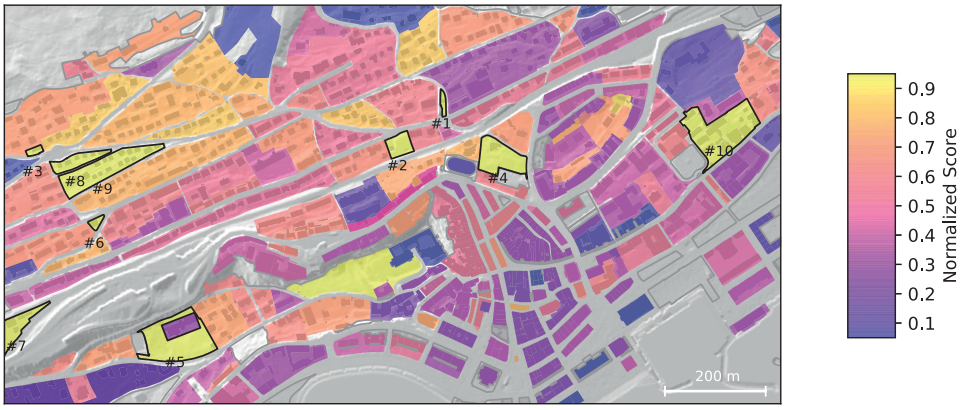


(b) Zone

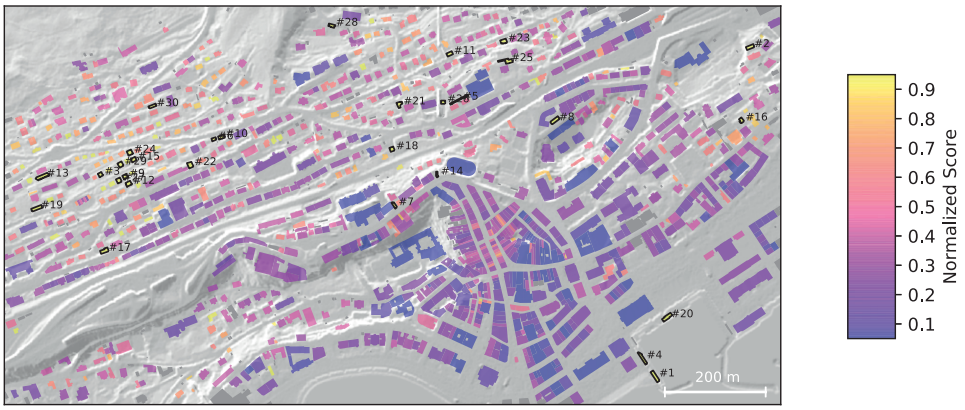


(c) Building

*Figure 12.18 – Normalized score for the integrated building retrofit and PV potential indicator (eq.* (11.9)*) using a SC-SS-balanced threshold. The top-ranked spatial locations are highlighted with a black outline; # identifies the rank. At the zone- and building-scale, high-potential locations are mostly located in mid-density areas close to the city center. Results are more extensively described and discussed in Section 12.2.2.*
*Background: Swisstopo SwissALTI$^{3D}$ - Footprints: SITN Cadastre*


(a) PV potential - Equation (11.8)


(b) Retrofit potential - Equation (11.9)


(c) PV and retrofit potential - Equation (11.10)

*Figure 12.19 – Normalized score for different indicators using a SC-SS-balanced threshold. The score is calculated on the value of each building interpolated to a 75-m grid using an Inverse Distance Weighting algorithm [275] considering a quadratic Euclidean distance from the 10 closest points in the x, y plane and then plotted using a bicubic interpolation. The historical inner-city area can be easily distinguished in (a) for its low PV potential and (b) for its relatively high building energy retrofit potential. Results are more extensively described and discussed in Section 12.2.2.*
*Background: Swisstopo SwissALTI3D - Footprints: SITN Cadastre*

### 12.2.3 Comparison of ranking

This section[2] compares the ranking conducted with different methods to show the effect of considering the uncertainty. For the sake of simplicity and clarity, we present a single spatial resolution only: a 'tile.' The tile was chosen to present the main results since it limits the number of locations to a manageable number for plotting and discussion while preserving an interesting variability between each location. Similarly, we will limit the analysis to just one metric, which is the PV solar potential, i.e., the gross electric energy production normalized by the peak power installed [kWh/kWp] (Equation (11.8)). Unlike in the previous sections, we will show the tile results including all PV modules with a non-null production, while discussing the effect of minimum thresholds in Section 12.2.3.3.

In order to be consistent with the vegetation scenarios, which present two extreme modeling approaches, we show in this section also the results from a 'high rad' scenario, which is obtained through the same method as the 'low rad' scenario (Algorithm 11.2) but using $q = 90$ instead of $q = 10$.

#### 12.2.3.1 Ranking based on single scenarios

As a baseline for comparison, we present the results obtained by ranking tiles based on simulations using a single scenario at a time, i.e., one combination of vegetation and weather. This is the state-of-the-art, i.e., decision-making without consideration of uncertainty.

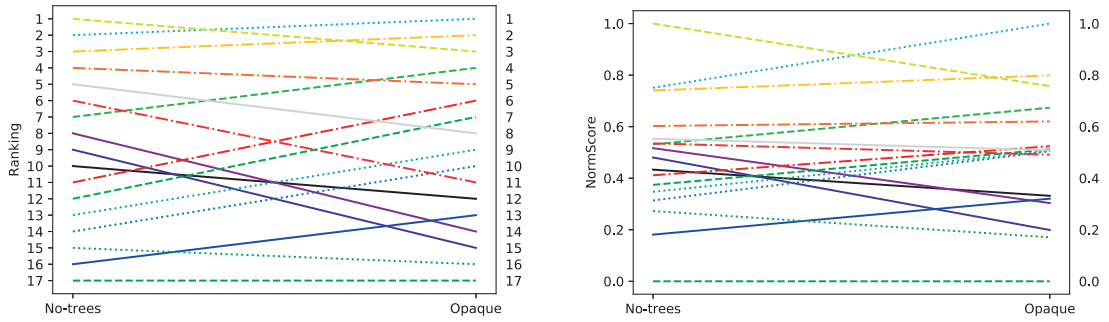


(a) Ranking

(b) Normalized Score

*Figure 12.20 – Ranking using single vegetation scenarios: the x-axes represent a scenario while the y-axes represent either rankings (a) or normalized score (b). The ranking (a) is calculated by sorting the gross electric energy production normalized by peak power installed and the score (b) is obtained by a min-max normalization. A large number of crossing lines indicates frequent and significant changes in ranking and scores between the two scenarios. The key in Figure 12.24c shows the tile IDs and the corresponding line style and color.*

Two sets of results are presented in Figure 12.20 and Figure 12.21: tile rankings and scores. The lines have been plotted to show changes between scenarios, so many crossing lines indicate more changes in rankings. The straight lines should not be interpreted to mean that the interpolation between the two

[2] This section contains some excerpts from Peronato et al. [226]: Peronato, G., Rastogi, P., Rey, E., & Andersen, M. (2018). A toolkit for multi-scale mapping of the solar energy-generation potential of buildings in urban environments under uncertainty. *Solar Energy*, 173, 861–874. https://doi.org/10.1016/j.solener.2018.08.017. The text is reproduced here as a courtesy of the publisher and with the agreement of the co-authors. G.P. contributed by running the simulations, analyzing the data and writing. Please consider that the analysis here has different numerical results than in the published paper, as slightly different assumptions and set of tiles were considered, so as to be consistent with the rest of the thesis.

extremes is linear. In fact, we do not know the intermediate states since we have not simulated them in this study. In Figure 12.20 we can see the ranking based on two vegetation scenarios and a typical weather file. Note that the two vegetation scenarios separately produce two very different rankings. On the contrary, there is very little difference in rankings based on different weather scenarios (simulated without vegetation), as shown in Figure 12.21.

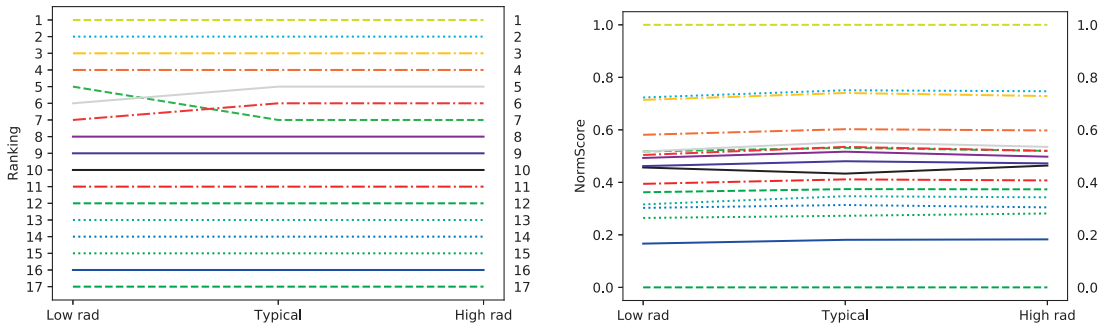


(a) Ranking

(b) Normalized score

*Figure 12.21 – Ranking using single weather scenarios (and 'no trees' vegetation conditions): the x-axes represent a weather scenario while the y-axes represent either rankings (a) or score (b), which are calculated as explained in Figure 12.20. The few changes in the ranking show that the ranking is not very sensitive to the different weather scenarios. The key in Figure 12.24c shows the tile IDs and the corresponding line style and color.*

#### 12.2.3.2 Risk-averse ranking based on multiple scenarios

We first analyzed the results treating the uncertainty in the factors one-at-a-time, presented in Figure 12.22.

In Figure 12.22c, we can see that the median difference in production between weather scenarios is about 0.15 times the 'high rad' simulation (15%), while, for vegetation, it is about 0.09 times the 'no trees' simulation (9%). In other words, when considering extreme weather scenarios, the magnitude of difference is high, while the spread of variation between tiles is almost null. This means that, while the production values are sensitive to weather, variation in the weather affects all tiles similarly. Conversely, the results for vegetation scenarios show that the magnitude of impact is lower but variation is higher. The vegetation scenarios of individual tiles are varied, but the difference between the extremes is smaller.

When we apply the risk-averse ranking based on pairwise comparison (Section 11.4.3.1) to vegetation scenarios under typical weather, with both boolean and fuzzy approaches, the decision matrices are visibly different (Figure 12.23). In the fuzzy approach, the pairwise comparisons result in more subtle differences, although tiles 200 and 203 clearly stand out respectively for their wins and losses.

The results of the ranking aggregation are shown in Figure 12.24. The overall score is calculated by summing the scores of each line of Figure 12.23, normalized to a $[0,1]$ scale (as described in Section 11.4.3.2). In the boolean approach, only 12 out of 17 possible ranks are assigned due to ties, while in the fuzzy approach all tiles have been assigned a rank. When considering the normalized score, the results have a larger spread than in the ranking. In addition, the fuzzy evaluation highlights some clusters, i.e. locations with a similar score, especially in the fuzzy approach.

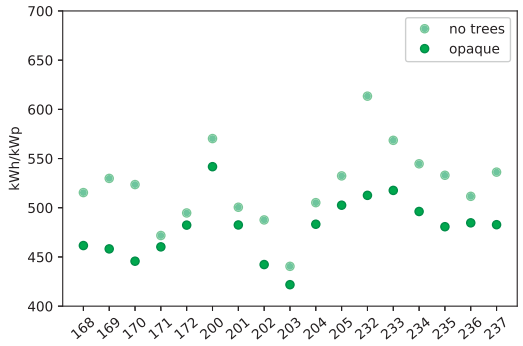


(a) Vegetation scenarios

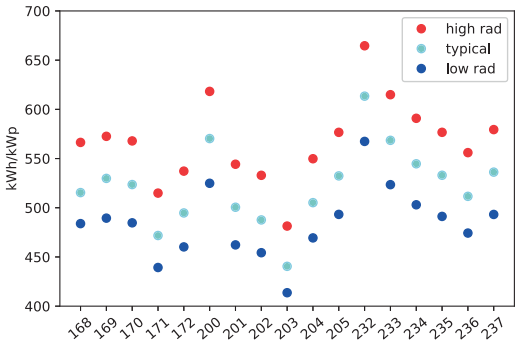


(b) Weather scenarios

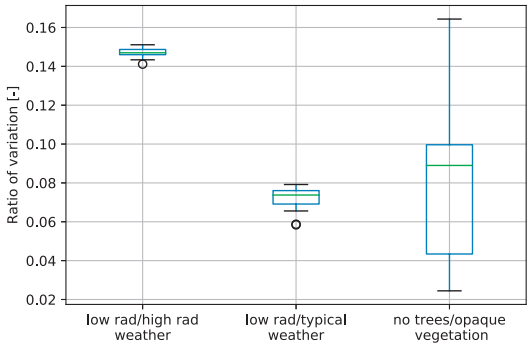


(c) Ratio between scenarios

*Figure 12.22 – The tile-by-tile scatter plots (a, b) and combined boxplots (c) show the difference of solar potential indicator between the scenarios among the different tiles. In (a) and (b), tiles are along the x-axes and the normalized production values are along the y-axes. In (a), vegetation scenarios with typical weather are shown. In (b), weather scenarios with 'no trees' vegetation conditions are shown. The box-plot (c) y-axis is the fractional change from the higher value of production for each tile and the x-axis shows the considered scenarios.*

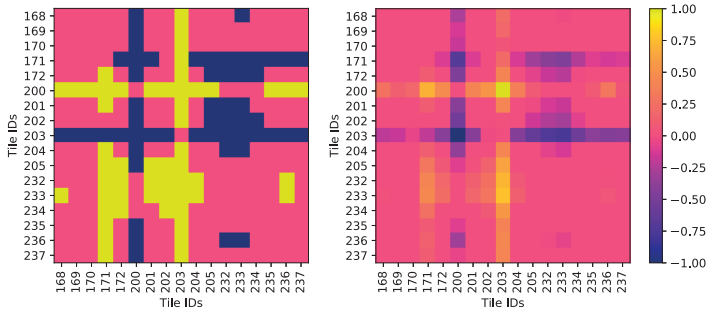


(a) Comparison matrix (boolean)

(b) Comparison matrix (fuzzy)

*Figure 12.23 – These matrices show the result of risk-averse pairwise comparisons (see Section 11.4.3.1) between the different tiles using a boolean (a) or fuzzy (b) logic. The colors represent the score value, as indicated in the color bar. The principal diagonal is filled with zeros, as it shows the comparison of each tile with itself. The total score of each tile is defined as the sum of each row.*

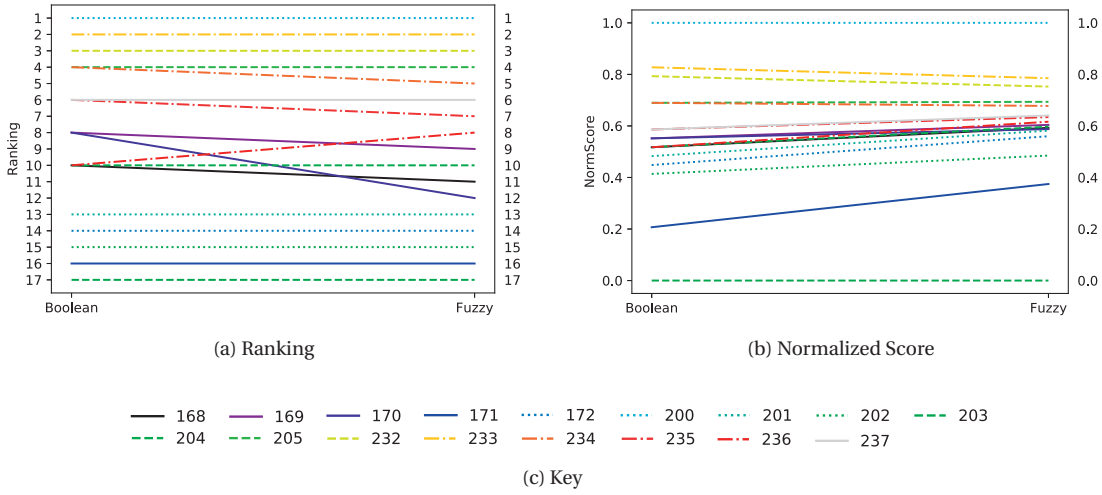


(a) Ranking

(b) Normalized Score

(c) Key

*Figure 12.24 – Ranking vegetation scenarios from risk-averse pairwise comparisons (see Section 11.4.3.1): a) shows the ranking and b) the normalized score. The fuzzy evaluation helps identify some clusters of tiles with similar scores (e.g. there is a large number of tiles with a score of about 0.7). The key in Figure 12.24c shows the tile IDs and the corresponding line style and color.*

#### 12.2.3.3 Low-yield avoidance at different thresholds

As we have seen in the previous section, the absolute difference between production in the radiation scenarios is considerable, at least when considering the two extremes 'high rad' and 'low rad'. While it is intuitive that the production should be very sensitive to solar availability, the decision-maker should consider the magnitude of this variability in the weather of their location. However, as seen in Section 12.2.3.1, the ranking does not significantly change because of weather. This is in line with our assumption that the mesoclimate and microclimate variations in solar availability affect all tiles more or less equally.

In order to overcome these limitations as well as those already discussed for the naive ranking (Section 12.2.3.1), we coupled a simple ranking based on summary statistics with the low-yield-avoidance method. This method excludes those PV modules that do not achieve a given production threshold for a specific weather scenario. As discussed in Sections 11.3.3.2 and 12.2.1, an annual minimum production threshold provides a sizing of the system for all buildings only based on their suitable surfaces and regardless of their energy demand.

Figure 12.25 shows the application of different minimum thresholds $t$ expressed in kWh of module gross electricity production normalized by the peak power installed on the tile. This threshold is calculated using the 'low rad' weather scenario. The ranking and the normalized score are highly affected by the introduction of minimum threshold. Only tile 203 is consistently ranked in the last positions, while all other tiles have their ranking changed multiple times. However, it should be considered that the actual difference of normalized gross electricity production between the different tiles becomes smaller at high thresholds. The ranking should be then considered on smaller spatial aggregation scales (e.g., buildings as in Section 12.2.2).

Figure 12.26 shows the ranking considering minimum thresholds $t$ and computed either on the typical weather ('typical') or on 'low rad' weather scenario ('conservative'). The ranking and the score are

highly affected by the introduction of minimum threshold and, to a minor extent, by the application of the 'conservative' weather scenario in the selection of modules.

The 'conservative' approach applied to normalized results determines higher potential for all tiles. This is because only the best-performing modules are considered. However, if we consider the non-normalized gross production of a tile shown in Table 12.4, we see a reduction due to the application of a threshold calculated on a 'low rad' weather scenario, especially at the upper thresholds. For example, if we discard PV modules not reaching the threshold of 800 kWh/kWp yearly production, only about 90% of the production at the 'typical' scenario (i.e., using a typical weather file) can be obtained in a 'conservative' scenario (i.e., using a 'low rad' weather file) .

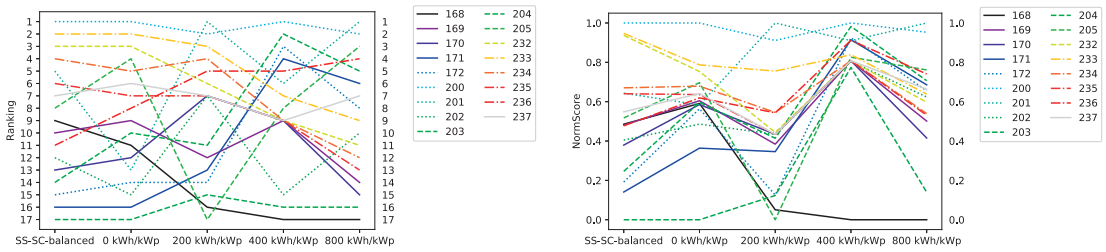


(a) Ranking

(b) Normalized score

*Figure 12.25 – Evaluation of tiles - PV Potential indicator Equation* (11.8) *- at different minimum thresholds t applied on a 'low rad' weather scenario. The SC-SS-balanced threshold is set per each building as shown in Figure 12.9. The key in Figure 12.24c shows the tile IDs and the corresponding line style and color. Apart for tile 203, which is always ranked in the last positions, we can see many changes in ranking and normalized score along with the change of threshold.*

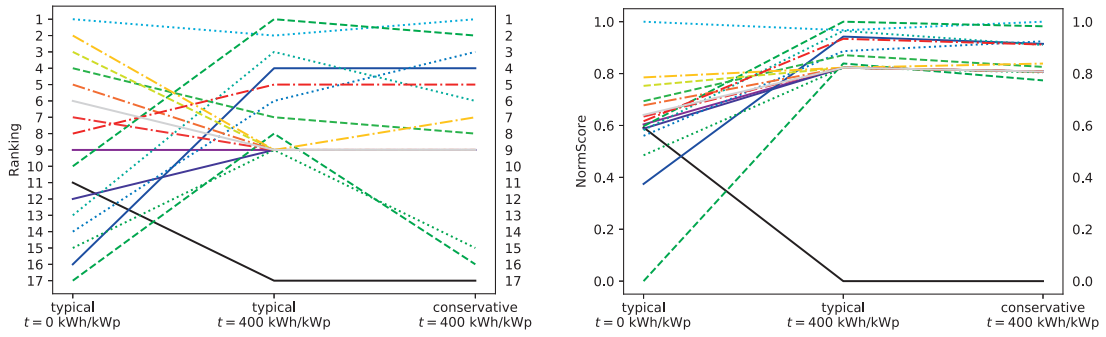


(a)

(b)

*Figure 12.26 – Ranking with a threshold applied on typical weather file ('typical') or 'low rad' weather scenario ('conservative'). The numerous crossing lines show that the use of thresholds, and, to a minor extent, of a 'conservative' risk-attitude, has a high impact on ranking and score. The key in Figure 12.24c shows the tile IDs and the corresponding line style and color.*

*Table 12.4 – Ratio between non-normalized module gross electricity production calculated using 'conservative' and 'typical' scenarios at different thresholds. At $t = 0$ the same number of modules are selected for both scenarios, that is why the ratio is 1. Along with the increasing threshold, we notice decreasing ratios, showing that only a small share of the modules achieve the threshold calculated using the 'conservative' weather scenario.*

| Tile IDs/Threshold | 0 kWh/kWp | 200 kWh/kWp | 400 kWh/kWp | 800 kWh/kWp |
|---|---|---|---|---|
| **168** | 1.0 | 0.99 | 0.97 | 0.95 |
| **169** | 1.0 | 0.99 | 0.96 | 0.93 |
| **170** | 1.0 | 0.99 | 0.96 | 0.83 |
| **171** | 1.0 | 0.99 | 0.97 | 0.83 |
| **172** | 1.0 | 0.99 | 0.95 | 0.90 |
| **200** | 1.0 | 0.99 | 0.96 | 0.86 |
| **201** | 1.0 | 0.99 | 0.98 | 0.91 |
| **202** | 1.0 | 0.99 | 0.97 | 0.94 |
| **203** | 1.0 | 0.99 | 0.97 | 0.88 |
| **204** | 1.0 | 0.99 | 0.97 | 0.91 |
| **205** | 1.0 | 0.99 | 0.98 | 0.88 |
| **232** | 1.0 | 0.99 | 0.95 | 0.91 |
| **233** | 1.0 | 0.99 | 0.96 | 0.87 |
| **234** | 1.0 | 0.99 | 0.96 | 0.88 |
| **235** | 1.0 | 0.99 | 0.94 | 0.88 |
| **236** | 1.0 | 0.99 | 0.97 | 0.93 |
| **237** | 1.0 | 0.99 | 0.98 | 0.94 |

### 12.2.4 Summary of findings

The application to the case study of Neuchâtel highlighted the potential of the proposed method. We summarize here[3] the main lessons learned: first, the ones related to the case-specific application in Neuchâtel, and, second, those that we assume can be generalized also to other applications.

#### 12.2.4.1 Case-specific findings

We have seen that, despite the high influence of vegetation in the absolute results, low-density residential areas rank better for PV potential compared to the ones located in the dense historical city center, when the proposed heuristic balancing SC and SS is used. However, the same inner areas have a higher potential for building retrofit and also have. This is probably a consequence of a combined effect of low solar gains, due to the shading of the compact fabric, and low insulation level, due to the presence of historical buildings.

For the same reasons, inner urban areas also have high self-consumption, but low self-sufficiency. Therefore, the algorithm implemented to find a balanced level between these two indicators determined a zero threshold for most of the buildings in this area, which means that all PV modules fitting the building surfaces were considered. Even at higher thresholds, the tile 203 located in the city center is consistently ranked in the last positions. However, if we consider only the modules reaching a minimum 650 kWh/kWp annual production, this tile contains some high-potential buildings.

[3] This section contains some excerpts from Peronato et al. [226]: Peronato, G., Rastogi, P., Rey, E., & Andersen, M. (2018). A toolkit for multi-scale mapping of the solar energy-generation potential of buildings in urban environments under uncertainty. *Solar Energy*, 173, 861–874. https://doi.org/10.1016/j.solener.2018.08.017. The text is reproduced here as a courtesy of the publisher and with the agreement of the co-authors. G.P. contributed by analyzing the data and writing.

We have also found that the three best-performing tiles are stable across the three considered indicators, when considering a balanced threshold. However, when applying restrictive minimum thresholds (> 200 kWh/kWp) to all building surfaces, their ranking decreases.

The building period of construction profoundly influences indicators including the energy retrofit potential. Since buildings of different periods are quite sparsed across the city, it is difficult to find spatial tendencies. A notable exception is the historical inner city center, which, as expected, generally has old buildings as well as low sun exposition and qualifies therefore for high building retrofit potential.

Another area located in the low-density zone North-West of the city center was found to have interesting potential for all indicators. The presence of multiple contiguous building zones and buildings with a high potential would suggest that a comprehensive intervention in this area is beneficial and should be prioritized.

#### 12.2.4.2 General findings

The ranking comparison presented in Section 12.2.3 showed that both the ranking and the absolute indicator values of spatial locations are highly influenced by the choice of the modeling scenario. In the case of vegetation, i.e. a typical epistemic uncertainty related to the difficulties of remote-sensing and modeling reality, the ranking is significantly changing depending on the considered modeling scenario, although the absolute difference between the scenarios is relatively small.

The opposite happens for weather uncertainty, which is temporally aleatory but spatially constant, as the proposed method does not consider local variations inside the same urban area. However, weather uncertainty does have an impact on sorting problems, as some locations could fall below the threshold. Indirectly, it has also an influence on ranking problems. We have shown in fact that, when applying minimum thresholds, the ranking order of spatial locations change. Moreover, the use of thresholds calculated on a conservative weather scenario helps choose the locations that meet the minimum threshold also in under-average years.

We have also shown that, by using a fuzzy approach, it was possible to establish a unique rank (i.e. without any tie) for every spatial location in the case of tiles. In this way, the normalized score can be used to define a consistent priority list for building retrofit or solar installations. The fuzzy logic also helps identify clusters of spatial locations with a similar performance. However, it should be considered that converting the normalized scores to rankings causes a loss of information, since small differences between scenarios could produce the same ranks as large differences, provided the sign does not change. This is why we recommend using the normalized score as the best indicator of solar potential

## 12.3 Conclusions

This chapter has shown the applicability of the proposed method to a real case study. The analyzed area of the city was large enough to provide a varied sample of the characteristics of the urban fabric, in terms of morphology, year of construction and architectural quality. However, this variety of characteristics prevented the definition of clear spatial tendencies, except a general specular opposition between the high-density historical center and the low-density areas. The former has lower PV potential but higher retrofit potential. Conversely, the latter has generally greater PV potential.

In general, we have seen that the finer the analysis granularity, the more difficult is determining these spatial trends, as the performance of spatial locations is highly influenced by local conditions. This can be seen as an added value for the proposed method, as it provides a consistent and robust evaluation at the different aggregation scales and takes into account these local conditions.

We also showed the relevance of the method in the decision-making, as it provides a score for each spatial location calculated from pairwise comparisons of modeling scenarios. When using fuzzy logic, the score is likely to be unique and helps the definition of priority lists. This can be used to assign limited resources for building energy retrofit or solar energy installations by prioritizing those with greater potential.

# 13 Comparison with measurements and reference tools

This chapter presents a critical comparison of the results obtained using our method with measurements from a real installation and with simulated values and features from alternative reference methods. This analysis is meant to show the effectiveness of the proposed method, while indicating areas of improvements.

## 13.1 Method and objectives

We used for the validation a roof-integrated PV installation , and as the main alternative method a Swiss-wide solar cadastre. The solar cadastre was chosen because, being promoted by the Swiss confederation, it has become a reference standard for solar potential assessments on both façades and roofs in Switzerland. The PV installation was selected because of its exemplary building integration, also attested by an award from the Swiss Solar Agency (Prix Solaire Suisse 2015), featuring the same BIPV module considered for the test application, as well as because of the availability of the owner to release the measurement data.

For the sake of consistency, the results were evaluated at the same weather conditions, whenever it is possible, and of system size, while highlighting the discrepancies in the models in predicting the actual size of the system. The scope is twofold:

- check the prediction error with regards to a ground-truth (measurements) and the prediction difference with alternative reference methods;
- discuss the main causes of differences with the compared data.

We should stress out that the focus of the comparisons is on the modeling and simulation part of the analysis workflow, and, to a minor extent, on the visualization features of the alternative method. These comparative studies are intended to show the accuracy of the predicted results obtained by coupling an advanced 3D city model (buildings, terrain and far-field obstructions presented in Section 11.2.1), the solar radiation model (Daysim), and the photovoltaic yield model (PVLIB DC performance model with a fixed Performance Ratio). We excluded the evaluation part of the workflow, as the main outcome of our method (i.e., a priority list) is not included in the compared method nor, to the best of our knowledge, in any existing alternative methods. Similarly, what we intend here for *validation*, i.e. the check of consistency of the simulated results with the physical measurements, is limited to what can be physically measured, that is the gross electricity energy production of a PV installation.

## 13.2 Confrontation to measured data from a roof-integrated PV installation

The section is aimed at comparing the outcome of the simulation of photovoltaic yield with the corresponding metered production from a real roof-integrated PV installation. To this end, we applied the same modeling ('no trees' scenario) and simulation workflow presented in Chapter 11, while using weather information and sizing hypotheses which are consistent with the measurements.

### 13.2.1 Description of the case-study installation

The PV installation is located in the roof of the *Hôtel des Associations*, a historical building located in the center of Neuchâtel (pictures in Figure 13.1 and map in Figure A.2) and inscribed in the ISOS heritage protection area.

The installation consists of 157 modules of 185 Wp (the same model described in Table 11.10 and applied in the case-study application of Chapter 12) and 5 modules of 135 Wp distributed as shown in Figure 13.1. This installation was carefully designed so as to respect high integration criteria standards. There is in fact large use of dummy modules mimicking the same appearance as the active PV modules. North-exposed façades (T1 and T2 in Figure 13.2) are entirely covered by these dummy modules, while the other surfaces include some custom-sized dummy modules to fit the irregular roof shape.

(a) Main façade facing West

(b) Roof faces facing North and East

*Figure 13.1 – View of the building. Its location can be seen in the map of Figure A.2.*
*Images: ©Prix Solaire Suisse 2015*

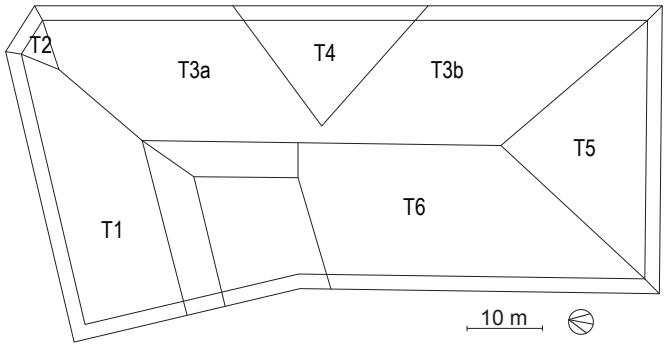


*Figure 13.2 – Plan of the roof surfaces.*
*Source: Viteos*

*Table 13.1 – Comparison of predicted and actual installation size. Refer to Figure 13.2 for surface keys. Surfaces T1 and T2 are not included as they have only dummy panels (non-active).*

| Surface | Area [m$^2$] | | Number of modules | | Nominal Power [kWp] | | |
|---|---|---|---|---|---|---|---|
| | Measured | Modeled | Measured | Modeled | Installed | Modeled | Difference |
| T3a | 52.7 | 49.9 | 32 | 30 | 5.920 | 5.55 | -6.2% |
| T3b | 46.6 | 50.4 | 31 | 28 | 5.735 | 5.18 | -9.7% |
| T4 | 21.7 | 19.2 | 13* | 6 | 2.155 | 1.11 | -48.5% |
| T5 | 34.1 | 33.9 | 19 | 13 | 3.515 | 2.40 | -31.7% |
| T6 | 73.6 | 67.1 | 57 | 46 | 10.545 | 8.51 | -19.3% |
| Total | 228.7 | 220.5 | 152* | 123 | 27.87 | 22.75 | -18.4% |

*including 5 modules of 135 Wp

### 13.2.2 Data processing and assumptions

The measured data comes from the local energy utility company, which consented to share the data on behalf of the building owner. The analyzed dataset contains the cumulative daily production of the installation [Wh] at a 5-minute resolution for each of the two inverters of the installation for the year 2017 (except for June and July which are from 2016). The use of these data required some pre-processing, which was conducted using the following procedure implemented in a Python script. We resampled the data by calculating the hourly mean of production and obtained the instantaneous power by subtracting the production of each hour from the production of the previous hour. The occurrences in which the instantaneous power was negative was set to 0, assuming that these were probably due to some problems in the data recording. We also corrected the daylight-saving time adjustment to be consistent with the one of the weather data.

The weather dataset was obtained from Meteosuisse, for the NEU station[1], which is only 1.65 km North-East in a straight line from the analyzed building (see map in Figure A.2). We used mean hourly values for global solar radiation (GHI), air temperature and wind speed. The DNI and DHI solar radiation values were obtained by applying the Reindl diffuse model [242] as implemented in Daysim subprogram `gen_reindl`. We then composed a weather file in both Daysim and EnergyPlus formats including the weather records from 2017, except for June and July values which were extracted from 2016, to be consistent with the measurements.

To obtain the hourly irradiances, we ran the Daysim subprogram `ds_illum` using the same daylight coefficients created for the analysis of Chapter 12, but using a new weather file composed of the DNI and DHI values obtained as explained here above. Similarly, the PVLIB libraries were applied on the same 185 Wp module whose data are presented in Table 11.10 and a weather file composed of GHI, wind and dry-bulb temperatures obtained as explained here above. The obtained DC electricity values were transformed to AC electricity by assuming a Performance Ratio of 0.85, as already explained in Section 11.3.

### 13.2.3 Results

We present here below the results of the comparison between the simulated results and the measurements. The output simulation values for each surface were scaled according to the actual installed

[1] More information can be found in this information sheet: https://www.meteoswiss.admin.ch/product/input/smn-stations/docs/NEU.pdf [Last accessed: June 26, 2018].

power:

$$P_s = P_s \cdot \frac{P_{mi}}{P_{ms}}, \tag{13.1}$$

where $P_s$ is the simulated PV production, and $P_{mi}$ and $P_{ms}$ are respectively the nominal installed power and the nominal simulated power from Table 13.1.

This scaling is necessary to differentiate between the modeling of the system size, which will be illustrated in Section 13.2.3.1, from the one of the energy output, which will be described in Section 13.2.3.2.

#### 13.2.3.1 System size and arrangement

The representation of surfaces in the 3D cadastre is somewhat simplified and some discrepancies are present with regards to the original construction drawings we received from Viteos. On the contrary, the integration of the BIPV modules was probably done taking into account an accurate survey of the roof surfaces in order to maximize the active surface area, and design the dummy modules with a custom size.

For these reasons, as can be seen Section 13.2.3.2, there is an overall underestimation of the number of modules that fit the surfaces. The underestimation is particularly significant for surfaces T4 and T5, two triangular roof faces for which the algorithm fail to recognize the orientation determining a less optimal fit of the surface (Section 13.2.3.1). Moreover, for surface T4 the underestimation of the number of modules is also caused by the fact that the surface belongs to two different land plots and since is represented as such in the 3D cadastre the grid algorithm consider it as two distinct surfaces, with one of the two being too small to fit any modules.

Nonetheless, considering that such a fine PV integration requires working with very restricted margins of error, we can argue that the overall differences found (-18.4%) are acceptable.

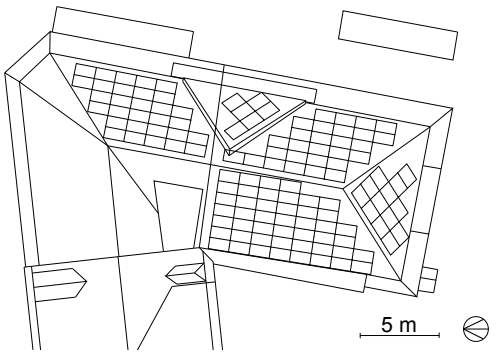


*Figure 13.3 – Arrangement of simulated modules on surfaces T3a, T3b, T4, T5 and T6 (Table 13.1). Surface T4 is split into two sub-surfaces as these correspond to two separate buildings registered in the cadastre. It should be noted that the reference solar installation includes some modules also on the overhang of the South-facing surface T5, which is modeled here as a distinct surface without modules. Source: SITN 3D cadastre*

#### 13.2.3.2 PV production

The PV production is compared after scaling using Equation (13.1). We compare here the data in terms of relative difference and Root Mean Square Error at different time granularities. The results are summarized in Table 13.2.

In terms of annual values, the model overestimated the PV production of about 1%. Figure 13.6 shows that the model slightly overestimates the production for all months except for December. The absolute difference is slightly lower in winter, while it is larger in relative values.

Figure 13.4 shows a small left offset of the simulated curve, which is probably due to the more eastern location of the weather station compared to the building. This is reflected in the daily RMSE (Table 13.2), which is only half of the daily value as the latter compensates the mismatch. The histograms in Figure 13.5 show an almost normal distribution for both hourly and daily comparisons.

*Table 13.2 – Summary of results of the comparison*

| | Annual | Monthly | Daily | Hourly |
|---|---|---|---|---|
| **Measured production** | 27.91 MWh | - | - | - |
| **Simulated production** | 28.21 MWh | - | - | - |
| **RMSE** | - | 35.35 kWh | 4.45 kWh | 2.13 kWh |

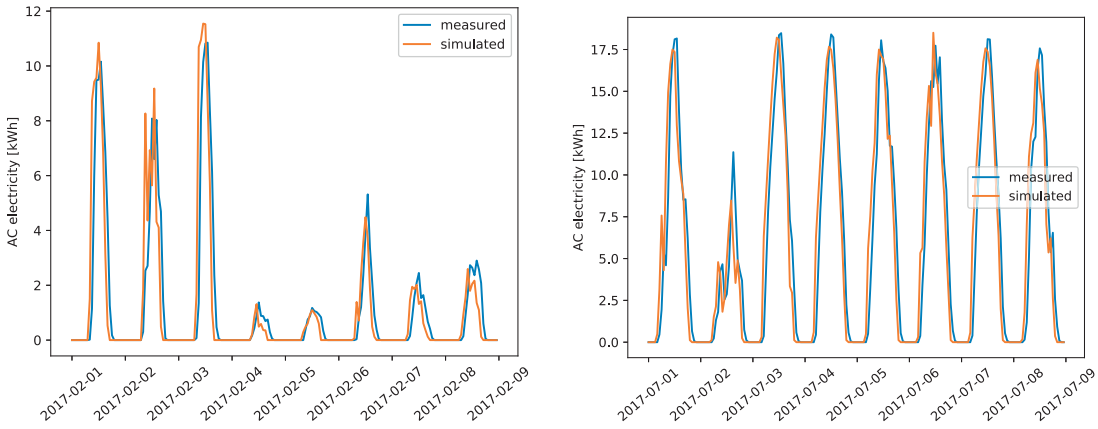


(a) First week of February 2017

(b) First week of July 2017

*Figure 13.4 – Comparison of hourly simulated and measured production for two sample weeks. Please note the difference in the scale of the y-axis.*

### 13.2.4 Discussion

The results show a good match of the predicted energy values, especially when the analysis is conducted at resolutions higher than daily. However, we should consider that simulated installation size was set to match with the actual one, while the former was about 18% smaller. We believe that this difference is acceptable, considering the particularly strict integration design conditions of the actual installation and the complex form and subdivision of the roof.

Moreover, we should consider that weather data used for this validation contains some assumptions,

which have probably affected the results. In particular, the location of the weather station is located about 1660 m North-East (heading = 70°) from the building. For this reason, the conditions might be different between the two locations. In particular, the direct solar radiation can be significantly affected by local cloud coverage and explain thus the small offset of the curves of Figure 13.4. It is in fact difficult to separate the error due to the solar radiation simulation and PV performance models from the one due to weather measurements and the application of the Reindl model. If the former error was the object of this investigation, the latter was clearly outside the scope.

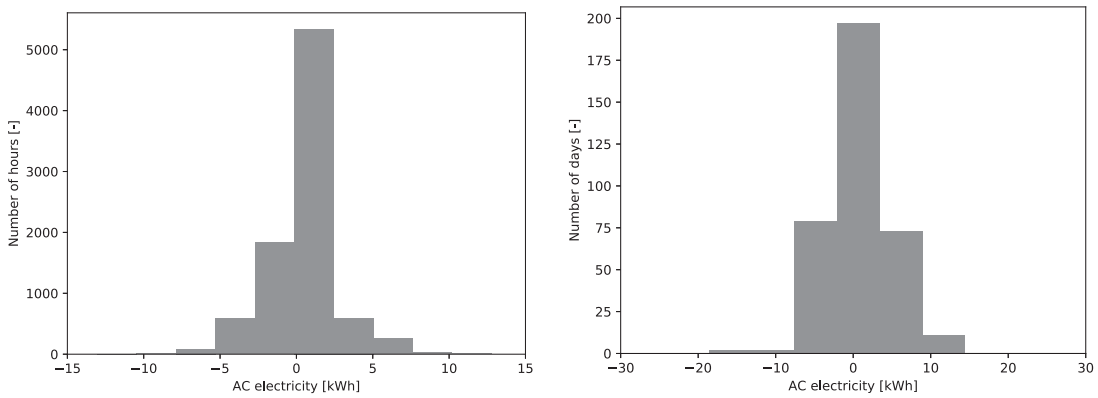


(a) Hourly (b) Daily

*Figure 13.5 – Histograms showing the difference between measured and simulated PV production at different resolutions.*

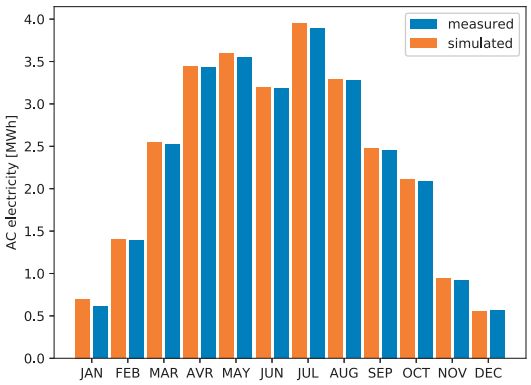


*Figure 13.6 – Comparison of monthly production.*

## 13.3 Confrontation to results from the Swiss Federal Solar Cadastre

This comparative analysis was conducted considering a reference tool for solar potential assessments in Switzerland. The Swiss Federal Solar Cadastre (SFSC) is in fact a web-based solar cadastre providing access to solar potential analysis for all buildings in Switzerland. At the best of our knowledge, the SFSC is the first public solar cadastre including and displaying information[2] for both façades and roofs, though in a 2D interface (see Figures 13.7a and 13.8a). Moreover, in opposition to the majority of solar cadasters based on raster or point-clouds, it is based as this thesis on a vector 3D city model. However, the Swiss Federal Solar Cadastre (SFSC) uses a Swiss-side 3D city model (Appendix A.1.4), which, even if at the same nominal LOD, has a lower representation accuracy than the 3D city model that we use in our method (Appendix A.1.5), in particular it includes fewer rooftop details (compare for example Figure 11.2 and Figure 13.8). Despite the differences in the data source, it is worth comparing the main features, parameters as well as the results for two case-study buildings.

The SFSC was developed by the company Meteotest as part of a joint project of the Federal Offices of Topography (Swisstopo), Meteorology (Meteoswiss) and Energy (BFE-OFEN-UFE). The calculation of the solar radiation on inclined surfaces is conducted using a view analysis on a DTM and a DSM from sensor points located on the surfaces of the vector 3D model. The solar radiation model considers both direct and diffuse POA irradiance calculated using the Perez sky model [214] from satellite data from the period 2004-2010. Reflected radiation is calculated by combining remote-sensed albedo with the view-factor. The PV model considers standard PV efficiency (17%) and Performance Ratio (80%). Further information on the underlying solar potential model can be found in Klauser [152] and the main data sources are also listed in Table 13.4.

It should be noted that this comparison cannot be considered as a validation of either our method or the Swiss Federal Solar Cadastre, because they are based on different hypotheses and data sources and none of them can be considered as a ground-truth. In Section 13.3.2 we added as a reference the measurements from the previous case-study, but also in this case it should be considered that the weather conditions are not always consistent.

*Table 13.3 – Comparison with the data types and sources used for the(Swiss Federal Solar Cadastre (SFSC) [152].*

| | SFSC | Our method |
|---|---|---|
| 3D building geometry | 3D vector cadastre (swissBUILDINGS$^{3D}$2.0) | 3D vector cadastre (Canton of Neuchâtel) |
| Heating demand | Estimated through statistical data | Simulated in CitySim |
| Weather data | MeteoSwiss 2004-2014 - 2km resolution | |
| Terrain | Digital Terrain Models at different resolutions, depending on the areas (SRTM at 100 m and swissALTI$^{3D}$ at 2 m) | Digital Surface Model at 100-m resolution |
| Vegetation | Digital Surface Model at 2 m resolution (interpolated at 0.5 m) | LiDAR point clouds |

### 13.3.1 Annual yield on tree-shaded surfaces

In order to make a critical comparison of the outputs of our method with the ones of the SFSC, we selected a building which has a fairly complex geometry and is significantly affected by vegetation shading, as a tree is placed at its East side. We compare here only two surfaces: the East-facing roof

[2] A similar visualization concept was already present in earlier work by Carneiro et al. [47].

surface and the main South-facing façade, which can be seen in Figure 13.7a and whose values are listed in Table 13.4. Since both the SFSC and our method include vegetation, we computed the difference between the values for the scenario "opaque trees", which is shown in the last column of Table 13.4. We do not consider here the coefficient ratios used in Table 11.11. The difference should be considered only for the annual irradiation, as the DC and AC generation are calculated with different parameters, which are also shown in the same table.

We can see that our method underestimates solar irradiation and shows a much greater impact of vegetation, while this difference is partially compensated in the DC and AC output by the use of less conservative parameters. Unlike the SFSC, our method allows a subdivision of the building surfaces to fit PV modules of a give size. As can be seen in the last image of Figure 13.7, in the considered sample building, the triangle-shaped roof surface fits 10 modules, which determines a reduction of the available area from 22.6 $m^2$ to 11.38 $m^2$. As we will confirm in the next section, we can consider that our method provides a better estimate of the size and arrangement of solar modules of a hypothetical solar installation on non-rectangular surfaces.

*Table 13.4 – Comparison of results for the building shown in Figure 13.7. The last column shows the difference between "opaque trees" scenarios.*

| | SFSC | Our method | | |
|---|---|---|---|---|
| Roof | | | | |
| | Opaque Trees | No Trees | Opaque Trees | Difference |
| Annual irradiation [kWh/$m^2$] | 910 | 973.5 | 283.3 | -69% |
| Efficiency | 17.0% | 17.2% | | |
| Actual efficiency | - | 17.5% | | |
| Performance ratio | 0.8 | 0.85 | | |
| Roof surface area [$m^2$] | 18 | 22.6 | | |
| N. of PV panels | - | 10 | | |
| Cell surface area [$m^2$] | | 1.0725 | | |
| Panel surface area [$m^2$] | - | 1.1375 | | |
| Effective panel surface [$m^2$] | - | 11.38 | | |
| DC Electricity generation [kWh] | 2'785 | 1'910 | 549 | -80% |
| AC Electricity generation [kWh] | 2'228 | 1'624 | 467 | -79% |
| Façade | | | | |
| Annual irradiation (kWh/$m^2$) | 673 | 782 | 581 | -14% |
| Efficiency | 17.0% | 17.2% | | |
| Actual efficiency | - | 17.5% | | |
| Performance ratio | 0.8 | 0.85 | | |
| Facade surface area ($m^2$) | 35 | 36 | | |
| N. of PV panels | - | 24 | | |
| Cell surface area ($m^2$) | | 1.0725 | | |
| Panel surface area ($m^2$) | - | 1.1375 | | |
| Effective panel surface ($m^2$) | - | 27.30 | | |
| DC Electricity generation (kWh) | 4'004 | 3'734 | 2'780 | -31% |
| AC Electricity generation (kWh) | 3'203 | 3'174 | 2'363 | -26% |

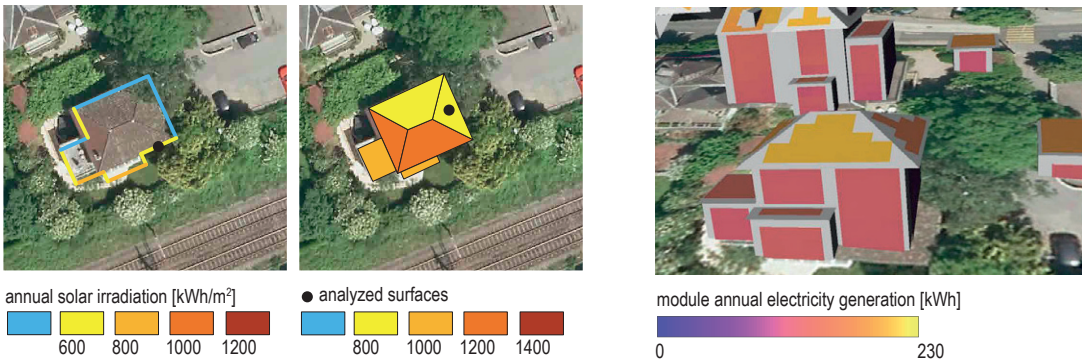


(a) SFSC (b) Our method

*Figure 13.7 – False-color view of the building solar potential as represented the different interfaces. The building location can be seen in the map of Figure A.2.*
*Sources: Imagery - Swisstopo CITIMAGE 2014 obtained through SITN*
*SFSC data (a) - ©2018 OFEN, Swisstopo, MétéoSuisse*
*3D model (b) - SITN Cadastre*

### 13.3.2 Monthly yield and sizing

We compare here the monthly electricity production as calculated by our method (simulated values) and the SFSC for the same installation analyzed in Section 13.2. For the sake of this analysis, we show the results of our method using both the typical weather scenario described in Section 11.2.3.1, which is appropriate for a multi-year solar potential estimation, and of a single year (2017, with two months from 2016), which is consistent with the measurements. We also include as a reference the values calculated[3] using the popular PV online calculator from PV-GIS (see Section 4.3.2).

Figure 13.9a shows that the SFSC greatly overestimates the electricity production for most of the months compared to all other methods, mainly because it considers an area almost 50% larger than the actual installation (Table 13.5) even after excluding part of the West surface which is covered by a rooftop superstructure. This determines a RMSE that is about 4 times the one of our method. In this sense, our method provides a better estimate of the size of the system, despite the underprediction of the number of modules already noted in Section 13.2.3.1.

If we compare the results considering the size factor (Figure 13.9b), all methods have similar profiles. Unsurprisingly, the simulated values of 2017 have the best fit with the measured values, resulting in the lowest RMSE. Simulations conducted using typical weather files (our method using Metonorm radiation for 1991-2010 and PV-GIS the CMSAF database for 2007-2016 ) determine smoother profiles than the one of the Swiss Federal Solar Cadastre (SFSC) and of single-year results. They also have a lower RMSE than the one of the SFSC, which has in turn a slightly more accurate prediction of the annual value than our method.

[3] The electricity producion was modeled with PV-GIS grid-connected PV calculator, using the calculated terrain shadows and the PVGIS-CMSAF solar radiation database (2007-2016) for a location with a location centered on the building (46.995°N, 6.933°W at 449 m asl). We selected building-integrated crystalline silicon PV modules, considering 15% of system losses. We conducted three separate simulations for the three main orientations of the roof surfaces: West (surface T6, 10.54 kWp) with slope 35° and azimuth 97° , South (surface T5, 3.515 kWp) slope 39° and azimuth 6° and East (surfaces T3a, T3b and T4, 13.81 kWp) slope 30° and azimuth -82°.

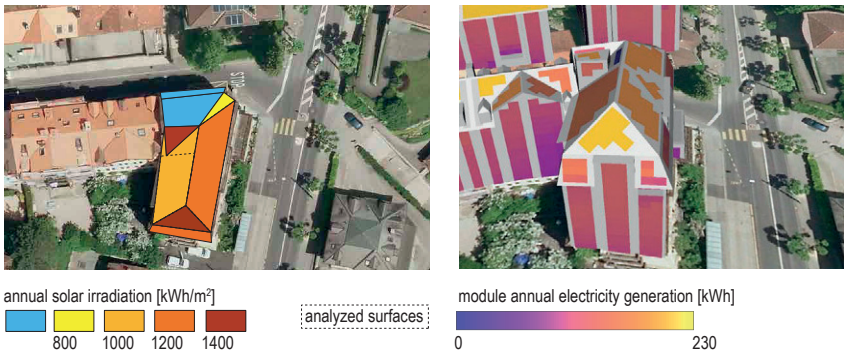


(a) SFSC (b) Our tool

*Figure 13.8 – False-color view of the building solar potential as represented in the different interfaces. The building location can be seen in the map of Figure A.2. Part of the West surface (24 m$^2$) is covered by a rooftop superstructure, which is not represented in the SFSC, but has been excluded from the analysis.*
*Sources: Imagery - Swisstopo CITIMAGE 2014 obtained via the SITN*
*SFSC data (a) - ©2018 OFEN, Swisstopo, MétéoSuisse*
*3D model (b) - SITN Cadastre*

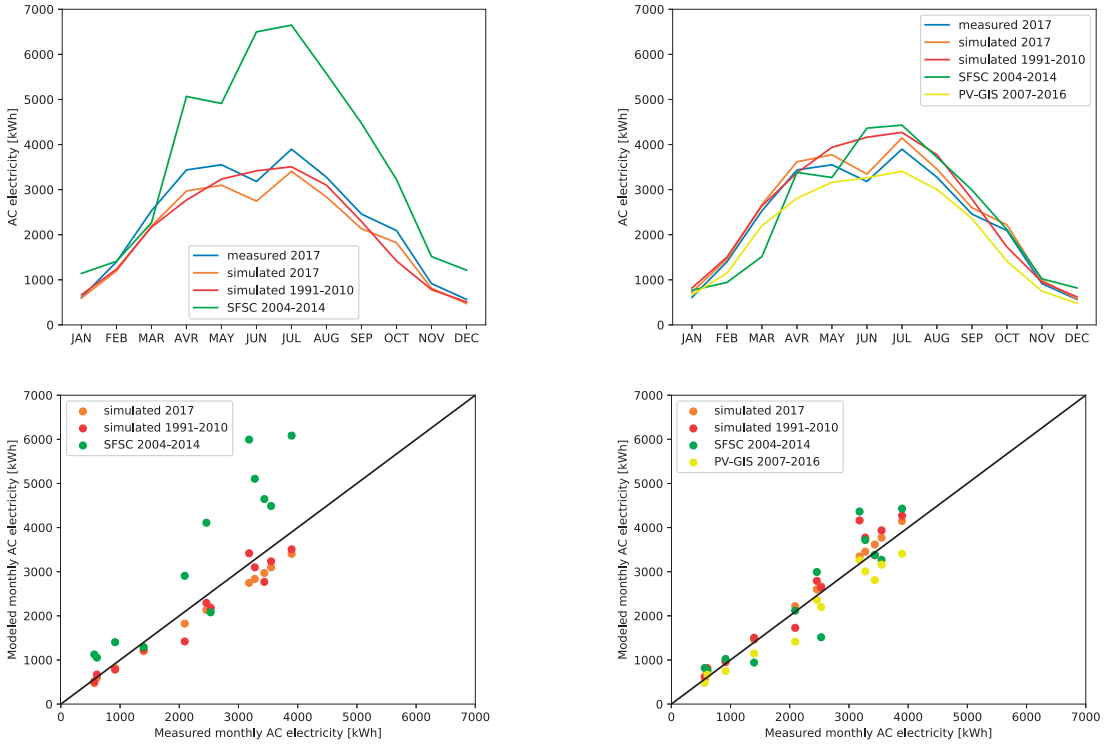


(a) Values (b) Values scaled to the actual surface/power

*Figure 13.9 – Monthly electricity production for the roof-integrated PV installation described in section 13.2. Values in (b) are scaled down (SFSC) or up (simulated) to the actual PV module surface area (Table 13.5), except for PV-GIS, which was set to the actual installed power (Table 13.1).*

*Table 13.5 – Comparison of results for the building presented in Section 13.2.*

| Weather year(s) | Measurements 2017* | Simulated 2017* | Simulated 1991-2010 (see Section 11.2.3.1) | SFSC** 2004-2014 [152] | PV-GIS 2007-2016 [249] |
|---|---|---|---|---|---|
| Roof area [$m^2$] | 229 | 220 | 220 | 234 | |
| PV module area [$m^2$] | 170 | 140 | 140 | 234 | |
| Annual electricity generation [kWh] | 27'910 | 24'282 | 25'101 | 40'290 | |
| Monthly RMSE [kWh] | - | 341 | 348 | 1377 | |
| | Scaled to the actual installation area | | | | Actual installation power[3] |
| Annual electricity generation [kWh] | 27'910 | 29'570 | 30'567 | 29'336 | 24658 |
| Monthly RMSE [kWh] | - | 153 | 389 | 547 | 359 |

*June and July data are from 2016
**Part of the West surface (24 $m^2$) has been excluded

## 13.4 Comparison of features with other tools

Table 13.6 shows the main decision-making features of some solar cadastres. The table presents only a very limited sample of existing solar cadastres, which present though some advanced features compared to the standard products solar maps (see Section 4.3.1). In particular, they all show multiple spatial aggregation scales (with our method having a particularly-extended list) and indicators. They also all show the relative potential of a given urban location with regards to other locations in the same area. As mentioned in Section 4.3.1, the rating of urban surfaces through minimum irradiation thresholds is a common feature in solar cadastres. Mapdwell and our method also display a solar score, which is an effective way of showing the ranking of a single buildings in a city. Most of these tools, including our method, include some sort of user interaction through parameters, while Mapdwell offers the most advanced features, bridging solar maps with PV calculators (Section 4.3.2) for an early-stage design of a specific installation. Similarly to Mapdwell, also our tool proposes some basic sizing of the solar, through a minimum threshold or an automated heuristic. Moreover, our tool also offers control over parameters for enabling some of the other proposed heuristics, such as the one for evaluating the geometric regularity and excluding low-yield locations.

With the notable exception of the SFSC, which has been already reviewed in the previous section, all tools are limited to roofs, while our method adds also 3D visualization capabilities. The other main specificities are the use of two distinct modeling scenarios for weather and vegetation, compared to the use of one static model for vegetation and only typical weather. Moreover, the use of the multiple modeling scenarios is incorporated in the calculation of the solar score and, therefore, also on the ranking of the buildings.

It should be noted that the actual effectiveness in decision-making has not been tested here, nor the accuracy of the results provided by the underlying analysis methods. It should also be considered that 2.5D analysis methods have a larger applicability than those based on 3D models, which are at the moment available only in a limited number of cities and countries (see Section 2.3). Moreover, our tool has been implemented in a desktop software, although it can possibly be installed in a web server, while all other analyzed tools are already implemented as web-based applications. Despite these caveats, we can argue that our method offers some unique features supporting decision making compared to the considered tools.

*Table 13.6 – Comparison of the decision-making features of some solar cadastres. The specificities of our method compared to other tools are highlighted in bold. Please see limitations in Section 13.4*

.

| Tool | Geometry | | Target | Spatial aggregations | Modeling scenarios | User parameters | Indicators | |
|---|---|---|---|---|---|---|---|---|
| | Input | Visualization | | | | | Absolute | Relative |
| Mapdwell [22] | 2.5D | 2D | Roof | PV module<br>Building | Opaque trees<br>Typical weather | Size<br>Efficiency | Electricity (generation)<br>Financial saving<br>Carbon saving | City-specific solar score |
| SFSC [272] | 3D | 2D | Roof<br>Façade | Surface<br>Building<br>Municipality | Opaque trees<br>Typical weather | Percentage of surface use | Electricity (generation)<br>Solar thermal<br>Financial saving | Rating of surfaces based on irradiation categories |
| Geneva's solar cadastre [69] | 2.5D | 2D | Roof<br>Façade* | Surface<br>Useful surface (≥1000 kWh/m$^2$ irradiation)<br>Building<br>Municipality | Opaque trees<br>Typical weather | | Electricity (generation)<br>PV power installed<br>Solar thermal (generation, surplus) | Rating of surfaces based on the different indicators |
| Our method | 3D | **3D** | Roof<br>Façade | PV module<br>Surface<br>Building<br>Zone<br>Grid | Opaque trees / **no trees**<br>**Low-rad** / typical weather | Sizing method<br>**Geometric regularity**<br>**Low-yield avoidance** | Electricity (generation and demand)<br>Retrofit potential | City-specific **solar score accounting for multiple vegetations scenarios** |

*not yet implemented in the web interface

## 13.5 Conclusions

This chapter focused on the comparison of the proposed modeling (Section 11.2) and simulation (Section 11.3) workflow with measurements and alternative solar potential analysis methods. It should be considered that the quantitative comparison did not focus on the evaluation (Section 11.4) and visualization (Section 11.5), which were compared in a more qualitative way.

The comparison showed in general a good match with the measured values. The greater the time resolution, the more accurate the model predicts the PV output. In this sense, the annual predicted electricity generation was only 1% higher than the measured one. However, it should be noted, that the surface fitting algorithm significantly (-18%) unpredicted the number of modules that have been actually installed on the surfaces, probably because of small deviations in the 3D model. Moreover, this comparison s was conducted in a simple situation, i.e,. a rooftoop mostly free of shading and reflections from other buildings or trees. The experimental validation should be conducted also in more challenging situations, such as on façade-mounted PV installations.

The comparison with the Swiss Federal Solar Cadastre (SFSC) is more difficult, as this is based on different assumptions and input data. We have seen that our method provides a more conservative estimation of the solar potential and, despite the under-prediction of the number of modules fitting the roof-installation, provides a better estimation of the size system than the SFSC. When considering the different sizes, both SFSC and our method provide similar annual relative error compared to the measurements in the reference installation, while the SFSC has a higher deviation for monthly values.

In terms of evaluation and visualization, the comparison showed that our method offers some unique features, notably in terms of using multiple modeling scenarios in the calculation of a solar score, which allows the ranking of urban locations within the analyzed area.

# 14 Conclusions

This thesis has presented a novel method for assessing and ranking the PV potential of buildings in urban environments using multiple modeling scenarios. The method is based on existing state-of-the-art methods for the simulation of solar radiation, building energy needs and photovoltaic yield, which are coupled in a comprehensive analysis and decision-support workflow.

## 14.1 Main findings

We can distinguish between the following two types of findings in this thesis:

- **Methodological results**, which are related to algorithms, software solutions, modeling strategies and scenarios that have been proposed in the thesis; as such, these findings present a flexible and extensible framework that can be directly applied in other studies.

- **Quantitative results**, which are the outcome of the preliminary studies and case-study application. Examples of these findings include the parameter selection based on sensitivity analyses as well as the general test of the impact of various parameters and input data on simulated solar potential. Since these results were obtained in case-study applications in Switzerland with specific urban contexts (Geneva and Neuchâtel), they are hardly generalizable to other conditions, but we believe that they can still be a valid reference for future studies.

### 14.1.1 Methodological results

The thesis proposed a software workflow for the modeling and simulation of a detailed 3D city model with a high spatial and temporal granularity. State-of-the-art models for solar radiation (Daysim), PV performance (PV-LIB) and building energy needs (CitySim) were coupled into a Rhino-Grasshopper and Python workflow.

The thesis has shown a method to provide robust decisions through the ranking of the urban locations. Unlike existing solar cadastres which are based on single modeling scenarios, our method provides a solar score integrating multiple modeling scenarios and allows the ranking of urban locations at different spatial aggregation scales according to their performance. In particular, we have shown the application of two preference models:

- the risk-averse preference model, which uses two extreme scenarios as the confidence interval in the decision (Figure 11.13); it has been integrated into a score-based ranking system derived by the application of the Copeland method;
- low-yield avoidance, which uses a low-performance scenario to discard solutions falling below a specific threshold (Figure 11.14).

We have applied both models in our case-study application showing their relevance in the decision-making process. Their implementation was made possible by the use of the following modeling scenarios in the preference models:

- for the application of the risk-averse model for vegetation
  - 'opaque trees' scenario, which corresponds to a fully-shading vegetation canopy, assimilated to the effect of trees during the summer season;
  - 'no trees' scenario, which corresponds to the absence of shading, assimilated to the effect of deciduous tree during winter;
- for the application of the low-yield avoidance model
  - 'low rad' weather, which corresponds to a year composed of the $q$-th percentile months, where $q$ is the 0.10-th month for Global Horizontal Irradiance (GHI);
  - 'typical' weather, which corresponds to a synthetic year with average weather conditions.

In this thesis, we also developed several algorithms that automated the analysis workflow. They are described in the text as pseudo-code, as most of them can be programmed with different programming languages, but have been all developed and implemented in the analysis and case-study application using Grasshopper 3D, Python or Radiance.

**Algorithm 6.1** provides a simple geometry healing method to correct the wrong orientation of surfaces in a 3D city model, which is a typical problem in many datasets.

**Algorithm 8.1** presents the concept of an algorithm for the assessment of the geometric regularity of the solar installation to comply with usual aesthetic requirements in Switzerland.

**Algorithm 9.1** describes a simple heuristic to allocate space for solar thermal and consequently assigning the remaining space to photovoltaics. It was implemented in Python.

**Algorithm 11.1** presents a method to obtain a structured grid, i.e. with equal distance between the sensor points.

**Algorithm 11.2** presents a method to generate weather scenarios from a long time-series of weather data by combination of months belonging to different years.

**Algorithm 11.3** describes the preparation of the geometry for the thermal simulation in CitySim.

**Algorithm 11.4** computes the area and volume of 3D buildings, which are needed as input for the thermal simulation. The algorithm is robust to the topological errors of the 3D model, in particular it succeeds calculating these indicators even on 3D models with non-closed building volumes.

**Algorithm 11.5** computes the hourly electricity loads of standard building typologies using the Swiss SIA 2024:2015 norm standard values, inspired from the PVOpti method [38].

**Algorithm 11.7** presents an implementation of the Algorithm 8.1 (considering only the conservative approach) for the thesis final workflow as described in Algorithm 11.7.

**Algorithm 11.6** sizes the solar system by finding the balance between Self-Consumption (SC) and Self-Sufficiency (SS), as also proposed by [6], assuming that that the owner wants to maximize self-consumption and self-sufficiency.

**Algorithm 11.8** (risk-averse preference model) is the core of the evaluation under epistemic uncertainty. It can applied to the decision between two extreme modeling scenarios.

**Algorithm 11.9** (low-yield avoidance) considers a minimum yield threshold calculated using a 'low rad' scenario for the selection of suitable locations for PV modules.

### 14.1.2 Quantitative results

Quantitative results are mostly the outcome of the preliminary studies that were presented in Part II. Although they are based on specific urban contexts, we argue that they can give relevant recommendation for future studies, especially in relative terms, which can be compared across different climates.

We have seen that, when modeled as a fully-opaque material, vegetation has a strong impact on façade solar irradiation and, in minor part, on rooftops. The impact depends of course on the quantity of vegetation and the built density. In the analyzed urban tiles in the city of Neuchâtel, its median effect is a reduction of 9% of the annual PV yield, and the maximum was found at -16%.

The thesis also explored discretization settings. In this sense, we have shown the relevance of the choice of the discretization algorithm and the resolution of the sensor points, impacting the number of sensor points and hence the computational cost of the simulations. We have seen that the Root Mean Square Error linearly increases with the spacing of a structured grid. However, at all considered levels of discretization (from 1 to 4 m spacing), the error is under 7%. The choice of an optimal grid spacing of 2 m was determined by its greater robustness to the simplifications of the simulation tool (Daysim) with regards to a Radiance `gendaylit` simulation.

In general, the solar potential indicators showed a sensitivity to the minimum considered evaluation threshold well as to the granularity of the analysis. We have seen that the grid spacing is likely to be more important at smaller thresholds and at increasing analysis spatial or temporal granularity. This is an indication for future assessments, which are likely to be conducted at lower irradiation thresholds than today, due to different factors including the decreasing price and the increasing efficiency of solar modules, and higher resolution, because of the need of hourly results for storage or self-consumption optimization. On the contrary, the Level of Detail, which is expected anyhow to improve in the future, is more important at higher thresholds. Similarly, at higher thresholds, the ranking stability is also more affected.

In the case study application, we have seen that the considered vegetation and weather scenarios have two different behaviors. The application of a 'low rad' weather scenario has a similar relative effect across different urban locations providing thus a similar ranking than at a typical weather scenario. Conversely, the uncertainty due to vegetation is significantly varying across urban locations, providing a different ranking at each considered scenario.

### 14.1.3 Validation

The validation, intended as a comparison with measurements, showed a good match of the simulated photovoltaic yield with the measured values from a roof-top installation, especially at resolutions higher than hourly. We also compared the outcomes with those of the Swiss Federal Solar Cadastre (SFSC), showing that our method provides a better sizing of the system based on the actual module size and available space. We highlighted the importance of the accuracy of the input 3D models in the results, which can greatly affect the results.

In more general terms, the case-study analysis proved the applicability of the analysis workflow in a large urban area of almost 1'400 buildings, with varied characteristics. By implementing a tile-based analysis, the method is scalable also to larger urban areas.

## 14.2 Applications

The proposed method was tested as a prototype software workflow in a case-study application. We discuss here its potential uses in real practice by decision-makers dealing with a large number of buildings in urban areas. In particular, we examine policy and planning applications of the priority lists resulted from the application of the proposed method.

### 14.2.1 Solar energy planning

As already noted in our earlier work [218] and in Section 2.4.1.2, solar access has been a core problem of urban planning since the origins of this discipline in modern times. We have seen that a powerful solar energy planning instrument exists for new buildings, the solar envelope, yet it is rarely applied in Europe. Solar easements and other regulatory tools (see Section 2.4.1.2) have transposed these requirements to the rights of direct sunlight for solar energy purpose, though generally limited to rooftops.

It is indeed more difficult to deal with solar energy in existing urban environments from an urban planning perspective. This is because the solar access is mostly dependent on the shading caused by the urban canopy, which - we assume - is not going change, unless new developments or densification interventions are built.

We argue that the method proposed in this thesis can have a twofold application to support solar energy planning in existing urban environments, by highlighting the following conditions of the different spatial locations:

- similarity of potential, suggesting that neighbor buildings could benefit from the same energy retrofit or PV installation; these interventions would possibly determine economy-of-scale savings;
- difference of potential, suggesting that the excess production of a high-potential building could profit neighboring low-potential buildings.

This application is possible thanks to the use of spatial aggregation at different scale levels and of spatial overlays, which provide a planning-targeted spatial representation of the solar energy potential.

### 14.2.2 Performance-based priority lists

We believe that a performance-based priority list would be useful for different applications and actors dealing with a large building portfolio in the same urban areas. In particular, we argue that it would provide substantial advantages for the allocation of incentives compared to the common practice.

As we have seen in Section 3.2.1.1, subsidies for photovoltaics are commonly assigned on a peak-power basis, i.e., based on the nominal peak power of the solar installation regardless of its actual yield. Conversely, subsidies for building energy retrofitting are normally based on an assessment of the energy performance of the building[1]. Even acknowledging that the estimated building energy performance is only an indicator and not an actual prediction of its energy needs, these estimations still give relevant information about building performance in real conditions (e.g. climate, context), especially in relative terms compared to other buildings.

We argue that a similar perfomance-based system could be used for photovoltaics as a *skill*-based allocation system. In this sense, the priority list provided by our method could give a first assessment of the eligibility to obtain financial or other kind support from the local authorities. The eligibility should consequently be certified by a qualified professional based on the expected performance or just checked by metering during the system operation, similarly to what happens in the Expected Performance Based Buydown (EPBB) and the Performance Based Incentive (PBI) of the California Solar Initiative [64].

In case of limited financial availability, we have seen that waiting lists are commonly used as a fair allocation method also in the field of renewable energy subsidization. However, we believe that performance-based priority lists provide higher aggregate welfare than waiting lists. They allow in fact to target the aid according to the *need* (e.g. energy saving potential) or *skill* (e.g. energy production potential) of the system, while ensuring the transparency of the evaluation through pairwise comparisons and a score-based method similar to the one of sport tournament. The solar score being normalized to the best and worst results, the system allows a fair comparison of spatial locations within a city as well as between different cities.

It is up to the decision-maker to assign incentives based on a standard priority list, i.e. prioritizing the best performing one at the top, or on a reversed one, i.e. prioritizing the worst performing ones. The second strategy would be useful, for instance, for decision-makers arguing that the best-performing installation locations do not actually need any financial aid, while the incentives should instead be targeted to low-performing locations so as to help them reach a minimum financial viability.

Moreover, priority lists can also be used by private stakeholders, such as owners of large building portfolio, their service management companies or also Energy Service Company (ESCo) that are interested in offering their services to building owners. Performance-based priority lists would offer a first estimation of the most interesting locations to invest on, either because of their energy saving or electricity generation potential.

[1] In Switzerland many cantons give financial incentives based on the achievement of a specific energy class of the energy performance certificate (GEAK© CECB© CECE©). Similarly, the 2010/31/EU Directive states that "Member States shall take account of the cost-optimal levels of energy performance when providing incentives for the construction or major renovation of buildings." (Art. 10,6 para. 6).

## 14.3 Discussion

This section discusses the proposed method with regards to the input data, method and validation phase, highlighting their main limitations. It also contains many elements that were highlighted during the thesis oral exam, thanks to the very stimulating comments from all the examiners. Finally, it describes future work to improve the shortcomings and finally proposes a broader research outlook.

### 14.3.1 Input data

The thesis proposed a method based on vector 3D city models. As we have seen in Section 2.3, the availability of these datasets is limited to some cities and, in only few cases, to whole states our countries, as in the case of Switzerland. Applications might thus be limited due to the non-availability of such data, but we can assume that their diffusion will be growing in the future. However, in the same Section 2.3, we also highlighted the increasing availability of LiDAR datasets. These datasets can be used either to create 3D vector data, using building reconstruction techniques, or in 2.5D solar potential assessments, directly, after meshing or after resampling to a raster model. The evaluation method proposed in Section 11.4 could thus have a larger applicability, as it can be implemented to any modeling and simulation method, as long as multiple modeling scenarios (notably, for vegetation and weather) can be produced.

In any case, it should be noted that the 3D city model we used is more detailed compared to the current practice and standard models available in other countries, yet lacks some important features such as the modeling of façade objects, notably windows and balconies, as well as of material properties of the surfaces. These aspects can be actually be seen as part of discussion on the consistency of the level of detail (see Section 14.3.2.1), which does not concern only the geometric Level of Detail (LOD) but also the different components of the analysis methods and data sources.

### 14.3.2 Method

One of the scopes of the proposed analysis method was to assure robust choices by taking into account different sources of uncertainty. The proposed method was then applied with regards to two typical, yet crucial uncertainties, i.e., the variability of weather based on past recorded data and the modeling of vegetation. However, the considered uncertainties were only used as examples to test the proposed method and are far from being an exhaustive list. Moreover, we cannot say whether they are the most relevant ones. Other aspects that should be considered to further check the robustness of the ranking prediction include:

- the influence of climate change on future weather, which will be also discussed in Section 14.3.2.3;
- the impact of large-scale PV deployment on the urban microclimate (e.g., UHI) and the surface properties (e.g., reflectivity);
- the changes in future energy demand, due for example to more efficient appliances or different user behavior;
- the different business models involving for example shared generation/consumption.

The modeling method was targeted to the analysis of PV potential with a simplified approach to architectural integration, neglecting for example the application in shading devices or railings. We considered in fact that the application of BIPV strategies is building specific and should be then conducted in later phases of the building design process. However, we proposed an algorithm for the

consideration of geometric regularity criteria since the planning phase, which can provide a better estimation of the actual solar potential of buildings under standard building integration guidelines.

With regards to the PV performance model, the proposed method did not incorporate system modeling, such as strings and inverters, but rather used a fixed Performance Ratio to convert DC to AC power. Modeling the string arrangement would have required an optimization process to avoid partial shading and we considered that, for the purpose of ranking urban locations, the DC electricity was a good proxy of the actual AC yield of the system.

The estimation of the building energy demand was largely based on normative data, including standard occupancy schedules and fixed annual energy demand depending on the building use. The effectiveness of the model would be of course much improved by the use of actual energy demand curves or stochastic models. The assumption that the demand curve after refurbishment does not take into account the changes in the heat capacity of the building nor the expected improved efficiency of the building systems working on an insulated and air-tight building. In particular, it does not consider interventions on the thermal mass, which could particularly useful for increasing the self-consumption of the building, as it will be discussed also in Section 14.3.2.2, as part of demand-side management (DSM) strategies.

Although vegetation does have an effect also on building energy performance, the geometry used for thermal simulation included only a 'no trees' scenario. The computational cost of the radiosity-based simulation engine behind CitySim (see Section 4.1.1) is highly affected by the high number of vegetation mesh faces, unless a simplified vegetation model is used (e.g., as in Coccolo et al. [58]).

The proposed workflow presented in Chapter 11 used a file-based data management system with generic data formats (e.g., text tabular data, or binary-encoded Python data structures), which are not optimal for accessing large datasets and do not include topological information. The whole computational workflow should be seen more as a prototype than as an actual software implementation: in particular, it has space of improvement for speed and memory handling. The workflow could integrate the recent advancements in standardized formats for 3D city models, i.e., CityGML [201] and its Application Domain Extension for energy [8], as well as of CityGML-compliant databases, such as the 3DCityDB [323]. This can be coupled with the popular open-source 3D mapping tool CesiumJS [65] for visualization purposes.

#### 14.3.2.1 Consistency in the level of detail

The proposed modeling and simulation method (Sections 11.2 and 11.3) couples different models, algorithms, heuristics, which make use of data from different sources. The overall goal behind the choice of the proposed comprehensive method was to maximize the accuracy, using state-of-the-art models and input data, while providing an acceptable computational time. The acceptability of the computational time is of course subjective and the actual computation time is expected to decrease in the future, if all other conditions (settings, input data) stay unchanged. The computational time proposed in Table 11.12 is hence indicative only of the present conditions, considering the given computational setting, and an acceptability threshold which is around 24 hours per 250x250-m tile for the longest-running job (in our case, the CitySim simulation).

We can describe here below some factors for which the mismatch between different analysis methods or input data is more evident.

- Photovoltaic *vs* building energy models. The implementation of the building energy model relies on simplified archetypes and occupancy behaviors, which have not been calibrated and are expected to provide large discrepancies with the actual demand; on the contrary, the simulation of the PV energy model relies on validated models, whose reliability has also been checked using the local data source and analysis methods (although in a simple case without many obstructions). In this sense, it should be considered that accuracy of the indicators is different, in particular for those including the prediction of the building energy saving potential (Equations (11.9) and (11.10)), which rely on the building energy models. The PV potential indicator (Equation (11.8)) is also supposed to be more reliable, as long as the sizing of the system is based on a fixed minimum energy yield threshold rather than on the sizing algorithm (Algorithm 11.6), as this is based on the self-consumption and self-sufficiency using also energy demand data.
- Level of Detail (LOD) of roofs *vs* façades. The original LOD definition (see Section 2.3.1) considers a Level of Detail that is higher for roofs than for façades, as it includes the real shape of the roof (although without overhangs), while the rest of the building is still modeled as a shoe-box. The 3D city model used in this work provides a refined LOD of roofs, including also the major roof-top superstructures and the overhangs, while the façades are still modeled as a shoebox, without protrusions (such as balconies, awnings) and any variations of the façade shape that are not included in the official cadastre footprints. In our understanding, the fact of including the overhanging eaves, which are a typical feature in traditional Swiss architecture, helps refine the solar potential on façades. However, there is still a mismatch between the architectural features of buildings and what can be modeled using commonly-available 3D models at LODs, which is still very limited with regards to façades.
- Geometric *vs* material properties of surfaces. The raytracing simulation ensures the inclusion on inter-reflections in the simulation, which was shown to be particularly important on façades and on denser urban environments, while these value are also dependent on the reflectivity of the surfaces. While the input 3D city model includes high LOD geometric information, it does not include information about the material properties of the surfaces. The short-wave reflectivity was then set using standard and fixed values, only differentiating between façades, roofs, ground and vegetation surfaces.

#### 14.3.2.2 Impact on the grid and self-consumption

The sizing of the system, which is based either on a minimum threshold or on a sizing heuristic balancing self-consumption and self-sufficiency, selects modules based on their annual electricity generation. This approach does not maximize the self-consumption of the building and, consequently, might affect the grid resilience. The grid is in fact likely to be overloaded by the injected surplus energy without undergoing major transformations, in terms for example of the power capacity of urban distribution transformers. In this sense, a location with a high solar potential calculated using our sizing heuristic might have a negative impact on the grid. However, the proposed method applied with a minimum threshold instead of the heuristic can be used by grid managers to check the impact of increasing PV energy penetrations at the different spatial aggregations levels.

The sizing heuristic is conceived to provide a first assessment of the solar potential when the financial attitude of the investors is not known. We consider in fact that the self-consumption is a proxy for the financial viability of the system for most of the final users, as it increases the financial value of the generated electricity and it should be then maximized. We also assume that most of the final users want to be as much independent from the grid as possible, to reduce the risk due to the fluctuation of the electricity price, and want thus to maximize the self-sufficiency. However, in the implementation

of the heuristic presented in Algorithm 11.6, the two indicators are opposing objectives: if we reduce the system of the system by discarding the modules with the lowest annual production, the self-consumption increases, at the detriment though of self-sufficiency, which will decrease. The heuristic can find only a single trade-off solution, which is likely not the optimal one, yet avoids an oversizing of the system while having a fair self-consumption. Maximizing the two indicators would have required the implementation of an optimization algorithm, which was outside the scope of this work and is of hard implementation for large-scale analysis comprising of multiple buildings.

Moreover, the proposed sizing heuristic does not consider alternative methods to increase the self-consumption, which were discussed also in Section 4.2.3.1. In particular, it can be argued that demand-side management is an effective method to match the demand curve with the electrictity generation curve; to this end, in the case of space heating, the building thermal mass can be used to store heating energy during daytime (when both passive and active energy sources have their peak) so as to use it later during nightime. Batteries can also be used as storage for the surplus energy to be used at night or at anytime the real-time production does not cover the demand. Finally, the optimized arrangement of PV modules, which tries to match the electricity generation curve with the demand curve, can also increase the self-consumption, using for examples East and West oriented modules reducing the midday peak.

#### 14.3.2.3 Weather variability and climate change

The weather scenarios were created based on past weather data, which excludes then the future variability due to climate change, affecting in particular solar radiation and temperature. However, we can examine some general trends with regards to the future weather. While the increasing solar radiation could have a positive effect on the energy yield, the temperature would negatively affect it. It was outside the scope of this work to predict the effect of the combined effect of solar radiation and temperature raise. We can however describe some general tendencies based on the results presented in Chapter 12.

As we have seen in Section 12.2.3 and already pointed out in Section 14.1.2, the ranking is only minimally influenced by the weather scenarios, while there is a significant effect of the weather scenarios on the absolute energy yield. In this sense, we could assume that future weather changes will likely not influence the ranking either. This means, for example, that a given location ranked as first is supposed to keep its rank, even if its actual energy performance value will change due to the consequences of global warming phenomena.

It should be noted that climate change might also create local and time-specific micro-climate conditions that are not taken into account by climate change models. These conditions, if actually occurring in the considered urban areas, will have an effect on the ranking of the different spatial locations composing that urban area. As a purely fictive scenario, fog or other weather phenomena regularly occurring in some specific moments of the day (e.g, in the morning) will have a higher impact on those spatial locations that are more dependent on energy produced/consumed in that period of time (e.g., buildings with larger East-exposed surfaces). Similar, these phenomena might also be occuring more often in a specific area of the city, possibly influenced by topography or other natural elements, and thus more significantly impacting the spatial locations in that area. If these phenomena are directly caused by climate change, will have a direct impact also on the ranking of the urban locations, while the proposed method is not able to predict this change.

### 14.3.3 Validation

The analysis method was applied to a case study to prove its applicability. However, in terms of validation, we limited the comparison based on the data we had accessed to, and was hence focused on validating the modeling and simulation workflow for solar radiation and PV performance on a roof-integrated installation. Further validation should be done for other systems in different locations and for façade-installed systems, as well as for testing the decision support effectiveness, which could only be done through user surveys.

Moreover, the validation should be completed with the data regarding the building energy demand. However, it should be considered that for space heating we used typical transmittance values already calibrated by a precedent study [213].

### 14.3.4 Outlook

This work focused on one main energy indicator, i.e. photovoltaic energy production in urban environments, while linking this potential to the energy retrofit potential. We can consider that other indicators could be provided to enlarge the spectrum of the analysis, considering for example comfort and $CO_2$ indicators.

Similarly, vegetation can be considered as a potential *per se*, in the same way as photovoltaics. Vegetation is in fact at the core of urban design and planning practice, while we have only considered it for its shading effect on solar energy systems. In addition to its aesthetics benefits, vegetation is widely used also for its multiple climatic-control features. Vegetation shading and evapotranspiration effect increase outdoor comfort by reducing the surface temperature. In this sense, we can expect that, thanks to the improved outdoor comfort, sustainable and healthy mobility patterns such as cycling and walking are also encouraged. Vegetation can also be used for reducing air pollution and for carbon sequestration and, as part of non-paved surfaces, to improve the soil permeability and decrease the risk of flooding in urban environments. However, its combined effects on different environmental indicators are rarely quantified and assessed in the design process. Recently, thermal comfort maps showing the predicted pedestrian comfort in outdoor spaces have been also proposed for planning applications [58], though using only evergreen trees. Therefore, we can foresee an extension of the tools for assessing the trade-offs of vegetation, in terms for example of $CO_2$ reduction compared to PV systems, as well as for comfort evaluation.

With the increasing use of photovoltaic systems also on façades (as well as of highly glazed buildings), glare discomfort will likely become more relevant due to the intense reflection of sunlight from their surfaces compared to traditional opaque materials. The Swiss federal legislation (see Section 3.1.2) requires solar installations to be "low-reflecting according to the scientific state of the art[2]". It is usually assumed that all manufactured solar systems sold in Switzerland comply with this requirement [287]. However, this does not prevent glare to occur in some situations, which can still have a negative impact on neighboring activities, as also tested by some cases in the Swiss cantonal jurisprudence[3]. Swissolar [287] has developed some simple guidelines to this regard. However, glare being based on different perception models, it is likely that some installations will still cause discomfort or even disability glare, as shown by previous work [130]. Recent work showed a possible evaluation of BIPV glare discomfort method based on a Radiance [266], which could be possibly integrated in our workflow, the main

[2] "*peu réfléchissantes selon l'état des connaissances techniques*", RPV-OAT-OPT, Art. 32a, §1.
[3] e.g., Administrative Cantonal Court of Graubunden, case R 14-53, 2005

limitation being though computational time and the sensing of the characteristics of the urban surfaces in terms of materiality.

It is known that some solar technologies perform better under non-optimal conditions, such as low- or diffuse light, than on standard test conditions. The applied PV performance model, as equivalent models used in standard practice, only considers global POA irradiance, neglecting the spectral response of the PV system. We acknowledge the fact that spectral lighting simulations are still on-going research [316] and would be probably excessive for such application, especially when analyzing crystalline modules as in this work. However, recently-developed PV performance models separating diffuse and direct irradiance (e.g., [151]) would be beneficial for analyzing the performance of non-crystalline technologies, in particular for façade applications.

## 14.4 Final remarks

As reminded by the latest report of the IPCC [121], the reduction of carbon emissions of the built environment cannot be postponed and should go beyond the binding 2°-C limit of the Paris agreement to avoid dramatic societal and economic consequences. The building sector in many countries is undergoing an energy and carbon transition, yet too slow in particular with regards to the carbon emissions of the existing building stock largely relying on fossil fuels for space heating. Intervention are still limited to discrete and soft interventions on single buildings, while we believe that they should be extended to large building areas so as to increase their effectiveness and speed.

We argue that decision-support under uncertainty can strategically favor the urban renewal process towards the energy and carbon-emissions goals. To this end, this thesis has provided a comprehensive work for the analysis of large urban areas, which could benefit planners, stakeholders, and large building owners prioritize robust energy interventions on existing buildings.

# A Appendix

## A.1 Characteristics of the 3D city models

The LOD classification of the 3D models is based on the definition by Biljecki et al. [30].

### A.1.1 Switzerland - LOD1

This 3D model is based on the product SwissBUILDINGS$^{3D}$ 1.0 by the Swiss Federal Office of Topography Swisstopo [295].

### A.1.2 Neuchatel - LOD1

These 3D models were automatically reconstructed using the software BuildingReconstruction [307] and as source data DSM and DTM at 0.5 m resolution and the cadastre building footprints (©2014 SITN).

### A.1.3 Neuchatel - LOD2

These 3D models were automatically reconstructed using the software BuildingReconstruction [307] and as source data DSM and DTM at 0.5 m resolution and the cadastre building footprints (©2014 SITN). Roofs are modeled with their actual shape but without super-structures nor overhangs.

### A.1.4 Switzerland - LOD2.3

This 3D model is based on the product SwissBUILDINGS$^{3D}$ 2.0 by the Swiss Federal Office of Topography Swisstopo [296]. Its main features are also described in Stoter et al. [290]. The CityGML dataset includes roof and façade semantics. Overhangs are represented twice: as part of the roof surface and as additional polygons (with their normals facing down).

### A.1.5 Neuchatel - LOD2.3

The 3D model is a recent 3D city cadastre from the Canton of Neuchâtel GIS department (SITN). The dataset we used is a preliminary release of the cadastre, extracted on June 21, 2017. It provides as separate files buildings and over-constructions, both divided into vertical and non-vertical (roof) surfaces, as well as the rooftops and footprints of other constructions not classified as buildings (e.g. garages). Unlike for the SwissBUILDINGS$^{3D}$ datasets presented here above, the building footprints are compliant with those of the official cadastre.

### A.1.6 Geneva - LOD2.3

This 3D model is available as open-data through the Canton of Geneva GIS department (SITG). The dataset provides as separate files buildings and over-constructions, both divided into vertical and non-vertical (roof) surfaces.

## A.2 Code snippets

### A.2.1 Processing PV modules

```
def getAC(nodes, values, LRvalues=[], threshold=0, PR=0.85, PanelPower=0.185, Regularity=True
  , Weighted=False, AllPanels=False, LowSuff=False):
    print("Processing panels...")
    # Add the weight info of each panel, differentiating between facades and roofs
    panels = getNodesWeight(nodes)

    # If there is no Low Rad data, use the typical data
    if len(LRvalues) == 0:
        LRvalues = values

    # DC to AC conversion
    panels["AC_notrees"] = pd.DataFrame(np.concatenate(values[0::2],axis=0)) * PR
    panels["AC_opaque"] = pd.DataFrame(np.concatenate(values[1::2],axis=0)) * PR
    panels["AC_notrees_lowrad"] = pd.DataFrame(np.concatenate(LRvalues[0::2],axis=0)) * PR


    # Make sure that panels in inter-tile buildings are counted only ones
    print("...removing duplicates")
    fishnet = parsing.getFishnet()
    panelscopy = pd.DataFrame()
    for tile in panels["tile"].unique(): #add geographic reference to panels
        selpanels = panels.loc[panels["tile"] == tile].copy()
        selpanels.Y += fishnet.loc[tile].Y
        selpanels.X += fishnet.loc[tile].X
        panelscopy = panelscopy.append(selpanels, ignore_index=True)
    panels = panelscopy
    panels = panels.round({'X': 4, 'Y': 4, 'Z': 4})
    #select the first occurrence of panels with the same coordinates
    panels = panels.groupby(by=["X","Y","Z"]).first()
    panels = panels.reset_index()

    # Remove "fake" panels located in too small surfaces
    panelswithcp = panels
    panels = panels[panels["SENSORTYPE"] == "panel"]
    print("Removed center points")
    panelsnocp = panels


    # Simple minimum threshold [kWh/kWp]
    print("...Applying threshold")
    if str(threshold) != "auto":
        # Threshold
```

```
42          panelsabove = panels[panels["AC_notrees_lowrad"]/PanelPower > threshold]
43
44      # "auto" threshold based on balance between self-sufficiency and self-consumption
45      else:
46          if LowSuff:
47              sufficiency = pd.read_csv("D:/SimulationData/neuchatel/CSV/
                  selfsufficiency_SIA_q10.csv",index_col=0)
48          else:
49              sufficiency = pd.read_csv("D:/SimulationData/neuchatel/CSV/selfsufficiency_SIA.
                  csv",index_col=0)
50          nodes = panelsnocp.copy() #only for counting purposes
51
52          # Get the bldgIDs that are both in thermal and PV simulations
53          bldgIDs1 = panels.groupby("BLDGID").first().index.values
54          bldgIDs2 = sufficiency.groupby(sufficiency.index).first().index.values
55          bldgIDs = np.intersect1d(bldgIDs1,bldgIDs2)
56          sufficiency = sufficiency.loc[bldgIDs]
57
58          # Select only panels belonging to thermally-simulated buildings ("panels heated")
59          panelsheated = panels[panels["BLDGID"].isin(bldgIDs)]
60          # Sort panels by AC and select only the panels that meet the SC/SS requirement
61          panelsabove = panelsheated.groupby("BLDGID").apply(lambda X: X.sort_values("
                AC_notrees",ascending=False).iloc[:int(sufficiency["npanels"].loc[X.name])])
62          panelsabove = panelsabove.reset_index(drop=True)
63
64      # Regularity algorithm
65      if Regularity:
66          print("...Applying regularity check")
67          countbefore = panels.groupby(['BLDGID','SURFID','ROWID'],sort=False).size() #number
                of panels per row before threshold
68          countafter = panelsabove.groupby(['BLDGID','SURFID','ROWID'],sort=False).size() #
                number of panels per row after threshold
69
70          counted = pd.concat([countbefore,countafter],axis=1) #number of panels per row before
                 and after threshold
71          # Reindex so that the order is the same as for panels
72          counted = counted.reindex(countbefore.index)
73
74          acceptability = abs(counted.iloc[:,0] - counted.iloc[:,1]) #number of panels that are
                 "left-overs" in that row
75          acceptability[acceptability.isnull().values] = -1 #nans to -1 (rows that have no
                panels achieving the threshold)
76
77          panels = panels.reset_index().set_index(["BLDGID","SURFID","ROWID"])
78          allpanels = panels #panels before the regularity algorithm
79
80          # Add the acceptability column
81          panels = pd.merge(panels,pd.DataFrame(acceptability,columns=["acceptability"]),
                left_index=True,right_index=True,how="inner")
82          # Only keep panels with complete rows (acceptability = 0 = 0 left overs)
83          panels = panels[panels.acceptability == 0]
84
85          #Keep the non-acceptable panels (for visualization and counting purposed)
86          acc = allpanels.index.isin(panels.index) #index of acceptaable panels
87          nonacceptable = allpanels[~acc]
88          panels = panels.reset_index()
89          nonacceptable = nonacceptable.reset_index()
90      else:
91          print("  Warning: no regularity check")
92          panelsabove = panelsabove.assign(acceptability = 0) #Assign fake regularity
93          allpanels = panels
94          panels = panelsabove
95          acc = allpanels.index.isin(panelsabove.index)
96          nonacceptable = allpanels[~acc]
97
98      print("Threshold: {} kWh/kWp\nNodes: {}\nPanels: {}\nPanels after threshold: {}\nPanels
            after threshold and regularity algorithm: {}".format(threshold,
99              panelswithcp.shape[0],
100             panelsnocp.shape[0],
101             panelsabove.shape[0],
102             panels.shape[0]))
```

```

    # Weight the panels differentiating between, differentiating between facades and roofs
    if Weighted:
        panels.loc[:,"AC_notrees"] = panels.loc[:,"AC_notrees"]*panels.loc[:,"weight"]
        panels.loc[:,"AC_opaque"] = panels.loc[:,"AC_opaque"]*panels.loc[:,"weight"]
        panels.loc[:,"AC_notrees_lowrad"] = panels.loc[:,"AC_notrees_lowrad"]*panels.loc[:,"
           weight"]
        print("AC production has been weighted")
    else:
        print("Wawning: AC production has not been weighted")

    # Keep geometry of non-suitable panels, to be visualized
    if AllPanels == True:
        print("Adding non-suitable panels")
        nonacceptable = nonacceptable.assign(acceptability = np.nan)
        panels = pd.concat([panels,nonacceptable],axis=0,ignore_index=True)
        if "geometry" in panels.columns:
            panels = gpd.GeoDataFrame(panels)

    return panels
```

### A.2.2 Hourly electricity loads

```
import pandas as pd
import numpy as np
import matplotlib.pyplot as plt


def ElectricLighting(use="singlefamily",scenario="standard",
                     epwfile=r"D:\SimulationData\neuchatel\EPW\Neuchatel.epw",
                     threshold=200,
                     hourly=True):
    if use == "singlefamily" or use == "multifamily":
        annualdemand = {'standard': 4, 'target': 2, 'existing': 4} #kWh/m2
        dayload = np.array([0.1,0.1,0.1,0.1,0.1,0.1,0.1,1.0,1.0,0.1,0.1,0.1,
                            0.6,0.6,0.1,0.1,0.1,0.1,0.5,1.0,1.0,0.5,0.1,0.1])
    elif use == "office":
        annualdemand = {'standard': 19, 'target': 5, 'existing': 19} #kWh/m2
        dayload = np.array([0.0,0.0,0.0,0.0,0.0,0.0,0.0,0.0,1.0,1.0,1.0,1.0,
                            1.0,1.0,1.0,1.0,1.0,1.0,1.0,0.0,0.0,0.0,0.0,0.0])

    if hourly:
        from pyepw.epw import EPW
        epw = EPW()
        epw.read(epwfile)
        GHI = []
        for wd in epw.weatherdata:
            GHI.append(wd.global_horizontal_radiation)
        GHI = np.array(GHI).reshape(365,24).transpose()
        daylit = np.greater(GHI,threshold)

        load = np.tile(dayload,365)
        load = load.reshape(365,24).transpose()
        need = load*(1-daylit)
        power = (annualdemand[scenario]*1000)/need.sum() * need

        return power
    else:
        return annualdemand[scenario]


def Ventilation(use="singlefamily",scenario="standard",hourly=True):
    if use == "singlefamily":
        annualdemand = {'standard': 0.7, 'target': 0.4, 'existing': 0.0} #kWh/m2
        dayload = np.array([1.0,1.0,1.0,1.0,1.0,1.0,0.6,0.4,0.0,0.0,0.0,0.0,0.0,
                            0.8,0.4,0.0,0.0,0.0,0.4,0.8,0.8,0.8,1.0,1.0,1.0]) #occupation
                              SIA2024
    if use == "multifamily":
        annualdemand = {'standard': 1.2, 'target': 0.7, 'existing': 0.0} #kWh/m2
        dayload = np.array([1.0,1.0,1.0,1.0,1.0,1.0,0.6,0.4,0.0,0.0,0.0,0.0,
```

```
47                              0.8,0.4,0.0,0.0,0.0,0.4,0.8,0.8,0.8,1.0,1.0,1.0]) #occupation
                                    SIA2024
48      elif use == "office":
49          annualdemand = {'standard': 2.1, 'target': 1.3, 'existing': 3.4} #kWh/m2
50          dayload = np.array([0.0,0.0,0.0,0.0,0.0,0.0,0.0,0.2,0.6,1.0,1.0,0.8,
51                              0.4,0.6,1.0,0.8,0.6,0.2,0.0,0.0,0.0,0.0,0.0,0.0]) #occupation
                                    SIA2024
52
53      if hourly:
54          load = np.tile(dayload,365)
55          load = load.reshape(365,24).transpose()
56          power = (annualdemand[scenario]*1000)/load.sum() * load
57          return power
58      else:
59          return annualdemand[scenario]
60
61
62  def Appliances(use="singlefamily",scenario="standard",hourly=True):
63      if use == "singlefamily" or use == "multifamily":
64          annualdemand = {'standard': 14, 'target': 7, 'existing': 18} #kWh/m2
65          dayload = np.array([0.1,0.1,0.1,0.1,0.1,0.1,0.1,0.2,0.6,0.8,1.0,0.8,
66                              0.4,0.6,1.0,0.8,0.6,0.2,0.1,0.1,0.1,0.1,0.1,0.1]) #appliances SIA
                                    2024
67      elif use == "office":
68          annualdemand = {'standard': 14, 'target': 6, 'existing': 29} #kWh/m2
69          dayload = np.array([0.1,0.1,0.1,0.1,0.1,0.2,0.8,0.2,0.1,0.1,0.1,0.1,
70                              0.8,0.2,0.1,0.1,0.1,0.2,0.8,1.0,0.2,0.2,0.2,0.1]) #appliances SIA
                                    2024
71
72      if hourly:
73          load = np.tile(dayload,365)
74          load = load.reshape(365,24).transpose()
75          power = (annualdemand[scenario]*1000)/load.sum() * load
76          return power
77      else:
78          return annualdemand[scenario]
```

### A.2.3 Risk-averse preference models

```
def PairWiseComparison(indata, fuzzy=False):
    matrix = []
    # Convert incoming data to numpy array if not already.
    if not isinstance(indata, np.ndarray):
        indata = np.array(indata)

    #Check which column represents a "low-prod scenario" and which one  a "high-prod scenario"
    # This only works for a two-column matrix.
    averagecolumn = indata.mean(axis=0)
    if averagecolumn[0] < averagecolumn[1]:
        l = 0 #low column is the first one
        h = 1 #high colum is the second one
    else:
        l = 1 #low colum is the second one
        h = 0 #high column is the first one

    # Scaling denominator for fuzzy calculation.
    # This only works for a two-column matrix.
    #we want the maximum distance between two barplots,
    #i.e. the difference between the max of the worst location (l column) and the min of the best location (h column)
    minmax = np.abs(np.max(indata[:,l]) - np.min(indata[:,h]))

    # If the incoming data is a 1D vector, it will be compared to no-PV,
    # i.e., an array of zeros.
    if indata.ndim == 1:
        indata = np.vstack((indata, np.zeros_like(indata))).T

    for p in range(0, indata.shape[0]):
        line = []
        for pp in range(0, indata.shape[0]):

        if (min(indata[p, :]) > max(indata[pp, :])):
            if fuzzy:
                line.append((min(indata[p, :])-max(indata[pp, :]))/minmax)
            else:
                line.append(1)
        elif (max(indata[p, :]) < min(indata[pp, :])):
            if fuzzy:
                line.append((max(indata[p, :])-min(indata[pp, :]))/minmax)
            else:
                line.append(-1)
        else:  # p and pp cannot be compared
            line.append(0)
            matrix.append(line)
        matrix = np.array(matrix)
    return matrix
```

### A.2.4 Support to horizon shading of sun direct contribution

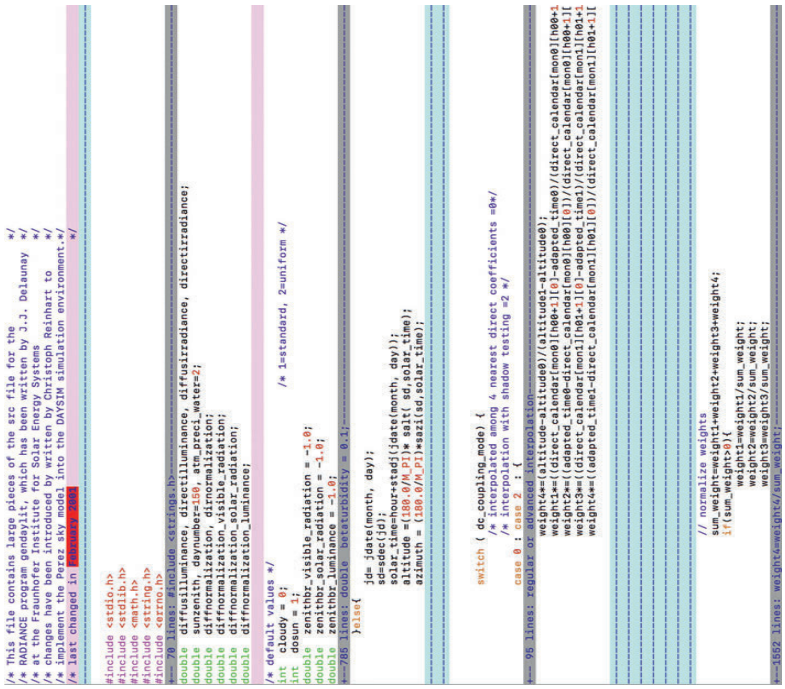

(a) Original

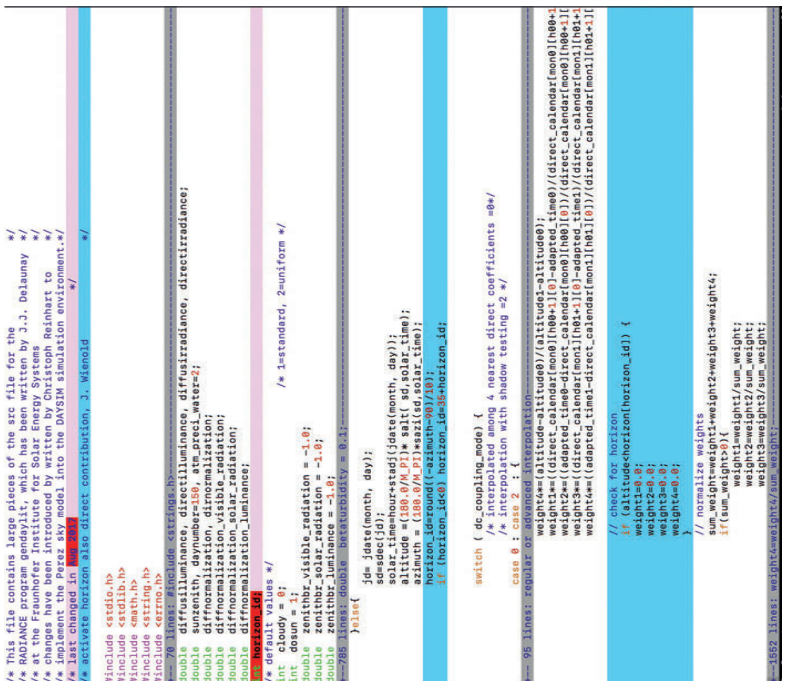

(b) Hacked version

*Figure A.1 – Screenshot of the modifications implemented by Jan Wienold in Daysim subprogram* `ds_illum` *to activate the horizon also for the direct contribution: if the sun altitude is lower than the horizon height, the direct contribution is forced to 0. The differences in the source code of the file* `calculate_Perez.c` *are highlighted in (b).*

## A.3 Map of case studies

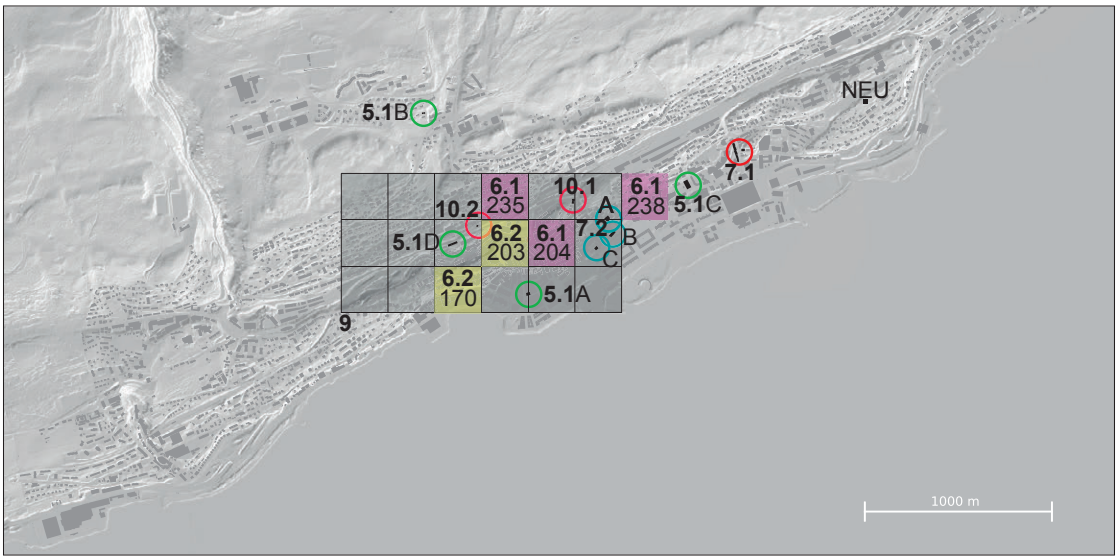


*Figure A.2 – Location of the case studies (buildings or tiles) in Neuchâtel. The numbers in bold refer to the chapter or section in which the case studies are described. They are followed by the case-study reference (if applicable). NEU indicates the position of the homonym weather station from Meteoswiss used for producing the weather files (see Section 11.2.3 and Section 13.2). The reference IDs for all tiles analyzed in Chapter 12 can be found in Figure 12.5.*
*Background: Swisstopo SwissALTI$^{3D}$ - Footprints: SITN Cadastre*


*Figure A.3 – Location of the case-study tile in Geneva (Section 6.2).*
*Background: Swisstopo SwissALTI$^{3D}$ - Footprints: SITG Cadastre*

## A.4 Animation frames

### A.4.1 Frames of Figure 6.13a


(a)

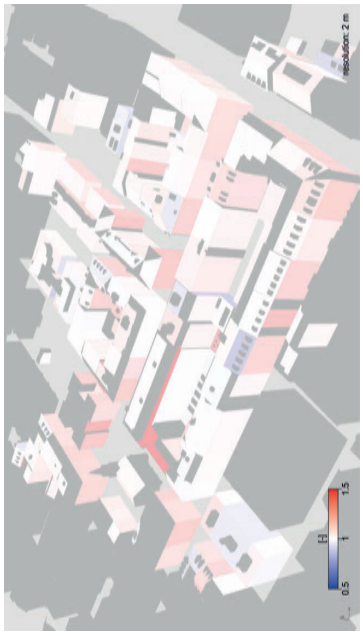


(b)

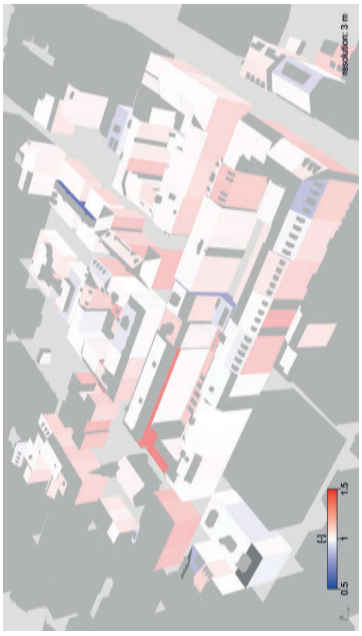


(c)

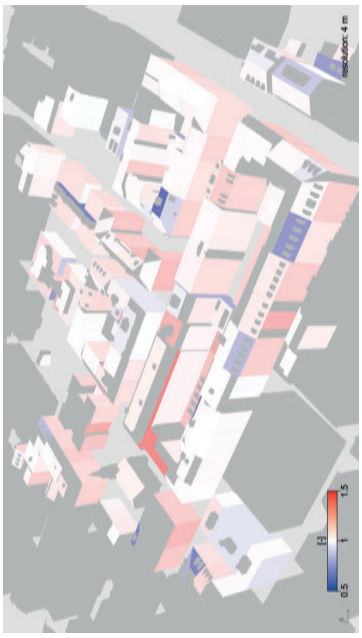


(d)

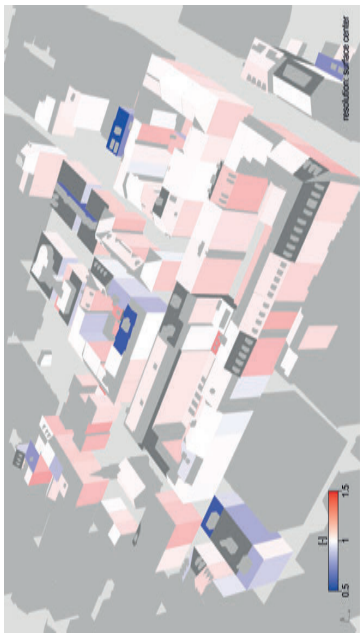


(e)

### A.4.2 Frames of Figure 6.13b

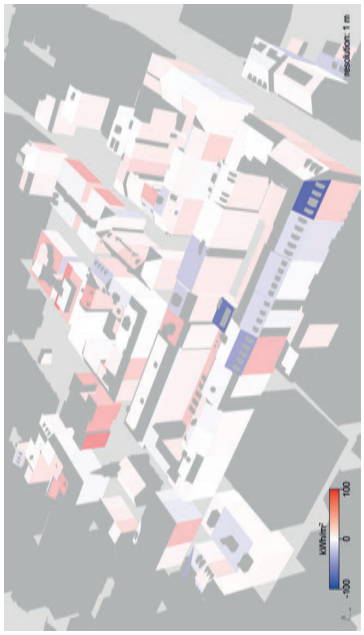

(a)

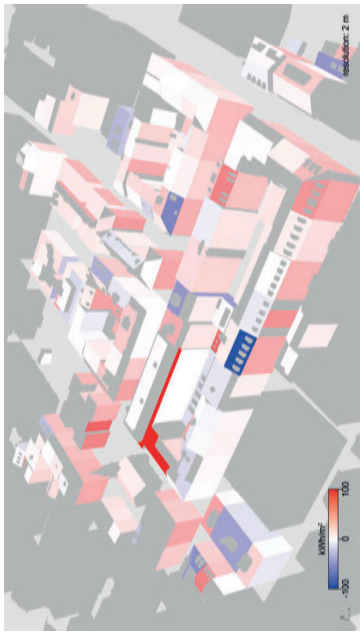

(b)

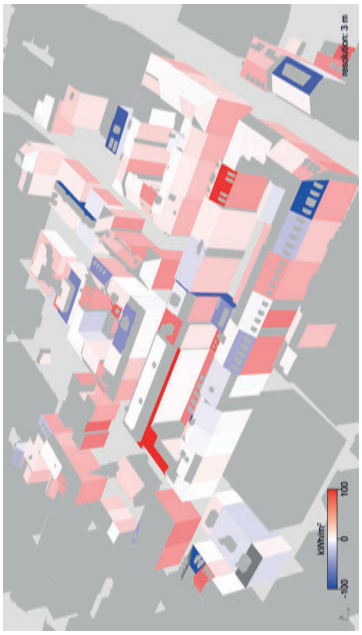

(c)

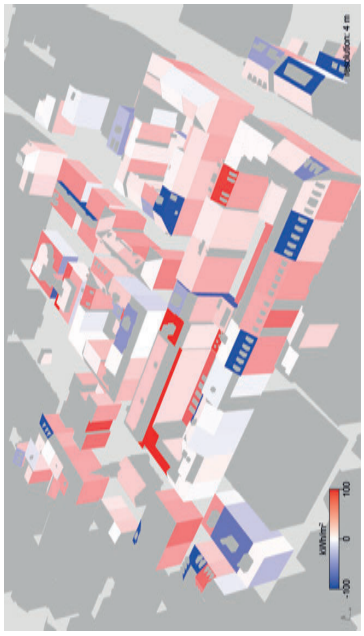

(d)

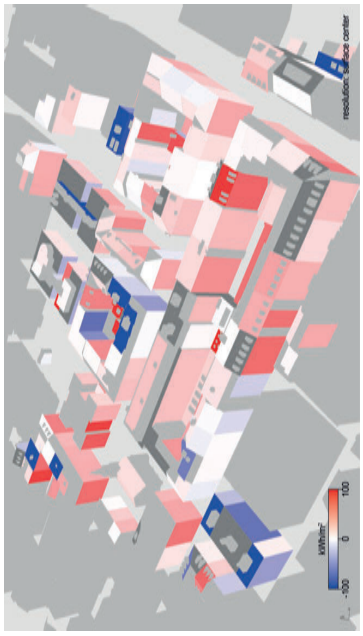

(e)

### A.4.3 Frames of Figure 11.16

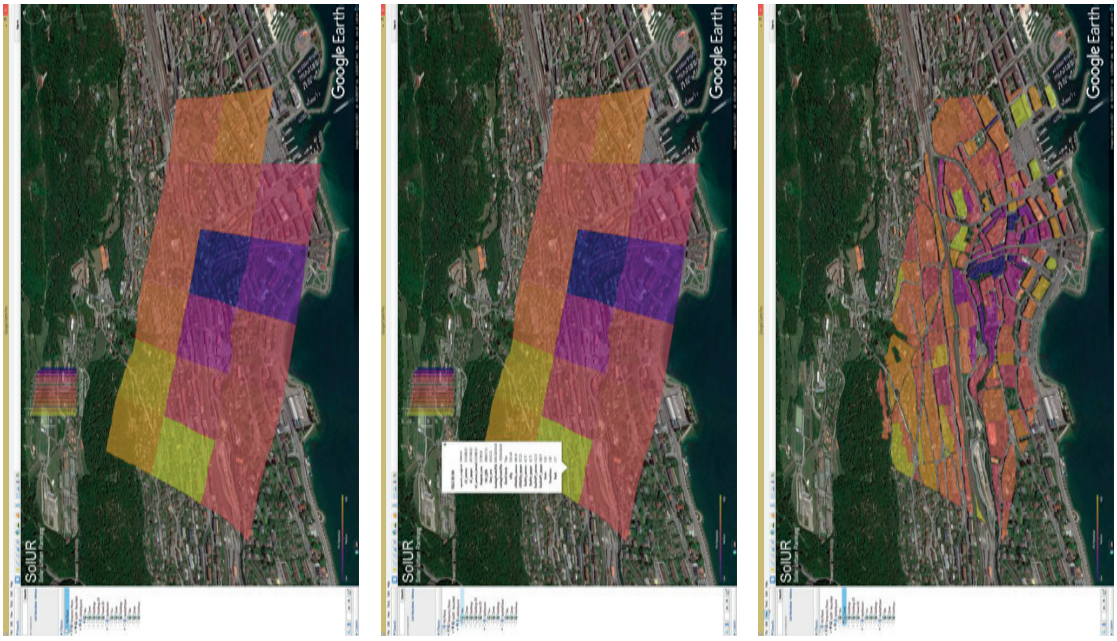


(a) (b) (c)

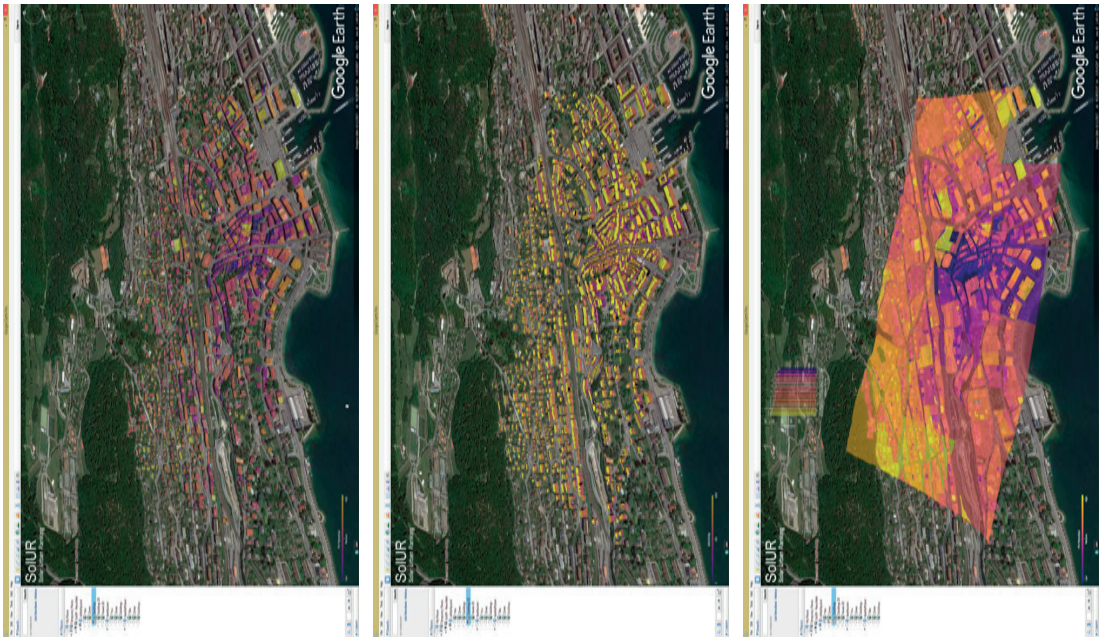


(d) (e) (f)

# Bibliography


[1] Andreas Abegg and Leonie Dörig. Die Erstellung von Solaranlagen auf oder im Umkreis von Schutzobjekten. *Energy Governance Working Paper*, 8, February 2017. doi: 10.21256/zhaw-1235. URL https://digitalcollection.zhaw.ch/handle/11475/1232.

[2] Acciona, Nobatek, and CEA. European regulatory framework for BIPV. Technical report, PVSITES Consortium, 2016.

[3] Ernst Basler + Partner AG. Das Gebäudeprogramm - Le Programme Bâtiments - Il Programma Edifici, 2014. URL http://www.dasgebaeudeprogramm.ch.

[4] Sergi Aguacil. *BIPV-driven refurbishment (provisional title)*. PhD thesis, Ecole polytechnique fédérale de Lausanne, Lausanne, 2019.

[5] Sergi Aguacil Moreno, Sophie Lufkin, and Emmanuel Rey. Towards integrated design strategies for implementing BIPV systems into urban renewal processes: preliminary case study in Neuchâtel (Switzerland). In *Proceedings of PLEA 2015*, Bologna, 2015.

[6] Sergi Aguacil Moreno, Sophie Lufkin, and Emmanuel Rey. Influence of energy-use scenarios in Life-Cycle Analysis of renovation projects with Building-Integrated Photovoltaics – Investigation through two case studies in Neuchâtel (Switzerland). In *Proceedings of the International Conference for Sustainable Design of the Built Environment 2017*, pages 1101–1112, 2017. URL https://infoscience.epfl.ch/record/233555.

[7] G. Agugiaro. From sub-optimal datasets to a CityGML-compliant 3d city model: experiences from Trento, Italy. *ISPRS - International Archives of the Photogrammetry, Remote Sensing and Spatial Information Sciences*, XL-4:7–13, April 2014. ISSN 2194-9034. doi: 10.5194/isprsarchives-XL-4-7-2014. URL http://www.int-arch-photogramm-remote-sens-spatial-inf-sci.net/XL-4/7/2014/.

[8] Giorgio Agugiaro, Joachim Benner, Piergiorgio Cipriano, and Romain Nouvel. The Energy Application Domain Extension for CityGML: enhancing interoperability for urban energy simulations. *Open Geospatial Data, Software and Standards*, 3(1):2, March 2018. ISSN 2363-7501. doi: 10.1186/s40965-018-0042-y. URL https://doi.org/10.1186/s40965-018-0042-y.

[9] Ali Aien, Mohsen Kalantari, Abbas Rajabifard, Ian Williamson, and Rohan Bennett. Utilising data modelling to understand the structure of 3d cadastres. *Journal of Spatial Science*, 58(2):215–234, September 2013. ISSN 1449-8596. doi: 10.1080/14498596.2013.801330. URL https://doi.org/10.1080/14498596.2013.801330.

[10] Ali Aien, Abbas Rajabifard, Mohsen Kalantari, and Ian Williamson. Review and Assessment of Current Cadastral Data Models for 3d Cadastral Applications. In *Advances in 3D Geoinformation*, Lecture Notes in Geoinformation and Cartography, pages 423–442. Springer, Cham, 2017. ISBN 978-3-319-25689-4 978-3-319-25691-7. doi: 10.1007/978-3-319-25691-7_24. URL https://link.springer.com/chapter/10.1007/978-3-319-25691-7_24.

[11] Nazmul Alam, Volker Coors, Sisi Zlatanova, and Peter van Oosterom. Resolution in photovoltaic potential computation. In *ISPRS Annals of Photogrammetry, Remote Sensing and Spatial Information Sciences*, volume IV-4-W1, pages 89–96, Split, Croatia, September 2016. Copernicus GmbH. doi: 10.5194/isprs-annals-IV-4-W1-89-2016. URL http://www.isprs-ann-photogramm-remote-sens-spatial-inf-sci.net/IV-4-W1/89/2016/.

[12] ARE. Raumkonzept Schweiz - Projet de Territoire Suisse - Progetto territoriale Svizzera, December 2012.

[13] ASHRAE. International weather for energy calculations (IWEC weather files), 2001.

[14] ASHRAE. International weather for energy calculations (IWEC weather files), v 2.0, 2012.

[15] Lydie Bahjejian. Patrimoine architectural et photovoltaïque: le chemin du dialogue. *Système solaires : le journal des énergies renouvelables*, 204:48–53, 2011.

[16] Priji Balakrishnan and J Alstan Jakubiec. Measuring Light Through Trees for Daylight Simulations: A Photographic and Photometric method. In *Proceedings of BSO2016*, page 9, Newcastle, United Kingdom, 2016.

[17] Tomas Balezentis and Dalia Streimikiene. Multi-criteria ranking of energy generation scenarios with Monte Carlo simulation. *Applied Energy*, 185, Part 1:862–871, January 2017. ISSN 0306-2619. doi: 10.1016/j.apenergy.2016.10.085. URL http://www.sciencedirect.com/science/article/pii/S0306261916315306.

[18] C. Bradford Barber, David P. Dobkin, and Hannu Huhdanpaa. The Quickhull Algorithm for Convex Hulls. *ACM Trans. Math. Softw.*, 22(4):469–483, December 1996. ISSN 0098-3500. doi: 10.1145/235815.235821. URL http://doi.acm.org/10.1145/235815.235821.

[19] Mike Barker, Tymandra Blewett-Silcock, Koen Eising, Marcel Gutschner, Elisabeth Kjellsson, Elvira Lutter, Stefan Nowak, Koem Steemers, and Gianluca Tondi. Solar ElectriCity Guide. Technical report, Institut Cerdà, Barcelona, 2001. URL http://ec.europa.eu/energy/renewables/solar_electricity/doc/pv_city_guide.pdf.

[20] Benoit Beckers, Luc Masset, and Pierre Beckers. Una proyección sintética para el diseño arquitectónico con la luz del sol. October 2007. URL https://orbi.uliege.be/handle/2268/15124.

[21] Benoit Beckers, Diana Rodríguez, Eduard Antaluca, and Jean-Louis Batoz. About solar energy simulation in the urban framework: The model of Compiegne. In *3rd International Congress Bauhass SOLAR*, pages 10–11, 2010.

[22] Eduardo Berlin, Christoph Reinhart, Alstan Jakubiec, and Nicolás Waissbluth. Mapdwell, 2013. URL http://www.mapdwell.com/en.

[23] Gonzalo Besuievsky, Santiago Barroso, Benoit Beckers, and Gustavo Patow. A Configurable LoD for Procedural Urban Models intended for Daylight Simulation. In Gonzalo Besuievsky and Vincent Tourre, editors, *Eurographics Workshop on Urban Data Modelling and Visualisation*, Strasbourg, 2014. The Eurographics Association. ISBN 978-3-905674-49-1. doi: 10.2312/udmv.20141073.

[24] BFE-OFEN-UFE. Principali novità del diritto in materia di energia dal 2018, February 2017.

[25] BFE-OFEN-UFE. Parc immobilier 2050 – Vision de l'OFEN, January 2018. URL http://www.bfe.admin.ch/themen/00507/00607/index.html?lang=fr&dossier_id=07007.

[26] Filip Biljecki. *Level of detail in 3D city models*. PhD thesis, Delft University of Technology, Delft, The Netherlands, 2017. URL doi:10.4233/uuid:f12931b7-5113-47ef-bfd4-688aae3be248. OCLC: 986240706.

[27] Filip Biljecki, Hugo Ledoux, Jantien Stoter, and Junqiao Zhao. Formalisation of the level of detail in 3d city modelling. *Computers, Environment and Urban Systems*, 48:1–15, November 2014. ISSN 0198-9715. doi: 10.1016/j.compenvurbsys.2014.05.004. URL http://www.sciencedirect.com/science/article/pii/S0198971514000519.

[28] Filip Biljecki, Gerard B. M. Heuvelink, Hugo Ledoux, and Jantien Stoter. Propagation of positional error in 3d GIS: estimation of the solar irradiation of building roofs. *International Journal of Geographical Information Science*, 29(12):2269–2294, August 2015. ISSN 1365-8816. doi: 10.1080/13658816.2015.1073292. URL http://dx.doi.org/10.1080/13658816.2015.1073292.

[29] Filip Biljecki, Jantien Stoter, Hugo Ledoux, Sisi Zlatanova, and Arzu Çöltekin. Applications of 3d City Models: State of the Art Review. *ISPRS International Journal of Geo-Information*, 4(4):2842–2889, December 2015. doi: 10.3390/ijgi4042842. URL http://www.mdpi.com/2220-9964/4/4/2842.

[30] Filip Biljecki, Hugo Ledoux, and Jantien Stoter. An improved LOD specification for 3d building models. *Computers, Environment and Urban Systems*, 59:25–37, September 2016. ISSN 0198-9715. doi: 10.1016/j.compenvurbsys.2016.04.005. URL http://www.sciencedirect.com/science/article/pii/S0198971516300436.

[31] Stéphane Bonjour and Jérémie Stoeckli. *The influence of the Level of Detail (LOD) and the surrounding materials reflectance on the assessment of the photovoltaic potential in urban environments*. Semester project report, Ecole polytechnique fédérale de Lausanne, Lausanne, January 2016.

[32] J.P. Brans. L'ingénierie de la decision. Elaboration dinstruments daide a la decision. Methode PROMETHEE. *Laide a La Decision: Nature, Instrument Set Perspectives Davenir*, pages 183–214, 1982.

[33] M. Breheny. Centrists, decentrists and compromisers: views on the future of urban form. In M. Jenks, E. Burton, and K. Williams, editors, *The Compact City. A Sustainable Urban Form?*, pages 13–35. Oxford Brookes University, Oxford, 1996.

[34] M. Bremer, A. Mayr, V. Wichmann, K. Schmidtner, and M. Rutzinger. A new multi-scale 3d-GIS-approach for the assessment and dissemination of solar income of digital city models. *Computers, Environment and Urban Systems*, 57:144–154, May 2016. ISSN 0198-9715. doi: 10.1016/j.compenvurbsys.2016.02.007. URL http://www.sciencedirect.com/science/article/pii/S0198971516300151.

[35] Claus Brenner. Building reconstruction from images and laser scanning. *International Journal of Applied Earth Observation and Geoinformation*, 6(3):187–198, March 2005. ISSN 0303-2434. doi: 10.1016/j.jag.2004.10.006. URL http://www.sciencedirect.com/science/article/pii/S030324340400087X.

[36] M. C. Brito, S. Freitas, S. Guimarães, C. Catita, and P. Redweik. The importance of facades for the solar PV potential of a Mediterranean city using LiDAR data. *Renewable Energy*, 111:85–94, October 2017. ISSN 0960-1481. doi: 10.1016/j.renene.2017.03.085. URL http://www.sciencedirect.com/science/article/pii/S0960148117302768.

[37] D. L. Bätzner, Y. Andrault, L. Andreetta, A. Büchel, W. Frammelsberger, C. Guerin, N. Holm, D. Lachenal, J. Meixenberger, P. Papet, B. Rau, B. Strahm, G. Wahli, and F. Wünsch. Properties of high efficiency silicon heterojunction cells. *Energy Procedia*, 8:153–159, 2011. ISSN 1876-6102. doi: 10.1016/j.egypro.2011.06.117. URL http://www.sciencedirect.com/science/article/pii/S1876610211016262.

[38] Bastian Burger and Monika Hall. PVopti – hourly based energy balance for building design. In *Energy Procedia*, volume 122 of *CISBAT 2017 International ConferenceFuture Buildings & Districts – Energy Efficiency from Nano to Urban Scale*, pages 769–774, September 2017. doi: 10.1016/j.egypro.2017.07.394. URL http://www.sciencedirect.com/science/article/pii/S1876610217329983.

[39] Jadranka Cace, Emil ter Horst, Katerina Syngellakis, Maíte Niel, Patrick Clement, Renate Heppener, and Eric Peirano. Urban wind turbines: guidelines for small wind turbines in the built environment. Technical report, WINEUR project (Wind Energy Integration in the Urban Environment), 2007. URL https://inis.iaea.org/search/search.aspx?orig_q=RN:40066905.

[40] Guido Calabresi and Philip Bobbitt. *Tragic Choices*. Norton, 1978. ISBN 978-0-393-05649-5. Google-Books-ID: 2CJwQgAACAAJ.

[41] Christopher P. Cameron, William E. Boyson, and Daniel M. Riley. Comparison of PV system performance-model predictions with measured PV system performance. In *Photovoltaic Specialists Conference, 2008. PVSC'08. 33rd IEEE*, pages 1–6. IEEE, 2008. URL http://ieeexplore.ieee.org/xpls/abs_all.jsp?arnumber=4922865.

[42] Xiaodong Cao, Xilei Dai, and Junjie Liu. Building energy-consumption status worldwide and the state-of-the-art technologies for zero-energy buildings during the past decade. *Energy and Buildings*, 128:198–213, September 2016. ISSN 0378-7788. doi: 10.1016/j.enbuild.2016.06.089. URL http://www.sciencedirect.com/science/article/pii/S0378778816305783.

[43] Massimiliano Capezzali and Gaëtan Cherix. Projet MEU : développer un outil qui réponde aux besoins des villes pour une planification performante des systèmes énérgetiques urbains. 2011.

[44] Nunzia Carbonara and Roberta Pellegrino. Public-private partnerships for energy efficiency projects: A win-win model to choose the energy performance contracting structure. *Journal of Cleaner Production*, 170:1064–1075, January 2018. ISSN 0959-6526. doi: 10.1016/j.jclepro.2017.09.151. URL http://www.sciencedirect.com/science/article/pii/S0959652617321492.

[45] Claudio Magalhães Carneiro. *Extraction of Urban Environmental Quality Indicators using LIDAR-Based Digital Surface Models*. PhD thesis, Ecole polytechnique fédérale de Lausanne, Lausanne, 2011.

[46] Cláudio Carneiro, Eugenio Morello, and Gilles Desthieux. Assessment of Solar Irradiance on the Urban Fabric for the Production of Renewable Energy using LIDAR Data and Image Processing Techniques. In Prof Monika Sester, Prof Lars Bernard, and Prof Volker Paelke, editors, *Advances in GIScience*, Lecture Notes in Geoinformation and Cartography, pages 83–112. Springer Berlin Heidelberg, January 2009. ISBN 978-3-642-00317-2 978-3-642-00318-9. URL http://link.springer.com/chapter/10.1007/978-3-642-00318-9_5.

[47] Cláudio Carneiro, Eugenio Morello, and Gilles Desthieux. Solar radiation over the urban texture: LIDAR Data and image Processing Techniques for environmental analysis at city scale. In Jiyeong Lee and Sisi Zlatanova, editors, *3D Geo-Information Sciences*, pages 319–340. Springer, 2009. URL http://link.springer.com/content/pdf/10.1007/978-3-540-87395-2_20.pdf.

[48] Craig Casey and Richard Mistrick. Simulation Tools for Architectural Daylighting and Integrated Controls (STADIC) - Utilities, August 2015. URL https://www.radiance-online.org/community/workshops/2015-philadelphia/presentations/day1/STADICUtilities-Radiance%20Workshop2015.pdf.

[49] C. Catita, P. Redweik, J. Pereira, and M. C. Brito. Extending solar potential analysis in buildings to vertical facades. *Computers & Geosciences*, 66:1–12, May 2014. ISSN 0098-3004. doi: 10.1016/j.cageo.2014.01.002. URL http://www.sciencedirect.com/science/article/pii/S0098300414000053.

[50] T. Cebecauer and M. Suri. Typical Meteorological Year Data: SolarGIS Approach. *Energy Procedia*, 69:1958–1969, May 2015. ISSN 1876-6102. doi: 10.1016/j.egypro.2015.03.195. URL http://www.sciencedirect.com/science/article/pii/S1876610215005019.

[51] CEC. California Energy Commission - Database of PV modules, January 2018. URL http://www.gosolarcalifornia.ca.gov/equipment/pv_modules.php.

[52] North Carolina Solar Center. Integrating Solar PV Into Energy Services Performance Contracts: Options for Local Governments Nationwide. Technical report, U.S. Department of Energy - SunShot Outreach Partnership, 2014. URL https://energy.gov/eere/solarpoweringamerica/integrating-solar-pv-energy-services-performance-contracts-options-local-governments-nationwide.

[53] Carlos Cerezo, Christoph Reinhart, and Jamie Bemis. Modeling Boston: A workflow for the generation of complete urban building energy demand models from existing urban geospatial datasets. Technical report, MIT, 2015. URL http://web.mit.edu/SustainableDesignLab/projects/BostonEnergyModel/_doc/CWES_MIT_SDL_NOV15.pdf.

[54] Giorgia Chinazzo. Refurbishment of Existing Envelopes in Residential Buildings: assessing robust solutions for future climate change. Master's thesis, EPFL, Lausanne, Switzerland, 2014. URL http://infoscience.epfl.ch/record/203438.

[55] Yosoon Choi, Jeffrey Rayl, Charith Tammineedi, and Jeffrey R. S. Brownson. PV Analyst: Coupling ArcGIS with TRNSYS to assess distributed photovoltaic potential in urban areas. *Solar Energy*, 85(11):2924–2939, November 2011. ISSN 0038-092X. doi: 10.1016/j.solener.2011.08.034. URL http://www.sciencedirect.com/science/article/pii/S0038092X11003070.

[56] T. J. Chung. *Computational Fluid Dynamics*. Cambridge University Press, 2002. doi: 10.1017/CBO9780511606205.

[57] Ekatina Chuprikova. An Assessment of the Solar Potential of Roofs within a Web-based Solar Cadastre. Case Study: Bolzano and Bressanone, Italy. Master's thesis, Technische Universität Wien, 2014. URL http://cartographymaster.eu/wp-content/theses/2014_Chuprikova_Thesis.pdf.

[58] Silvia Coccolo, David Pearlmutter, Jerome Kaempf, and Jean-Louis Scartezzini. Thermal Comfort Maps to estimate the impact of urban greening on the outdoor human comfort. *Urban Forestry & Urban Greening*, August 2018. ISSN 1618-8667. doi: 10.1016/j.ufug.2018.08.007. URL http://www.sciencedirect.com/science/article/pii/S1618866718300189.

[59] R. Compagnon. Solar and daylight availability in the urban fabric. *Energy and Buildings*, 36(4):321–328, April 2004. ISSN 0378-7788. doi: 10.1016/j.enbuild.2004.01.009.

[60] Daniele Condorelli. What Money Can't Buy: Allocations with Priority Lists, Lotteries and Queues. SSRN Scholarly Paper ID 1420899, Social Science Research Network, Rochester, NY, June 2009. URL https://papers.ssrn.com/abstract=1420899.

[61] Daniele Condorelli. What money can't buy: Efficient mechanism design with costly signals. *Games and Economic Behavior*, 75(2):613–624, July 2012. ISSN 0899-8256. doi: 10.1016/j.geb.2012.02.018. URL http://www.sciencedirect.com/science/article/pii/S0899825612000395.

[62] V. Costanzo, R. Yao, E. Essah, L. Shao, M. Shahrestani, A. C. Oliveira, M. Araz, A. Hepbasli, and E. Biyik. A method of strategic evaluation of energy performance of Building Integrated Photovoltaic in the urban context. *Journal of Cleaner Production*, 184:82–91, May 2018. ISSN 0959-6526. doi: 10.1016/j.jclepro.2018.02.139. URL http://www.sciencedirect.com/science/article/pii/S0959652618304517.

[63] Swiss Federal Council. Message relatif au premier paquet de mesures de la Stratégie énergétique 2050, September 2013. URL https://www.admin.ch/opc/fr/federal-gazette/2013/6771.pdf.

[64] CPUC. California Solar Initiative Program Handbook, 2017. URL http://www.gosolarcalifornia.ca.gov/documents/CSI_HANDBOOK.PDF.

[65] Declan G. De Paor, Steven J. Whitmeyer, and Callan Bentley. CESIUM — A virtual globe with strong potential applications in geoscience education. In *Geological Society of America Abstracts with Programs*, Albany, New York, 2016. The Geological Society of America (GSA). doi: 10.1130/abs/2016NE-272098. URL https://gsa.confex.com/gsa/2016NE/webprogram/Paper272098.html.

[66] W. De Soto, S. A. Klein, and W. A. Beckman. Improvement and validation of a model for photovoltaic array performance. *Solar Energy*, 80(1):78–88, January 2006. ISSN 0038-092X. doi: 10.1016/j.solener.2005.06.010. URL http://www.sciencedirect.com/science/article/pii/S0038092X05002410.

[67] Jesse Dean, Alicen Kandt, Kari Burman, Lars Lisell, and Christopher Helm. Analysis of web-based solar photovoltaic mapping tools. In *ASME 2009 3rd International Conference on Energy Sustainability collocated with the Heat Transfer and InterPACK09 Conferences*, pages 85–96. American Society of Mechanical Engineers, 2009.

[68] Jean-Jaques Delaunay, Jan Wienold, and Wendelin Sprenger. gendaylit, 1994. URL https://www.radiance-online.org//learning/documentation/manual-pages/pdfs/gendaylit.pdf.

[69] Gilles Desthieux, Claudio Carneiro, Reto Camponovo, Pierre Ineichen, Eugenio Morello, Anthony Boulmier, Nabil Abdennadher, Sébastien Dervey, and Christoph Ellert. Solar Energy Potential Assessment on Rooftops and Facades in Large Built Environments Based on LiDAR Data, Image Processing, and Cloud Computing. Methodological Background, Application, and Validation in Geneva (Solar Cadaster). *Frontiers in Built Environment*, 4, 2018. ISSN 2297-3362. doi: 10.3389/fbuil.2018.00014. URL https://www.frontiersin.org/articles/10.3389/fbuil.2018.00014/full.

[70] DIM-SEMO. Bâti 3d Spécifications techniques, 2008. URL http://ge.ch/sitg/geodata/SITG/CATALOGUE/INFORMATIONS_COMPLEMENTAIRES/BATI_3D_SPECIFICATIONS_TECHNIQUES.pdf.

[71] A. P. Dobos, Paul Gilman, and Michael Kasberg. P50/P90 Analysis for Solar Energy Systems Using the System Advisor Model. In *Proceedings of the WREF 2012*. National Renewable Energy Laboratory (NREL), Golden, CO., 2012.

[72] Aron P. Dobos. An Improved Coefficient Calculator for the California Energy Commission 6 Parameter Photovoltaic Module Model. *Journal of Solar Energy Engineering*, 134(2):021011–021011–6, March 2012. ISSN 0199-6231. doi: 10.1115/1.4005759. URL http://dx.doi.org/10.1115/1.4005759.

[73] Aron P. Dobos. PVWatts version 5 manual. Technical report, National Renewable Energy Laboratory (NREL), Golden, CO., 2014.

[74] Swapnil Dubey, Jatin Narotam Sarvaiya, and Bharath Seshadri. Temperature Dependent Photovoltaic (PV) Efficiency and Its Effect on PV Production in the World – A Review. *Energy Procedia*, 33:311–321, 2013. ISSN 1876-6102. doi: 10.1016/j.egypro.2013.05.072. URL http://www.sciencedirect.com/science/article/pii/S1876610213000829.

[75] DVRPC. Renewable Energy Ordinance Framework - Solar PV (Draft). Technical report, Delaware Valley Regional Planning Commission, 2015. URL https://www.dvrpc.org/EnergyClimate/ModelOrdinance/Solar/pdf/2016_DVRPC_Solar_REOF_Reformatted_Final.pdf.

[76] H. Edelsbrunner, D. Kirkpatrick, and R. Seidel. On the shape of a set of points in the plane. *IEEE Transactions on Information Theory*, 29(4):551–559, July 1983. ISSN 0018-9448. doi: 10.1109/TIT.1983.1056714.

[77] Herbert Edelsbrunner and Ernst P. Mücke. Three-dimensional Alpha Shapes. *ACM Trans. Graph.*, 13(1): 43–72, January 1994. ISSN 0730-0301. doi: 10.1145/174462.156635. URL http://doi.acm.org/10.1145/174462.156635.

[78] Ursula Eicker, Romain Nouvel, Eric Duminil, and Volker Coors. Assessing Passive and Active Solar Energy Resources in Cities Using 3d City Models. In *Energy Procedia*, volume 57 of *2013 ISES Solar World Congress*, pages 896–905, January 2014. doi: 10.1016/j.egypro.2014.10.299. URL http://www.sciencedirect.com/science/article/pii/S187661021401666X.

[79] john Elster. *Local justice. How institutions allocate scare goods and necessary burdens*. Russell Sage Foundation, New York, 1992.

[80] Joan Esteban and Debraj Ray. Inequality, Lobbying, and Resource Allocation. *American Economic Review*, 96(1): 257–279, March 2006. ISSN 0002-8282. doi: 10.1257/000282806776157533. URL https://www.aeaweb.org/articles?id=10.1257/000282806776157533.

[81] Karoline Fath, Julian Stengel, Wendelin Sprenger, Helen Rose Wilson, Frank Schultmann, and Tilmann E. Kuhn. A method for predicting the economic potential of (building-integrated) photovoltaics in urban areas based on hourly Radiance simulations. *Solar Energy*, 116:357–370, June 2015. ISSN 0038-092X. doi: 10.1016/j.solener.2015.03.023. URL http://www.sciencedirect.com/science/article/pii/S0038092X15001413.

[82] Bakhtiar Feizizadeh, Majid Shadman Roodposhti, Piotr Jankowski, and Thomas Blaschke. A GIS-based extended fuzzy multi-criteria evaluation for landslide susceptibility mapping. *Computers & Geosciences*, 73(Supplement C):208–221, December 2014. ISSN 0098-3004. doi: 10.1016/j.cageo.2014.08.001. URL http://www.sciencedirect.com/science/article/pii/S0098300414001873.

[83] Kaspar Fischer. Introduction to Alpha Shapes, 2000. URL https://graphics.stanford.edu/courses/cs268-11-spring/handouts/AlphaShapes/as_fisher.pdf.

[84] Pietro Florio, C. Roecker, M. C. Munari Probst, and Jean-Louis Scartezzini. *Visibility of Building Exposed Surfaces for the Potential Application of Solar Panels: A Photometric Model*. The Eurographics Association, 2016. ISBN 978-3-03868-013-0. URL https://diglib.eg.org:443/handle/10.2312/udmv20161419.

[85] Michal Fogl and Vítězslav Moudrý. Influence of vegetation canopies on solar potential in urban environments. *Applied Geography*, 66:73–80, January 2016. ISSN 0143-6228. doi: 10.1016/j.apgeog.2015.11.011. URL http://www.sciencedirect.com/science/article/pii/S0143622815300175.

[86] Jimeno A. Fonseca, Thuy-An Nguyen, Arno Schlueter, and Francois Marechal. City Energy Analyst (CEA): Integrated framework for analysis and optimization of building energy systems in neighborhoods and city districts. *Energy and Buildings*, 113:202–226, February 2016. ISSN 0378-7788. doi: 10.1016/j.enbuild.2015.11.055. URL http://www.sciencedirect.com/science/article/pii/S0378778815304199.

[87] Adrian Fozzard. *The Basic Budgeting Problem: Approaches to Resource Allocation in the Public Sector and their Implications for Pro-poor Budgeting*. Overseas Development Institute, London, 2001. ISBN 978-0-85003-527-8. OCLC: 778245627.

[88] S. Freitas, C. Catita, P. Redweik, and M. C. Brito. Modelling solar potential in the urban environment: State-of-the-art review. *Renewable and Sustainable Energy Reviews*, 41:915–931, January 2015. ISSN 1364-0321. doi: 10.1016/j.rser.2014.08.060. URL http://www.sciencedirect.com/science/article/pii/S1364032114007461.

[89] S. Freitas, F. Serra, and M. C. Brito. Pv layout optimization: String tiling using a multi-objective genetic algorithm. *Solar Energy*, 118:562–574, August 2015. ISSN 0038-092X. doi: 10.1016/j.solener.2015.06.018. URL http://www.sciencedirect.com/science/article/pii/S0038092X15003266.

[90] S. Freitas, T. Santos, and M.C. Brito. Sizing of Urban Distribution Transformers in a Neighbourhood with PV Generation and Energy Storage. *33rd European Photovoltaic Solar Energy Conference and Exhibition; 2761-2765*, 2017. doi: 10.4229/eupvsec20172017-6bv.3.95. URL http://www.eupvsec-proceedings.com/proceedings?paper=43782.

[91] S. Freitas, C. Reinhart, and M. C. Brito. Minimizing storage needs for large scale photovoltaics in the urban environment. *Solar Energy*, 159:375–389, January 2018. ISSN 0038-092X. doi: 10.1016/j.solener.2017.11.011. URL http://www.sciencedirect.com/science/article/pii/S0038092X1730991X.

[92] Rolf Frischknecht, René Itten, Franziska Wyss, Isabelle Blanc, Garvin Heath, Marco Raugei, Parikhit Sinha, and Andreas Wade. Life cycle assessment of future photovoltaic electricity production from residential-scale systems operated in Europe. Technical Report IEA-PVPS

Task 12, Subtask 2.0, LCA Report IEA-PVPS T12-05:2015, IEA, 2014.

[93] Pinde Fu and Paul M. Rich. A geometric solar radiation model and its applications in agriculture and forestry. In *Proceedings of the Second International Conference on Geospatial Information in Agriculture and Forestry*, volume 1, pages 357–364, 2000. URL http://solar.maps.umn.edu/assets/pdf/fu_rich_2000.pdf.

[94] Luc Girardin, François Marechal, Matthias Dubuis, Nicole Calame-Darbellay, and Daniel Favrat. EnerGis: A geographical information based system for the evaluation of integrated energy conversion systems in urban areas. *Energy*, 35(2):830–840, February 2010. ISSN 0360-5442. doi: 10.1016/j.energy.2009.08.018. URL http://www.sciencedirect.com/science/article/pii/S0360544209003582.

[95] R Giridharan, S Ganesan, and S. S. Y Lau. Daytime urban heat island effect in high-rise and high-density residential developments in Hong Kong. *Energy and Buildings*, 36(6):525–534, June 2004. ISSN 0378-7788. doi: 10.1016/j.enbuild.2003.12.016. URL http://www.sciencedirect.com/science/article/pii/S0378778804000684.

[96] Adolf Goetzberger and Volker Uwe Hoffmann. *Photovoltaic Solar Energy Generation*. Springer Series in Optical Sciences. Springer-Verlag, Berlin Heidelberg, 2005. ISBN 978-3-540-23676-4. URL //www.springer.com/la/book/9783540236764.

[97] Clara Good, Jinfeng Chen, Yanjun Dai, and Anne Grete Hestnes. Hybrid Photovoltaic-thermal Systems in Buildings – A Review. *Energy Procedia*, 70:683–690, May 2015. ISSN 18766102. doi: 10.1016/j.egypro.2015.02.176. URL http://linkinghub.elsevier.com/retrieve/pii/S1876610215002982.

[98] Brian Goss, Ian Cole, Thomas Betts, and Ralph Gottschalg. Irradiance modelling for individual cells of shaded solar photovoltaic arrays. *Solar Energy*, 110:410–419, December 2014. ISSN 0038-092X. doi: 10.1016/j.solener.2014.09.037. URL http://www.sciencedirect.com/science/article/pii/S0038092X14004770.

[99] Chris Gueymard and José A. Ruiz-Arias. Performance of Separation Models to Predict Direct Irradiance at High Frequency: Validation over Arid Areas. In *Proceedings of Eurosun 2015*, pages 1–10. International Solar Energy Society, 2015. ISBN 978-3-9814659-3-8. doi: 10.18086/eurosun.2014.08.06. URL http://proceedings.ises.org/citation?doi=eurosun.2014.08.06.

[100] Sandeep Gupta, Holger Weinacker, and Barbara Koch. Comparative Analysis of Clustering-Based Approaches for 3-D Single Tree Detection Using Airborne Fullwave Lidar Data. *Remote Sensing*, 2(4):968–989, April 2010. doi: 10.3390/rs2040968. URL http://www.mdpi.com/2072-4292/2/4/968.

[101] Aron Habte, Thomas Stoffel, Richard Perez, Daryl Myers, Christian Gueymard, Philippe Blanc, and Stefan Wilbert. Overview of solar radiation resource concepts. In *Best Practices Handbook for the Collection and Use of Solar Resource Data for Solar Energy Applications*. NREL, December 2017. doi: 10.2172/1411856. URL http://www.osti.gov/servlets/purl/1411856/.

[102] Monika Hall, Bastian Burger, and Achim Geissler. Entwicklung eines Planungsinstruments zur Bestimmung der Netzinteraktion von Gebäuden. In . *September*, page 16, 2016.

[103] Amina Harzallah. *Émergence et évolution des préconisations solaires dans les théories architecturales et urbaines en France, de la seconde moitié du XIXe siècle à la deuxième guerre mondiale*. PhD thesis, Ecole nationale supérieure d'architecture de Nantes, Nantes, 2007. Thèse de doctorat discipline science de l'ingénieur spécialité architecture soutenue le 11 janvier 2007 à l'École nationale supérieure d'architecture de Nantes, Laboratoire CERMA, UMR-CNRS 1563.

[104] John E. Hay. Calculation of monthly mean solar radiation for horizontal and inclined surfaces. *Solar Energy*, 23(4):301–307, January 1979. ISSN 0038-092X. doi: 10.1016/0038-092X(79)90123-3. URL http://www.sciencedirect.com/science/article/pii/0038092X79901233.

[105] Heinrich Häberlin. *Photovoltaics System Design and Practice*. John Wiley & Sons, Chichester, UK, January 2012. ISBN 978-1-119-97838-1. URL http://dx.doi.org/10.1002/9781119976998.

[106] Hans Karl Heidemann. Lidar base specification (ver. 1.3, February 2018). In *U.S. Geological Survey Techniques and Methods, book 11, chap. B4*, page 101. U.S. Department of the Interior U.S. Geological Survey, 2018. URL https://doi.org/10.3133/tm11b4.

[107] Peter Hettich and Gian Luca Peng. Erleichterte Bewilligung von Solaranlagen in der Rechtspraxis : gut gemeint, wenig effektiv und verfassungsrechtlich fragwürdig. *Aktuelle Juristische Praxis AJP*, 24(10):1427–1438, November 2015. ISSN 1660-3362. URL https://www.alexandria.unisg.ch/245718/.

[108] Bernd Hirschl. *Acceptability of solar power systems a study on acceptability of photovoltaics with special regard to the role of design*. IÖW, Berlin, 2005. ISBN 978-3-932092-81-7.

[109] Jaroslav Hofierka and Ján Kaňuk. Assessment of photovoltaic potential in urban areas using open-source solar radiation tools. *Renewable Energy*, 34(10):2206–2214, October 2009. ISSN 0960-1481. doi: 10.1016/j.renene.2009.02.021. URL http://www.sciencedirect.com/science/article/pii/S0960148109000949.

[110] Jaroslav Hofierka and Marian Zlocha. A New 3-D Solar Radiation Model for 3-D City Models: New 3-D Solar Radiation Model. *Transactions in GIS*, 16(5):681–690, October 2012. ISSN 13611682. doi: 10.1111/j.1467-9671.2012.01337.x. URL http://doi.wiley.com/10.1111/j.1467-9671.2012.01337.x.

[111] W. F. Holmgren and D. G. Groenendyk. An open source solar power forecasting tool using PVLIB-Python. In *2016 IEEE 43rd Photovoltaic Specialists Conference (PVSC)*, pages 0972–0975, June 2016. doi: 10.1109/PVSC.2016.7749755.

[112] W. F. Holmgren, R. W. Andrews, A. T. Lorenzo, and J. S. Stein. PVLIB Python 2015. In *2015 IEEE 42nd Photovoltaic Specialist Conference (PVSC)*, pages 1–5, June 2015. doi: 10.1109/PVSC.2015.7356005.

[113] Tianzhen Hong, Yixing Chen, Sang Hoon Lee, and Mary Ann Piette. CityBES: A web-based platform to support city-scale building energy efficiency. *Urban Computing*, 2016.

[114] Christiana Honsberg and Stuart Bowden. PVeducation.org, 2018. URL www.pveducation.org.

[115] E. Howard. *Garden Cities of Tomorrow*. Swan Sonnenschein & Company, Limited, London, 1902. URL https://archive.org/details/gardencitiestom00howagoog.

[116] Chiung-Wen Hsu. Using a system dynamics model to assess the effects of capital subsidies and feed-in tariffs on solar PV installations. *Applied Energy*, 100:205–217, December 2012. ISSN 0306-2619. doi: 10.1016/j.apenergy.2012.02.039. URL http://www.sciencedirect.com/science/article/pii/S0306261912001389.

[117] Y. J. Huang, H. Akbari, H. Taha, and A. H. Rosenfeld. The Potential of Vegetation in Reducing Summer Cooling Loads in Residential Buildings. *Journal of Climate and Applied Meteorology*, 26(9):1103–1116, September 1987. ISSN 0733-3021. doi: 10.1175/1520-0450(1987)026<1103:TPOVIR>2.0.CO;2. URL https://journals.ametsoc.org/doi/abs/10.1175/1520-0450%281987%29026%3C1103%3ATPOVIR%3E2.0.CO%3B2.

[118] Gianluca Iaccarino. Quantification of uncertainty in flow simulations using probabilistic methods. Technical report, DTIC Document, 2009. URL http://oai.dtic.mil/oai/oai?verb=getRecord&metadataPrefix=html&identifier=ADA568130.

[119] IEA. Potential for Building Integrated Photovoltaics. Full Technical Report PVPS T7- 4, International Energy Agency, 2002.

[120] IESNA. IES LM-83-12 IES Spatial Daylight Autonomy (sDA) and Annual Sunlight Exposure (ASE). Technical Report IES LM-83-12, Illuminating Engineering Society of North America, New York, NY, USA, 2012.

[121] IPCC. Special Report, on Global Warming of 1.5 °C. Technical report, IPCC, Incheon, Republic of Korea, October 2018.

[122] Fraunhofer ISE. Photovoltaics Report. Technical report, Fraunhofer-Institut für Solare Energiesysteme ISE, 2018. URL https://www.ise.fraunhofer.de/content/dam/ise/de/documents/publications/studies/Photovoltaics-Report.pdf.

[123] T. F. Ishugah, Y. Li, R. Z. Wang, and J. K. Kiplagat. Advances in wind energy resource exploitation in urban environment: A review. *Renewable and Sustainable Energy Reviews*, 37:613–626, September 2014. ISSN 1364-0321. doi: 10.1016/j.rser.2014.05.053. URL http://www.sciencedirect.com/science/article/pii/S1364032114003785.

[124] J. E. Jackson and J. W. Palmer. A Simple Model of Light Transmission and Interception by Discontinuous Canopies. *Annals of Botany*, 44(3):381–383, September 1979. ISSN 1095-8290, 0305-7364. doi: 10.1093/oxfordjournals.aob.a085744. URL https://academic.oup.com/aob/article/154349/A.

[125] J. Jacobs. *The death and life of great American cities*. Random House, New York, 1961.

[126] Abdul Qayoom Jakhrani, Al-Khalid Othman, Andrew Ragai Henry Rigit, and Saleem Raza Samo. Determination and comparison of different photovoltaic module temperature models for Kuching, Sarawak. In *Clean Energy and Technology (CET), 2011 IEEE First Conference on*, pages 231–236. IEEE, 2011. URL http://ieeexplore.ieee.org/xpls/abs_all.jsp?arnumber=6041469.

[127] Martin Jakob. Marginal costs and co-benefits of energy efficiency investments: The case of the Swiss residential sector. *Energy Policy*, 34(2):172–187, January 2006. ISSN 0301-4215. doi: 10.1016/j.enpol.2004.08.039. URL http://www.sciencedirect.com/science/article/pii/S030142150400271X.

[128] Martin Jakob, Sonja Kallio, Claudio Nägeli, Walter Ott, Roman Bollinger, and Stefan von Grünigen. Integrated Strategies and Policy Instruments for Retrofitting Buildings to reduce Primary Energy Use and GHC emissions (INSPIRE). Final Report, Swiss Federal Office of Energy, 2014.

[129] Alstan Jakubiec and Christoph F. Reinhart. DIVA 2.0: integrating daylight and thermal simulations using Rhinoceros 3d, DAYSIM and EnergyPlus. In *Proceedings of BS2011*, pages 2202–2209, Sidney, Australia, 2011. IBPSA.

[130] J. Jakubiec and Christoph Reinhart. Assessing Disability Glare Potential of Reflections from New Construction. *Transportation Research Record: Journal of the Transportation Research Board*, 2449:114–122, December 2014. ISSN 0361-1981. doi: 10.3141/2449-13. URL http://trrjournalonline.trb.org/doi/abs/10.3141/2449-13.

[131] J. Alstan Jakubiec and Priji Balakrishnan. Quantifying Materials in Lighting Simulations, August 2015.

[132] J. Alstan Jakubiec and Christoph F. Reinhart. A method for predicting city-wide electricity gains from photovoltaic panels based on LiDAR and GIS data combined with hourly Daysim simulations. *Solar Energy*, 93:127–143, July 2013. ISSN 0038-092X. doi: 10.1016/j.solener.2013.03.022. URL http://www.sciencedirect.com/science/article/pii/S0038092X13001291.

[133] Ted James, Alan Goodrich, Michael Woodhouse, Robert Margolis, and Sean Ong. Building-Integrated Photovoltaics (BIPV) in the residential sector: an analysis of installed rooftop system prices. Technical Report NREL/TP-6A20-53103, National Renewable Energy Laboratory (NREL), Golden, CO, USA, November 2011.

[134] Bjørn Petter Jelle, Christer Breivik, and Hilde Drolsum Røkenes. Building integrated photovoltaic products: A state-of-the-art review and future research opportunities. *Solar Energy Materials and Solar Cells*, 100:69–96, May 2012. ISSN 09270248. doi: 10.1016/j.solmat.2011.12.016. URL http://linkinghub.elsevier.com/retrieve/pii/S0927024811006970.

[135] M. Jenks, E. Burton, and K. Williams, editors. *The Compact City. A Sustainable Urban Form?* Oxford Brookes University, Oxford, 1996.

[136] Christoph Jäger. Installations solaires: un premier commentaire du nouvel article 18a LAT. *Territoire & Environnement*, 6:2–22, 2014.

[137] A. Jochem, B. Höfle, M. Hollaus, and M. Rutzinger. Object detection in airborne LIDAR data for improved solar radiation modeling in urban areas. In *Proceedings of Laser scanning '09*, volume 38 prt 3/W8, Paris, 2009. ISPRS. URL https://research.utwente.nl/en/publications/object-detection-in-airborne-lidar-data-for-improved-solar-radiat.

[138] Martin Kada and Laurence McKinley. 3d building reconstruction from LiDAR based on a cell decomposition approach. *International Archives of Photogrammetry, Remote Sensing and Spatial Information Sciences*, 38(Part 3):W4, 2009. URL http://www.pf.bgu.tum.de/isprs/cmrt09/pub/CMRT09_Kada_McKinley.pdf.

[139] Daniel M. Kammen and Deborah A. Sunter. City-integrated renewable energy for urban sustainability. *Science*, 352(6288):922–928, May 2016. ISSN 0036-8075, 1095-9203. doi: 10.1126/science.aad9302. URL http://science.sciencemag.org/content/352/6288/922.

[140] Jouri Kanters, Maria Wall, and Elisabeth Kjellsson. The Solar Map as a Knowledge Base for Solar Energy Use. *Energy Procedia*, 48:1597–1606, 2014. ISSN 1876-6102. doi: 10.1016/j.egypro.2014.02.180. URL http://www.sciencedirect.com/science/article/pii/S1876610214004421.

[141] Yuliya Karneyeva and Rolf Wüstenhagen. Solar feed-in tariffs in a post-grid parity world: The role of risk, investor diversity and business models. *Energy Policy*, 106:445–456, July 2017. ISSN 0301-4215. doi: 10.1016/j.enpol.2017.04.005. URL http://www.sciencedirect.com/science/article/pii/S0301421517302306.

[142] M. Karteris, Th. Slini, and A. M. Papadopoulos. Urban solar energy potential in Greece: A statistical calculation model of suitable built roof areas for photovoltaics. *Energy and Buildings*, 62:459–468, July 2013. ISSN 0378-7788. doi: 10.1016/j.enbuild.2013.03.033. URL http://www.sciencedirect.com/science/article/pii/S0378778813002016.

[143] Brian Kehoe. Getting Communities Up to Speed. *Plan on it. A Dutchess County Planning Federation eNewsletter*, October 2015.

[144] James Keirstead, Nouri Samsatly, and Nilay Shah. SynCity: an integrated tool kit for urban energy systems modelling. 2009. URL https://workspace.imperial.ac.uk/urbanenergysystems/public/URS_Keirstead2009.pdf.

[145] V. O. Key. The Lack of a Budgetary Theory. *American Political Science Review*, 34(6):1137–1144, December 1940. ISSN 1537-5943, 0003-0554. doi: 10.2307/1948194. URL https://www.cambridge.org/core/journals/american-political-science-review/article/the-lack-of-a-budgetary-theory/1F85359A51547F524B127D582FE876B8.

[146] Hla Hla Khaing, Yit Jian Liang, Nant Nyein Moe Htay, and Jiang Fan. Characteristics of Different Solar PV Modules under Partial Shading. *International Journal of Electrical, Computer, Electronics and Communication Engineering*, 8(9):1333–1337, 2014. URL http://www.waset.org/publications/9999229.

[147] Jad Khoury, Zeinab Alameddine, and Pierre Hollmuller. Understanding and bridging the energy performance gap in building retrofit. *Energy Procedia*, 122:217–222, 2017. ISSN 1876-6102. URL https://archive-ouverte.unige.ch/unige:97004.

[148] Yeonjoo Kim, Eun-Sung Chung, Sang-Mook Jun, and Sang Ug Kim. Prioritizing the best sites for treated wastewater instream use in an urban watershed using fuzzy TOPSIS. *Resources, Conservation and Recycling*, 73:23–32, April 2013. ISSN 0921-3449. doi: 10.1016/j.resconrec.2012.12.009. URL http://www.sciencedirect.com/science/article/pii/S0921344912002236.

[149] D. L. King, G. M. Galbraith, W. E. Boyson, S. Gonzalez, A. T. Murray, J. W. Ginn, and W. I. Bower. Array Performance Characterization and Modeling for Real-Time Performance Analysis of Photovoltaic Systems. In *2006 IEEE 4th World Conference on Photovoltaic Energy Conference*, volume 2, pages 2308–2311, May 2006. doi: 10.1109/WCPEC.2006.279634.

[150] David L. King, William Earl Boyson, and Jay A. Kratochvil. Photovoltaic array performance model. Technical Report SAN2004-3535, Sandia National Laboratories, 2004.

[151] Blaz Kirn, Kristijan Brecl, and Marko Topic. A new PV module performance model based on separation of diffuse and direct light. *Solar Energy*, 113:212–220, March 2015. ISSN 0038-092X. doi: 10.1016/j.solener.2014.12.029. URL http://www.sciencedirect.com/science/article/pii/S0038092X14006203.

[152] Daniel Klauser. Solarpotentialanalyse für Sonnendach.ch. Technical report, Metotest, 2016.

[153] Geoffrey T. Klise and Joshua S. Stein. Models Used to Assess the Performance of Photovoltaic Systems. Technical Report SAND2009-8258, Sandia National Laboratories, 2009.

[154] Jérôme Henri Kämpf. On the modelling and optimisation of urban energy fluxes. 2009. doi: 10.5075/epfl-thesis-4548,urn:nbn:ch:bel-epfl-thesis4548-9. URL https://infoscience.epfl.ch/record/141956.

[155] Ralph L. Knowles. *Sun Rhythm Form*. The MIT Press, Cambridge, MA, USA, 1981.

[156] Seiki Koma, Yuichiro Yamabe, and Akinori Tani. Research on urban landscape design using the interactive genetic algorithm and 3d images. *Visualization in Engineering*, 5:1, February 2017. ISSN 2213-7459. doi: 10.1186/s40327-016-0039-5. URL https://doi.org/10.1186/s40327-016-0039-5.

[157] Angela Köppl, Kathrin Reisberger, and Stefan Schelicher. National Renewable Energy Action Plan (NREAP-AT) - Progress Report 2011 for Austria under Directive 2009/28/EG. Technical report, Bundesministerium für Wirtschaft, Familie un Jugend, 2011. URL http://aei.pitt.edu/88662/1/article_22_austria_report_en.pdf.

[158] Ronald M. Kruhlak. A Legal Review of Access to Sunlight in Sunny Alberta. Technical report, The Alberta Environmental Research Trust, Edmonton, AB, Canada, 1981.

[159] K. Kumar, H. Ledoux, and J. Stoter. Comparative analysis of data structures for storing massive TINS in a DBMS. In *ISPRS - International Archives of the Photogrammetry, Remote Sensing and Spatial Information Sciences*, volume XLI-B2, pages 123–130. Copernicus GmbH, June 2016. doi: https://doi.org/10.5194/isprs-archives-XLI-B2-123-2016. URL https://www.int-arch-photogramm-remote-sens-spatial-inf-sci.net/XLI-B2/123/2016/.

[160] Michael Kwartler and Robert N. Bernard. CommunityViz. In Richard K. Brail and Richard E. Klosterman, editors, *Planning Support Systems: Integrating Geographic Information Systems, Models, and Visualization Tools*. Esri Press, Redlands, CA, 2001. URL http://static1.1.sqspcdn.com/static/f/947001/23447497/1378331642313/Planning+Support+Systems.pdf?token=N8d7MVHB1NZqv6Lgf5eWUyYQNww%3D.

[161] Tillmann Lang, David Ammann, and Bastien Girod. Profitability in absence of subsidies: A techno-economic analysis of rooftop photovoltaic self-consumption in residential and commercial buildings. *Renewable Energy*, 87:77–87, March 2016. ISSN 0960-1481. doi: 10.1016/j.renene.2015.09.059. URL http://www.sciencedirect.com/science/article/pii/S0960148115303384.

[162] Adrien Legrain and Sylvain Vitali. *Definition of design scenarios for the arrangement of tilted solar arrays and estimation of their electricity production from horizontal irradiances*. Semester project report, Ecole polytechnique fédérale de Lausanne, 2018. URL https://infoscience.epfl.ch/record/257766.

[163] Anika Lemar. Zoning as Taxidermy: Neighborhood Conservation Districts and the Regulation of Aesthetics. *90 Indiana Law Journal 1525 (2015)*, 90 (4), October 2015. ISSN 0019-6665. URL https://www.repository.law.indiana.edu/ilj/vol90/iss4/4.

[164] Ronnen Levinson, Hashem Akbari, Melvin Pomerantz, and Smita Gupta. Solar access of residential rooftops in four California cities. *Solar Energy*, 83(12):2120–2135, December 2009. ISSN 0038-092X. doi: 10.1016/j.solener.2009.07.016. URL http://www.sciencedirect.com/science/article/pii/S0038092X0900173X.

[165] Jianming Liang, Jianhua Gong, Wenhang Li, and Abdoul Nasser Ibrahim. A visualization-oriented 3d method for efficient computation of urban solar radiation based on 3d–2d surface mapping. *International Journal of Geographical Information Science*, 28 (4):780–798, April 2014. ISSN 1365-8816. doi: 10.1080/13658816.2014.880168. URL http://dx.doi.org/10.1080/13658816.2014.880168.

[166] Jianming Liang, Jianhua Gong, Jieping Zhou, Abdoul Nasser Ibrahim, and Ming Li. An open-source 3d solar radiation model integrated with a 3d Geographic Information System. *Environmental Modelling & Software*, 64:94–101, February 2015. ISSN 13648152. doi: 10.1016/j.envsoft.2014.11.019. URL http://www.sciencedirect.com/science/article/pii/S1364815214003454.

[167] Shenshen Liang and Luca de Alfaro. Efficient Selection of Pairwise Comparisons for Computing Top-heavy Rankings. 2017.

[168] Dexter H. Locke, J. Morgan Grove, Jacqueline WT Lu, Austin Troy, Jarlath PM O'Neil-Dunne, and Brian D. Beck. Prioritizing preferable locations for increasing urban tree canopy in New York City. *Cities and the Environment (CATE)*, 3(1):4, 2010.

[169] Cristina S. Polo López and Francesco Frontini. Energy Efficiency and Renewable Solar Energy Integration in Heritage Historic Buildings. *Energy Procedia*, 48:1493–1502, 2014. ISSN 1876-6102. doi: 10.1016/j.egypro.2014.02.169. URL http://www.sciencedirect.com/science/article/pii/S1876610214004317.

[170] E. Lucchi, G. Garegnani, L. Maturi, and D. Moser. Architectural integration of photovoltaic systems in historic districts. The case study of Santiago de Compostela. In *International Conference in Energy Efficiency in Historic Buildings*, volume 29, page 30th, 2014. URL https://www.wopapa.it/en/research/institutes/renewableenergy/Publications2/Documents/PaperLucchi-Gar.-Mat.pdf.

[171] David Luebke, Martin Reddy, Jonathan D. Cohen, Amitabh Varshney, Benjamin Watson, and Robert Huebner. Chapter 1 - Introduction. In *Level of Detail for 3D Graphics*, The Morgan Kaufmann Series in Computer Graphics, pages 3–ii. Morgan Kaufmann, San Francisco, 2003. ISBN 978-1-55860-838-2. doi: 10.1016/B978-155860838-2/50003-0. URL https://www.sciencedirect.com/science/article/pii/B9781558608382500030.

[172] Niko Lukač, Danijel Žlaus, Sebastijan Seme, Borut Žalik, and Gorazd Štumberger. Rating of roofs' surfaces regarding their solar potential and suitability for PV systems, based on LiDAR data. *Applied Energy*, 102:803–812, February 2013. ISSN 0306-2619. doi: 10.1016/j.apenergy.2012.08.042. URL http://www.sciencedirect.com/science/article/pii/S0306261912006162.

[173] Lukas Lundström. Weather data for building simulation. New actual weather files for North Europe combining observed weather and modeled solar radiation. Master's thesis, Mälardalen University Sweden, Västerå, 2012. URL https://www.diva-portal.org/smash/get/diva2:574999/FULLTEXT01.pdf.

[174] Rasmus Luthander, Bengt Stridh, and Joakim Widén. PV system layout for optimized self-consumption. In *DIVA*, 2014. URL http://urn.kb.se/resolve?urn=urn:nbn:se:uu:diva-234181.

[175] Rasmus Luthander, Joakim Widén, Daniel Nilsson, and Jenny Palm. Photovoltaic self-consumption in buildings: A review. *Applied Energy*, 142:80–94, March 2015. ISSN 0306-2619. doi: 10.1016/j.apenergy.2014.12.028. URL http://www.sciencedirect.com/science/article/pii/S0306261914012859.

[176] Ardeshir Mahdavi, Ulrich Pont, Feryal Shayeganfar, Neda Ghiassi, Amin Anjomshoaa, Stefan Fenz, Johannes Heurix, Thomas Neubauer, and A Min Tjoa. EXPLORING THE UTILITY OF SEMANTIC WEB TECHNOLOGY IN BUILDING PERFORMANCE SIMULATION. 2012.

[177] Jacek Malczewski. *GIS and multicriteria decision analysis*. John Wiley & Sons, Inc., New York, 1999.

[178] Jacek Malczewski and Claus Rinner. Dealing with Uncertainties. In *Multicriteria Decision Analysis in Geographic Information Science*, Advances in Geographic Information Science, pages 191–221. Springer, Berlin, Heidelberg, 2015. ISBN 978-3-540-74756-7 978-3-540-74757-4. doi: 10.1007/978-3-540-74757-4_7. URL https://link.springer.com/chapter/10.1007/978-3-540-74757-4_7.

[179] Ivan Marović, Ivica Završki, and Nikša Jajac. Ranking zones model – a multicriterial approach to the spatial management of urban areas. *Croatian Operational Research Review*, 6(1):91–103, March 2015. ISSN 18480225, 18489931. doi: 10.17535/crorr.2015.0008. URL http://hrcak.srce.hr/index.php?show=clanak&id_clanak_jezik=204296&lang=en.

[180] Annika Messmer and Rolf Frischknecht. Umweltbilanz Strommix Schweiz 2014. Technical report, 2016.

[181] J. Marshall Miller, editor. *New life for cities around the world : International handbook on urban renewal*. Books International, New York, 1959.

[182] R.C. Miller and D.S. Herrmann. System and method for producing suitability score for energy management system on building rooftop, April 2016. URL https://www.google.ch/patents/US20160110663.

[183] Nahid Mohajeri, Govinda Upadhyay, Agust Gudmundsson, Dan Assouline, Jérôme Kämpf, and Jean-Louis Scartezzini. Effects of urban compactness on solar energy potential. *Renewable Energy*, 93:469–482, August 2016. ISSN 0960-1481. doi: 10.1016/j.renene.2016.02.053. URL http://www.sciencedirect.com/science/article/pii/S0960148116301549.

[184] Marylène Montavon. *Optimisation of Urban Form by the Evaluation of the Solar Potential*. PhD thesis, École Polytechnique Fédérale de Lausanne (EPFL), Lausanne, 2010. URL http://infoscience.epfl.ch/record/145897.

[185] José L Moraga and Machiel Mulder. Electrification of heating and transport. Technical report, 2018.

[186] David Morley. Planning for Solar Energy. Technical Report 575, American Planning Association, 2014. URL https://www.growsolar.org/wp-content/uploads/2014/10/Planning-for-Solar-Energy-2014_PAS-575.pdf.

[187] R. W. Mueller, C. Matsoukas, A. Gratzki, H. D. Behr, and R. Hollmann. The CM-SAF operational scheme for the satellite based retrieval of solar surface irradiance — A LUT based eigenvector hybrid approach. *Remote Sensing of Environment*, 113(5):1012–1024, May 2009. ISSN 0034-4257. doi: 10.1016/j.rse.2009.01.012. URL http://www.sciencedirect.com/science/article/pii/S0034425709000224.

[188] Maria Cristina Munari Probst and Christian Roecker. Urban acceptability of building integrated solar systems: Leso QSV approach. In *Proceedings of ISES 2011*, Kassel, 2011.

[189] Maria Cristina Munari Probst and Christian Roecker. Criteria for Architectural Integration of Active Solar Systems IEA Task 41, Subtask A. *Energy Procedia*, 30:1195–1204, 2012. ISSN 1876-6102. doi: 10.1016/j.egypro.2012.11.132. URL http://www.sciencedirect.com/science/article/pii/S1876610212016487.

[190] Eric Munford. *The CIAM discourse on urbanism, 1928-1960*. The MIT Press, Cambridge, MA, USA, 2000.

[191] Syed Monjur Murshed, Amy Lindsay, Solène Picard, and Alexander Simons. PLANTING: Computing High Spatio-temporal Resolutions of Photovoltaic Potential of 3d City Models. In Ali Mansourian, Petter Pilesjö, Lars Harrie, and Ron van Lammeren, editors, *Geospatial Technologies for All*, pages 27–53. Springer International Publishing, Cham, 2018. ISBN 978-3-319-78207-2 978-3-319-78208-9. doi: 10.1007/978-3-319-78208-9_2. URL http://link.springer.com/10.1007/978-3-319-78208-9_2.

[192] S. H. Naderi, P. Shams, and H. S. Shahhoseini. Fuzzy-Copeland ranking method to evaluate multi-disjoint paths selection algorithms. In *2012 IEEE International Conference on Computer Science and Automation Engineering*, pages 761–764, June 2012. doi: 10.1109/ICSESS.2012.6269578.

[193] Emilie Nault. *Solar Potential in Early Neighborhood Design. A Decision-Support Workflow Based on Predictive Models*. PhD Thesis, Ecole polytechnique fédérale de Lausanne, Lausanne, Switzerland, 2016.

[194] Emilie Nault, Emmanuel Rey, and Marilyne Andersen. Early design phase evaluation of urban solar potential: Insights from the analysis of six projects. In *Proceedings of BS2013*, pages 177–184, Chambéry, France, 2013. URL http://infoscience.epfl.ch/record/187120/.

[195] Emilie Nault, Giuseppe Peronato, and Marilyne Andersen. Forme urbaine et potentiel solaire. In Emmanuel Rey, editor, *Urban Recovery*. Presses Polytechniques et Universitaires Romandes (PPUR), Lausanne, 2015.

[196] Emilie Nault, Peter Moonen, Emmanuel Rey, and Marilyne Andersen. Predictive models for assessing the passive solar and daylight potential of neighborhood designs: A comparative proof-of-concept study. *Building and Environment*, 2017. ISSN 0360-1323. doi: 10.1016/j.buildenv.2017.01.018. URL https://www.sciencedirect.com/science/article/pii/S0360132317300197.

[197] Pradip Niyogi, S. K. Chakrabartty, and M. K. Laha. *Introduction to Computational Fluid Dynamics*. Pearson India, February 2006. ISBN 978-81-317-9390-9. URL http://proquest.safaribooksonline.com/book/electrical-engineering/computer-engineering/9788177587647/firstchapter.

[198] Romain Nouvel, Maryam Zirak, Volker Coors, and Ursula Eicker. The influence of data quality on urban heating demand modeling using 3d city models. *Computers, Environment and Urban Systems*, 64:68–80, July 2017. ISSN 0198-9715. doi: 10.1016/j.compenvurbsys.2016.12.005. URL http://www.sciencedirect.com/science/article/pii/S0198971516304306.

[199] Manasseh Obi and Robert Bass. Trends and challenges of grid-connected photovoltaic systems – A review. *Renewable and Sustainable Energy Reviews*, 58:1082–1094, May 2016. ISSN 1364-0321. doi: 10.1016/j.rser.2015.12.289. URL http://www.sciencedirect.com/science/article/pii/S136403211501672X.

[200] City of Los Angeles. *Solar Envelope Zoning: Application to the City Planning Process, Los Angeles Case Study*. Technical Information Office, Solar Energy Research Institute, 1980. Google-Books-ID: nBHOt0FeLg4C.

[201] OGC. OGC City Geography Markup Language (CityGML) Encoding Standard - version 2.0, April 2012. URL https://portal.opengeospatial.org/files/?artifact_id=47842.

[202] Kristina Orehounig, Ralph Evins, Viktor Dorer, and Jan Carmeliet. Assessment of Renewable Energy Integration for a Village Using the Energy Hub Concept. *Energy Procedia*, 57:940–949, 2014. ISSN 1876-6102. doi: 10.1016/j.egypro.2014.10.076. URL http://www.sciencedirect.com/science/article/pii/S187661021401443X.

[203] Kristina Orehounig, Georgios Mavromatidis, Ralph Evins, Viktor Dorer, and Jan Carmeliet. Towards an energy sustainable community: An energy system analysis for a village in Switzerland. *Energy and Buildings*, 84:277–286, December 2014. ISSN 0378-7788. doi: 10.1016/j.enbuild.2014.08.012. URL http://www.sciencedirect.com/science/article/pii/S0378778814006549.

[204] Najd Ouhajjou, Wolfgang Loibl, Amin Anjomshoaa, Stefan Fenz, and A Min Tjoa. Ontology-based urban energy planning support building-integrated solar PV. In *eWork and eBusiness in Architecture, Engineering and Construction*, pages 543–550. CRC Press, August 2014. ISBN 978-1-138-02710-7. URL http://www.crcnetbase.com/doi/abs/10.1201/b17396-89.

[205] Najd Ouhajjou, Wolfgang Loibl, Stefan Fenz, and A Min Tjoa. Multi-Actor Urban Energy Planning Support: Building refurbishment and Building-integrated Solar PV. In *Proceedings of the 28th EnviroInfo 2014 Conference*, pages 77–84. BIS-Verlag, 2014. URL http://enviroinfo.eu/sites/default/files/pdfs/vol8514/0077.pdf.

[206] Najd Ouhajjou, Wolfgang Loibl, Stefan Fenz, and A Min Tjoa. Stakeholder-oriented Energy Planning Support in Cities. In *Energy Procedia*, volume 78, pages 1841–1846, November 2015. doi: 10.1016/j.egypro.2015.11.327.

[207] Najd Ouhajjou, Wolfgang Loibl, Stefan Fenz, and A. Min Tjoa. Multi-actor Urban Energy Planning Support: Building Refurbishment & Building-Integrated Solar PV. In *Advances and New Trends in Environmental and Energy Informatics*, Progress in IS, pages 157–176. Springer, Cham, 2016. ISBN 978-3-319-23454-0 978-3-319-23455-7. doi: 10.1007/978-3-319-23455-7_9. URL https://link.springer.com/chapter/10.1007/978-3-319-23455-7_9.

[208] Matthew Parkan. Digital-Forestry-Toolbox: A Collection of Digital Forestry Tools for Matlab, 2017. URL http://mparkan.github.io/Digital-Forestry-Toolbox/.

[209] M. Patriarche and D. Dumortier. Experimental Validation of Simulation Software for Daylight Evaluation in Street Canyons (WIP). In *Proceedings of the 2012 Symposium on Simulation for Architecture and Urban Design*, SimAUD '12, pages 13:1–13:5, San Diego, CA, USA, 2012. Society for Computer Simulation International. ISBN 978-1-61839-790-4. URL http://dl.acm.org/citation.cfm?id=2339453.2339466.

[210] Manolis Patriarche. *Mesure et modélisation de la lumière naturelle dans les canyons urbains*. PhD thesis, ENTPE, 2014. URL https://hal.archives-ouvertes.fr/tel-01088928/.

[211] Changhai Peng, Ying Huang, and Zhishen Wu. Building-integrated photovoltaics (BIPV) in architectural design in China. *Energy and Buildings*, 43(12):3592–3598, December 2011. ISSN 0378-7788. doi: 10.1016/j.enbuild.2011.09.032. URL http://www.sciencedirect.com/science/article/pii/S0378778811004348.

[212] Wei Peng, Junnan Yang, Xi Lu, and Denise L. Mauzerall. Potential co-benefits of electrification for air quality, health, and CO2 mitigation in 2030 China. *Applied Energy*, 218:511–519, May 2018. ISSN 0306-2619. doi: 10.1016/j.apenergy.2018.02.048. URL http://www.sciencedirect.com/science/article/pii/S0306261918301739.

[213] Diane Perez. *A framework to model and simulate the disaggregated energy flows supplying buildings in urban areas*. PhD thesis, Ecole polytechnique fédérale de Lausanne, 2014. URL https://infoscience.epfl.ch/record/197073?ln=en.

[214] R. Perez, R. Stewart, C. Arbogast, R. Seals, and J. Scott. An anisotropic hourly diffuse radiation model for sloping surfaces: Description, performance validation, site dependency evaluation. *Solar Energy*, 36(6):481–497, 1986. ISSN 0038-092X. doi: 10.1016/0038-092X(86)90013-7. URL http://www.sciencedirect.com/science/article/pii/0038092X86900137.

[215] R Perez, P. Ineichen, R. Seals, J. Michalsky, and R. Stewart. Modeling daylight availability and irradiance components from direct and global irradiance. *Solar Energy*, 44(5):271–289, 1990.

[216] R. Perez, R. Seals, and J. Michalsky. All-weather model for sky luminance distribution— preliminary configuration and validation. *Solar Energy*, 50(3):235–245, 1993.

[217] Richard Perez, James Schlemmer, Karl Hemker, Sergey Kivalov, Adam Kankiewicz, and Christian Gueymard. Satellite-to-irradiance modeling - a new version of the SUNY model. pages 1–7. IEEE, June 2015. ISBN 978-1-4799-7944-8. doi: 10.1109/PVSC.2015.7356212. URL http://ieeexplore.ieee.org/document/7356212/.

[218] Giuseppe Peronato. *Built density, solar potential and daylighting: Application of parametric studies and performance simulation tools in urban design*. MArch thesis, Università Iuav di Venezia, Venice, March 2014. URL https://infoscience.epfl.ch/record/201758?ln=en.

[219] Giuseppe Peronato, Emmanuel Rey, and Marilyne Andersen. Sampling of building surfaces towards an early assessment of BIPV potential in urban contexts. In *Proceedings of PLEA2015 Architecture in (R)Evolution*, Bologna, 2015. ISBN 978-88-941163-1-1. URL https://infoscience.epfl.ch/record/209966/files/PLEA2015_Peronato_final.pdf.

[220] Giuseppe Peronato, Stéphane Bonjour, Jérémie Stoeckli, Emmanuel Rey, and Marilyne Andersen. Sensitivity of calculated solar irradiation to the level of detail: insights from the simulation of four sample buildings in urban areas. In *PLEA 2016 - Cities, Buildings, People: Towards Regenerative Environments, Proceedings of the 32nd International Conference on Passive and Low Energy Architecture;*, volume 2, Los Angeles, July 2016. ISBN 978-1-365-29354-2.

[221] Giuseppe Peronato, Emmanuel Rey, and Marilyne Andersen. 3d-modeling of vegetation from LiDAR point clouds and assessment of its impact on façade solar irradiation. In *ISPRS - International Archives of the Photogrammetry, Remote Sensing and Spatial Information Sciences*, volume XLII-2/W2, pages 67–70, Athens, October 2016. doi: 10.5194/isprs-archives-XLII-2-W2-67-2016.

[222] Giuseppe Peronato, Jérôme Kämpf, Emmanuel Rey, and Marilyne Andersen. Integrating urban energy simulation in a parametric environment: a Grasshopper interface for CitySim. In *Proceedings of PLEA 2017*, Edinburgh, 2017. URL https://infoscience.epfl.ch/record/228832?ln=en.

[223] Giuseppe Peronato, Parag Rastogi, and Marilyne Andersen. Robustesse de l'évaluation du potentiel solaire de formes urbaines différenciées. In Emmanuel Rey, editor, *Suburban polarity*. Presses Polytechniques et Universitaires Romandes (PPUR), Lausanne, 2017.

[224] Giuseppe Peronato, Emmanuel Rey, and Marilyne Andersen. ACTIVE INTERFACES. From 3d geodata to BIPV yield estimation: towards an urban-scale simulation workflow. 2017. URL https://infoscience.epfl.ch/record/226576.

[225] Giuseppe Peronato, Sergi Aguacil Moreno, Adrien Legrain, Sylvain Vitali, Emmanuel Rey, and Marilyne Andersen. Assessing the photovoltaic potential of flat roofs: insights from the analysis of optimised array arrangements. Hong Kong, China, 2018.

[226] Giuseppe Peronato, Parag Rastogi, Emmanuel Rey, and Marilyne Andersen. A toolkit for multi-scale mapping of the solar energy-generation potential of buildings in urban environments under uncertainty. *Solar Energy*, 173:861–874, October 2018. ISSN 0038-092X. doi: 10.1016/j.solener.2018.08.017.

[227] Giuseppe Peronato, Emmanuel Rey, and Marilyne Andersen. 3d model discretization in assessing urban solar potential: the effect of grid spacing on predicted solar irradiation. *Solar Energy*, 176:334–349, December 2018. doi: 10.1016/j.solener.2018.10.011.

[228] L.E. Perret-Aebi, P. Heinstein, M. Despeisse, C. Ballif, and M. Stückelberger. Solar module and its production process, July 2015. URL https://encrypted.google.com/patents/EP2898540A1?cl=un.

[229] Ronen Perry and Tal Z. Zarsky. Queues in law. *Iowa L. Rev.*, 99:1595, 2013.

[230] Ravi Peters. *Geographical point cloud modelling with the 3D Medial Axis Transform*. PhD thesis, Delft University of Technology, Delft, The Netherlands, 2018.

[231] Christophe Piguet and Alexandre Dyens. Analyse critique de l'art. 18a LAT revisé : genèse, conditions d'application et portée /, 2014.

[232] Cristina Silvia Polo Lopez. Recupero Sostenibile di Edifici Storici : Concetti di Integrazione Solare, March 2012. URL http://www.enea.it/it/comunicare-la-ricerca/events/fotovoltaico-energymed_22mar12/SUPSI_PoloLopez.pdf/at_download/file.

[233] Jean-Charles Pomerol and Sergio Barba-Romero. *Multicriterion Decision in Management: Principles and Practice*. Springer Science & Business Media, December 2012. ISBN 978-1-4615-4459-3. Google-Books-ID: sk_hBwAAQBAJ.

[234] Anne Power. Does demolition or refurbishment of old and inefficient homes help to increase our environmental, social and economic viability? *Energy Policy*, 36(12):4487–4501, December 2008. ISSN 0301-4215. doi: 10.1016/j.enpol.2008.09.022. URL http://www.sciencedirect.com/science/article/pii/S0301421508004709.

[235] Alessandro Prada, Giovanni Pernigotto, Paolo Baggio, Andrea Gasparella, and Ardeshir Mahdavi. Effect of Solar Radiation Model on the Predicted Energy Performance of Buildings. In *International High Performance Buildings Conference*, January 2014. URL http://docs.lib.purdue.edu/ihpbc/130.

[236] Prognos. Die Energieperspektiven für die Schweiz bis 2050. Technical report, BFE, Basel, 2012. URL http://www.bfe.admin.ch/themen/00526/00527/06431/index.html?lang=en&dossier_id=06421.

[237] Volker Quaschning. *Systemtechnik einer klimaverträglichen Elektrizitätsversorgung in Deutschland für das 21. Jahrhundert*. VDI-Verlag, 2000. ISBN 978-3-18-343706-1. Google-Books-ID: oB_jAAAACAAJ.

[238] F. Javier Ramírez, A. Honrubia-Escribano, E. Gómez-Lázaro, and Duc T. Pham. Combining feed-in tariffs and net-metering schemes to balance development in adoption of photovoltaic energy: Comparative economic assessment and policy implications for European countries. *Energy Policy*, 102:440–452, March 2017. ISSN 0301-4215. doi: 10.1016/j.enpol.2016.12.040. URL http://www.sciencedirect.com/science/article/pii/S0301421516307078.

[239] J. Ranalli, K. Calvert, M. Bayrakci Boz, and J. R. S. Brownson. Toward comprehensive solar energy mapping systems for urban electricity system planning and development. *The Electricity Journal*, 31(1):8–15, January 2018. ISSN 1040-6190. doi: 10.1016/j.tej.2018.01.002. URL http://www.sciencedirect.com/science/article/pii/S1040619017303524.

[240] Parag Rastogi. *On the sensitivity of buildings to climate*. PhD Thesis, Ecole polytechnique fédérale de Lausanne, Lausanne, Switzerland, 2016. URL https://infoscience.epfl.ch/record/220971.

[241] P. Redweik, C. Catita, and M. Brito. Solar energy potential on roofs and facades in an urban landscape. *Solar Energy*, 97:332–341, November 2013. ISSN 0038-092X. doi: 10.1016/j.solener.2013.08.036. URL http://www.sciencedirect.com/science/article/pii/S0038092X13003460.

[242] D. T. Reindl, W. A. Beckman, and J. A. Duffie. Diffuse fraction correlations. *Solar Energy*, 45(1):1–7, January 1990. ISSN 0038-092X. doi: 10.1016/0038-092X(90)90060-P. URL http://www.sciencedirect.com/science/article/pii/0038092X9090060P.

[243] Christoph F. Reinhart and Sebastian Herkel. The simulation of annual daylight illuminance distributions — a state-of-the-art comparison of six RADIANCE-based methods. *Energy and Buildings*, 32(2):167–187, July 2000. ISSN 0378-7788. doi: 10.1016/S0378-7788(00)00042-6. URL http://www.sciencedirect.com/science/article/pii/S0378778800000426.

[244] Christoph F. Reinhart and Oliver Walkenhorst. Validation of dynamic RADIANCE-based daylight simulations for a test office with external blinds. *Energy and Buildings*, 33(7):683–697, September 2001. ISSN 0378-7788. doi: 10.1016/S0378-7788(01)00058-5. URL http://www.sciencedirect.com/science/article/pii/S0378778801000585.

[245] J. Remund, S. C. Müller, C. Schilter, and B. Rihm. The use of Meteonorm weather generator for climate change studies. pages EMS2010–417, September 2010. URL http://adsabs.harvard.edu/abs/2010ems..confE.417R.

[246] Jan Remund, Stefan Mueller, Stefan Kunz, and Christoph Schilter. METEONORM Handbook Part II : Theory. Technical report, May 2012. URL http://meteonorm.com/download/software/mn70/.

[247] Emmanuel Rey, Sophie Lufkin, Christophe Ballif, Rolf Wuestenhagen, Stephen Wittkopf, and Jean-Philippe Bacher. Building integrated photovoltaics | ACTIVE INTERFACES, April 2015.

[248] Marcel Šúri and Jaroslav Hofierka. A New GIS-based Solar Radiation Model and Its Application to Photovoltaic Assessments. *Transactions in GIS*, 8(2):175–190, April 2004. ISSN 1467-9671. doi: 10.1111/j.1467-9671.2004.00174.x. URL http://onlinelibrary.wiley.com/doi/10.1111/j.1467-9671.2004.00174.x/abstract.

[249] Marcel Šúri, Thomas A. Huld, and Ewan D. Dunlop. PV-GIS: a web-based solar radiation database for the calculation of PV potential in Europe. *International Journal of Sustainable Energy*, 24(2):55–67, June 2005. ISSN 1478-6451, 1478-646X. doi: 10.1080/14786450512331329556. URL http://www.tandfonline.com/doi/abs/10.1080/14786450512331329556.

[250] Maria Gracia Riera Pérez and Emmanuel Rey. A multi-criteria approach to compare urban renewal scenarios for an existing neighborhood. Case study in Lausanne (Switzerland). *Building and Environment*, 65:58–70, July 2013. ISSN 0360-1323. doi: 10.1016/j.buildenv.2013.03.017. URL http://www.sciencedirect.com/science/article/pii/S0360132313000978.

[251] Maria Gracia Riera Pérez, Emmanuel Rey, Ulrick Liman, Yves Roulet, and Adeline Favris-Donzel. SméO, a sustainability assessment tool targeting the 2000 Watts society. *Proceedings of PLEA 2014*, 2014. URL http://infoscience.epfl.ch/record/204708?ln=fr.

[252] D. Robinson and A. Stone. A simplified radiosity algorithm for general urban radiation exchange. *Building Services Engineering Research & Technology*, 26(4):271–284, 2005. ISSN 0143-6244.

[253] Darren Robinson. *Computer Modelling for Sustainable Urban Design: Physical Principles, Methods and Applications*. Routledge, November 2012. ISBN 978-1-136-53935-0. Google-Books-ID: J_xAVFrEqeUC.

[254] Darren Robinson and Andrew Stone. Irradiation modelling made simple: the cumulative sky approach and its applications. In *Proceedings of PLEA 2004*, Eindhoven, The Netherlands, 2004.

[255] Darren Robinson and Andrew Stone. Solar radiation modelling in the urban context. *Solar Energy*, 77(3):295–309, September 2004. ISSN 0038-092X. doi: 10.1016/j.solener.2004.05.010. URL http://www.sciencedirect.com/science/article/pii/S0038092X04001161.

[256] Darren Robinson, Frédéric Haldi, Jérôme Henri Kämpf, Philippe Leroux, Diane Perez, Adil Rasheed, and Urs Wilke. CitySim: Comprehensive micro-simulation of resource flows for sustainable urban planning. In *Proceedings of BS2009*, pages 1083–1090, Glasgow, July 2009. IBPSA.

[257] Laura Romero Rodríguez, Romain Nouvel, Eric Duminil, and Ursula Eicker. Setting intelligent city tiling strategies for urban shading simulations. *Solar Energy*, 157:880–894, November 2017. ISSN 0038-092X. doi: 10.1016/j.solener.2017.09.017. URL http://www.sciencedirect.com/science/article/pii/S0038092X17307855.

[258] Thomas Rose and Alexander Wollert. The dark side of photovoltaic — 3d simulation of glare assessing risk and discomfort. *Environmental Impact Assessment Review*, 52:24–30, April 2015. ISSN 0195-9255. doi: 10.1016/j.eiar.2014.08.005. URL http://www.sciencedirect.com/science/article/pii/S0195925514000730.

[259] Mostapha Sadeghipour Roudsari and Michelle Pak. Ladybug: a parametric environmental plugin for grasshopper to help designers create an environmentally-conscious design. In *Proceedings of the 13th International IBPSA Conference*, 2013. URL http://www.ibpsa.org/proceedings/BS2013/p_2499.pdf.

[260] B. Roy and Ph. Vincke. Relational Systems of Preference with One or More Pseudo-Criteria: Some New Concepts and Results. *Management Science*, 30(11):1323–1335, 1984. ISSN 0025-1909. URL http://www.jstor.org/stable/2631567.

[261] Patrick Rérat. The New Demographic Growth of Cities: The Case of Reurbanisation in Switzerland. *Urban Studies*, (pending publication), 2014.

[262] Thomas L. Saaty. *The Analytic Hierarchy Process: Planning, Priority Setting, Resource Allocation*. McGraw-Hill, 1980. ISBN 978-0-07-054371-3. Google-Books-ID: Xxi7AAAAIAAJ.

[263] Hans-Rudolf Schalcher, Hans-Jakob Boesch, Kathrin Bertschy, Heini Sommer, Dominik Matter, Johanna Gerum, and Martin Jakob. Quels seront les coûts futurs des bâtiments et des infrastructures suisses et qui les paiera ? Technical report, SNSF, 2011. URL http://www.uspi.ch/fileadmin/user_upload/documents/USPI_INFO_03.2011_ANNEXE_RAPPORT_FNS.pdf.

[264] Andreas Schüler, Deepanshu Dutta, Estelle de Chambrier, Christian Roecker, Gregory De Temmerman, Peter Oelhafen, and Jean-Louis Scartezzini. Sol–gel deposition and optical characterization of multilayered SiO2/Ti1-xSixO2 coatings on solar collector glasses. *Solar Energy Materials and Solar Cells*, 90(17):2894–2907, November 2006. ISSN 0927-0248. doi: 10.1016/j.solmat.2006.05.003. URL

http://www.sciencedirect.com/science/article/pii/S092702480600184X.

[265] T. Schoen, D. Prasad, D. Ruoss, P. Eiffert, and H. Sørensen. Task 7 of the IEA PV power systems program–achievements and outlook. In *Proceedings of the 17th European Photovoltaic Solar Conference*, 2001. URL http://ptp.irb.hr/upload/mape/solari/paper_task7_17th_eu_pvsec.pdf.

[266] Roland Schregle, Christian Renken, Stephen Wittkopf, Roland Schregle, Christian Renken, and Stephen Wittkopf. Spatio-Temporal Visualisation of Reflections from Building Integrated Photovoltaics. *Buildings*, 8(8):101, August 2018. doi: 10.3390/buildings8080101. URL https://www.mdpi.com/2075-5309/8/8/101.

[267] Alain Schärlig. *Décider sur plusieurs critères: Panorama de l'aide à la décision multicritère*. Presses Polytechniques et Universitaires Romandes (PPUR), 1985.

[268] Alain Schärlig. *Pratiquer Electre et Prométhée*. Presses Polytechniques et Universitaires Romandes (PPUR), 1996.

[269] Nils Seifert, Michael Mühlhaus, Gerhard Schubert, Dietrich Fink, and Frank Petzold. Decision support for inner-city development. In *Proceedings of eCAADe 2014*, pages 43–52, Newcastle, United Kingdom, 2014.

[270] Nils Seifert, Michael Mühlhaus, and Frank Petzold. A Parametric 3d City Model: Basis for Decision Support in Inner-City Development. In *Proceedings of the 16th International Conference on Computing in Civil and Building Engineering*, pages 1285–1292, 2016.

[271] Manajit Sengupta, Jésus Polo, Christian Gueymard, and Yu Xie. Modeling Solar Radiation - Current practices. December 2017. doi: 10.2172/1411856. URL http://www.osti.gov/servlets/purl/1411856/.

[272] SFOE-MétéoSuisse-Swisstopo. Toit solaire, 2016. URL www.toit-solaire.ch. Swiss Federal Office of Energy SFOE - Federal Office of Meteorology and Climatology MeteoSwiss - Federal Office of Topography swisstopo http://www.uvek-gis.admin.ch/BFE/sonnendach/?lang=en.

[273] Nihar B. Shah and Martin J. Wainwright. Simple, Robust and Optimal Ranking from Pairwise Comparisons. *arXiv:1512.08949 [cs, math, stat]*, December 2015. URL http://arxiv.org/abs/1512.08949. arXiv: 1512.08949.

[274] Ayyoob Sharifi and Yoshiki Yamagata. Principles and criteria for assessing urban energy resilience: A literature review. *Renewable and Sustainable Energy Reviews*, 60: 1654–1677, July 2016. ISSN 1364-0321. doi: 10.1016/j.rser.2016.03.028. URL http://www.sciencedirect.com/science/article/pii/S136403211600263X.

[275] Donald Shepard. A Two-dimensional Interpolation Function for Irregularly-spaced Data. In *Proceedings of the 1968 23rd ACM National Conference*, ACM '68, pages 517–524, New York, NY, USA, 1968. ACM. doi: 10.1145/800186.810616. URL http://doi.acm.org/10.1145/800186.810616.

[276] SIA. SIA 380/1:2009 Thermische Energie im Hochbau - Besoins de chaleur pour le chauffage - L'energia termica nell'edilizia, 2009.

[277] SIA. SIA 2024:2015 Raumnutzungsdaten für Energie- und Gebäudetechnik - Données d'utilisation des locaux pour l'énergie et les installations du bâtiment - Dati d'utilizzo di locali per l'energia e l'impiantistica degli edifici, January 2015. URL http://shop.sia.ch/normenwerk/architekt/sia%202024/d/2015/F/Product/.

[278] SIA. SIA 380/1:2016 Thermische Energie im Hochbau - Besoins de chaleur pour le chauffage, 2016.

[279] Daniel Siret. Rayonnement solaire et environnement urbain : de l'héliotropisme au désenchantement, histoire et enjeux d'une relation complexe. *Développement Durable et Territoires*, 4(2), 2013. ISSN 1772-9971. doi: 10.4000/developpementdurable.9767.

[280] Daniel Siret and Amina Harzallah. Architecture et contrôle de l'ensoleillement. In *Congrès IBPSA France*, 2006. URL https://halshs.archives-ouvertes.fr/halshs-00572362/.

[281] SMS. Panneaux solaires: fiche des recommandations, 2013. URL https://www.ge.ch/patrimoine/sms/inc/pub/img-pub/conseils/conseils_panneaux_solaires.pdf.

[282] Solargis. Solargis Solar Resource: Description and accuracy, 2016. URL https://solargis.com/assets/doc/Solargis-database-description-and-accuracy.pdf.

[283] K. H. Soon and V. H. S. Khoo. CityGML modelling for Singapore 3d national mapping. *ISPRS - International Archives of the Photogrammetry, Remote Sensing and Spatial Information Sciences*, XLII-4/W7:37–42, 2017. ISSN 2194-9034. doi: 10.5194/isprs-archives-XLII-4-W7-37-2017. URL https://www.int-arch-photogramm-remote-sens-spatial-inf-sci.net/XLII-4-W7/37/2017/.

[284] Iain Staffell, Daniel J. L. Brett, Nigel P. Brandon, and Adam D. Hawkes. *Domestic Microgeneration: Renewable and Distributed Energy Technologies, Policies and Economics*. Routledge, June 2015. ISBN 978-1-317-44885-3. Google-Books-ID: sZvwCQAAQBAJ.

[285] Clarence Stein. *Toward new towns for America*. Reinhold, New York, 1957.

[286] J. S. Stein. The photovoltaic Performance Modeling Collaborative (PVPMC). In *2012 38th IEEE Photovoltaic Specialists Conference*, pages 003048–003052, June 2012. doi: 10.1109/PVSC.2012.6318225.

[287] David Stickelberger and Christian Moll. Guide pratique des installations solaires. Technical report, Swissolar, Bern, 2017. URL https://www.swissolar.ch/fileadmin/user_upload/Shop/171127_Leitfaden_RPG_Kurzfassung_FRA.pdf.

[288] Jérémie Stoeckli and Stéphane Bonjour. *The influence of the Level of Detail (LOD) on the assessment of the photovoltaic (PV) potential in urban environments*. Semester project report, Ecole polytechnique fédérale de Lausanne, Lausanne, January 2016.

[289] Jantien Stoter, Henk de Kluijver, and Vinaykumar Kurakula. Towards 3d environmental impact studies: example of noise. In Peter van Oosterom, Sisi Zlatanova, Friso Penninga, and Elfriede M. Fendel, editors, *Advances in 3D Geoinformation Systems*, Lecture Notes in Geoinformation and Cartography, pages 341–359. Springer Berlin Heidelberg, 2008. ISBN 978-3-540-72134-5 978-3-540-72135-2. doi: 10.1007/978-3-540-72135-2_19. URL http://link.springer.com/chapter/10.1007/978-3-540-72135-2_19.

[290] Jantien Stoter, Bruno Vallet, Thomas Lithen, Maria Pla, Piotr Wozniak, Tobias Kellenberger, Andre Streilein, Risto Ilves, and Hugo Ledoux. State-of-the-art of 3d national mapping in 2016. *ISPRS - International Archives of the Photogrammetry, Remote Sensing and Spatial Information Sciences*, XLI-B4:653–660, June 2016. ISSN 2194-9034. doi: 10.5194/isprs-archives-XLI-B4-653-2016. URL http://www.int-arch-photogramm-remote-sens-spatial-inf-sci.net/XLI-B4/653/2016/.

[291] Rudi Stouffs. Strict and automatic mapping of IFC-BIM Models into sematically enriched 3d CityGML Building Models (Exterios and Interior), 2017. URL http://3dgeoinfo2017.com/Files/rudi.pdf.

[292] Aneta Strzalka, Dirk Monien, Athanasios Koukofikis, and Ursula Eicker. Sensitivity analysis for minimization of input data for urban scale heat demand forecasting. In *Proceedings of SET 2015*, Nottingham, UK, 2015.

[293] SWISS-ENERGYSCOPE. POURQUOI LE TAUX DE RÉNOVATION DES BÂTIMENTS EST-IL SI FAIBLE MALGRÉ LE PROGRAMME DE SUBSIDE?, 2018. URL http://www.energyscope.ch/100-questions/politique-energetique/p-pourquoi-le-taux-de-renovation-des-batiments-est-il-si-faible-malgre-le-programme-de-subsides-p.

[294] Swissolar. Calculateur d'énergie solaire, 2018. URL https://www.swissolar.ch/fr/pour-maitres-douvrage/outils-de-calcul/calculateur-denergie-solaire/.

[295] Swisstopo. swissBUILDINGS3d Version 1.0 Les bâtiments de la Suisse en 3d simplifiés, September 2010. URL https://www.swisstopo.admin.ch/content/swisstopo-internet/fr/home/products/landscape/build3d/_jcr_content/contentPar/tabs/items/dokumente/tabPar/downloadlist/downloadItems/766_1464677452832.download/swissbuildings1.0f2010.pdf.

[296] Swisstopo. Information produit - swissBUILDINGS3d 2.0, October 2016. URL https://www.swisstopo.admin.ch/content/swisstopo-internet/fr/home/products/landscape/build3d2/_jcr_content/contentPar/tabs/items/dokumente/tabPar/downloadlist/downloadItems/768_1464679037931.download/swissBUILDINGS3D%202.0_Produktinfo_fr_2016_bf.pdf.

[297] Haider Taha. The potential for air-temperature impact from large-scale deployment of solar photovoltaic arrays in urban areas. *Solar Energy*, 91:358–367, May 2013. ISSN 0038-092X. doi: 10.1016/j.solener.2012.09.014. URL http://www.sciencedirect.com/science/article/pii/S0038092X12003386.

[298] Owen Temby, Konstantinos Kapsis, Harris Berton, Daniel Rosenbloom, Geoffrey Gibson, Andreas Athienitis, and James Meadowcroft. Building-Integrated Photovoltaics: Distributed Energy Development for Urban Sustainability. *Environment: Science and Policy for Sustainable Development*, 56(6):4–17, November 2014. ISSN 0013-9157. doi: 10.1080/00139157.2014.964092. URL https://doi.org/10.1080/00139157.2014.964092.

[299] Tomorrow. Electricity map. Emissions co2 de la consommation électrique en temps réel, 2018. URL https://www.electricitymap.org.

[300] Thoreau Rory Tooke, Nicholas C. Coops, James A. Voogt, and Michael J. Meitner. Tree structure influences on rooftop-received solar radiation. *Landscape and Urban Planning*, 102(2):73–81, August 2011. ISSN 0169-2046. doi: 10.1016/j.landurbplan.2011.03.011. URL http://www.sciencedirect.com/science/article/pii/S0169204611001526.

[301] Thoreau Rory Tooke, Nicholas C. Coops, Andreas Christen, Ozgur Gurtuna, and Arthur Prévot. Integrated irradiance modelling in the urban environment based on remotely sensed data. *Solar Energy*, 86(10):2923–2934, October 2012. ISSN 0038-092X. doi: 10.1016/j.solener.2012.06.026. URL http://www.sciencedirect.com/science/article/pii/S0038092X12002381.

[302] P.R. Tregenza. Subdivision of the sky hemisphere for luminance measurements. *Lighting Research and Technology*, 19:13–14, 1987.

[303] UN. World Urbanization Prospects 2018. Technical report, United Nations, 2018. URL https://population.un.org/wup/.

[304] Raymond Unwin. *Town Planning in Practice: An Introduction to the Art of Designing Cities and Suburbs*. T. F. Unwin, London-Leipzig, 1909. URL https://archive.org/details/townplanninginp00unwigoog.

[305] Jari Vauhkonen, Ilkka Korpela, Matti Maltamo, and Timo Tokola. Imputation of single-tree attributes using airborne laser scanning-based height, intensity, and alpha shape metrics. *Remote Sensing of Environment*, 114(6):1263–1276, June 2010. ISSN 0034-4257. doi: 10.1016/j.rse.2010.01.016. URL http://www.sciencedirect.com/science/article/pii/S0034425710000386.

[306] Frank Vignola, Cathy Grover, Nick Lemon, and Andrew McMahan. Building a bankable solar radiation dataset. *Solar Energy*, 86(8):2218–2229, August 2012. ISSN 0038-092X. doi: 10.1016/j.solener.2012.05.013. URL http://www.sciencedirect.com/science/article/pii/S0038092X1200182X.

[307] virtualcitySystems. BuildingReconstruction, 2014.

[308] Didier Vuarnoz and Thomas Jusselme. Temporal variations in the primary energy use and greenhouse gas emissions of electricity provided by the Swiss grid. *Energy*, 161:573–582, October 2018. ISSN 0360-5442. doi: 10.1016/j.energy.2018.07.087. URL http://www.sciencedirect.com/science/article/pii/S0360544218313847.

[309] Adi Vulkan, Itai Kloog, Michael Dorman, and Evyatar Erell. Modeling the potential for PV installation in residential buildings in dense urban areas. *Energy and Buildings*, 169:97–109, June 2018. ISSN 0378-7788. doi: 10.1016/j.enbuild.2018.03.052. URL http://www.sciencedirect.com/science/article/pii/S0378778817339877.

[310] Paul Waddell. UrbanSim: Modeling Urban Development for Land Use, Transportation, and Environmental Planning. *Journal of the American Planning Association*, 68(3):297–314, September 2002. ISSN 0194-4363. doi: 10.1080/01944360208976274. URL http://dx.doi.org/10.1080/01944360208976274.

[311] Christoph Waibel, Ralph Evins, and Jan Carmeliet. Using interpolation to generate hourly annual solar potential profiles for complex geometry. In *Proceedings of BSO2016*, Newcastle, United Kingdom, 2016. URL http://www.ibpsa.org/proceedings/BSO2016/p1059.pdf.

[312] Yiping Wang, Wei Tian, Li Zhu, Jianbo Ren, Yonghui Liu, Jinli Zhang, and Bing Yuan. Interactions between Building Integrated Photovoltaics and Microclimate in Urban Environments. *Journal of Solar Energy Engineering*, 128 (2):168–172, August 2005. ISSN 0199-6231. doi: 10.1115/1.2188533. URL http://dx.doi.org/10.1115/1.2188533.

[313] Yunsheng Wang, Holger Weinacker, and Barbara Koch. A Lidar Point Cloud Based Procedure for Vertical Canopy Structure Analysis And 3d Single Tree Modelling in Forest. *Sensors*, 8(6):3938–3951, June 2008. doi: 10.3390/s8063938. URL http://www.mdpi.com/1424-8220/8/6/3938.

[314] P. Wate, V. Coors, D. Robinson, and M. Iglesias. Qualitative screening method for impact assessment of uncertain building geometry on thermal energy demand predictions. *ISPRS - International Archives of the Photogrammetry, Remote Sensing and Spatial Information Sciences*, XLII-2/W2:127–134, October 2016. ISSN 2194-9034. doi: 10.5194/isprs-archives-XLII-2-W2-127-2016. URL http://www.int-arch-photogramm-remote-sens-spatial-inf-sci.net/XLII-2-W2/127/2016/.

[315] Manfred Wieland, Alexandru Nichersu, Syed Monjur Murshed, and Jochen Wendel. Computing solar radiation on CityGML building data. In *18th AGILE international conference on geographic informaton science*, 2015.

[316] Jan Wienold, Aicha Diakite, Martine Knoop, and Marilyne Andersen. Making simulations more colorful: Extension of gendaylit to create a colored sky, 2018.

[317] S Wilcox and W Marion. Users Manual for TMY3 Data Sets. Technical Report NREL/TP-581-43156, National Renewable Energy Laboratory (NREL), 2008.

[318] Donald Wittman. First Come, First Served: An Economic Analysis of "Coming to the Nuisance". *The Journal of Legal Studies*, 9(3):557–568, 1980. ISSN 0047-2530. URL http://www.jstor.org/stable/724004.

[319] Donald Wittman. Efficient Rules in Highway Safety and Sports Activity. *The American Economic Review*, 72(1): 78–90, 1982. ISSN 0002-8282. URL http://www.jstor.org/stable/1808576.

[320] Ran Xu and Stephen Wittkopf. Visual assessment of BIPV retrofit design proposals for selected historical buildings using the saliency map method. *Journal of Facade Design and Engineering*, 2(3-4):235–254, May 2015. ISSN 2213302X, 22133038. doi: 10.3233/FDE-150022. URL http://www.medra.org/servlet/aliasResolver?alias=iospress&doi=10.3233/FDE-150022.

[321] Dazhi Yang. Solar radiation on inclined surfaces: Corrections and benchmarks. *Solar Energy*, 136:288–302, October 2016. ISSN 0038-092X. doi: 10.1016/j.solener.2016.06.062. URL http://www.sciencedirect.com/science/article/pii/S0038092X16302432.

[322] Hong Yang, Xianjin Huang, and Julian R. Thompson. Tackle pollution from solar panels. *Nature*, 509:563, May 2014. URL http://dx.doi.org/10.1038/509563c.

[323] Zhihang Yao, Claus Nagel, Felix Kunde, György Hudra, Philipp Willkomm, Andreas Donaubauer, Thomas Adolphi, and Thomas H. Kolbe. 3dcitydb - a 3d geodatabase solution for the management, analysis, and visualization of semantic 3d city models based on CityGML. *Open Geospatial Data, Software and Standards*, 3(1):5, May 2018. ISSN 2363-7501. doi: 10.1186/s40965-018-0046-7. URL https://doi.org/10.1186/s40965-018-0046-7.

[324] Katharine G. Young. Rights and Queues: On Distributive Contests in the Modern State. *Columbia Journal of Transnational Law*, 55:65–137, 2016.

[325] Katherine Young. Examining the Interface Between Rights and Queues, 2017. URL https://blog.harvardlawreview.org/examining-the-interface-between-rights-and-queues/.

[326] Isa Zanetti, Kim Nagel, and Domenico Chianese. Concepts for Solar Integration. Development of Technical and Architectural Guidelines for Solar System Integration in Historical Buildings. In *EU PVSEC Proceedings*, pages 5105–5109, Valencia, Spain, 2010. ISBN 3-936338-26-4. doi: 10.4229/25thEUPVSEC2010-5BV.5.4. URL http://www2.isaac.supsi.ch/isaac/pubblicazioni/Fotovoltaico/Conferences/Valencia%20(Spain)%20-%2025%20EU%20PVSEC%20-%20September%202010/5bv.5.4%20concepts%20for%20solar%20integration%20(i.%20zanetti).pdf.

[327] Zhen Zhen, Lindi J. Quackenbush, and Lianjun Zhang. Trends in Automatic Individual Tree Crown Detection and Delineation—Evolution of LiDAR Data. *Remote Sensing*, 8(4):333, April 2016. doi: 10.3390/rs8040333. URL http://www.mdpi.com/2072-4292/8/4/333.

[328] Helen Wei Zheng, Geoffrey Qiping Shen, and Hao Wang. A review of recent studies on sustainable urban renewal. *Habitat International*, 41:272–279, January 2014. ISSN 0197-3975. doi: 10.1016/j.habitatint.2013.08.006. URL http://www.sciencedirect.com/science/article/pii/S0197397513000908.

[329] Zongwei Zhou. Integration of renewable energy with urban design. Master's thesis, Massachusetts Institute of Technology, Cambridge, MA, USA, 2011.

[330] Mark Zimmermann. Sustainable Renovation of Historical Buildings (SuRHiB). Final Report, Swiss Federal Office of Energy, Bern, March 2013.

[331] Urs Zuppinger. Planification et projets de construction : étude exploratoire. Technical report, Secrétariat d'Etat à l'économie (SECO), Lausanne, September 2005.

[332] ARE Zurich. Leitfaden Solaranlagen. Technical report, Amt für Raumentwicklung des Kantons Zürich, 2016.

# Acronyms

**AC** Alternate Current. 167

**BAPV** Building-Applied Photovoltaics. 4, 125, 129

**BIPV** Building-Integrated Photovoltaics. 3, 4, 125, 129, 217

**CAD** Computer-Aided Drafting. 154

**DEM** Digital Elevation Model. 35

**DHI** Diffuse Horizontal Irradiance. 151, 152

**DHM** Digital Height Model. 35

**DHW** Domestic Hot Water. 133–135, 160, 161

**DNI** Direct Normal Irradiance. 151, 152

**DSM** Digital Surface Model. 35, 126, 203

**DTM** Digital Terrain Model. 35, 126, 137, 147, 149, 164, 203

**ESCo** Energy Service Company. 28, 75, 172

**FiT** Feed-in tariff. 28, 29, 77

**GHI** Global Horizontal Irradiance. 152, 153, 160, 212

**GIS** Geographic Information Systems. 5, 154, 228

**ISOS** Inventaire fédéral des sites construits d'importance nationale â protéger en Suisse. 177, 178, 199

**LCOE** Levelized Cost of Electricity. 29

**LiDAR** Light Detection and Ranging or Laser Imaging Detection and Ranging. 84, 128, 149, 151, 154, 164, 204

**LOD** Level of Detail. 5, 7, 8, 85, 89–94, 112, 115, 119, 133, 134, 147, 219

**NPV** Net Present Value. 134

**POA** Plane of Array. 26, 84, 162, 203, 217

**PV** Photovoltaics. 133, 134, 167, 211

**RACN** Récensement Architectural du Canton de Neuchâtel. 176–178

**RegBL** Swiss Federal Register of Buildings and Dwellings. 158, 176–178, 228

**RMSE** Root Mean Square Error. 202, 206

**SC** Self-Consumption. 163, 181, 183, 185, 187, 188, 194, 213

**SFSC** Swiss Federal Solar Cadastre. 203, 204, 206–208, 213

**SIA** Swiss Society of Engineers and Architects. 157

**SS** Self-Sufficiency. 163, 181, 183, 185, 187, 188, 194, 213

**ST** Solar Thermal. 133, 134

**STC** Standard Test Conditions. 163

**TMY** Typical Meteorological Year. 152

**WWR** Window-to-wall ratio. 157, 158, 164

# Acknowledgements

I owe thanks to many people and organizations for making this thesis possible. First, I wish to thank my advisor Prof. Marilyne Andersen for giving me the chance to join LIPID, a really stimulating interdisciplinary research environment, which forged me in many ways. Throughout my master project and the subsequent PhD, she has always trusted my work and skills, providing prompt encouragement and advice. I also want to thank Prof. Emmanuel Rey, co-advisor of this thesis, for creating the research context of this PhD as Principal Investigator of its umbrella project. I am also grateful to Prof. François Golay, who chaired both my candidacy and thesis oral exams, and the other members of the thesis jury, Prof. Miguel Centeno Brito, Prof. François Maréchal and Prof. Christoph Reinhart. I have really appreciated their in-depth comments and feedback on an earlier version of this manuscript as well as the interesting discussion at the oral exam.

This thesis is also the fruit of many enriching exchanges and collaborations with senior scientists, colleagues and students that I also wish to acknowledge here: Sergi Aguacil, for the discussions on sizing of PV systems and solar potential indicators; Dr. Filip Biljecki, for his precious expertise on 3D city models and the Level of Detail; Prof. Jacques Dubey, for his advice on reviewing Swiss legislation on solar energy; Dr. Pietro Florio, for many useful discussions, especially on geo-visualization techniques, as well as for reviewing some parts of the thesis' manuscript and other papers; Dr. Francesco Frontini, for providing measurements and suggestions on the modeling of PV modules; Prof. François Golay, for the feedback on decision-support methods; Prof. Jérôme Kämpf, for the support with CitySim and collaboration on the development of the Grasshopper interface; Prof. Jan Kleissl, subject editor of *Solar Energy*, and the anonymous reviewers for their feedback on the submitted papers; Dr. Matthew Parkan, for the help with GIS software, LiDAR datasets and the reconstruction of vegetation; Dr. Parag Rastogi, for many useful discussions and the collaboration on weather uncertainty and solar potential indicators; Dr. Emilie Nault, for reviewing many papers of mine and her useful feedback and advice since my master's project; Dr. Jan Wienold, for the help and prompt support with Radiance/Daysim and with the lab's Linux machine; Romain Nouvel, Prof. Ursula Eicker and Prof. Volker Coors for hosting my research stay at HFT Stuttgart in February 2017; Kynthia Chamilothori and Minu Agarwal for patiently reviewing some parts of this thesis' early manuscript; Stéphane Bonjour, Adrien Legrain, Jérémie Stoeckli, Sylvain Vitali, former or current master students at EPFL in Energy Management and Sustainability (SB, AL, JS) and Environmental Sciences and Engineering (SV), for their contributions to specific projects that are part of this thesis; Dr. Frédéric Pont, Dr. Antoine Guillemin and Martin Gonzenbach for the technology transfer advising, which contributed to the definition of the application part of the thesis.

The friendly working environment was also very important for the development of this thesis. I want to acknowledge all colleagues who passed by the IDEAS-LE offices during the last 4 years: in roughly

chronological order, Boris, Mandana, Emilie, Maria, María, Shevy, Martine, Loïc, Aleksis, Lorenzo, Jan, Giorgia, Kynthia, Sergi, Jean-Denis, Luisa, Judith, Angela, Peter, Victoria, Joëlle, Clotilde, Forrest and Geraldine. Thank you, in particular, for the useful feedback during the LIPID research meetings, LAST PhD workshops and IDEAS talks.

I also gratefully acknowledge all funding organizations, and, through them, all tax payers in Switzerland making publicly-funded research possible. This thesis was in fact conducted in the framework of the ACTIVE INTERFACES research project [247], which is part of the National Research Program "Energy Turnaround" (NRP 70) of the Swiss National Science Foundation (SNSF). Further information on the National Research Program can be found at www.nrp70.ch. In addition to the SNSF, the PhD was also supported by the Ecole polytechnique fédérale de Lausanne (EPFL) and by Movetia, through the Swiss-European Mobility Programme (SEMP) / ERASMUS.

Finally, I want to acknowledge the organizations and individuals that provided the datasets used in this thesis and the support to their use:

- The GIS department of the Canton of Neuchâtel (*Système d'Information du Territoire Neuchâtelois* - SITN) and its head, Marc Riedo. The use of SITN data in this work is regulated by a contract established on November 10, 2014. For all figures in which the SITN is acknowledged in the figure captions, the following copyright note applies: *Données cartographiques du SITN © 2014-2017 / Service de la Géomatique et du Registre Foncier*.
- The Swiss Federal Office of Topography (Swisstopo). Swisstopo's geodata are obtained through a commercial license (Switzerland - LOD2.3 model), the EPFL geodata service (Switzerland - LOD1 model), and the GeoVITe service (all other cases). Their use in this thesis complies with the Article 5(f) of the Swiss Federal Ordinance on the Swisstopo Emoluments (GebV-swisstopo, OEmol-swisstopo, OEm-swisstopo) and is acknowledged in the figure captions.
- The GIS department of the Canton of Geneva (*Système d'information du territoire à Genève* - SITG). The use of SITG data (extracted in June 2016) in this work is possible thanks to an open license and is acknowledged in the figure captions.
- The Swiss Federal Office of Statistics providing access to the Swiss Federal Register of Buildings and Dwellings (RegBL) records for the city of Neuchâtel. Their use in this thesis complies with the Articles 11 and 12 of the Swiss Federal Ordinance on the RegBL (VGWR, ORegBL, OREA).
- The *Fondation du Home de l'Ermitage et des Rochettes - Hôtel des Associations* and VITEOS for the measurement data presented in Section 13.2. I want to thank, in particular, Daniel Perdrizat (HdA) and Remigio Pian, Raphaël Planas, and Kenny Du Terrail Couvat (VITEOS).

The acknowledgments above are not enough, as completing the PhD would not have been possible without also supporting friends and family.

A special mention goes to the LÉA 1 113 crew, Emilie, Parag and Sergi. I would not probably have started this PhD without Emilie's example and encouragements during my master's thesis. I also thank Sergi and Emilie for feeding me in many occasions and Parag for checking whether my screensaver was on. Another special mention goes to the most recent LE 1 114 occupants (Kynthia, Giorgia, Forrest and Minu) and their couch, which during the last year "hosted many writing breaks, existential crises and a lot of fun. Thank you, Kynthia, for your enormous support since the very beginning of the PhD, Giorgia and Forrest, for being the best bros, and Forrest also the best buddy in this important year.

I also want to thank Pietro, the best "PhD mate", with whom I shared all the challenges of these years, but also many good moments. I cannot count all the times I knocked at his door during these years, and I really appreciated his precious help and understanding. I am also glad that even if, unfortunately, *non #bastaunsi*, we have kept caring about the future of our home country.

Despite living far from each other, my long-time friends Leo and Matteo have also been always there and I want to thank them for their continuing support and friendship, as I look forward to our next periodic meeting.

Beside the research, I had the opportunity to be involved in many activities in the EPFL campus. I feel that I greatly benefited from doing my PhD in such a lively working and studying environment. I really enjoyed working with students in class and projects and, as a novice TA, instructor and supervisor, I probably learned more than I gave. The 2-year term at EPFL School Council (AE) was also a very instructive contact with Swiss research management and political culture. I am grateful to my fellow AE members with whom I participated in numerous meetings and contributed to many position documents. I am also glad to have joined Polydoc in the very first steps of this adventure and I want to thank the fellow committee members for their trust and collaboration during the past year.

I also had the enormous chance of joining the EPFL and UNIL student chamber orchestra at the very beginning of my PhD. The OChE provided through music, *après-répètes* and *randoches* some of the best moments I have spent in Lausanne. I met here many inspiring musicians, who became also great friends. A special thank to Xavier, Sam, Thomas, Flo and Manu, for all the fun times and great memories, with or without music.

The PhD has been a 4-year journey with many other travel mates joining hikes, treks, ski outings, pétanque matches, road trips, political events, music retreats, and soirées of which I keep some excellent memories. I wish to thank all those who took part in this unforgettable journey.

Finally, I want to thank my parents for their unconditional love and support. This thesis is dedicated to them.

*Lausanne, December 2018*

# CV

# Giuseppe PERONATO

Born on 17.08.1989 in Vicenza, Italy. Italian-EU citizen, Swiss resident (Permit B EU/EFTA)
Permanent email address: gperonato@gmail.com

## EDUCATION

2014.09-present **PhD Candidate**
**Ecole polytechnique fédérale de Lausanne (EPFL),** Lausanne, Switzerland
Laboratory of Integrated Performance in Design (LIPID)
Thesis title: *Photovoltaic and building energy retrofit potential in urban areas: a planning-support system under uncertainty*
Advisor: Prof. Marilyne Andersen; Co-advisor: Prof. Emmanuel Rey

2017.02 **Visiting researcher, HFT Stuttgart** (13-17.02), funded by the SEMP program

2011.10-2014.03 **Master degree in Architecture** (Laurea Magistrale in Architettura)
**Università Iuav di Venezia,** Venice, Italy
Grade: 110/110 *cum laude*
Track: Urban Studies (Architettura e città)
Thesis title: *Built density, solar potential and daylighting: application of performance simulation tools in urban design.* Full text
Advisors: Dr. F. Cappelletti, Prof. F. Peron; Co-Advisors: Prof. M. Andersen, E. Nault

2012.09-2013.09 **Exchange Student,** awarded LLP Erasmus scholarship
**Ecole polytechnique fédérale de Lausanne (EPFL),** Lausanne, Switzerland

2008.10-2011.07 **Bachelor degree in Architecture** (Laurea in Scienze dell'Architettura)
**Università Iuav di Venezia**, Venice, Italy

2011.01-2011.05 **Exchange Student**, awarded MIUR scholarship for ExtraEU mobility
**McGill University**, Montréal, Canada

1998.11-2010.09 **Diploma in cello performance** (Diploma di Conservatorio in Violoncello)
Conservatorio di Musica "A. Pedrollo", Vicenza, Italy

## EMPLOYMENT

2018.10-present **Research assistant** – 5% FTE
**Uppsala universitet,** Uppsala, Sweden
Division of Construction Engineering
Advisor: Prof. Joakim Widén

2014.09-present **Doctoral assistant** (Teaching and research assistant) – 100% FTE
**Ecole polytechnique fédérale de Lausanne (EPFL),** Lausanne, Switzerland
Laboratory of Integrated Performance in Design (LIPID)
Advisor: Prof. Marilyne Andersen

2013.02-2013.09 **Student assistant** (Research assistant) – 10-20% FTE
**Ecole polytechnique fédérale de Lausanne (EPFL),** Lausanne, Switzerland
Laboratory of Integrated Performance in Design (LIPID)
Advisors: Prof. Marilyne Andersen, E. Nault

## INSTITUTIONAL RESPONSIBILITIES

2016.09-2018.08 **Representative of the scientific staff**
2018.01-2018.08 **Vice president and member of the executive board**
**School Council (*Assemblée d'Ecole*)**
**Ecole polytechnique fédérale de Lausanne (EPFL),** Lausanne, Switzerland
http://ae.epfl.ch

## STUDENT SUPERVISION

2015.09-2018.06 **Project supervisor (project tutor: Prof. Marilyne Andersen)**
**Master-level semester projects**, 10 ECTS credits
Stéphane Bonjour and Jérémie Stoeckli (MES program)
*The influence of the Level of Detail (LOD) on the assessment of the photovoltaic (PV) potential in urban environments.* Fall 2015
*Solar-optimized building form: a parametric design platform for PV and ST systems. Application to the Solar Decathlon pavilion.* Spring 2016
Mathieu Desmarescaux and Mélanie Gaillet-Tournier (MES program)
*Energy modeling of the Solar Decathlon pavilion: development and fine-tuning of solar passive strategies.* Fall 2016
*Assessing the viability of BIPV installations in building energy retrofitting projects.* Spring 2017
Adrien Legrain (MES program) and Sylvain Vitali (Enegy minor)
*Definition of design scenarios for the arrangement of tilted solar arrays and estimation of their electricity production from horizontal irradiances.* Fall 2017
Adrien Legrain (MES program)
*Energy and spatial comfort assessment of an office space with semi-transparent PV modules.* Spring 2018
**Master-level semester project**, 4 ECTS credits
Karni Siraganyan (SIE program)
*Energy modeling of the Solar Decathlon pavilion: testing the thermal resilience under unplanned use.* Fall 2016

2015.12-2016.01 **Co-advisor**
**Master's thesis in Geography**, Université de Lausanne
Zohreh Shafi Zadeh
*Energy scenarios in urban renewal processes: a GIS-based approach to analyze the urban-scale installation of photovoltaics. Case study of two neighborhoods in Neuchâtel.*
Advisors: Dr. M. Tonini, Dr. C. Kaiser, Prof. M. Andersen, G. Peronato

## TEACHING

Spring 2017-2018 **Lecturer**
**Renewable energy and solar architecture in Davos**
Co-instructors: Ph. Bélanger, J. Bunyesc Palacín, H. Huwald, M. Lehning, L. Pastore
Bachelor-level intensive class, 4 ECTS credits
Role: lecturer on solar energy in buildings, student supervision, grading

02.2017 **Guest lecturer**
**1.5-day seminar and workshop on "Integrated daylight and thermal simulation"**
**University of Aarhus, Denmark**
Master-level class **"**Daylighting design" - Prof. W. Osterhaus
Content: Lecture, software hands-on tutorials, and student advising.

Fall 2016-2017 **Teaching assistant**
**Comfort and architecture: sustainable strategies**
Instructors: M. Andersen, L. Pastore, J. Wienold
Master-level class, 3 ECTS credits
Role: Participated in the design of exercises and grading, taught simulation software tutorials.

## REVIEWING

2018.06-present **Solar Energy, Applied Energy**

2016-2017 **PLEA International Conference**

2016, 2018, 2019 **SimAUD International Symposia**

## SOFTWARE DEVELOPMENT

**GHCitySim.** Set of Grasshopper components for interfacing with CitySim, an urban-scale building energy simulation engine. Licensed under GNU-GPL3.

**getHorizon.** Tool to get the horizon profile (skyline) from a viewpoint using online elevation services. Licensed under BSD-3-Clause.

## VOLOUNTEER EXPERIENCE

2015.11-2018.06 **Member of the board, Vice-president (2015-2017), President (2017-2018) EPFL and UNIL Student Chamber Orchestra (OChE),** Lausanne, Switzerland
*Manager of the orchestra, with various leading and executive responsibilities including communication, IT, fundraising and public relations.*
http://www.oche.ch

2017.11-2018.12 **Founding member, member of the board, internal relations manager PolyDoc** (EPFL PhD student association), Lausanne, Switzerland
*In charge of the relations with EPFL elected bodies.*
http://polydoc.epfl.ch

## PERSONAL SKILLS

IT

| | |
|---|---|
| Algorithmic 3D modeling | Rhinoceros+Grasshopper |
| Building energy modeling | EnergyPlus (DesignBuilder, Honeybee, ArchSim), CitySim |
| Daylight and irradiance modeling | Radiance/Daysim (DIVA, Honeybee) |
| PV performance modeling | SAM, PVLIB |
| GIS | ArcGIS, QGIS, GeoPandas |
| Coding and scientific computing | Python, MATLAB; Bash and PHP (basics) |
| Graphics | Photoshop, InDesign, Illustrator |
| OS | MacOs, Linux (Raspbian, Ubuntu), Windows |
| Web | HTML, CSS, PHP (basics) |
| Markup languages | LaTeX, Markdown (typesetting); KML (geodata), HTML (web) |

Languages

Italian (native), English and French (fluent, C1-C2), German (basic, A2)

## SELECTED PUBLICATIONS

### Journal articles

Peronato, G., Rey, E., & Andersen, M. (2018). 3D model discretization in assessing urban solar potential: the effect of grid spacing on predicted solar irradiation. Solar Energy, 176, 334–349. https://doi.org/10.1016/j.solener.2018.10.011

Peronato, G., Rastogi, P., Rey, E., & Andersen, M. (2018). A toolkit for multi-scale mapping of the solar energy-generation potential of buildings in urban environments under uncertainty. Solar Energy, 173, 861–874. https://doi.org/10.1016/j.solener.2018.08.017.

Nault, E., Peronato, G., Rey, E., Andersen, M., 2015. Review and critical analysis of early-design phase evaluation metrics for the solar potential of neighborhood designs. Building and Environment 92, 679–691. doi:10.1016/j.buildenv.2015.05.012

### Peer-reviewed conference papers

Peronato, G., Aguacil Moreno, S., Legrain, A., Vitali, S., Rey, E., & Andersen, M. (2018). Assessing the photovoltaic potential of flat roofs: insights from the analysis of optimised array arrangements. To be presented at PLEA 2018 conference, Hong Kong, China.

Peronato, G., Kaempf, J.H., Rey, E., Andersen, M., 2017. Integrating urban energy simulation in a parametric environment: a Grasshopper interface for CitySim, in: PLEA 2017, Proceedings of the 33rd International Conference on Passive and Low Energy Architecture. Full text.

Peronato, G., Rey, E., Andersen, M., 2016. 3D-modeling of vegetation from LiDAR point clouds and assessment of its impact on façade solar irradiation, in: ISPRS - International Archives of the Photogrammetry, Remote Sensing and Spatial Information Sciences. pp. 67–70. doi:10.5194/isprs-archives-XLII-2-W2-67-2016.

Peronato, G., Bonjour, S., Stoeckli, J., Rey, E., Andersen, M., 2016. Sensitivity of calculated solar irradiation to the level of detail: insights from the simulation of four sample buildings in urban areas, in: PLEA 2016 - Cities, Buildings, People: Towards Regenerative Environments, Proceedings of the 32nd International Conference on Passive and Low Energy Architecture. Full text.

Peronato, G., Rey, E., Andersen, M., 2015. Sampling of building surfaces towards an early assessment of BIPV potential in urban contexts, in: Proceedings of PLEA2015 Architecture in (R)Evolution. Full text.

Peronato, G., Nault, E., Cappelletti, F., Peron, F., Andersen, M., 2015. A parametric design-based methodology to visualize building performance at the neighborhood scale, in: Proceedings of BSA 2015. Bozen-Bolzano University Press, Bolzano/Bozen, pp. 351–358. Full text.

### Book chapters

Peronato, G., Rastogi P., Andersen, M., 2017. Robustesse de l'évaluation du potentiel solaire de formes urbaines différenciées, in: Rey, E. (Ed.), Suburban Polarity. Presses Polytechniques et Universitaires Romandes (PPUR), Lausanne.

Nault, E., Peronato, G., Andersen, M., 2015. Forme urbaine et potentiel solaire, in: Rey, E. (Ed.), Urban Recovery. Presses Polytechniques et Universitaires Romandes (PPUR), Lausanne.

*The full list of publications is available through EPFL institutional repository Infoscience.*

**Ce document a été imprimé au Centre d'impression EPFL,
imprimerie climatiquement neutre, certifiée myClimate.**